7. SITE 651: TYRRHENIAN SEA[1]

Shipboard Scientific Party[2]

HOLE 651A

Date occupied: 11 January 1986

Date departed: 18 January 1986

Time on hole: 7 days 17.5 hr

Position: 40°09.03′N, 12°45.39′E

Water depth (sea level, corrected m, echo-sounding): 3578.0

Water depth (rig floor, corrected m, echo-sounding): 3589.0

Bottom felt (m, drill pipe length from rig floor): 3590.9

Total depth (m): 4141.8

Penetration (m): 550.9

Number of cores: 58

Total length of cored section (m): 550.9

Total core recovered (m): 189.8

Core recovery (%): 34.5

Deepest sedimentary unit cored:
Depth sub-bottom (m): 387.6
Nature: clays and nannofossil ooze
Age: early Pliocene
Measured vertical sound velocity (km/s): 1.7 to 2.1

Igneous or metamorphic basement:
Depth sub-bottom (m): 387.6 (top) to 550.9 (bottom)
Nature: basalt (Unit 1), dolerite and metadolerite (Unit 2), basalt and basalt breccia (Unit 3), and serpentinized peridotite (Unit 4)
Velocity range (km/s): 3.4–6.1

Principal results: Site 651 was located on the eastern flank of a basement swell which lies at the axis of the Vavilov Basin (Fig. 1). Drilling established the presence of a basement complex consisting predominantly of basalts overlying serpentinized peridotite. The sedimentary cover is of Pliocene to Pleistocene age and includes abundant volcaniclastics in the upper section.

Two major sedimentary units were recovered between the seafloor and 388 mbsf, and three basement units were recovered between 388 and 551 mbsf (Fig. 2). The lithologic units (Fig. 3) were as follows:

Sedimentary Unit I: depth: 0–136.0 mbsf; age: late Pleistocene. Sedimentary Unit I consists mostly of volcanogenic sediments interbedded with volumetrically subordinate (< 15%) marly, nannofossil-rich mud. Beneath the superficial muds, the succession is dominated by pumiceous sand and gravel. Cemented pumice breccia decreases in average grain size and abundance downhole.

Sedimentary Unit II: depth: 136.0–387.6 mbsf; age: Pliocene to late Pleistocene. Sedimentary unit II is composed of nannofossil chalk with very subordinate volcanogenic turbiditic claystones and siltstone. The upper levels (136–309 mbsf) are lithologically very heterogeneous and include volcaniclastic siltstone and sandstone, whereas the lower levels (309–348 mbsf) are more uniform, dominated by nannofossil chalk. A 40-m-thick subunit immediately above basement (348–387.6 mbsf) comprises brilliantly colored dolomite-rich sediment, apparently relatively enriched in Fe and Mn. No microfossils have been detected in the lower 39 m of this dolomitic subunit; the fauna in the top meter are from the base of biostratigraphic zone MPl6/NN18 (upper Pliocene, 2 m.y. ago). Extrapolation of the sedimentation rate curve from the lowest datable portion of the sediment column down to basement suggests a date of approximately 3.6 m.y. for the basalt/sediment contact.

Basement Unit 1: depth: 387.6–464 mbsf. The upper part of the basement section consists of basalt with carbonate veins which decrease downhole, plus carbonate-opal-cemented basaltic breccias. The basalt is aphanitic, highly altered, and of low vesicularity. Several distinct flows were recognized by the presence of altered glassy chilled margins.

Basement Unit 2: depth: 464–492 mbsf. Basement Unit 1 grades into Unit 3 through a complex transition zone. This transition zone comprises highly altered peridotite, dolerite, dolomitic chalk, alkali-feldspar-rich leucocratic rocks, carbonate-cemented basaltic breccias, a very coarse sand to fine gravel graded layer (possible drilling disturbance), and a few rounded loose pebbles of metadolerite. The deepest occurrence of planktonic foraminifers was in a dolomitic breccia at 465 mbsf; a very tentative date of early Pliocene has been assigned.

Basement Unit 3: depth: 492–522 mbsf. Thin layer of basalt and carbonate-cemented breccias, similar to Unit 1.

Basement Unit 4: depth: 522–551 mbsf. Highly serpentinized peridotites showing a tectonite fabric. Relict mineralogy suggests that these peridotites are prevalently lherzolitic.

Standard downhole measurements (DIL-LSS-GR-CAL and LDT-CNT-NGT) were made from 119 mbsf to approximately 325 mbsf. The logs agree well with the laboratory physical properties measurements and lithostratigraphy in intervals of good core recovery. In intervals of poor recovery, the logs indicate that volcaniclastics are dominant, and suggest that the coring process preferentially sampled

---

[1] Kastens, K. A., Mascle, J, Auroux, C., et al., 1987. *Proc., Init. Repts. (Pt. A), ODP*, 107.

[2] Kim A. Kastens (Co-Chief Scientist), Lamont-Doherty Geological Observatory, Palisades, NY 10964; Jean Mascle (Co-Chief Scientist), Laboratoire de Géodynamique Sous-Marine, Université Pierre et Marie Curie, BP 48, 06230 Villefranche-sur-Mer, France; Christian Auroux, Staff Scientist, Ocean Drilling Program, Texas A&M University, College Station, TX 77843; Enrico Bonatti, Lamont-Doherty Geological Observatory, Palisades, NY 10964; Cristina Broglia, Lamont-Doherty Geological Observatory, Palisades, NY 10964; James Channell, Department of Geology, 1112 Turlington Hall, University of Florida, Gainesville, FL 32611; Pietro Curzi, Istituto di Geologia Marina, Via Zamboni, 65, 40127 Bologna, Italy; Kay-Christian Emeis, Ocean Drilling Program, Texas A&M University, College Station, TX 77843; Georgette Glaçon, Laboratoire de Stratigraphie et de Paleoécologie, Centre Saint-Charles, Université de Provence, 3, Place Victor Hugo, 13331 Marseille Cedex, France; Shiro Hasegawa, Institute of Geology, Faculty of Science, Tohoku University, Aobayama, Sendai, 980, Japan; Werner Hieke, Lehrstuhl für Allgemeine, Angewandte und Ingenieur-Geologie, Abt. Sedimentforschung und Meeresgeologie, Technische Universität München, Lichtenbergstrasse 4, D-8046 Garching, Federal Republic of Germany; Floyd McCoy, Lamont-Doherty Geological Observatory, Palisades, NY 10964; Judith McKenzie, Department of Geology, University of Florida, 1112 Turlington Hall, Gainesville, FL 32611; Georges Mascle, Institut Dolomieu, Université Scientifique et Médicale de Grenoble, 15 Rue Maurice Gignoux, 38031 Grenoble Cedex, France; James Mendelson, Earth Resources Laboratory E34-366, Department of Earth, Atmospheric and Planetary Sciences, Massachusetts Institute of Technology, 42 Carleton Street, Cambridge, MA 02142; Carla Müller, Geol.-Paläont. Institut, Universität Frankfurt/Main, 32–34 Senckenberg-Anlage, D-6000 Frankfurt/Main 1, Federal Republic of Germany (current address: 1 Rue Martignon, 92500 Rueil-Malmaison, France); Jean-Pierre Réhault, Laboratoire de Géodynamique Sous-Marine, Université Pierre et Marie Curie, BP 48, 06230 Villefranche-sur-Mer, France; Alastair Robertson, U.S. Geological Survey, 345 Middlefield Road, Menlo Park, CA 94025 (current address: Department of Geology, Grant Institute, University of Edinburgh, Edinburgh, EH9 3JW, United Kingdom); Renzo Sartori, Istituto di Geologia Marina, Via Zamboni, 65, 40127 Bologna, Italy; Rodolfo Sprovieri, Istituto di Geologia, Corso Tukory, 131, Palermo, Italy; Masayuki Torii, Department of Geology and Mineralogy, Faculty of Science, Kyoto University, Kyoto, 606, Japan.

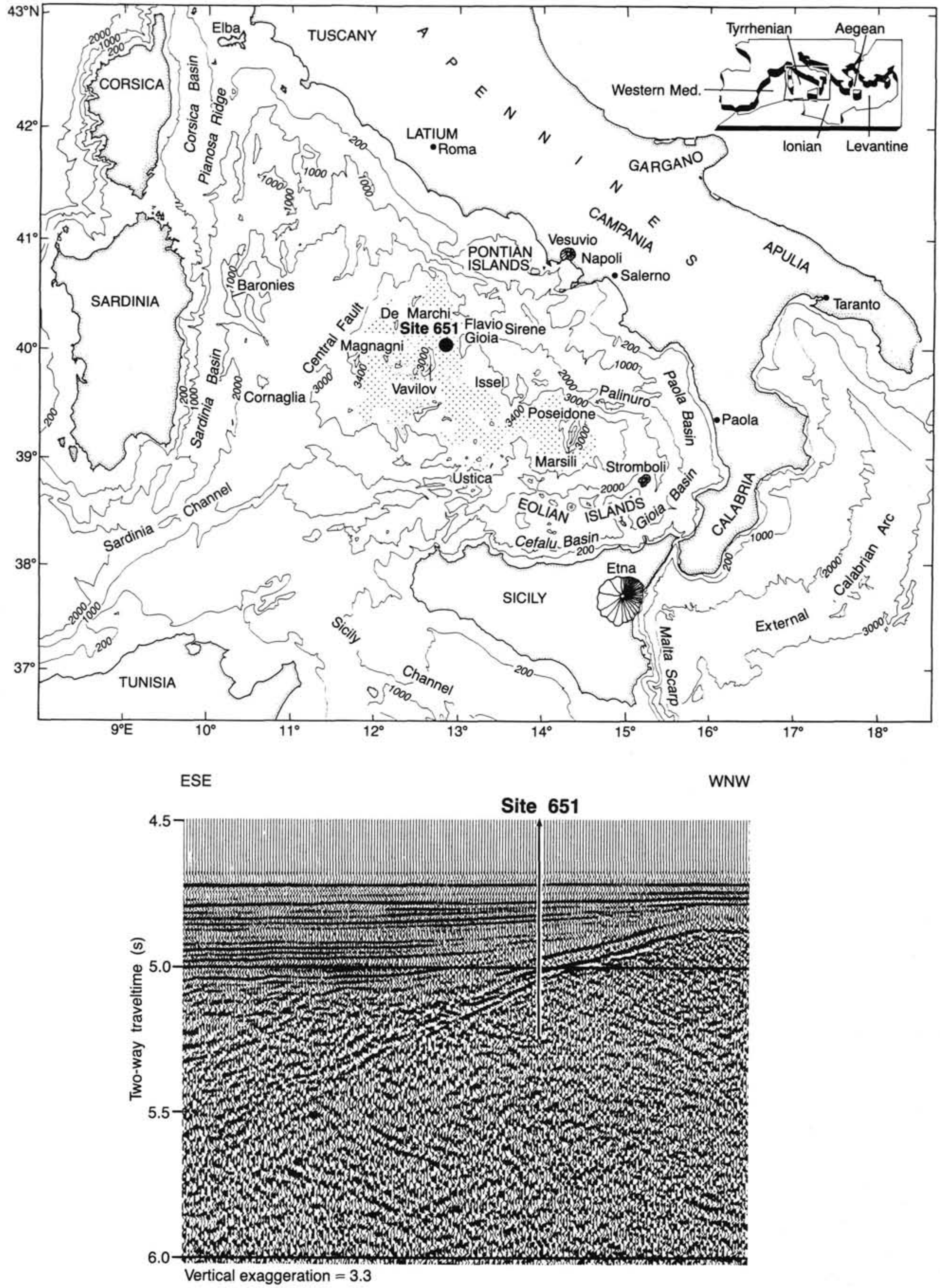

Figure 1. Location of Site 651 on bathymetric map and on MCS profile (line ST12). Bathymetry in meters.

an unrepresentative fraction dominated by carbonate-rich fine-grained sediment.

BACKGROUND AND OBJECTIVES

Regional Setting and Previous Work

Site 651 is located in the axis of the Vavilov Basin in the central Tyrrhenian Sea (Fig. 4). The Vavilov Basin is the northwestern of the two deep Tyrrhenian basins. The basin contains a narrow (60 km across) bathyal plain (water depth 3530 m). To the west, the Vavilov Basin is bounded by a prominent north-trending sialic ridge, de Marchi Seamount, which is interpreted as the easternmost fault-bounded, tilted block associated with the Sardinian continental margin (Fig. 5) (Moussat, 1983). The mirror image of de Marchi seamount is Flavio Gioia Seamount, another north-trending sialic ridge lying to the east of Vavilov Basin. To the north and northeast, the Vavilov Basin connects with a series of wide submarine valleys originating from the Tuscanian and Campanian continental shelves (Fig. 4). To the south, the Vavilov bathyal plain contains a prominent (>2000 m relief) north-northeast-trending elongate volcano, Vavilov Seamount.

As was the case for the Marsili Basin (Site 650), the Vavilov Basin is thought to be underlain by oceanic-type lithosphere. Indirect evidence for the nature of the lithosphere includes a Moho depth of less than 10 km (Fig. 6; Ferruci et al., 1973; Panza et al., 1980; Recq et al., 1984; Steinmetz et al., 1983), high amplitude magnetic anomalies (Bolis et al., 1981), and a relatively high heat flow (Fig. 7; Erickson et al., 1977; Della Vedova et al., 1984; Hutchison et al., 1985). A negative magnetic anomaly (> 150 gammas) is associated with Vavilov Seamount. In addition to these geophysical arguments, the existence of oceanic crust is supported by the recovery of tholeiitic basalts from the Vavilov Seamount (Selli et al., 1977; Gennesseaux et al., 1986) and at DSDP Site 373. Samples from Vavilov Seamount have been dated at 3.5 m.y. (Selli et al., 1977) and early Pleistocene (Gennesseaux et al., 1986). DSDP Site 373 was located on the flank of a small volcano about 30 km east-southeast of Vavilov volcano (Hsü, Montadert, et al., 1978). Drilling at DSDP Site 373 recovered brecciated basalt and basalt flows. The Site 373 basalts are of mid-ocean ridge (MORB) type and have been dated between 7.3 and 3.5 m.y. using the K/Ar technique (Barberi et al., 1978; Dietrich et al., 1978).

Single channel and multichannel seismic (MCS) profiles (Fig. 8) across the Vavilov Basin show a diffractive and irregular acoustic basement at several hundred meters to 1 km below seafloor; this basement is inferred to be the top of oceanic layer 2. Interval velocities within this unit range from 3.46 to 4.33 km/s, confirming seismic refraction data (Fig. 6) which give a velocity value of about 4.0 km/s (Recq et al., 1984). In the Vavilov Basin, acoustic basement rises as a broad northeast-trending swell, which bisects the basin into almost symmetrical parts. The basement swell lies approximately along the northward prolongation of Vavilov Seamount. A saddle separates the crest of the basement swell from the peak of the volcano; this geometry suggests that the basement swell does not represent lava flows originating from Vavilov volcano. The two sub-basins of the Vavilov bathyal plain are locally filled with as much as 800–900 m of well-layered sediments whose acoustic signature is numerous subparallel, subhorizontal, high-amplitude reflectors. The well-layered units have been interpreted as ponded turbidites, ash layers, and hemipelagic sediments of early Pliocene through Pleistocene age (Fabbri and Curzi, 1979; Moussat, 1983). Locally, an intermediate-depth acoustic unit can be detected underlying the well-layered upper unit and pinching out against the acoustic basement swell. Interval velocities measured in the intermediate depth unit are high, 3.4–3.7 km/s. The intermediate layer had been tentatively interpreted as a Messinian facies, either "evaporites of marginal zone" (Fabbri and Curzi, 1979), a subaerial lacustrine facies (Malinverno et al., 1981), or a subaerial volcaniclastic series (Moussat, 1983).

Objectives

Age and Geochemistry of the Basaltic Basement

Site 651 is a companion site to Site 650 (in the Marsili Basin) and shares many of the same objectives. The overall goal of the pair of sites was to provide constraints for the hypothesis that back-arc spreading has occurred in the Tyrrhenian Sea at two distinct centers, and that the locus of basaltic magma formation has jumped from west to east (i.e., from Vavilov to Marsili Basin), possibly as an effect of southeastward retreat of the subduction zone. Thus, the first objective at Site 651 was to recover and date the sediment/basalt contact; then to penetrate sufficiently deep into basalt to recover relatively unaltered samples for determination of age and geochemical affinity. Although some of this information was available from drilling at DSDP Site 373, that site was thought to be possibly atypical because it was located on a small seamount out of the main part of the basin.

"Basal" Sediments

Cores from numerous DSDP sites on oceanic crust formed at mid-ocean ridges have recovered a metalliferous layer at the base of the sedimentary section, just above the basalt (Bonatti, 1975). There are, however, relatively few well-documented cases of metalliferous basal sediments in back-arc basin settings (e.g., Bonatti et al., 1979). This is particularly unfortunate because back-arc basins are thought by many researchers to be the precursors of many ophiolites, including some ophiolites where the basal metalliferous sediments are economically important (Robertson and Boyle, 1983). Recovering such basal metalliferous sediments, if they exist, was the second objective of Site 651.

Messinian Paleoenvironment

Finetti and Morelli (1973) first noted that the central portion of the Tyrrhenian Sea lacks the acoustic signature diagnostic of the Messinian salt layer, which is seen on seismic reflection profiles from other deep basins in the Mediterranean Sea. This apparent lack of salt raises the question of what exactly was happening in the central Tyrrhenian during the Messinian desiccation. Fabbri and Curzi (1979) inferred that evaporites were probably present, but that the Messinian unit (if any) must be very thin, including only the upper gypsiferous part of the total evaporite sequence. Fabbri and Curzi (1979) felt that such "marginal" evaporites could be deposited in a shallow water or continental setting. In contrast, Malinverno et al. (1981) felt that no evaporites were present in the central Tyrrhenian Sea. Instead, they mapped a Messinian facies of subaerial clastic deposits interspersed with pockets of lacustrine sediment, from which they inferred that the central Tyrrhenian area stood higher than the elevation at which evaporites were being deposited. Moussat (1983) followed Fabbri and Curzi (1979) in mapping a limited occurence of "marginal evaporites" in the central Tyrrhenian. In addition he stressed the importance of a chaotic acoustic unit immediately above basement which he interpreted as volcaniclastic sediments of possible Messinian age; Site 651 lies within Moussat's volcaniclastic facies. Finally, after our experience of finding post-Messinian basement at Site 650 we had to consider a fourth hypothesis—that the central Tyrrhenian did not yet exist in the Messinian, as originally proposed by Selli and Fabbri (1971). The third objective of Site 651 was to determine the Messinian paleoenvironment (if any) of the central Tyrrhenian Sea.

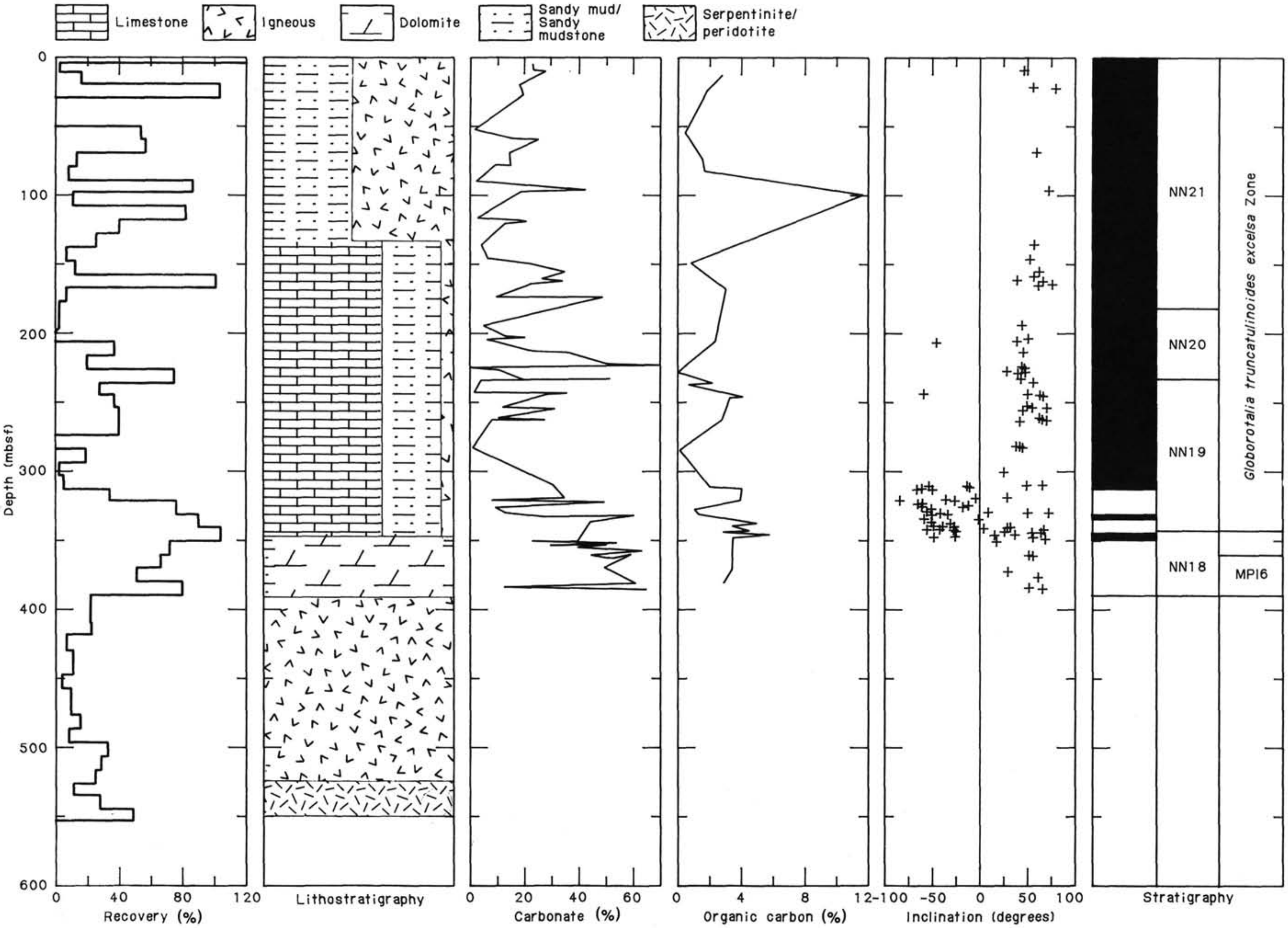
Limestone
Igneous
Dolomite
Sandy mud/ Sandy mudstone
Serpentinite/ peridotite
Depth (mbsf)
0
100
200
300
400
500
600
0
40
80
120
Recovery (%)
Lithostratigraphy
0
20
40
60
Carbonate (%)
0
4
8
12
Organic carbon (%)
-100
-50
0
50
100
Inclination (degrees)
NN21
NN20
NN19
NN18
Globorotalia truncatulinoides excelsa Zone
MPl6
Stratigraphy

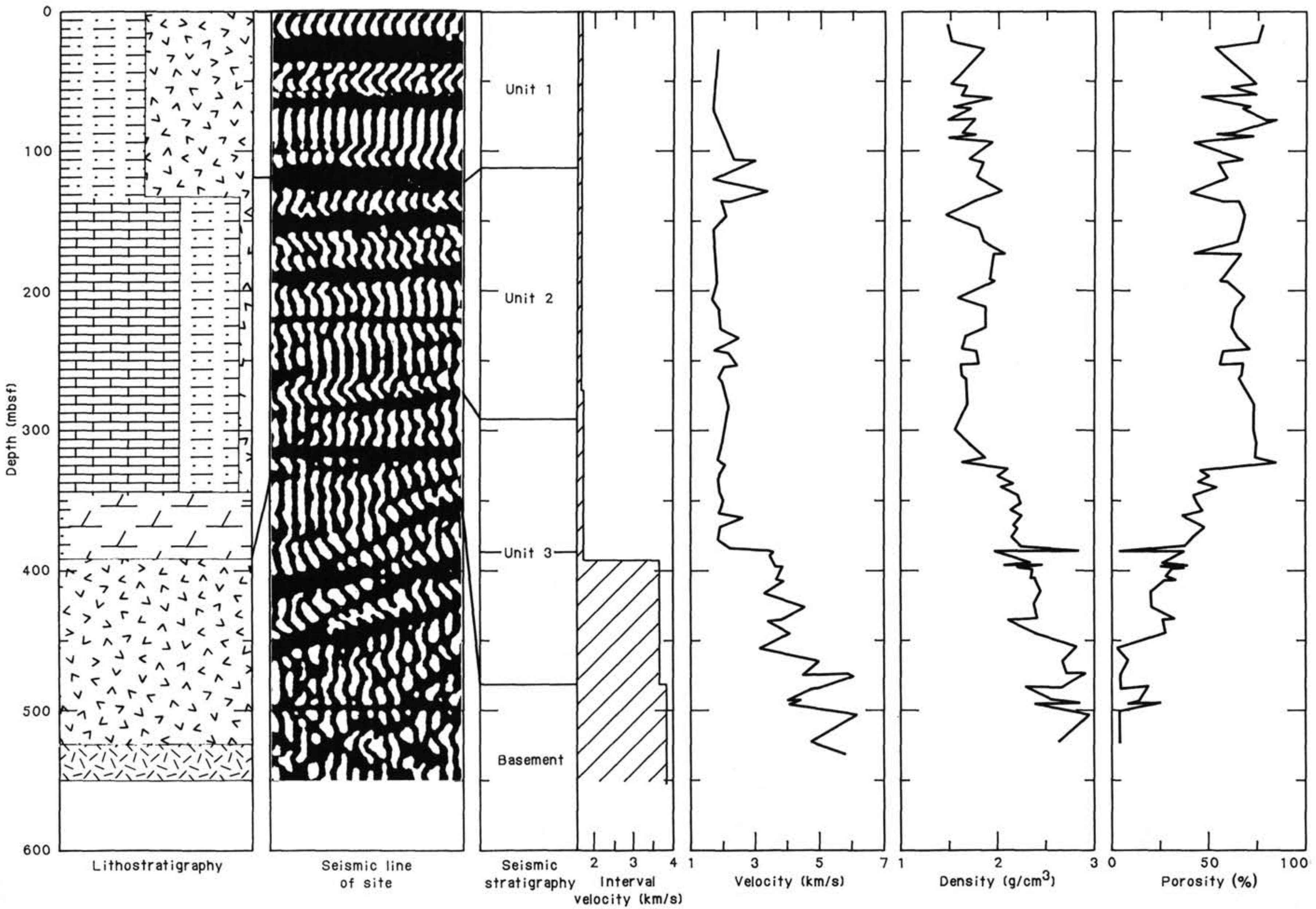

Figure 2. Summary of measurements made at Site 651.

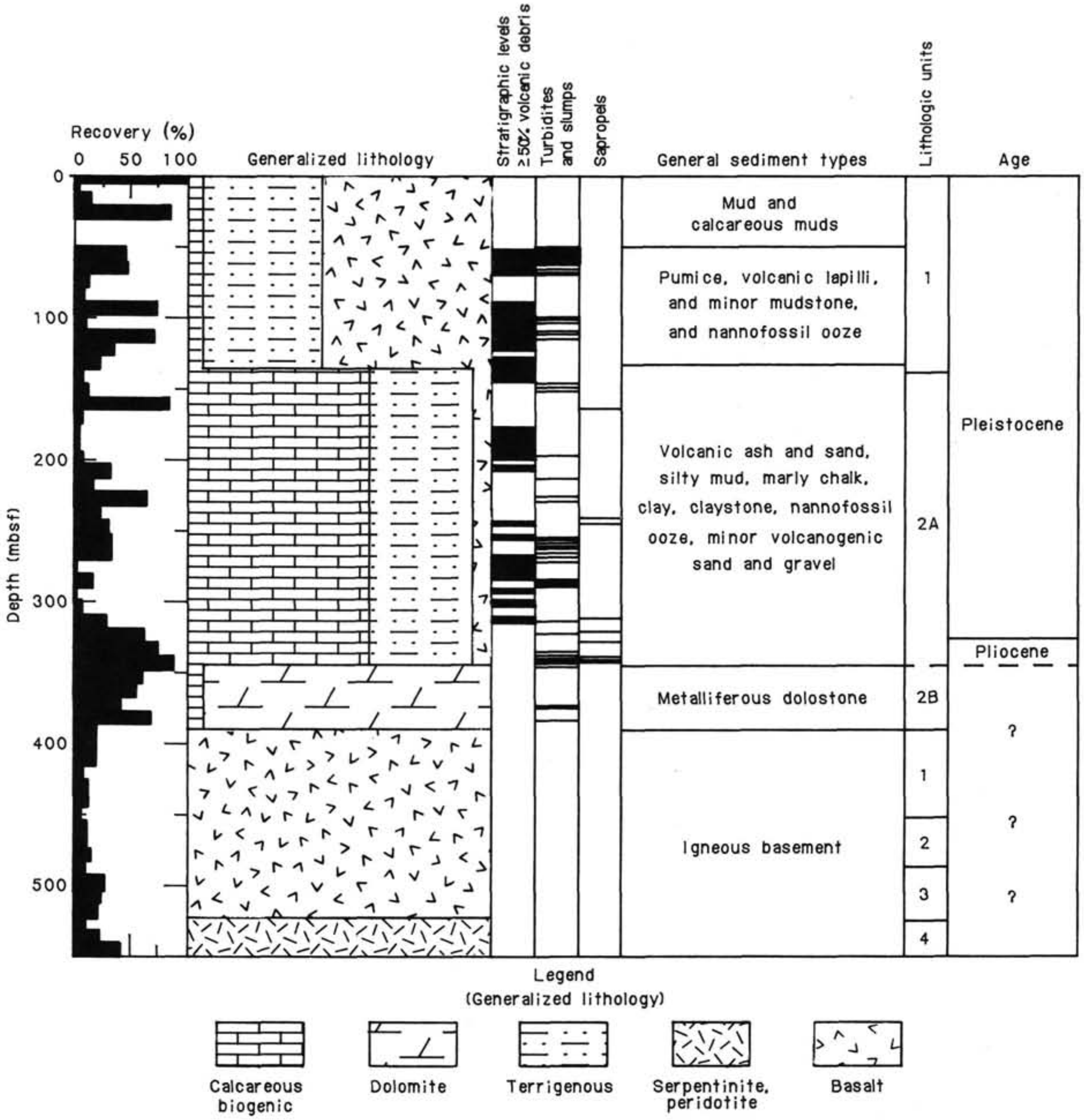

Figure 3. Generalized lithostratigraphic column, showing the main lithologies described and subdivision into units. In the stratigraphic column, the width of each vertical division is proportional to the percent of the indicated lithology recovered in that lithostratigraphic unit; lithologies are major groups as described in "Explanatory Notes" chapter, this volume.

Pliocene-Pleistocene Stratigraphy

As at Site 650, we planned to continuously core the (inferred) Pliocene-Pleistocene sedimentary sequence to develop biostratigraphic, tephrochronologic, and paleomagnetic time scales. The goals for tephrochronology remained the same as described for Site 650, but we hoped to obtain more discrete, undiluted, identifiable tephra layers in a region where the sedimentation rate was expected to be lower. After our unexpectedly successful paleomagnetic measurements at Site 651, we were optimistic that we could obtain a second detailed magnetic reversal chronology if we again encountered volcanogenic turbidites rich in magnetite.

Site Selection

The ponded sediments in the structurally deepest portion of Vavilov Basin exceed 1 s (perhaps 900 m) in thickness. Drilling through this extremely thick sequence would have been excessively time-consuming, as well as uncomfortably close to the outer limit for technical feasibility on a single bit hole. Instead we chose to drill on a basement swell which lies northward along strike from Vavilov Seamount (Fig. 9). If Vavilov Basin approximates the geometry of an organized spreading center, then Vavilov Seamount and its along-strike continuation would be the axis of spreading. In that case, basalts from the Site 651 target basement swell would be among the youngest in the Vavilov basin. At Site 650 we had recovered basalts which were thought to be among the oldest in the Marsili Basin. A comparison between the youngest basalts in Vavilov Basin with the oldest basalts in Marsili Basin was the appropriate comparison to test the working hypothesis that spreading at Marsili Basin began after the cessation of spreading in Vavilov Basin.

Although various investigators disagreed about the interpretation of the Messinian acoustic facies (see above), there was at

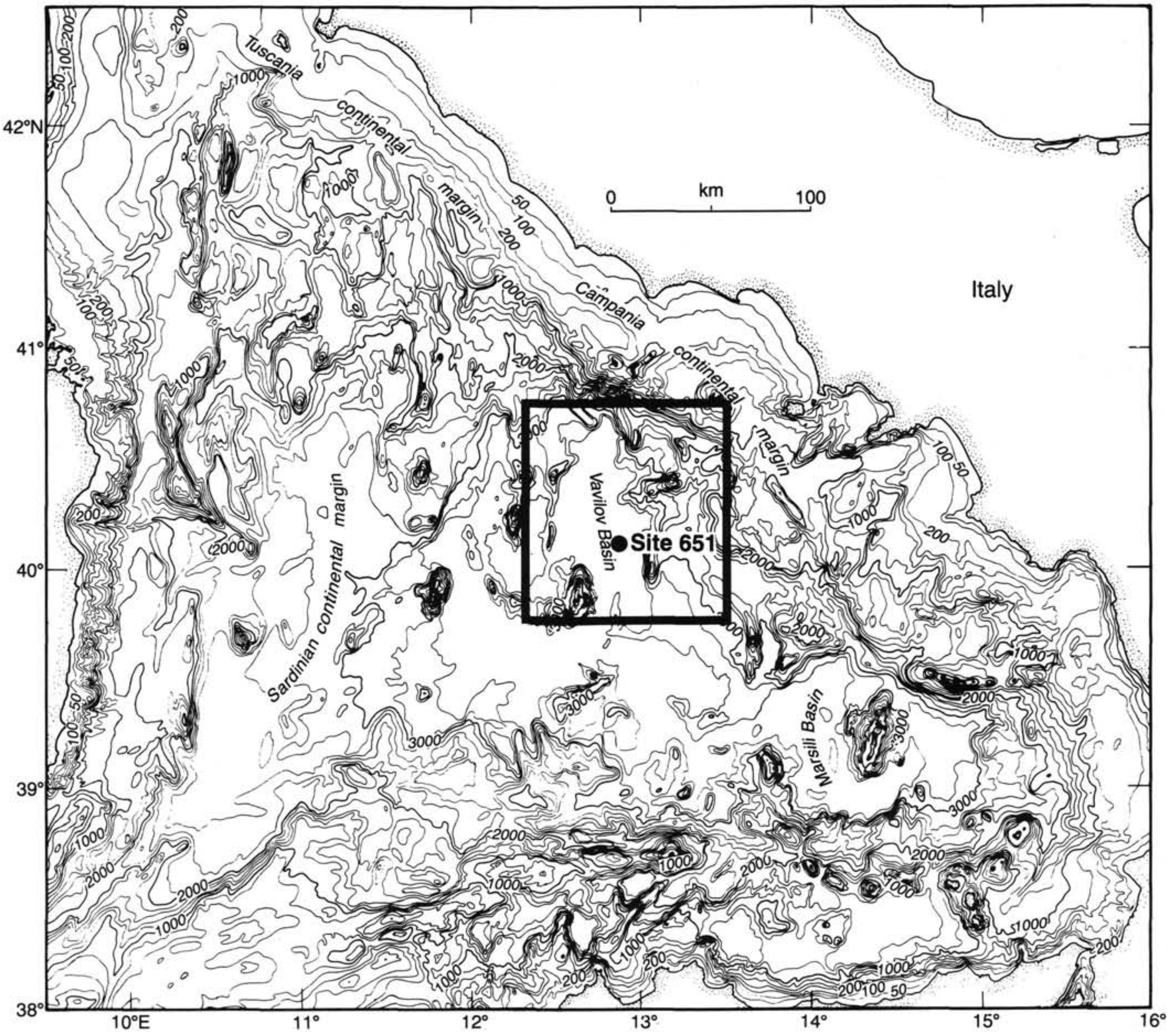

Figure 4. Site 651 is located in the Vavilov Basin, which is the northwestern of the two deep basins in the central Tyrrhenian Sea. Bathymetry in meters.

least a partial consensus on where in the seismic section the Messinian should occur: at the unit referred to as the "intermediate-depth unit" in the "Regional Setting and Previous Work" discussion above, i.e., at about 0.5 s below seafloor. The second factor guiding our selection of the Vavilov Basement site was that we wished to penetrate this "intermediate unit." This could be accomplished by drilling on the flank rather than the crest of the basement swell.

An appropriate location was identified on site survey seismic reflection profile ST12 (shotpoint 168) near its intersection with profile ST03 (shotpoint 2865) (Fig. 8).

OPERATIONS

Strategy

The proposed site is located on the eastern flank of an acoustic basement swell about 8 km from the crest of the swell, at a point where depth to basement is 500 ms. Interval velocities, obtained just prior to the departure of the leg, indicated that at the proposed site the seismic unit just above the basement (which had been tentatively identified as a Messinian facies) was characterized by a seismic velocity of 3.7 km/s. The relatively high seismic velocity suggested that the unit might be difficult to penetrate. The site objectives included identifying both the nature of the basement and the nature of the allegedly Messinian unit. To improve the possibility of achieving both goals, we planned to drop the positioning beacon 400 m west (updip) of the drill site, at the pinch-out of the 3.7 km/s unit. If the first hole failed to reach basement, a second hole could be positioned 400 m east of the beacon, where only 300 m of sediment overlies the basement.

The unknown but potentially hard nature of the 3.7 km/s layer, as well as the need to penetrate sufficiently deeply into basement to obtain relatively unaltered samples, dictated a rotary cored (RCB) hole. The planned downhole measurements program consisted of 4 or 5 Uyeda-probe heat flow measure-

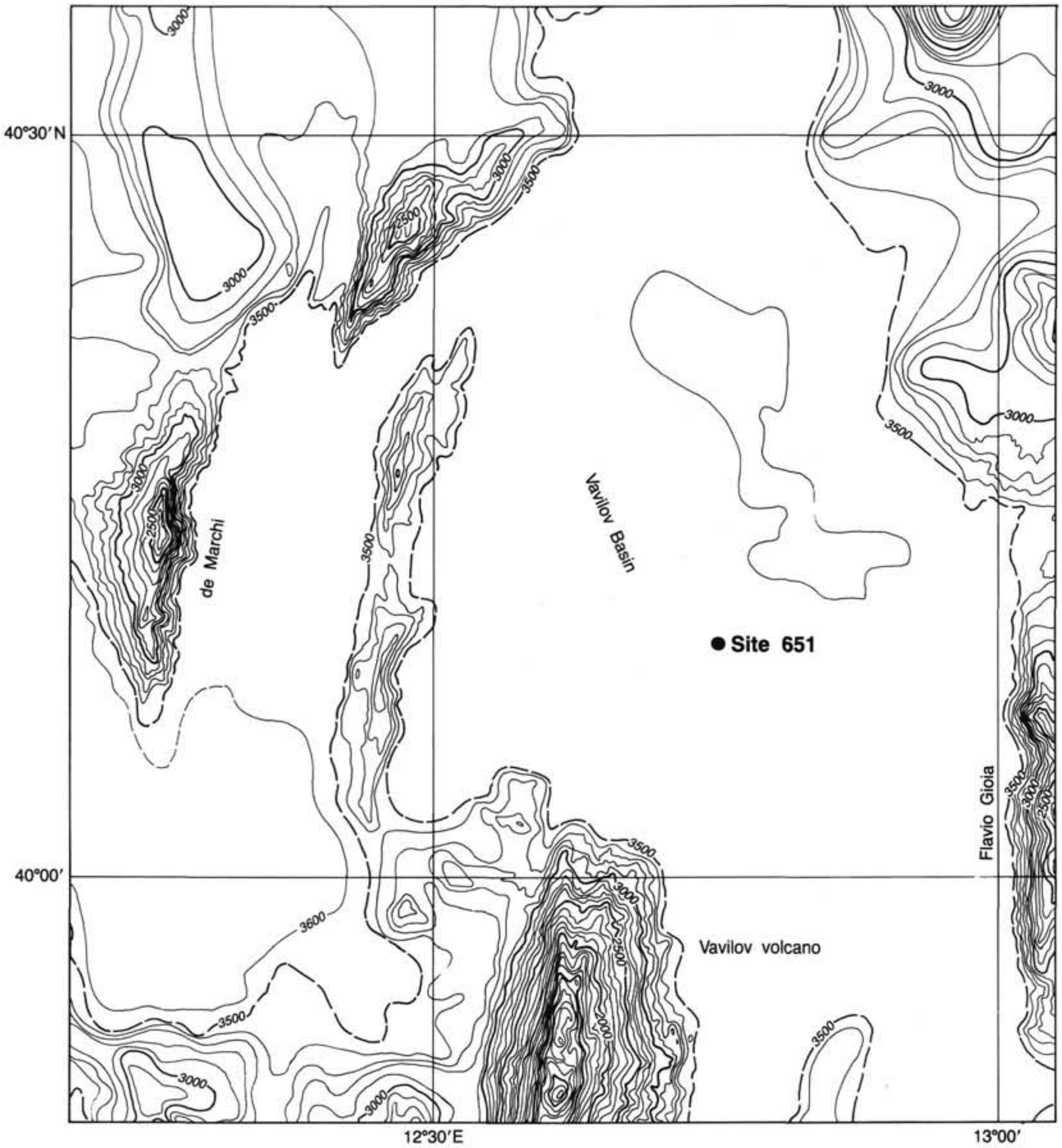

Figure 5. Site 651 is in the axis of the Vavilov bathyal plain. The bathyal plain is bounded to the west and east by prominent north-trending ridges (de Marchi and Flavio Gioia), which are asymmetrical in cross section and sialic in composition. These ridges are interpreted as the innermost fault-bounded, tilted blocks of the continental margin. Vavilov volcano, lying south of the bathyal plain, emerges from the deep basin with a total relief of almost 3 km. Bathymetry in meters.

ments at 40-m-spacing, and three logging runs: DIL/LSS/GR, LDT/CNT/NGT, and borehole televiewer.

The approach to Site 651 was planned to duplicate line ST12 of the site survey, beginning 15 nmi east of the proposed site. Along this line the seafloor is flat bathyal plain, so the target would need to be recognized from the seismic records. Since the target lay on the east side of a basement high it would probably be difficult to recognize in real time on an east to west pass because of the delay between the time when the ship passes over a piece of seafloor and the time the corresponding processed water-gun record is seen in the lab. Therefore the plan was to cross the target from east to west, come around to the reciprocal course, and drop the beacon on a west to east pass.

Approach to Site

At 0112 on 11 January (local time equals GMT), the ship slowed to 6 kt and changed course to 275° to begin the site approach. Two Bolt 80-in.^{3} water guns and a 500-m Teledyne streamer were streamed beginning at 0116. Seismic data were filtered and recorded as described in "Explanatory Notes" and "Underway Geophysics" sections, this chapter. Bathymetric data were also collected at 12 and 3.5 kHz during the approach.

On the latter part of the transit from Site 650, the ship was navigated using the Global Positioning System (GPS). Loran C appeared to be functioning consistently, although the Loran fixes plotted approximately 1 mi west-southwest of the GPS fixes. After the ship slowed and turned west to begin the site approach, the discrepancy between the GPS and Loran fixes gradually widened. GPS fixes plotted on the desired line and showed a speed made good of 4.8 kt; whereas Loran fixes plotted south of the line and showed a speed made good of 6.2 kt. The Loran speed was more consistent with the shaft rpm. At 0203 a transit satellite fix was received which agreed with the Loran. Although its elevation was low (10°), we decided at this point to believe

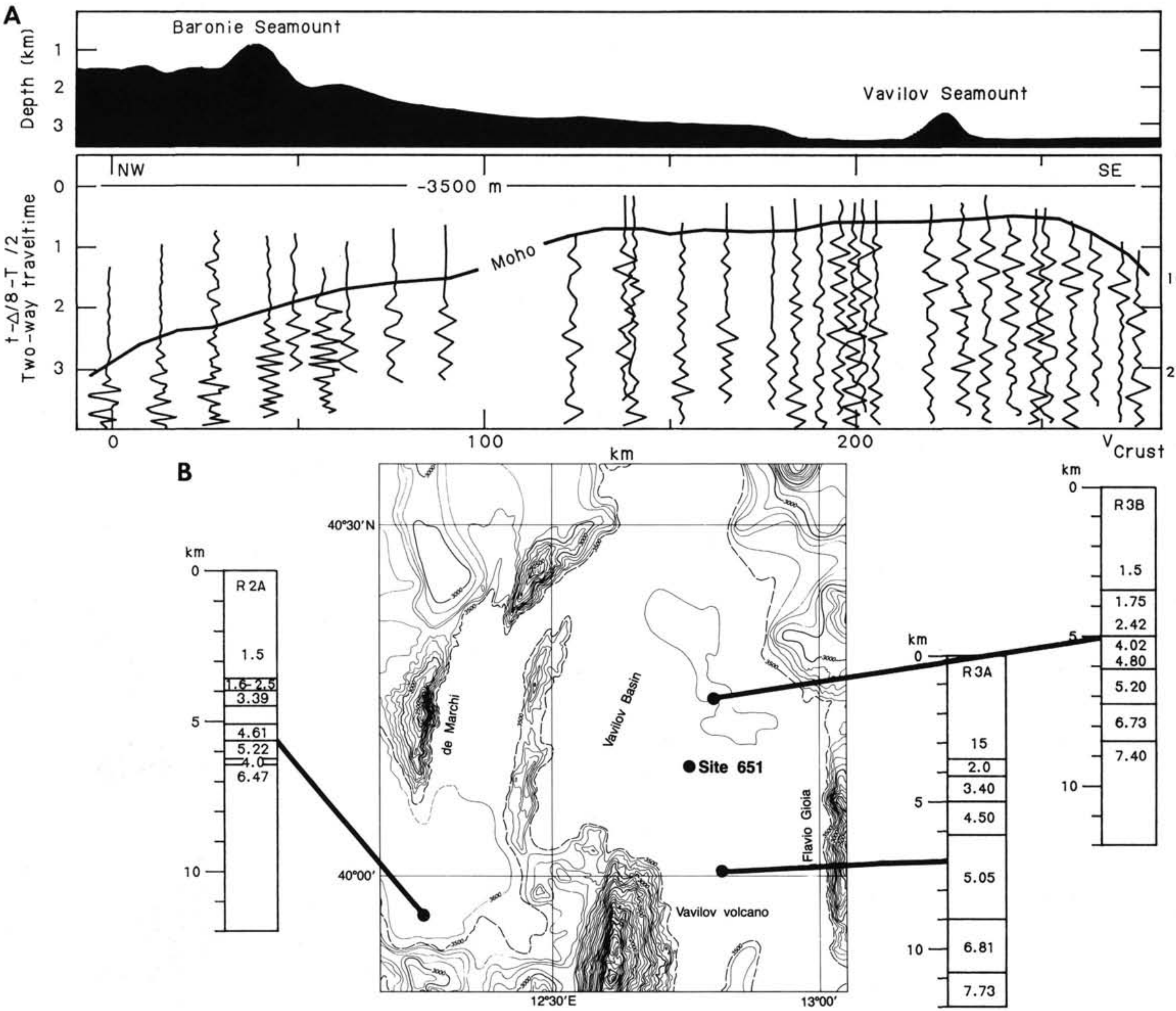

Figure 6. A. Profile of the depth to Moho, obtained from seismic refraction experiments using ocean-bottom seismometers as receivers (after Steinmetz et al., 1985). B. Sonobuoy refraction data (after Recq et al., 1984) from the Vavilov Basin. Both data sets support a mantle depth less than 10 km below sea level. Bathymetry in meters.

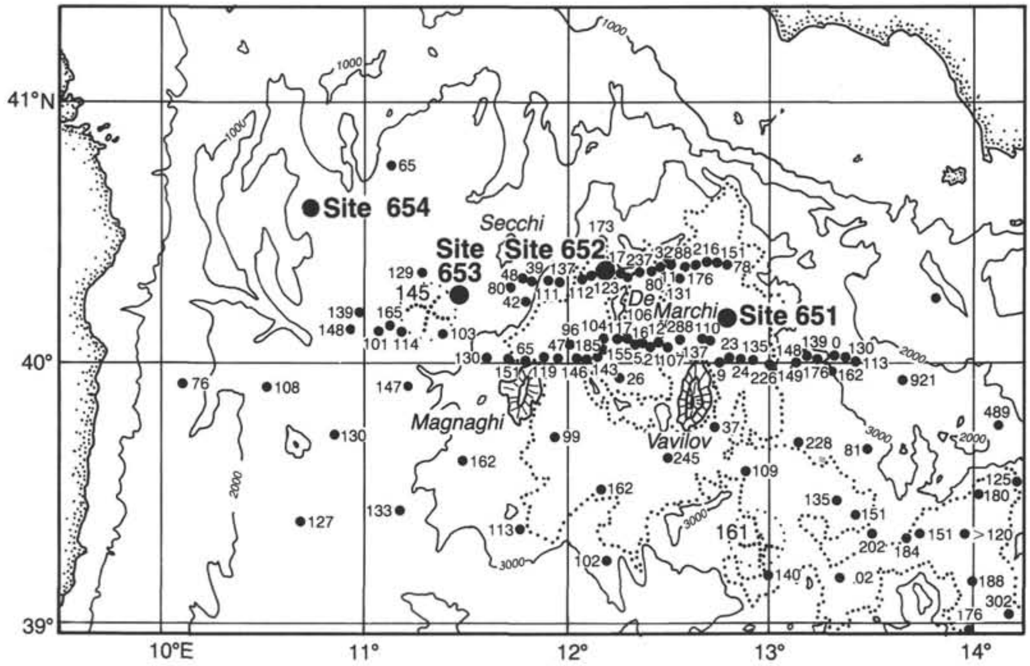

Figure 7. Heat flow distribution across central and western Tyrrhenian Basins (after Erickson, 1970; Della Vedova et al., 1984; Hutchison et al., 1985). Heat flow units are shown in m/Wm^2. Bathymetry in meters.

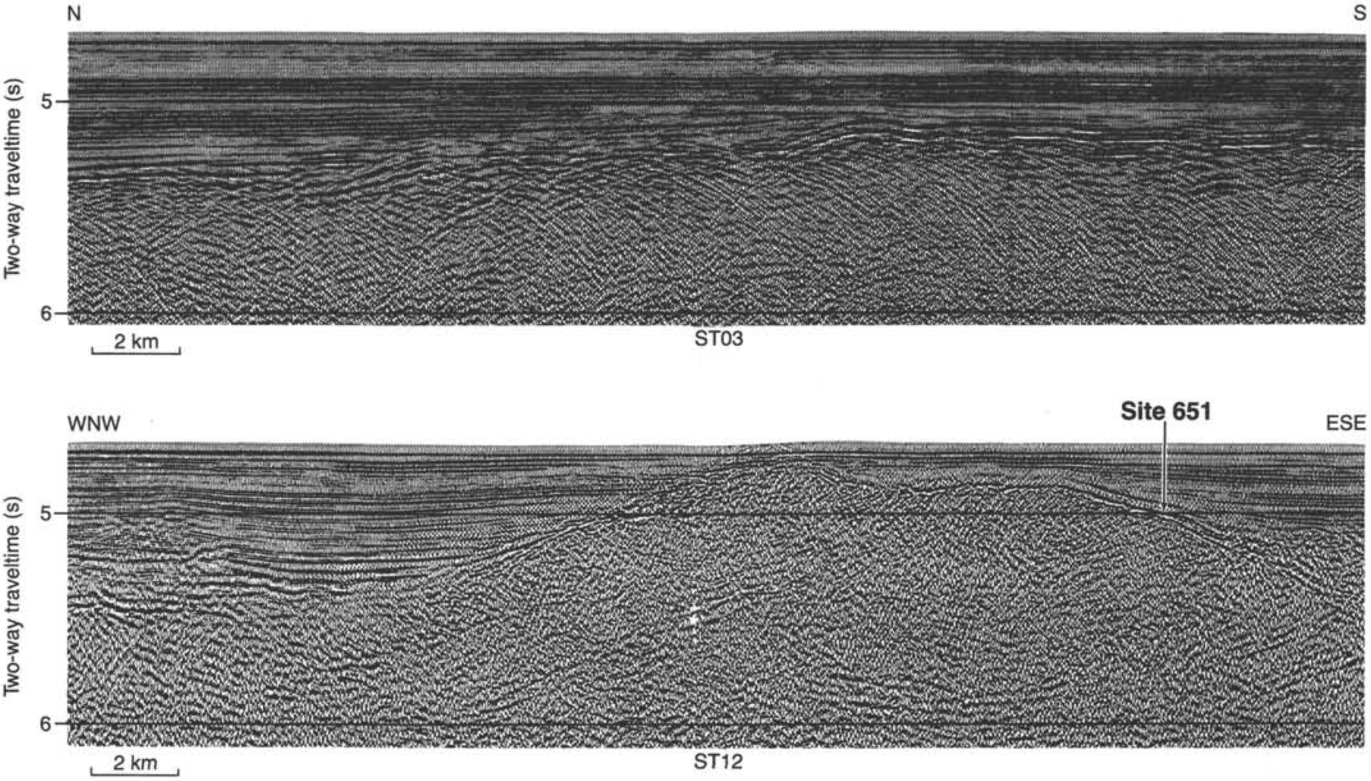

Figure 8. Multichannel seismic lines ST03 and ST12 across the Vavilov Basin; position of these profiles shown in Figure 10. Site 651 is located on ST12 on the eastern flank of a basement swell. This swell lies on trend with the long axis of Vavilov Seamount. Throughout Vavilov Basin, the acoustic basement is an irregular and diffracting surface.

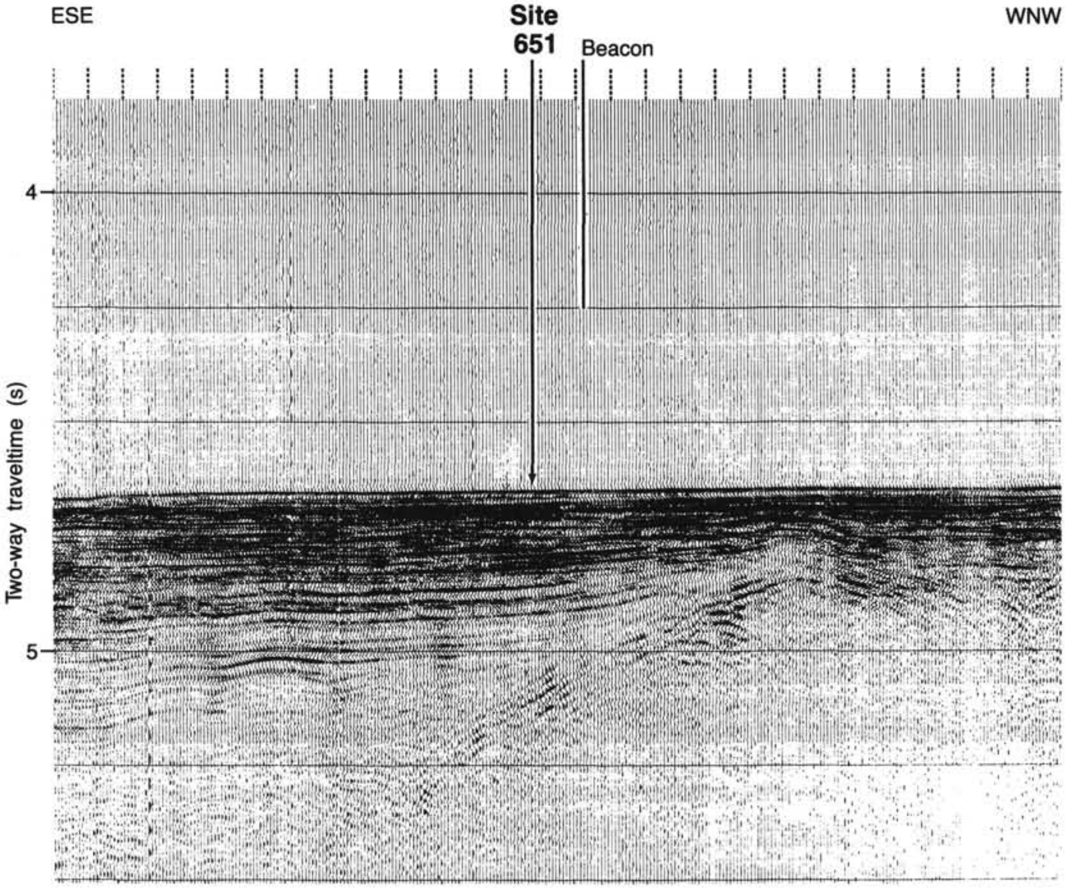

Figure 9. Single channel water-gun profile from the *Resolution* site survey for Site 651. The site was selected to allow documentation of the basin-filling sediments (particularly the unit which pinches against the basement slope), as well as penetration into basement.

the Loran/transit satellite position rather than the GPS position in light of the agreement between Loran and inferred ship speed; furthermore GPS was approaching the end of its night window, which is the time when it is most likely to be unreliable. In retrospect it seems that the GPS went astray between 0045 and 0100 (see Fig. 10), when an unexpected northward shift in GPS position occurred. At 0228, the ship changed course to 295° to come up to the desired track as given by Loran rather than GPS. This decision was confirmed when the fix from a 0232 transit satellite (at elevation 18°) was computed and was also found to agree with the Loran positions. By 0253 the ship was back on the desired track (according to Loran), and the course was changed back to 275°. At this point the ship was 4 nmi from the beacon drop point.

Shortly after 0300, the ship came over the edge of the target basement swell. The agreement between site survey profile ST12 and the *Resolution* water-gun profile was excellent, and the position of the pinch-out of the 3.7 km/s unit could be unambiguously recognized. The ship continued westward across the entire basement swell (about 5 nmi past the site) to confirm the agreement of the site survey and *Resolution* seismic profiles. At 0355 a Williamson turn was initiated to reverse course to 095°. The eastbound profile closely resembled the westbound profile. The decision of when to drop the beacon was made by comparison of the two profiles, with an allowance of 3 min for the 500-m offset between Loran antenna and seismic streamer plus 1 min to communicate and execute the command to drop it. The beacon was dropped at 0522, at Loran position 40°08.95′N, 12°45.01′E. The survey was continued a mile beyond the beacon position to confirm the geometry of the sub-bottom reflectors, and then seismic gear was retrieved at 0536.

The ship reversed course and returned toward the beacon to begin dynamic positioning at a position 400 m east (095°) of the beacon. The average of GPS and transit satellites received while drilling gave a final position for Hole 651A of 40°09.03′N; 12°45.39′E. The Loran position on site was 40°08.97′N; 12°45.23′E using the X and Z slaves. Loran master/slave time delays were as follows: X, 13239; Y, 35321; Z, 52536.

Coring

Hole 651A was spudded using a conventional rotary coring bottom-hole assembly at 1330 on January 11. Following the first four soft-mud cores, a successful heat flow measurement was taken at 30 mbsf. Cores 107-651A-5R through 107-651A-12R were taken in an unlithified turbidite-rich sequence; abundant coarse, loose, flowing sand continually threatened the stability of the hole. Mud was circulated before each core to clean out the hole. Heat flow runs planned for 80, 120, and 160 mbsf were cancelled because of the danger that the hole would collapse and the pipe would be irrevocably stuck.

Beginning with Core 107-651A-11R, discrete cemented layers within the coarse volcaniclastic sands and gravels were recovered. The number and thickness of the cemented layers increased downsection. By Core 107-651A-13R the worst of the flowing sands were past, and the hole appeared to be relatively stable. Rotary core barrel (RCB) coring continued without incident through the chalks, oozes, and finer grained turbidites (lithostratigraphic Unit II) of Cores 107-651A-15R through 651A-42R. Recovery

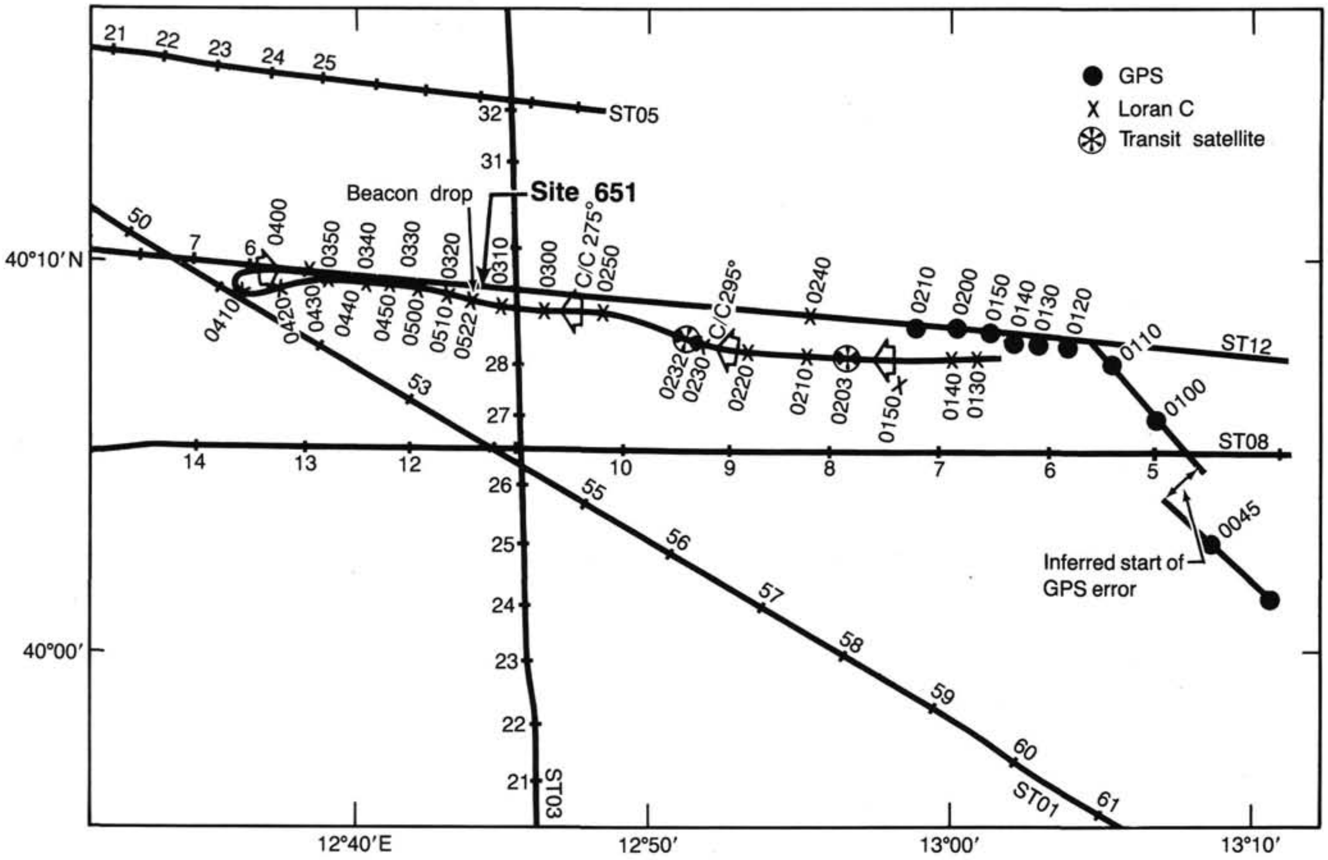

Figure 10. Navigation on approach to Site 651, along MCS line ST12. Positions indicated from GPS, transit satellite, and Loran C indicated as time of day. C/C = change of course. Positions along site survey lines indicated by shotpoint/100.

was highly variable (Fig. 11), from 2% to 100%, better in clay-rich units and poorer in sandy layers. Cores 107-651A-42R through 651A-56R penetrated a wide variety of hard rocks including dolomite breccia, basalt, gabbro, and peridotite. Most of the recovered rock fragments were smaller in all dimensions than the core trimming diameter of the bit. This has been taken as evidence that they were pervasively fractured and perhaps transported by geological processes; however, coring disturbance has not been conclusively ruled out. Core 107-651A-55R included a 60-cm section of sand, graded from very coarse sand at its base to medium sand at its top. A majority of the experienced drilling personnel felt that this sand was made of cuttings forced up into the core barrel by "back pressure," i.e., the weight of the mud/water mixture in the annulus of the borehole outside the pipe. A minority opinion held that the occurrence of large rock fragments downcore from the sandy layer ruled out the back pressure hypothesis. Everyone agreed that if loose sand of this sort were present in the section, the drilling parameters chosen to penetrate the hard rock would result in minimal recovery of such sand; thus if the sand was *in situ*, the 60 cm recovered is probably representative of a thicker unit.

Cores 107-651A-57R and 651A-58R recovered peridotite. Unlike the overlying hard rocks, the peridotite was recovered as cylinders rather than as fist-sized fragments. This is taken as evidence that the peridotite was undisturbed and *in situ*, whereas the overlying hard rocks need not have been.

During Cores 107-651A-54R through 651A-58R, there were indications that the hole condition was deteriorating. When the pipe was raised during core retrieval operations, the bit tended to "ratchet" up the hole as though it were catching on bumps and ledges. Some fill was detected, and once again mud was circulated between cores to try to clear the hole. After Core 107-651A-58R was recovered, the pipe was found to be stuck and required working and circulating for almost 2 hr to come completely free. At this point, since further penetration seemed risky and the objectives of the site had been met, coring was terminated. The coring summary for Hole 651A appears in Table 1.

Logging

The bit was released using a hydraulic bit release, and the now-open-ended pipe was raised to 119 mbsf (equivalent to Core 107-651A-13R) to begin logging; this depth was chosen to be below the loose, flowing sand which had caused hole instability problems while coring, and to keep the majority of the bottom hole assembly buried for safety of the pipe. The first logging run consisted of the dual induction log (DIL), natural gamma ray (GR), long spacing sonic (LSS), and caliper. As this set of tools was being lowered through the pipe, the pipe was found to be stuck again. While the logging tools are in the pipe it is not possible to rotate the pipe; the driller can only pull up and circulate fluid to try to break loose. In this case, an overpull of 100,000 lb was required to free the pipe. The DIL-LSS-GR combination was lowered downhole to a depth of 339 mbsf (equivalent to Core 107-651A-35R), where an impassable bridge or ledge was encountered. Good data were collected both going down and coming up.

The second logging run consisted of the litho-density tool (LDT), dual porosity compensated neutron tool (CNT), and

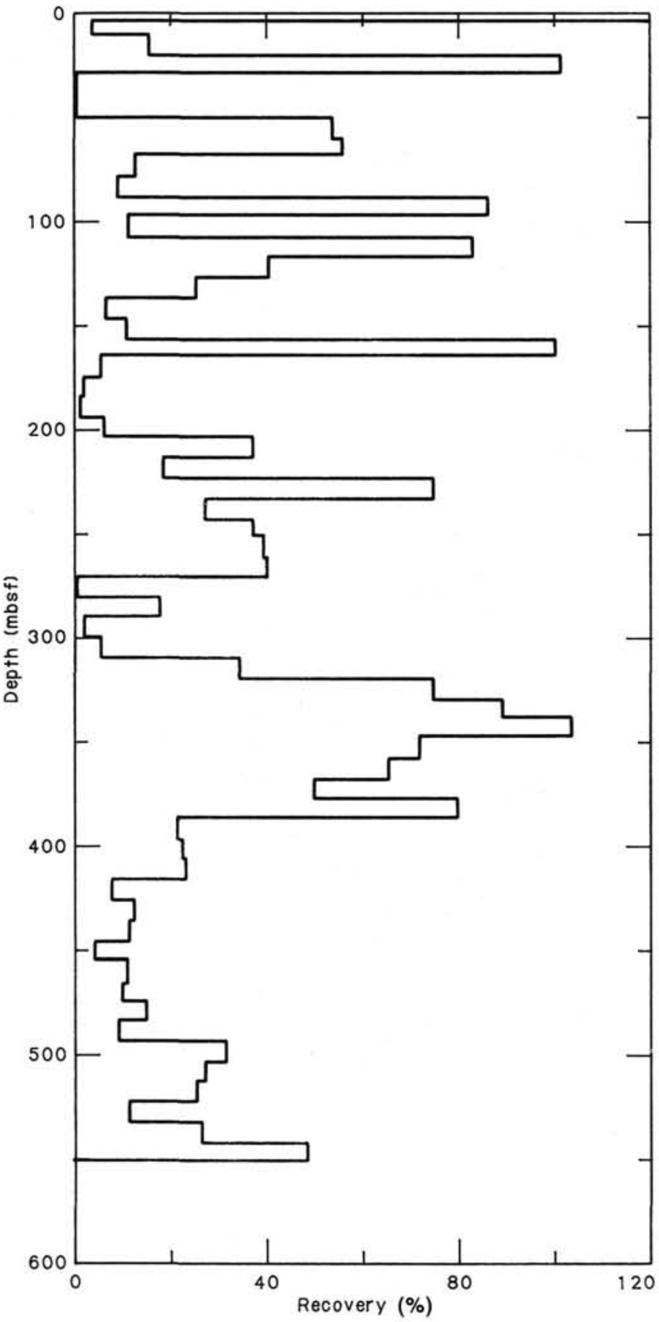

Figure 11. Percentage recovery from RCB coring at Site 651.

natural gamma ray spectrometry tool (NGT). This suite of tools was run down to 273 mbsf where it, in turn, encountered an impassable obstruction (66 m shallower than the first run's obstruction). LDT-CNT-NGT data were successfully collected from this depth up to the bottom of the pipe.

The pipe was then run down into the hole in an attempt to clear out the obstructions to allow logging of the lower half of the hole, particularly the basement. At a depth of 271 mbsf the end of the pipe tagged a firm bridge and became stuck. The pipe was pulled and worked continuously with as much as 155,000 lb overpull, but refused to come free. Finally, the top drive (which is normally not used during logging) was attached to the pipe so the pipe could be rotated. The pipe was finally freed with torque and overpull.

Table 1. Coring summary table for Site 651.

Core no.	Date (Jan. 1986)	Time (hr)	Sub-bottom depths (m)	Length cored (m)	Length recovered (m)	Recovery (%)
1R	11	1430	0.0–3.7	3.7	9.5	256.2
2R	11	1600	3.7–10.3	6.6	0.2	3.5
3R	11	1745	10.3–19.8	9.5	1.5	15.9
4R	11	1930	19.8–29.4	9.6	9.8	101.7
5R	11	2300	29.4–39.8	10.4	0.0	0.0
6R	11	0100	39.8–49.5	9.7	0.0	0.0
7R	11	0245	49.5–59.2	9.7	5.2	53.8
8R	12	0600	59.2–68.8	9.6	5.4	56.2
9R	12	0830	68.8–78.3	9.5	1.2	13.0
10R	12	1015	78.3–88.0	9.7	0.9	9.1
11R	12	1215	88.0–97.4	9.4	8.2	86.9
12R	12	1430	97.4–107.0	9.6	1.1	11.5
13R	12	1645	107.0–116.7	9.7	8.1	83.3
14R	12	1845	116.7–126.3	9.6	3.9	40.7
15R	12	2100	126.3–136.0	9.7	2.5	25.5
16R	13	0000	136.0–145.7	9.7	0.6	6.4
17R	13	0145	145.7–154.9	9.2	1.0	11.2
18R	13	0330	154.9–164.6	9.7	9.8	100.7
19R	13	0530	164.6–174.2	9.6	0.6	6.1
20R	13	0715	174.2–183.9	9.7	0.2	1.9
21R	13	0845	183.9–193.5	9.6	0.1	1.3
22R	13	1015	193.5–203.2	9.7	0.6	6.6
23R	13	1200	203.2–212.9	9.7	3.7	37.7
24R	13	1330	212.9–222.6	9.7	1.8	19.0
25R	13	1445	222.6–232.3	9.7	7.4	75.8
26R	13	1630	232.3–242.0	9.7	2.6	27.2
27R	13	1745	242.0–251.6	9.6	3.6	37.4
28R	13	1930	251.6–261.2	9.6	3.8	39.3
29R	13	2045	261.2–270.8	9.6	3.9	40.1
30R	13	2215	270.8–280.4	9.6	0.1	0.5
31R	13	2330	280.4–290.0	9.6	1.7	18.0
32R	14	0115	290.0–299.6	9.6	0.2	2.1
33R	14	0300	299.6–309.3	9.7	0.5	5.6
34R	14	0500	309.3–318.9	9.6	3.3	34.5
35R	14	0630	318.9–328.6	9.7	7.3	75.5
36R	14	0815	328.6–338.2	9.6	8.6	90.0
37R	14	1000	338.2–347.8	9.6	10.0	103.7
38R	14	1215	347.8–357.5	9.7	7.0	72.2
39R	14	1430	357.5–367.2	9.7	6.4	65.5
40R	14	1615	367.2–376.8	9.6	4.8	50.2
41R	14	1800	376.8–386.5	9.7	7.8	80.0
42R	14	2030	386.5–396.2	9.7	2.1	22.0
43R	15	2230	396.2–405.9	9.7	2.2	22.5
44R	15	0045	405.9–415.6	9.7	2.3	23.3
45R	15	0315	415.6–425.3	9.7	0.8	7.7
46R	15	0615	425.3–435.0	9.7	1.2	12.3
47R	15	0845	435.0–444.7	9.7	1.1	11.2
48R	15	1115	444.7–454.3	9.6	0.4	4.4
49R	15	1330	454.3–464.0	9.7	1.1	11.1
50R	15	1515	464.0–473.6	9.6	1.0	9.9
51R	15	1730	473.6–483.3	9.7	1.5	15.0
52R	15	2000	483.3–492.9	9.6	0.9	8.9
53R	15	2230	492.9–502.6	9.7	3.1	32.0
54R	16	0200	502.6–512.2	9.6	2.6	27.5
55R	16	0530	512.2–521.9	9.7	2.4	25.1
56R	16	1000	521.9–531.5	9.6	1.1	11.5
57R	16	1400	531.5–541.2	9.7	2.6	26.5
58R	16	1730	541.2–550.9	9.7	4.7	48.7

The hole was filled with weighted mud and the pipe was retrieved, thus ending Site 651. The vessel departed for Site 652 at 2300 on 17 January.

LITHOSTRATIGRAPHY

Introduction

At Site 651 the sedimentary succession above the igneous basement was subdivided into two units as follows (Fig. 3):

Unit I: Cores 107-651A-1R to 651A-15R (inclusive); depth: 0–136.0 mbsf; thickness: 136.0 m; age: late Pleistocene (NN19).

Unit II: Cores 107-651A-16R to 107-651A-42R; depth: 136.0-387.6 mbsf; thickness: 251.6 m; age: Pleistocene and late Pliocene (NN18/NN20).

Unit I

Unit I (0-136 mbsf, Cores 107-651A-1R through 651A-15R) consists mostly of volcanogenic sediments interbedded with volumetrically subordinate (<15%) marly nannofossil-rich mud. Overall, beneath superficial muds, the succession in Unit I is dominated by pumiceous sand, gravel, and cemented breccia that decrease in average grain-size and relative abundance toward the base, giving way to finer-grained more calcareous facies in Unit II. The recovery in Cores 107-651A-2R, 651A-3R, 651A-5R, 651A-6R, 651A-9R, 651A-10R, and 651A-12R was minimal, or nonexistent. Details of the Unit I succession are as follows:

In downward succession, the first lithology encountered is homogeneous soupy mud with minor graded volcaniclastic sands (<2% carbonate) (e.g., Sample 107-651A-1R-7, 5-40 cm) extending from 0 to 10.3 mbsf (Cores 107-651A-1R, 651A-2R). From 10.3 to 25.1 mbsf (107-651A-3R and 107-651A-4R, Sections 1-4, inclusive), the minor recovery consisted of marly nannofossil mud (<25% $CaCO_3$), rich in volcanic glass (up to 15% glass) in smear slides. At 25.1 mbsf (107-651A-4R-6) there is the first appearance of homogeneous sand that is largely volcaniclastic, but also siliciclastic in composition. There was no recovery at all from 29.4 to 49.23 mbsf (107-651A-5R and 651A-6R). Below this (29.4-49.2 mbsf; 107-651A-5R and 651A-6R) the recovery comprised mostly gravel-sized pumice and volcanic lapilli, showing large-scale (as thick as 5.2 m) inverse graded units (49.5-54.7 mbsf; Core 107-651A-7R), suggestive of redeposition by gravity flow (e.g., mass-flow and/or turbidity currents). A similar pumiceous facies present from 59.2 to 68.8 mbsf (Core 107-651A-8R) includes several 10-30-cm-thick zones, of which one (Section 107-651A-8R-1) is normally graded and the other two (Samples 107-651A-8R-1, 60-73 cm, and 651A-8R-1, 92-124 cm) are reverse graded. In this core, pumice, sand-size vitric fragments, and lapilli tuff are interbedded with three 10-30-cm-thick horizons of marly nannofossil mud and calcareous clay. The lack of sedimentary structures in the unconsolidated coarse-grained clastic sediments at this level may well reflect drilling disturbances.

From 69 mbsf (107-651A-9R) downward, the clastic sediments are slightly less coarse-grained and are interbedded with fine-grained sediments that are more clay rich. From 68.8 to 88.0 mbsf the recovery is dominated by weakly laminated to homogeneous mudstone (about 25% $CaCO_3$), sandy mudstone (about 15% $CaCO_3$), and sand (about 3% $CaCO_3$) in 5-50-cm-thick units. These sediments are interpreted as turbidites mainly on the basis of graded bedding and laminations. From 88.8 to 97.4 mbsf (107-651A-11R) there is a return to nearly homogeneous unconsolidated sand and gravel.

The composition of the siliciclastic sediments present from 97.4 to 107.0 mbsf (107-651A-12R) indicates a mainly extrusive igneous provenance with minor contribution from metamorphic rocks (schist). Below this, from 107 to 125.7 mbsf (107-651A-13R), volcaniclastic sands and breccias consist mostly of pumice pebbles that are rounded to subrounded with clasts as much as 1 cm in diameter (Fig. 12). This sediment is more lithified, with a common, albeit patchy, cement composed of opaline silica. This cement may be related to the dissolution of volcanic glass and growth of zeolites during diagenesis. Intercalated intervals that are less consolidated may include material washed down from above. The lowest levels of Unit I, located at 113.0-136.0 mbsf (107-651A-13R-5 through 651A-15R), again comprise poorly consolidated volcanic lapilli, volcanic breccia, and volcaniclastic sand, together with intercalations of calcareous clay as thick as 80 cm (107-651A-14R-3, 1-83 cm). A marked homogeneity of grain size could indicate the destruction of primary sedimentary structures by drilling.

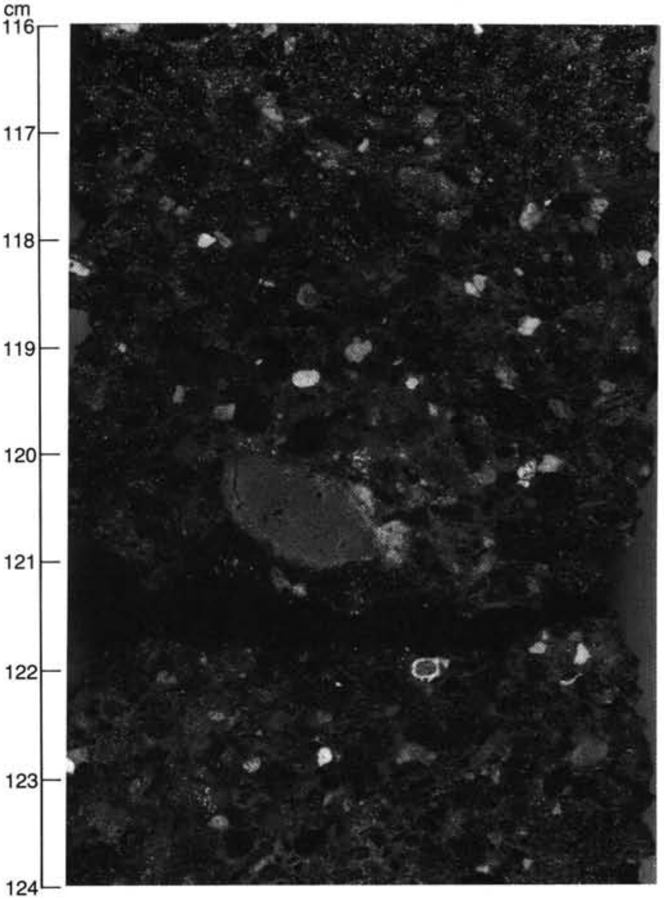

Figure 12. Well-cemented volcaniclastic rudite. The clasts are rounded to subangular and are composed mostly of pumice. The white cement is opaline silica that is thought to have formed by the early diagenetic dissolution of volcanic glass (107-651A-13R-2, 116-124 cm).

Discussion and Interpretation

Paleontological data from nannofossils and foraminifers, as well as paleomagnetic reversal chronology (see "Paleomagnetism" section, this chapter), indicate that Unit I accumulated rapidly at greater than 72 cm/1000 yr. The nonrecovered intervals may comprise largely unconsolidated coarse-grained volcanogenic sediments (e.g., sand and gravel). Below the superficial soupy muds (below 10.3 mbsf), the succession is dominated by volcaniclastic sands, gravels, and breccias, together with volcanic ashes and lapilli tuffs of mostly pyroclastic origin that were reworked and deposited by mass flow and turbidity current mechanisms. The radioactivity logs indicate that volcaniclastic sediment was much more extensive than the minimal recovery would suggest (see "Downhole Measurements" section, this chapter). The provenance was mainly extrusive igneous rocks, but also sedimentary rocks and possibly metamorphic rocks. Four factors suggest that provenance was mainly located in the Italian mainland to the east and to the northeast: (1) present day adjacent submarine canyons mainly originate to the east and northeast; (2) schists occur in the Italian mainland, but not in the Eolian islands to the south, for example; (3) K-feldspar phenocrysts are common, similar to the Campanian province; and (4) the radioactive nature (U, Th) of the volcaniclastic sediment mirrors that of the Roman province (see "Downhole Measurements" section, this chapter). Numerous occurrences of shelf-derived microfauna (foraminifers, ostracodes, bryozoa) suggest that much of the clastic sediment was reworked across the shelf and through submarine canyons before it reached the present location. Clastic accumulation was, on occasion, slow enough to allow the deposition of calcareous clays and nannofossil mud that probably reflect *in-situ* hemipelagic sedimentation.

Unit II

Unit II (Cores 107-651A-16R to 651A-42R) consists mostly of marly nannofossil chalk, volcanic ash, calcareous siltstone, calcareous mudstone, nannofossil ooze, calcareous claystone, dolomitic claystone, metalliferous claystone, dolostone, and Fe-Mn-enriched dolostone. Unit II is differentiated from Unit I on the basis of finer grain size, increased clay, increased calcium carbonate content, and a greatly reduced volcaniclastic component within the sediments recovered.

Within Unit II, a marked transition in facies is noted downsection. The upper levels (136–309.3 mbsf, Cores 107-651A-16R to 651A-34R) are lithologically heterogeneous, comprising interbedded volcaniclastic siltstones and sandstones, claystones (about 5.6% $CaCO_3$), calcareous mudstones (20%–25% $CaCO_3$), and rare nannofossil chalk (50%–60% $CaCO_3$). Toward the base of the interval (270.8–309.3 mbsf; Cores 107-651A-30R to 651A-34R) there was minimal recovery. This could reflect the presence of a major unconsolidated volcaniclastic unit, as suggested by the radioactivity and sonic logs (see "Downhole Measurements" section, this chapter). Then, below this (309.3–347.8 mbsf) the succession is much more uniform, dominated by nannofossil chalk (30%–60% $CaCO_3$) with very subordinate claystone, siltstone, and volcanic ash, which, together amount to $< 10\%$ of the succession. In view of the extremely variable recovery, all of the above lithologies are grouped into a single subunit of Unit II (Subunit IIa). Below this (347.8–387.6 mbsf; Cores 107-651A-38R to 651A-42R), there is the appearance of abundant dolomite and a change from subdued to brilliant colors, which together constitute the criteria for recognition of Subunit IIb.

Subunit IIa, from 136.0 mbsf (107-651A-16R) to 347.8 mbsf (107-651A-37R): thickness: 211.8 m.

The interval from 136.0 to 145.7 mbsf is transitional between Units I and II and comprises marly chalks containing volcanic ash. Beneath this, from 145.7 to 174.2 mbsf (Cores 107-651A-17R to 651A-19R, inclusive), the succession becomes more indurated and is dominated by homogeneous marly nannofossil chalk with scattered laminated siliciclastic silts (e.g., Sample 107-651A-19R-1, 1–50 cm). Between 183.9 and 193.5 mbsf (107-651A-21R) 11 cm of reworked vitric tuff was recovered from the core catcher of an otherwise empty core.

From 193.5 to 203.2 mbsf (Cores 107-651A-22R to 651A-25R, inclusive) claystone, mudstone, siltstone, and minor sand and gravel are present. Exceptionally, in 107-651A-23R-1, 0–20 cm, there is a very well-cemented coarse-grained sandstone containing moderately well-rounded grains as much as 5 mm in diameter. Below, the interval 203.4–222.6 mbsf in this core (and in Core 107-651A-24R) is dominated by marly nannofossil chalk rich in planktonic foraminiferal tests (Fig. 13). This sediment type is interbedded with numerous thin (< 5 cm) grayish and greenish calcareous siltstones that show normal grading, parallel lamination, cross-lamination, and convolute-lamination. These features are most numerous from 222.60 to 242.0 mbsf (Cores 107-651A-25R and 651A-26R). In Sample 107-651A-25R-3, 52–54 cm, there is a thin dark-colored, possibly sapropelic, interval that was not analyzed for organic carbon content. In the interval 242.0–251.6 mbsf (Core 107-651A-27R) three thin (< 3 cm) siltstones were noted that contain altered volcanic glass and zeolites. The interval from 251.6 to 309.3 mbsf (Cores 107-651A-28R to 651A-33R, inclusive) comprises extensively bioturbated nannofossil chalk and marly nannofossil chalk with very subordinate graded calcareous siltstones and fine-grained calcareous sandstones of both siliciclastic and volcaniclastic composition. Slumping and microfaulting not considered to be an artifact of drilling were observed in Sample 107-651A-29R-2, 95–105 cm, and in the core catcher.

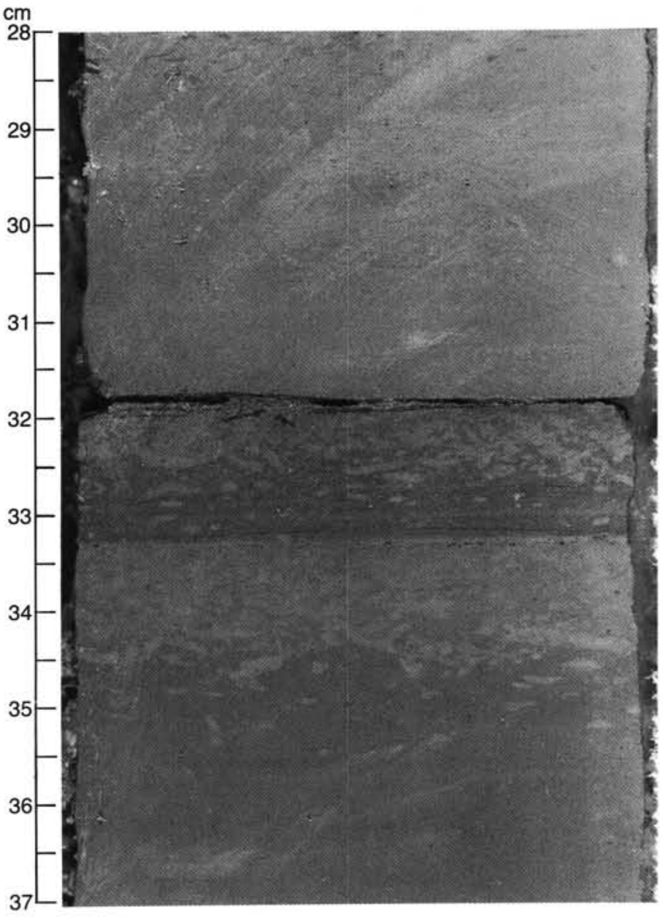

Figure 13. The photograph illustrates the typical background hemipelagic sediments of Subunit IIa, burrowed marly nannofossil chalk. The interval from 32 to 33.5 cm is an example of a typical volcaniclastic silt turbidite, showing basal scour, grading, and parallel lamination; in this case it is quite strongly burrowed.

The recovery of Unit IIa from 309.3 to 347.8 mbsf (Cores 107-651A-34R to 651A-38R) was much better than in the interval above. This interval becomes progressively more clay-rich downsection, but otherwise is again volumetrically dominated by planktonic foraminiferal chalks that are burrowed (30%–61% $CaCO_3$), with thin (< 5 cm) interbedded calcareous siltstones and mudstones. The radioactivity logs (U, Th) suggest that abundant volcaniclastic material disappears below 315 mbsf in Core 651A-34R (see "Downhole Measurements" section, this chapter). Sapropelic horizons occur at 329.14 mbsf (107-651A-36R-1, 54–56 cm; 4.16% organic carbon), 318.96 mbsf (Sample 107-651A-35R-1, 6–8 cm; 2.88% organic carbon), and 345.60 mbsf (107-651A-37R-5, 140–142 cm; 2.94% organic carbon) (see "Geochemistry" section, this chapter). The sapropelic layer in Section 107-651A-35R-1 was tentatively correlated by the shipboard paleontologists with similar sapropelic layers at Site 650 within the same time interval (107-650A-51X, 650A-52X) near the base of the Jaramillo event (see "Biostratigraphy" and "Paleomagnetism" sections, this chapter). Similarly, the sapropel at Site 651 in Section 107-651A-37R-2 may correspond to the sapropel in Core 107-650A-64X. Episodes of basin-wide sapropel genesis thus appear to occur in the Tyrrhenian Sea during late Pliocene and early Pleistocene time.

Subunit IIb: 347.8 mbsf (107-651A-38R) to the contact with the igneous basement near 387.6 mbsf (107-651A-42R); thickness: 39.8 m.

Subunit IIb differs from Subunit IIa on the basis of, first, the appearance of abundant dolomite, commonly as sharp-sided euhedral rhombohedra (2–20 μm in size) and, second, a downward transition from subdued to very bright colors (see below).

The upper level of Subunit IIb from 347.6 to 378.5 mbsf (Core 107-651A-38R) comprises dolomitic claystone, dolostone, apparently metalliferous mud, and minor volcanic ash. The dolomitic sediments fizz only weakly in 5% HCl. Volcanic ash was noted at 357.9 mbsf in Sample 107-651A-38R-1, 43–45 cm, and shows grading, parallel-, and microcross-lamination. A notable feature is the presence of a subvertical, 10 cm long × 2.5 cm wide water-escape neptunian dike located in Sample 107-651A-38R-1, 30–42 cm (Fig. 14); this is interpreted as a water-escape structure. In this core the apparent dip of the lamination reaches a maximum of 45°. Between Sections 107-651A-38R-2 and 107-651A-39R, CC the dip varies from 0° to 45°; then in Section 107-651A-40R-1 the angle of lamination returns to subhorizontal. The angle of drill-string deviation does not exceed 2.3°. The majority view of the shipboard sedimentologists is that the dip is real, reflecting tilting of the basement after deposition in late Pliocene time and/or deposition of the flank of a structural high. A minority view is that the apparent dip is an artifact of drilling, bearing in mind the locally variable dip and the drilling disturbance (e.g., Sample 107-651A-12R-4, 2 cm).

Below Core 107-651A-38R in the interval from 357.5 to 387.6 mbsf (Cores 107-651A-39R to 651A-42R) the sediments recovered are dominated by brightly colored dolostones that are probably enriched in Fe, Mn, and trace metals. Bioturbation is very abundant, ranging from weak to locally intense. An indistinct primary current lamination is generally visible but in some cases lamination is a diagenetic effect. The colors of the metal-enriched sediments vary intergradationally between various hues of orange, greenish, grays, yellowish, reddish, brownish to nearly black (see the barrel sheets for a complete list of colors). Black manganese oxide segregations are present in burrow fills and disseminated dendritic patterns ("dendrites") as much as several millimeters in diameter. In 107-651A-40R-1, 63–65 cm, there is a thin interval of black crystalline material that may be manganese oxide (?pyrolusite). In the same core there is evidence of instability during sedimentation, observable as mudflow and resedimented soft pebbles (107-651A-40R-3, 60–66 cm). Just above the basalt contact a feldspathized volcanic ash horizon within dolostone was noted (389.9 mbsf, Sample 107-651A-41R-3, 47 cm). The precise lava/sediment contact was not recovered. However, large pieces (as much as 4 cm in diameter) of pink dolostone were recovered from just above the first occurrence of basalt (387.6 mbsf; Sample 107-651A-42R-1, 105 cm). Also, as described further below, the underlying basalts and basalt-derived breccias include indurated dolomitic sediments similar to those above the basalt; poorly preserved planktonic foraminifers are present within basalt-derived breccia at 465.1 mbsf, 78.6 m below the first occurrence of basalt downhole (Core 107-651A-50R; see "Biostratigraphy" and "Igneous Petrology" sections, this chapter).

Discussion and Interpretation

Subunit IIa, of late Pliocene age, is dominated by hemipelagic nannofossil chalk, calcareous mudstone, and calcareous

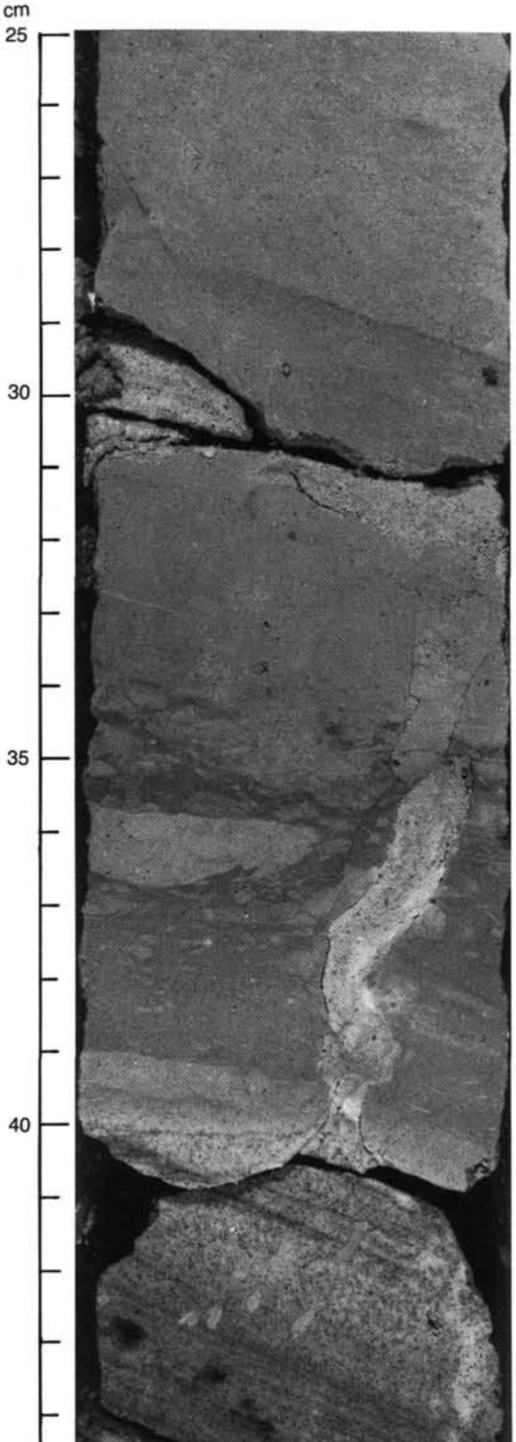

Figure 14. Neptunian dike. This is a sedimentary dike formed by water-escape during early diagenesis. In the lower end of the photographed section (at 40–45 cm), volcanic ash was deposited, probably as a turbidite, and was then depositionally overlain by extensively burrowed nannofossil ooze. Possibly due to tectonic instability (e.g., earthquakes), water was expelled from the sediment beneath and was injected upward into the nannofossil oozes as the neptunian dike. Note also the markedly inclined bedding; this is thought to be a primary structure rather than an artifact of drilling (see text for discussion), but may well have resulted from post-depositional tectonic tilt (348.05 mbsf; Sample 107-651A-38R-1, 25–45 cm).

claystone with the addition of minor, mostly volcaniclastic siltstones and mudstones. The volcaniclastic sediments are interpreted as fine-grained turbidites, probably derived from source areas on the Italian mainland, such as the Roman and Campanian volcanic provinces. Toward the igneous basement, there is evidence of minor tectonic instability, evidenced by slumping, small-scale reverse faulting (350.46 mbsf; Section 107-651A-38R-3, 10–25 cm), and dewatering structure (a neptunian dike).

It is considered that throughout the time of formation of the igneous basement (?early Pliocene, see "Biostratigraphy" section, this chapter) and during the accumulation of both Subunits IIa and IIb, background carbonate sediment became admixed with the igneous basement rocks (see "Igneous Petrology" section, this chapter). Later, during diagenesis, the dolomite formed within the basal carbonate sediments, possibly related to low-temperature hydrothermal alteration of the igneous basement. Additional data are needed to decide if the apparent enrichment in Fe and Mn of the basal sediments of Subunit IIb is related to the alteration of basalt, or, alternatively, if the metal-enrichment is connected with subseafloor hydrothermal activity during the original basaltic extrusion and/or doleritic intrusions.

SEDIMENT ACCUMULATION RATES

The sediment accumulation rate curve (Fig. 15) was constructed using results obtained from paleomagnetic, planktonic foraminifers, and nannoplankton studies; no correction for compaction has been applied. Within the upper part of the Pleistocene (NN21) the sediment accumulation rate of 72 cm/1000 yr is rather high; this is attributed to the large amount of coarse-grained redeposited sediment located from Core 107-651A-4R to Core 651A-16R (29–136 mbsf). Below this, sediment accumulation rate decreases to 27 cm/1000 yr down to the base of the Brunhes magnetic event at 0.73 m.y.b.p. in Section 107-651A-34R-1 (about 310 mbsf). This decrease in rate corresponds to a lithological change from predominantly coarse-grained turbiditic sediments to finer-grained calcareous and tuffaceous mud and sand. Sediment accumulation rate changes sharply to 3.3 cm/1000 yr within the time interval 0.73 to 1.67 m.y.b.p. (base Brunhes–Pliocene/Pleistocene boundary). The sequence in this interval consists mainly of calcareous mud and ooze, with minor intercalations of tuffaceous mud and clay. This distinct change in sediment accumulation rate might be linked to the onset of the glacial Pleistocene at about 0.8 m.y.b.p. and/or to a high volcanic activity. Applying the same sediment accumulation rate inferred for the upper Pliocene down to the top of the basalt at 387 mbsf, suggests an age of about 3.6 m.y.b.p. for the top of the basalts.

Evidence for Sedimentary Instability in Hole 651A

The entire section shows indications of sedimentary instability that are particularly well-expressed by the frequency of turbidites (e.g., about 70 turbidites in 7.40 m recovered in Core 107-651A-22R between 222.6 and 232.3 mbsf). Short periods without significant turbidites characterize the intervals: 0–29.4 mbsf (Cores 107-651A-1R to 651A-5R), 49.5–68.8 mbsf (Cores 107-651A-7R to 651A-9R), 154.9–174.2 mbsf (Cores 107-651A-18R to 651A-20R), 203.2–212.9 mbsf (part of Core 107-651A-23R), and 280.4–290.0 mbsf (Core 107-651A-31R).

Microslumps occur between 222.6 and 232.3 mbsf (Core 107-651A-25R) and below 261.2 mbsf in Core 107-651A-29R (261.2–270.8 mbsf), Core 107-651A-31R (280.4–290.0 mbsf), and 107-651A-34R (309.3–318.9 mbsf). Microfaults occur downsection from 309.3 mbsf, which corresponds to the limit between sedimentary Subunits IIa and IIb; microfaults are present in Cores 107-651A-34R (309.3–318.9 mbsf), 107-651A-36R (328.6–338.2 mbsf), and 107-651A-38R (347.8–357.5 mbsf) (Fig. 16). Between 347.8 and 376.8 mbsf (Cores 107-651A-38R through 651A-40R) pronounced dip is indicated by inclined burrowing and layering of the sediments (Fig. 17). The dip is typically 30°, reaching 55° locally (Core section 107-651A-38R-3). As discussed above, we

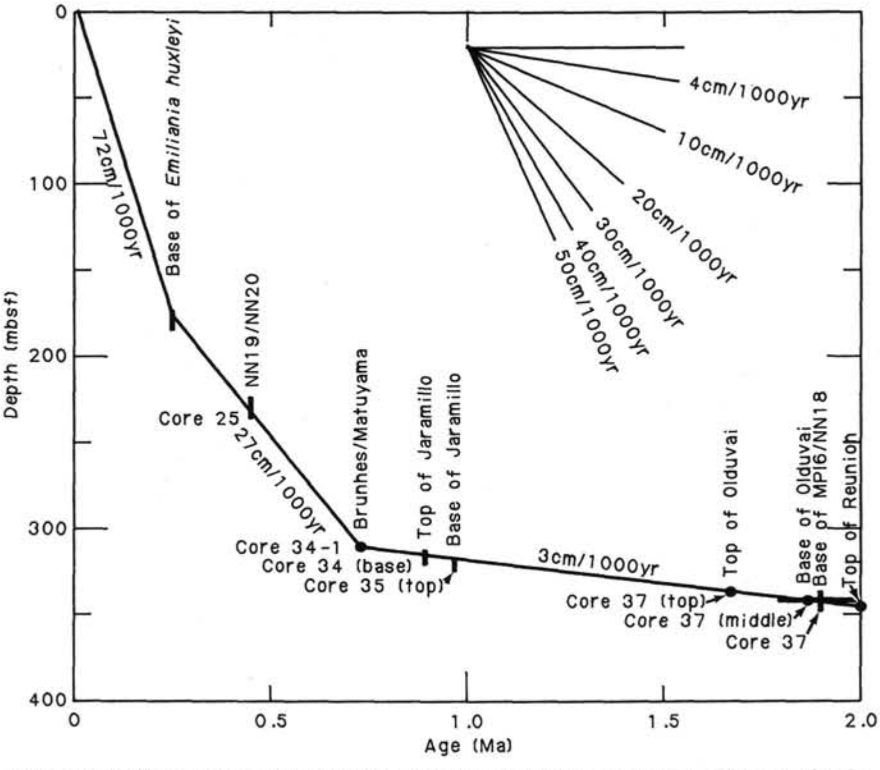

Figure 15. Sediment accumulation rate curve not corrected for compaction. The upsection increase in sedimentation rate is mainly attributed to increased volcaniclastic sediment input (see text).

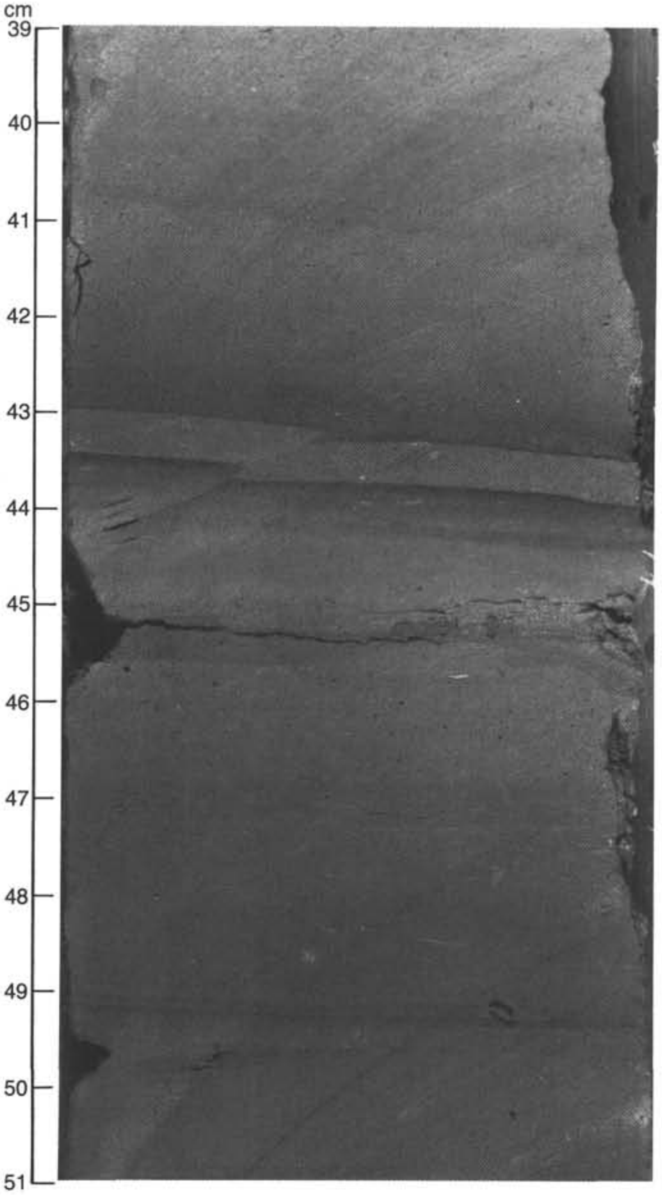

Figure 16. Photograph showing an example of a microfault, Sample 107-651A-36R-2, 43–44 cm. Note that the laminations above and below the fault are not disturbed.

considered the possibility that this dip could be related to a non-vertical borehole, and/or to drilling disturbance. An inclination measurement performed within the hole indicated a vertical deviation of no more than 2.3°, and thus drill-string deviation is not an important factor. We instead prefer to relate the apparent dip to tectonic tilting of the igneous basement that took place after accumulation of the basal part of the overlying sediment succession. It is interesting to note that the neptunian dike occurs in this interval (Fig. 14; 107-651A-38R-1). Its formation could possibly have been due to water escape related to normal faulting and tilting.

PETROLOGY

Description of Units

The basement drilled at Site 651 consists of a complex rock assemblage which includes basalts and basaltic breccias, dolerites

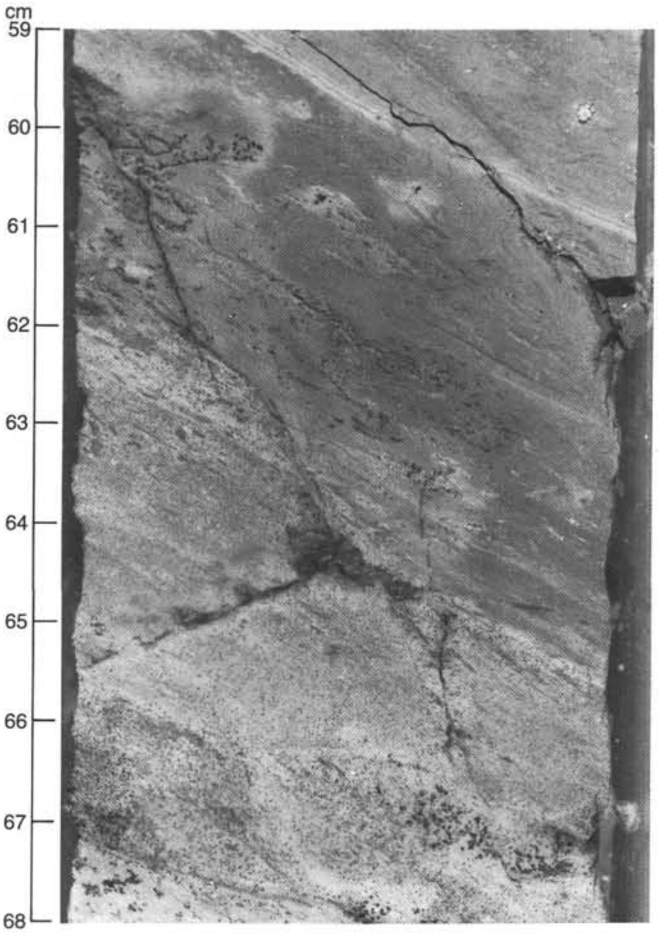

Figure 17. Photograph showing example of dipping strata (about 30°) in Section 107-651A-39R-5. This dip is attributed to tectonic tilt. The black speckles are diagenetically-formed manganese dendrites.

and metadolerites, serpentinized peridotites, and a few granodiorite fragments. The following units have been recognized.

Unit 1: Upper Basalt

Basalt was penetrated from about 386.7 mbsf, below a basal sedimentary unit consisting of dolomitic and metalliferous deposits (see "Lithostratigraphy" section, this chapter), to 464 mbsf. Several former chilled glass margins were observed in this section, suggesting that the unit consists of several flows. At the top of the unit and decreasingly with depth the rock is dissected by carbonate-filled veins, which were probably produced by deposition from seawater circulating in fissures and fractures within the basalt (Fig. 18). Some sediment filling may also have occurred. The basalt is generally aphanitic; its degree of vesicularity is generally low (< 10% by volume). The basalt is moderately to highly altered, though less altered than at Site 650 in the Marsili Basin. The rock shows relatively constant textural and mineralogical features throughout this unit. Texture ranges from intergranular to intersertal. Microphenocrysts of olivine and Ca-plagioclase are scattered in a groundmass of plagioclase laths and alteration products. In a few cases the groundmass is made of mildly altered glass, and some specimens display a crust of palagonite.

The geochemical affinity of Unit 1 basalt cannot be assessed yet owing to lack of complete chemical data. However, preliminary major element data suggest that Unit 1 basalts are similar

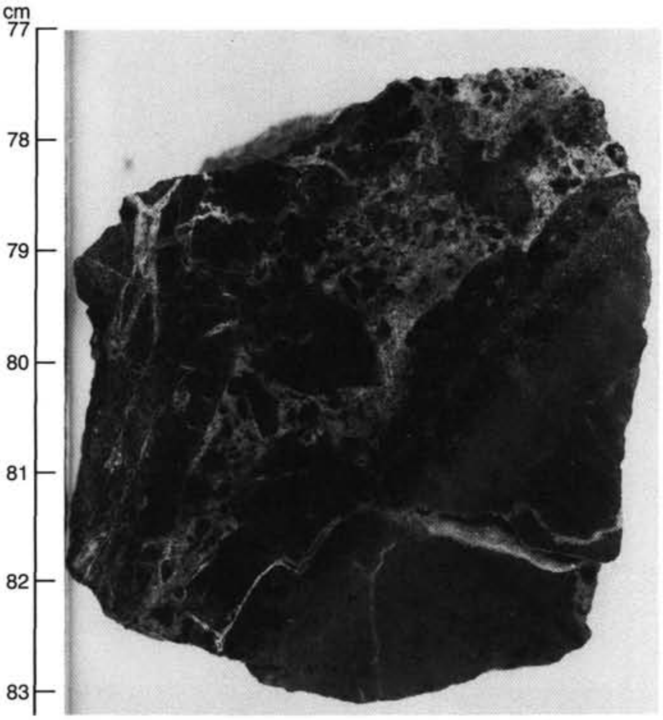

Figure 18. Basaltic breccia cemented by carbonates, above a former chilled glass margin, in Sample 107-651A-43R-1, 77–84 cm.

to basalt of tholeiitic to intermediate affinity drilled near Vavilov Seamount at DSDP Site 373 during Leg 42 (Barberi et al., 1978; Dietrich et al., 1978).

Unit 2: Dolerites and Metadolerites

From approximately 464 to 492 mbsf coarse grained dolerites and metadolerites constitute the prevalent rock types of the recovered cores (Fig. 19). The dominant mineral assemblage of the dolerites is Ca-plagioclase and olivine, which in some discrete zones within the unit change gradually into Na-plagioclase/actinolite metadolerites and into leucocratic Na-plagioclase-rich rocks. The dolerite is interpreted tentatively as representing a basaltic sill which was emplaced below Unit 1 basalt, and which reacted during intrusion probably with patches of wet sediment giving rise to the amphibole- and Na-plagioclase-rich rocks. A thin (approximately 30 cm) dolomitic sediment layer lies near the top of Unit 2, apparently little affected by the doleritic intrusion. The chemistry of the dolerite might be similar to that of Unit 1 basalt, though as yet lacking analytical data this statement is only conjectural.

Unit 3: Lower Basalts and Basaltic Breccias

A relatively thin layer of basalt and carbonate-cemented breccias was drilled below the doleritic unit, from 492 to 522 mbsf. The basalt is very altered near the top of the unit, less so further down. At least one former glassy chilled margin was recognized. Texturally and mineralogically Unit 3 basalt appears to be similar to Unit 1 basalt. The breccias could represent tectonic and/or talus basaltic breccias which have been cemented by carbonate sediment filling and by carbonate precipitation from circulating seawater.

Unit 4: Serpentinized Peridotites

Serpentinized peridotites were drilled from 522 mbsf to the bottom of the drilled section, 551 mbsf. The ultramafic rocks range in color from the classic olive green to very dark green to brown. White veins of chrysotile criss-cross the peridotites (Fig. 20), which appear to be highly sheared in more than one direction (Fig. 21). Both high-temperature plastic deformation and several phases of lower temperature deformation can be recognized (Fig. 22). No cumulate textures were recognized. The peridotites are strongly serpentinized, with mesh-texture lizardite and chrysotile developed after olivine, and large bastite plates after orthopyroxene. Relict primary phases include significant quantities of clinopyroxene in several samples, suggesting that the original rocks were prevalently lherzolites. Red brown Cr-spinel is ubiquitous, while trains of secondary magnetite are abundant particularly along chrysotile veins.

The tectonite texture and the inferred primary modal composition of the Site 651 peridotites suggest that they are derived from the upper mantle. We note that two small (approximately 5 cm in diameter) fragments of sheared biotite-containing quartz-feldspar rock were found within the Unit 4 peridotites.

Preliminary Evaluation of the Results

1. If our preliminary assessment that Unit 4 ultramafics are derived from the upper mantle is correct, two alternative origins for Site 651 peridotites can be considered: (1) they are a fragment of pre-Cenozoic, Alpine or Apennine ophiolite; (2) they are part of an upper mantle protrusion emplaced into stretched and thinned crust during the early stages of rifting of the central Tyrrhenian. Case (1) would imply that continental crust lies at Site 651. Case (2) implies a situation similar to that of other modern or ancient rifted passive margins, such as the Red Sea or the Atlantic Iberian margin, where protrusions of upper mantle bodies have been documented (Boillot et al., 1980; Bonatti et al., 1981).
2. The small quartz-feldspar-biotite rock fragments found within Unit 4 could be fragments of continental basement. If this is so, they could either have been transported by the peridotite body during its protrusion through the continental crust, or they could be detrital fragments derived from a nearby outcrop of continental crust during the emplacement of the peridotite body. In either case, they would suggest that the emplacement of the peridotite body took place through continental crust, though probably stretched and thinned.
3. The following simplified sequence of events could be tentatively inferred from the basement section drilled at Site 651: (1) protrusion of an upper mantle body, probably through stretched and thinned continental crust, sometime during or before the early Pliocene (inferred age of the oldest sediments above basement; see "Biostratigraphy" section, this chapter); (2) basalt injection which forms a thin layer of basaltic flows above the peridotite, i.e., "Basement Unit 3 lower basalt"; (3) a thin layer of sediment is deposited on the basalt; (4) new basaltic injections produce a 60-m-thick layer of basalt flows, i.e., "Basement Unit 1 upper basalt"; (5) a new basaltic injection forms a doleritic sill below Unit 1 upper basalt, i.e., "Basement Unit 2." The dolerite sill could have been injected after the whole of Basement Unit 1, or only part of it, had been emplaced.

BIOSTRATIGRAPHY

Summary

At Site 651 a sedimentary sequence 387.6 m thick overlies fragmented basaltic rocks representing the local top of the basement. Only the upper 348 m of a total sedimentary sequence of 386.5 m yields fossils. The lower part, represented by brownish, dolomite-rich mudstone, is barren. The upper segment was referred to the latest Pliocene-Pleistocene interval (*Discoaster brouweri* (NN18)/*Globorotalia inflata* (MPl6)-*Emiliania huxleyi*

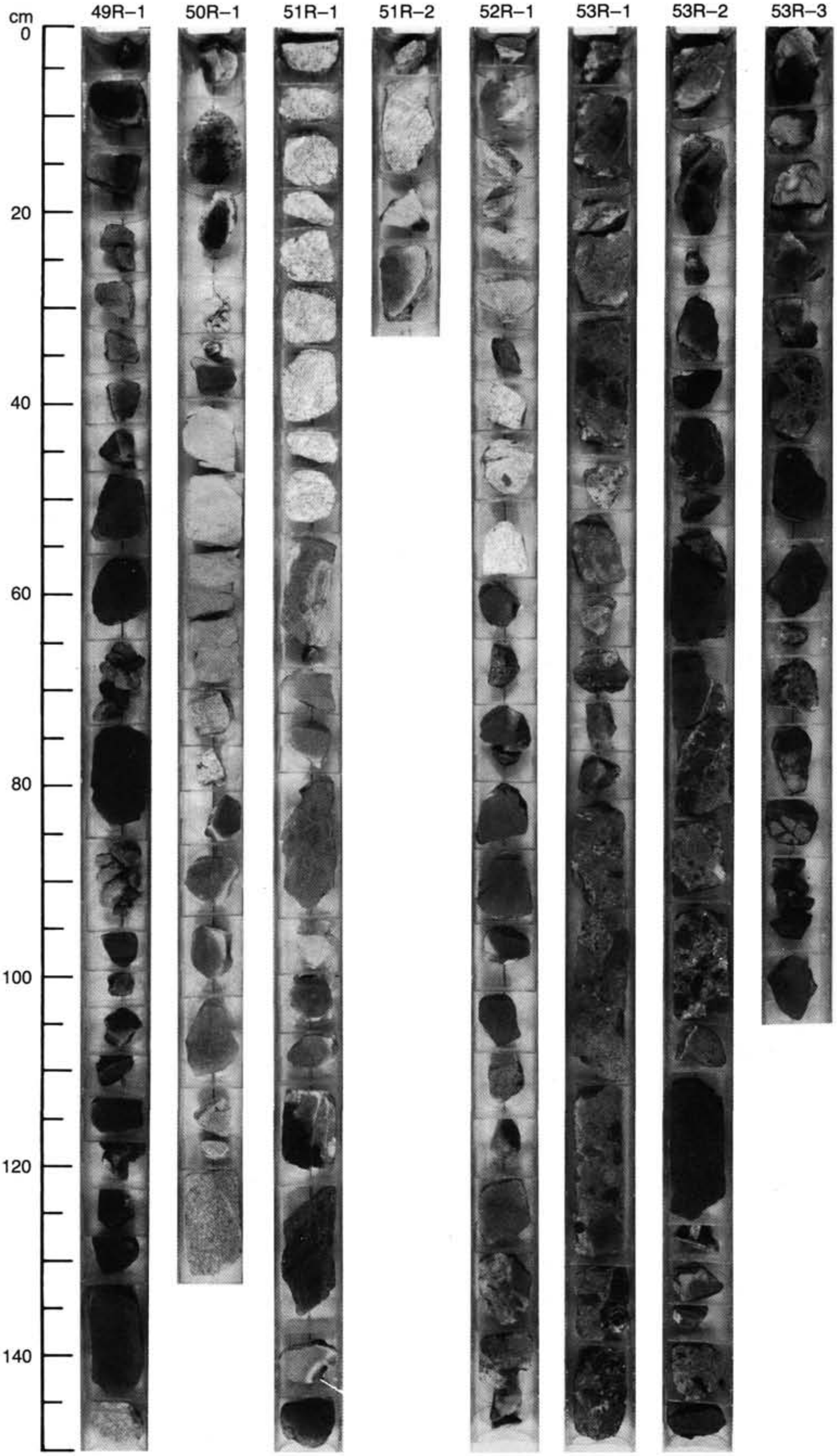

Figure 19. Transition from Unit 1, upper basalt, to Unit 2, dolerites and metadolerites, to Unit 3, lower basalt and basaltic breccia, observed from Cores 107-651A-49R through 651A-53R.

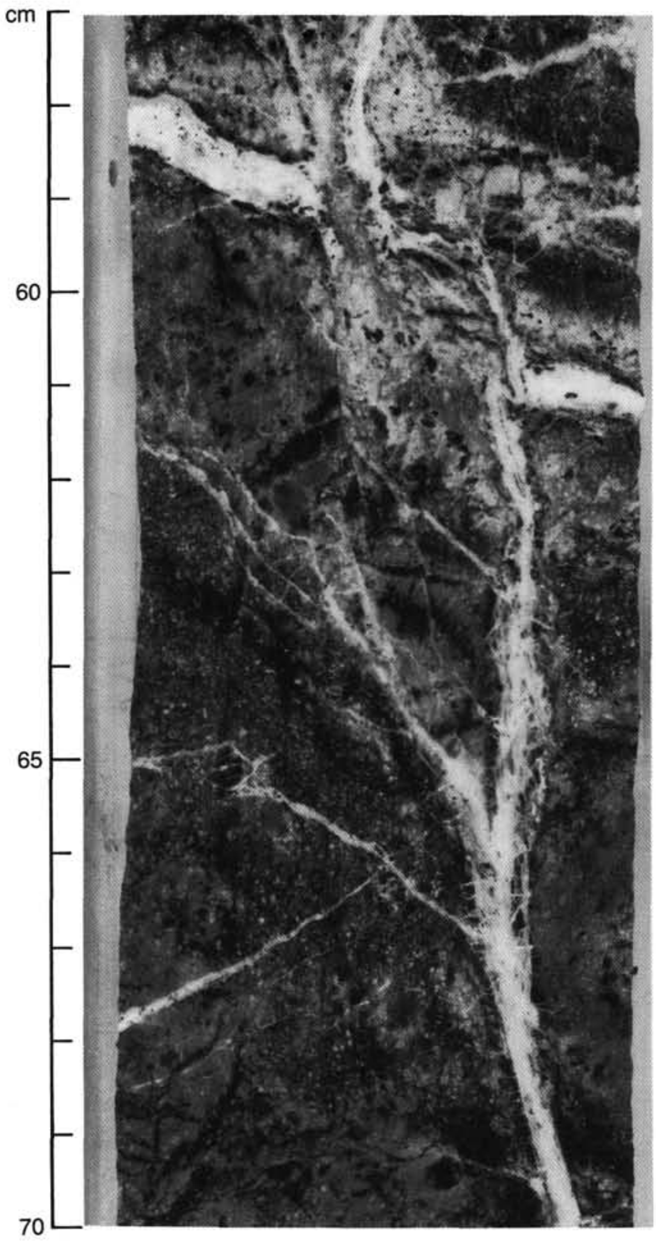

Figure 20. Veins of chrysotile criss-crossing a serpentinized peridotite sample, in Sample 107-651A-57R-1, 57–70 cm.

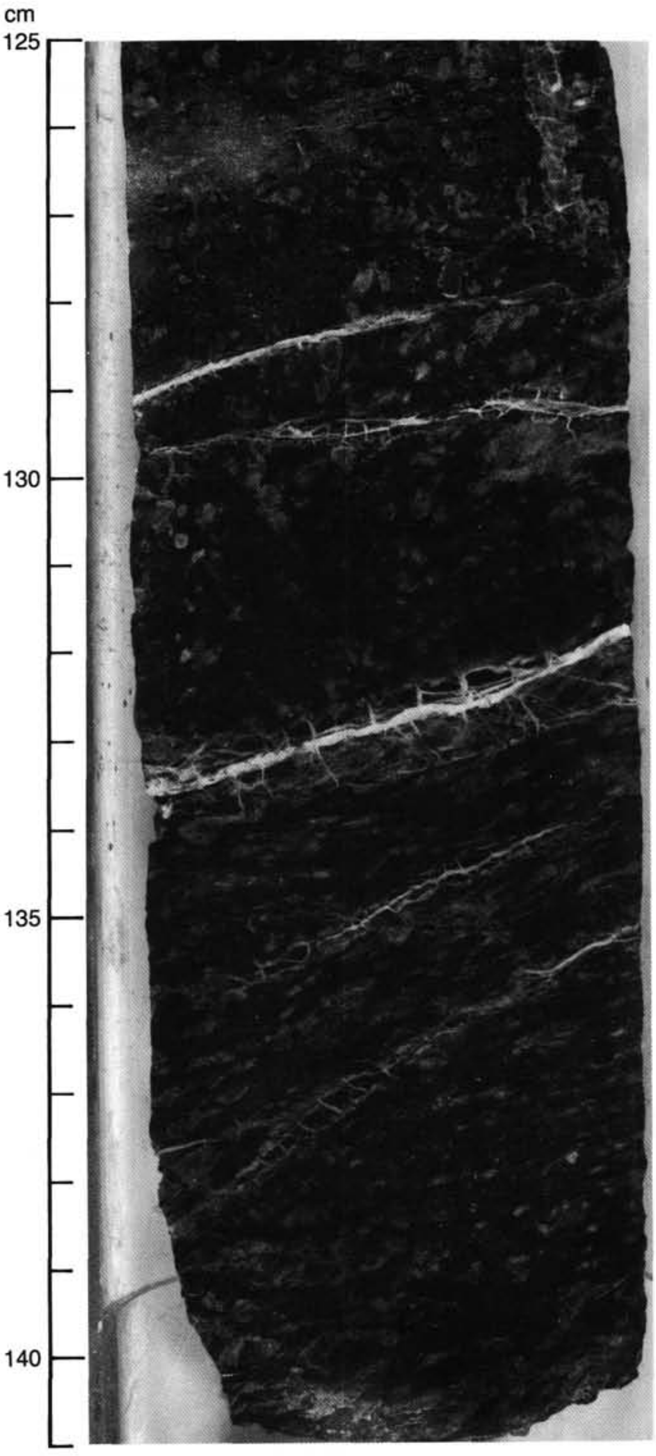

Figure 21. Sample of serpentinized peridotite showing foliation, in Sample 107-651A-58R-4, 125–141 cm.

(NN21)/*Globorotalia truncatulinoides excelsa* biozones) (Fig. 23). Using a paleoclimatic approach, additional data were obtained to subdivide the upper part of the Pleistocene.

The Pliocene/Pleistocene boundary, recognized by planktonic foraminifers (first strong peak of left-coiling *Neogloboquadrina pachyderma*) was determined between 343.8 and 343.1 mbsf near the top of the Olduvai paleomagnetic event. The base of MPl6 is at 348 mbsf. Planktonic foraminifers are generally poor from the top to 300 mbsf, often diluted by volcanic glass and pumice. From 300 mbsf to the base of the fossiliferous interval the foraminiferal assemblage is common and diversified. Nannofossils are abundant within the calcareous mud and ooze, whereas they are diluted in the volcanic material, in which reworked species are always few to common.

Benthic foraminifers occur in the interval from the top to 348 mbsf of the hole. The faunas above 155 mbsf are composed only of displaced specimens from an upper bathyal or shallower environment. In the interval between 165 and 334 mbsf, mixed fauna of middle to lower bathyal species and shallower species have been found. From 335 until 348 mbsf the faunae consist of autochthonous lower bathyal species.

Planktonic Foraminifers

Pleistocene

The Pleistocene interval was recovered from Core 107-651A-1R to about 343.5 mbsf (Sample 107-651A-37R-4, 40–42 cm). Two planktonic foraminiferal biozones (Ruggieri and Sprovieri,

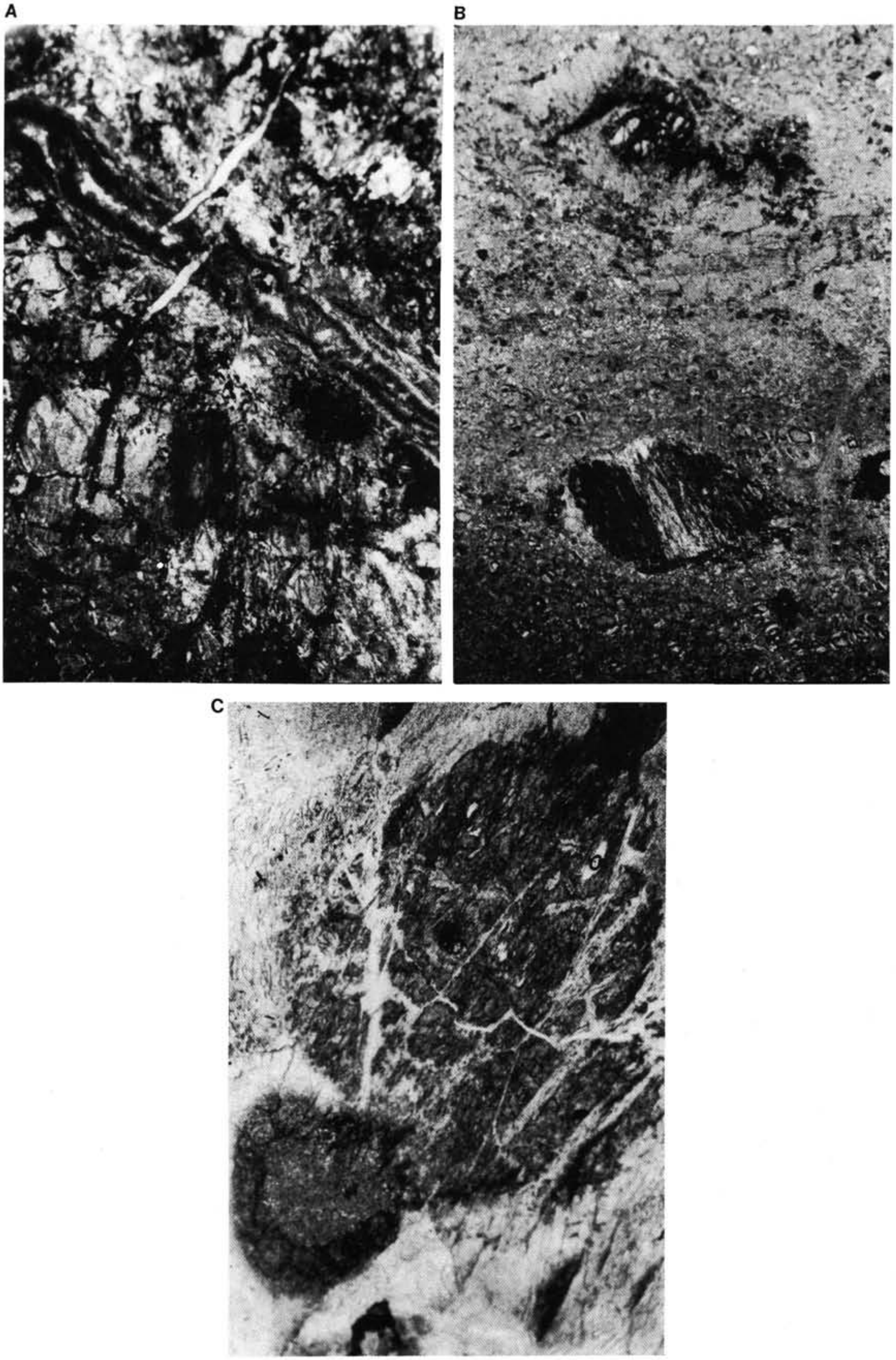

Figure 22. A. Photomicrograph showing two generations of serpentine-filled veins in serpentinized peridotite. B. Pyroxene crystal in serpentinized peridotite. C. Orthopyroxene crystal sheared with pressure shadow and dissected by secondary veins. Samples are from Core 107-651A-58R-1, 145–149, 102–103, and 139–140 cm, respectively.

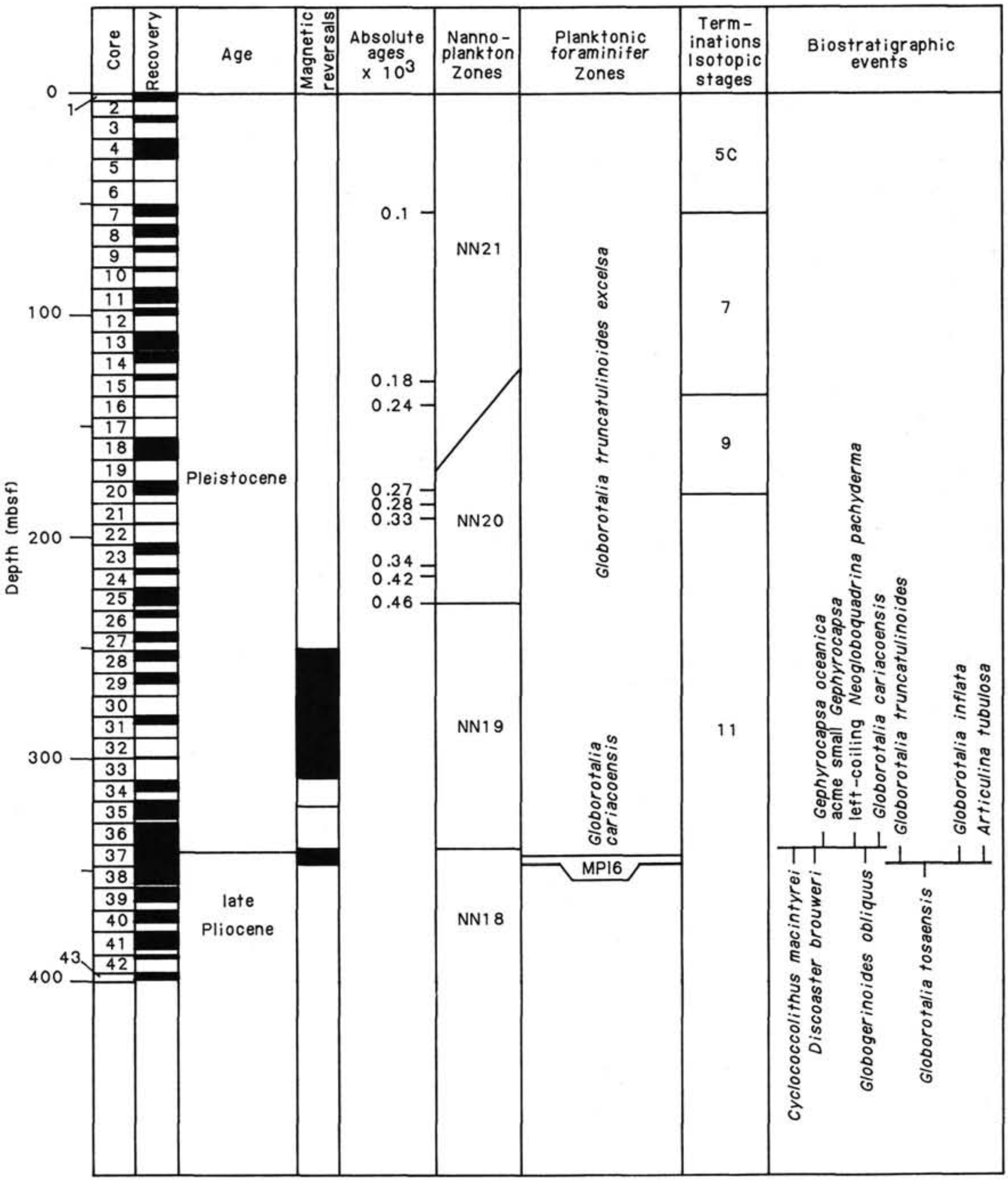

Figure 23. Summary of biostratigraphic information, Site 651.

1983; Ruggieri et al., 1984 as amended in the "Explanatory Notes" section, this chapter) were recognized, but the boundaries between them could not be detected with accuracy since the biostratigraphic markers are generally rare or absent. The *Globorotalia truncatulinoides excelsa* biozone ought to be present from the top down to about 328 mbsf. This marker species appears in coincidence with the last occurrence of (frequent) *Helicosphaera sellii* (and just below the base of the small *Gephyrocapsa* acme interval) (Ruggieri et al., 1984) and therefore, in the absence of the nominate taxon, the upper level of frequent *H. sellii* is used here to recognize the base of the *Globorotalia truncatulinoides excelsa* biozone. The *Globigerina cariacoensis* biozone was recognized from about 328 mbsf to about 343.5 mbsf (Sample 107-651A-37R-4, 40–42 cm). The zonal marker is present only in some discrete levels and never abundant.

Chronostratigraphic units were recognized according to the biostratigraphic indications coming from the pertinent stratotype sections or boundary-stratotype sections. The Pliocene/Pleistocene boundary (about 1.67 m.y.b.p.; Colalongo et al., 1982; Tauxe et al., 1983) was well detected just below 343.1 mbsf by the appearance of abundant specimens of *Neogloboquadrina pachyderma* left coiling, immediately followed upward by the appearance of *Globigerina cariacoensis*. *Globigerinoides obliquus* disappears at about 339.30 mbsf (Sample 107-651A-37R-1, 137–140 cm).

Pliocene

The latest Pliocene (Piacenzian Stage) is present between 343.5 and 348 mbsf, where the MPl6 biozone (Cita, 1975; Rio et al., 1984b) was recognized. The zonal marker is always abundant. The very few specimens of *Globorotalia inflata* recognized in the two samples from Section 1 of Core 107-651A-38R (about 348-349 mbsf) together with sparse planktonic foraminifers (includes left-coiling *Neogloboquadrina pachyderma*, generally rare in the Pliocene) are here considered as downhole contaminants. Indeed, the brownish, dolomite rich interval present down to about 390 mbsf, is always barren. At 348 mbsf (Sample 107-651A-37R, CC) a peculiar assemblage with *Globorotalia truncatulinoides, Globorotalia tosaensis, Globorotalia tosaensis tenuitheca*, and *Sphaeroidinella dehiscens* has been recognized. In the nannoplankton assemblage, *Discoaster brouweri* and *Discoaster brouweri triradiatus* are present. According to Rio et al. (1984a) this interval is present at the base of the MPl6 biozone. *Globorotalia crassaformis* was tentatively recognized in thin section coming from level at 465 mbsf, within the cemented breccia interval.

Paleoclimatic Approach

At Site 651, the paleoclimatic approach is difficult due to both contemporaneous slidings and strongly reworked polygenic material. The comparison with Site 650 indicates that we caught only some glimpses of a story.

The top of Core 107-651A-1R is a fine-grained turbidite, of Holocene age, but not recent. No living specimens have been found and some are reworked from cooler assemblages. In Core 107-651A-1R, CC, at 3.7 mbsf, reworked Pliocene species are present. The unit seems to start in 107-651A-4R, CC (29.4 mbsf) with a polygenic conglomerate including reworked Pliocene species. There was no recovery in Cores 107-651A-5R and 651A-6R.

At 49.5 mbsf (Core 107-651A-7R), a very poor assemblage indicates a temperate-cool climate. The presence of sinistral *Globorotalia truncatulinoides excelsa* can be correlated with an equivalent level observed at Site 650, Core 107-650A-7H, CC. It may correspond probably with stage 5c of Emiliani (1978) at 100,000 years (Fig. 23). This second turbiditic sequence seems to start with an indurated volcaniclastite 20 m thick. At the base (107-651A-15R, CC) a thin layer of nannofossil ooze with abundant sinistral *Globorotalia truncatulinoides excelsa* is compared with Cores 107-651A-13R, CC and -14R, CC at Site 650, attributed to isotopic stage 7 (188,000-244,000 years). Cores 107-651A-17R to 651A-20R represent a 29-m-thick homogenite; dextral *Globorotalia truncatulinoides excelsa* indicates a temperate-warm environment, as well as a thin ooze of Core 107-651A-20R, CC (183.9 mbsf).

Presently we have recognized four levels with dextral forms at Site 650; they are tentatively correlated with isotopic stages 1, 5c, 9, and 14. By correlation, Stage 9 seems to be the best constrained and seems to occur within the NN20 nannozone. It is possible that the top of NN20 is missing because at Site 650 the top of this zone falls within the isotopic stage 8. Below 107-651A-20R, CC we should reach the Termination IV as defined by Broecker and Van Donk (1970). In fact, from 193.3 mbsf until 212.9 mbsf in Cores 107-651A-21R, CC, 651A-22R, CC, and 651A-23R, CC only a very poor temperate assemblage diluted within volcanic inputs was found. In Core 107-651A-24R, CC (222.6 mbsf) an assemblage with sinistral *Globorotalia truncatulinoides excelsa* in a temperate-warm assemblage is tentatively correlated with isotopic stage 11 (347,000-421,000 years).

At 232.6 mbsf in Core 107-651A-25R, CC the sediment is clearly sorted but below an ooze layer occurring at 242 mbsf (Core 107-651A-26R, CC), the sediment is characterized by a relative abundance of *Globorotalia inflata* difficult to correlate with the acme at Site 650 because the underlying Core 107-651A-27R, CC shows an assemblage characterized by *Globorotalia viola* and *Globorotalia crassaformis* not found at Site 650. If we admit that Core 107-651A-25R, CC (at 232.3 mbsf) is still within the NN19 this may introduce a gap of about 120,000 yr or a very strong condensation including isotopic stages 12, 13, and part of 14. At 261.2 mbsf the Core 107-651A-28R, CC also contains the *Globorotalia inflata* acme. The underlying 39-m-thick ashes are barren of planktonic foraminifers. Cores 107-651A-34R, CC and 651A-35R, CC are also barren; Core 107-651A-36R, CC at 338.2 mbsf is the last of the Pleistocene characterized by the presence of *Globigerina cariacoensis*.

At Site 651 very few cool levels have been identified making the identification of the terminations difficult. One may suggest that the cool periods have been dominated by a turbiditic sedimentation.

Benthic Foraminifers

Benthic foraminifers occurred sporadically in intervals from the top, down to 348 mbsf of Site 651. The fossil faunae in this site are roughly divided into three assemblages, i.e., upper, middle, and lower assemblages. The upper assemblage is characterized by high species diversity, and is found in the interval between top and 155 mbsf (Core 107-651A-17R, CC). In each sample, shallow-water species such as *Ammonia beccarii* and *Elphidium crispum* occur together with middle bathyal ones such as *Uvigerina mediterranea*. Lower bathyal species, however, cannot be found through the interval. These foraminiferal tests are accompanied by terrigenous and/or volcanogenic materials without exception. Thus, most of the specimens in this assemblage are regarded as displaced by turbidity currents. The middle assemblage, which is found in samples from 146 mbsf (Core 107-651A-18R, CC) down to 334 mbsf (Sample 107-651A-36R-4, 101-105 cm), consists of mixed fauna of middle to lower bathyal species plus shallower ones. The former species (ex. *Pyrgo lucernula, Chilostomella mediterranensis, Articulina tubulosa*) seem to be autochthonous. On the other hand, the latter ones (ex. *Asterigerina mamilla, Elphidium crispum, Rosalina* spp., *Cibicides lobatulus*) are concluded to be displaced from upper bathyal or shallower zones. Terrigenous materials are seen in some samples. The lower assemblage is found in the samples from 335 mbsf (Sample 107-651A-36R-5, 97-101 cm) to 348 mbsf (Sample 107-651A-37R, CC), in which terrigenous materials are not included at least in sand-size fraction. It is characterized by autochthonous *Oridorsalis stellatus, Gyroidina altiformis*, and *Articulina tubulosa*.

In the Ionian region, the first appearance level of *A. tubulosa* is reported in the MPl6 zone (D'Onofrio, 1981; Raffi and Sprovieri, 1984). In the present hole, its lowest occurrence is at 342 mbsf (Sample 107-651A-37R-3, 105-109 cm) assigned to the *Globigerina cariacoensis* biozone at the base of the Pleistocene.

Nannoplankton

The upper Pleistocene (Zones NN20/NN21) was recognized from Core 107-651A-1R to Sample 107-651A-25R, CC, 30 cm. The upper part of this series consists mainly of volcanogenic sediments interbedded with volumetrically subordinated marly nannofossil-rich mud. Cemented pumice breccias increase in average grain size and abundance downhole. Nannofossils are strongly diluted within the turbidites by detrital carbonates, volcanic ash, and reworked Cretaceous to Pliocene nannoplankton species. The presence of *Micrascidites* spines shows that these sediments are provided partially from the shelf.

As at Site 650, *Coccolithus pelagicus* is missing in the Holocene. It occurs from Core 107-651A-3R downsection with varying abundance. The small *Gephyrocapsa* is very abundant in Sample 107-651A-20R, CC, 18 cm. However, this level does not correspond to the small *Gephyrocapsa* zone.

Helicosphaera sp. characterized by two large pores was observed in Sections 1 and 2 of Core 107-651A-25R. It seems to be typical for the lower part of Zone NN20.

The *Pseudoemiliania lacunosa* Zone (NN19) was encountered from Samples 107-651A-25R, CC, 30 cm, to 107-651A-37R-1, 70 cm (from 232.0 to 339.0 mbsf). Nannofossils become more abundant due to decreasing number of turbidites. This lithological change is well expressed in an important drop of accumulation rates.

The distinct acme of the small *Gephyrocapsa* ranges from Core 107-651A-34R to Section 1 of Core 107-651A-36R. At the same time several sapropel layers can be observed. The extinction level of *Helicosphaera sellii* was observed in Sample 107-651A-34R-4, 45 cm, that means within the small *Gephyrocapsa* Zone and very close to the top of the Jaramillo magnetic event.

Braarudosphaera bigelowi becomes abundant within the sapropels of Cores 107-651A-36R and 107-651A-37R. This species is also common in Sections 3 and 4 of Core 107-651A-37R (just below the Pliocene/Pleistocene boundary) where it constitutes thin layers. These results are in good agreement with those obtained at Site 650.

The Pliocene/Pleistocene boundary (NN18/NN19) was recognized between Samples 107-651A-37R-1, 111-112 cm, and 107-651A-37R-1, 120 cm (339.3 mbsf) based on the extinction of *Cyclococcolithus macintyrei* and *Discoaster brouweri*. This boundary falls almost together with the top of the Olduvai magnetic event which was determined preliminarily at 342.0 mbsf.

Within the uppermost Pliocene some turbidites occur which are rich in detrital carbonates and reworked nannoplankton species. This level corresponds to the slumps and synsedimentary breccias observed at Site 650, just below the Pliocene/Pleistocene boundary.

Discoasters are extremely rare or absent within the uppermost Pliocene. They are restricted to several layers, implying climatic oscillations.

In Core 107-651A-38R nannofossils become very rare or they are absent due to diagenesis and formation of secondary dolomite. Based on extrapolation of sedimentation rates, oldest sediments overlying the basalt would have an age of about 3.6 Ma.

PALEOMAGNETISM

Hole 651A was drilled using a rotary core barrel. The resulting poor recovery and drilling disturbance did not allow us to resolve an unambiguous or continuous magnetostratigraphy. In addition, the sedimentation rate in the late Pliocene/early Pleistocene interval is about five times lower than at Site 650. The reversals between the base of the Brunhes chron and the top of the Olduvai subchron are condensed into 32 m of core at Site 651, as opposed to 160 m at Site 650.

One hundred fourteen discrete 7-cm^3 samples were collected at this site. They were measured on the Molspin magnetometer and progressively demagnetized using the Schonstedt alternating field demagnetizer. Data quality was improved by onshore thermal demagnetization and measurement with the cryogenic magnetometer.

The magnetic properties of the sediments at this site were similar to those at Site 650. The natural remanent magnetizations (NRM) usually have intensities of about 10^{-5} G/cm^3 but this is reduced by as much as an order of magnitude after demagnetization at peak fields of 100-200 Oe. The inclinations of the NRM are nearly always steep and positive, probably as a result of a drill-string (viscous) magnetization which dominates NRM. Fortunately, this viscous magnetization has very low coercivity and can be removed at peak demagnetization fields of 100-200 Oe. The remaining higher coercivity component thus records a magnetic stratigraphy down to the Reunion event.

In spite of the very poor recovery, we were able to discern the main features of the early Pleistocene/late Pliocene polarity time scale (Table 2).

Table 2. Preliminary determination of magnetozone boundaries for Site 651. The samples which bracket the magnetozone boundaries are given.

Magnetozone boundary	Core	Section	Interval (cm)	Depth (mbsf)
Base of Brunhes	between 34R	1	6-8	309.37
	and 34R	1	17-19	309.48
Top of Jaramillo	between 35R	1	66-68	319.57
	and 35R	1	130-132	320.21
Base of Jaramillo	between 35R	1	130-132	320.21
	and 35R	2	148-150	321.89
Top of Olduvai	between 37R	3	34-36	341.55
	and 37R	3	72-74	341.93
Base of Olduvai	between 37R	4	146-148	344.16
	and 37R	5	108-110	345.29
Top of Reunion	between 37R	6	52-54	346.23
	and 37R	6	134-136	347.05
No data below	37R	7	12-14	347.42

PHYSICAL PROPERTIES

Introduction

Physical properties measured at site 651 include GRAPE density and thermal conductivity from full round core sections, vane shear strength, compressional wave velocity, and index properties (porosity, bulk density, and grain density) from split sections. The different methods of analysis are described in the "Explanatory Notes" chapter, this volume.

Results

GRAPE Density

Bulk density was determined by gamma ray attenuation and porosity evaluation (GRAPE) for the entire length of every core. unfortunately, due to the drilling disturbances, the results are difficult to interpret.

Index Properties and Compressional Velocity

Porosity, bulk density, compressional velocity, and grain density are plotted relative to sub-bottom depth in Figures 24 and 25 and are listed in Tables 3 and 4.

The bulk density values are in good agreement with the porosity values and reflect the same trend changes along the cores. Four main trends can be distinguished in Hole 651A:

1. From the mud line to 92 mbsf, we measured decreasing porosity (77% to 45%) and increasing bulk density (1.5 to 2.2 g/cm^3).
2. From 92 to about 320 mbsf, porosity increased up to 74%, which corresponds to a weak decrease in bulk density down to about 2.1 g/cm^3.
3. From 320 to 445 mbsf, a clear decrease of the porosity (50%-26%) and increase of density (from 2.1 to 2.5 g/cm^3) were noted.
4. Between 445 and 551 mbsf: this deepest interval presents very low porosity values (3%-5%) with some relative high porosity data points (about 25%) and density as high as 2.9 g/cm^3.

The grain density curve at Hole 651A is difficult to interpret but three "units" could be differentiated: between the mud line and 320 mbsf, from 320 mbsf to about 385 mbsf, and from 385 mbsf to the bottom of the hole. The upper unit is characterized by heterogeneous values around 2.6 g/cm^3, the second interval shows homogeneous grain density of about 2.85 g/cm^3 and the deeper interval has a good homogeneity of grain density around 2.6 g/cm^3.

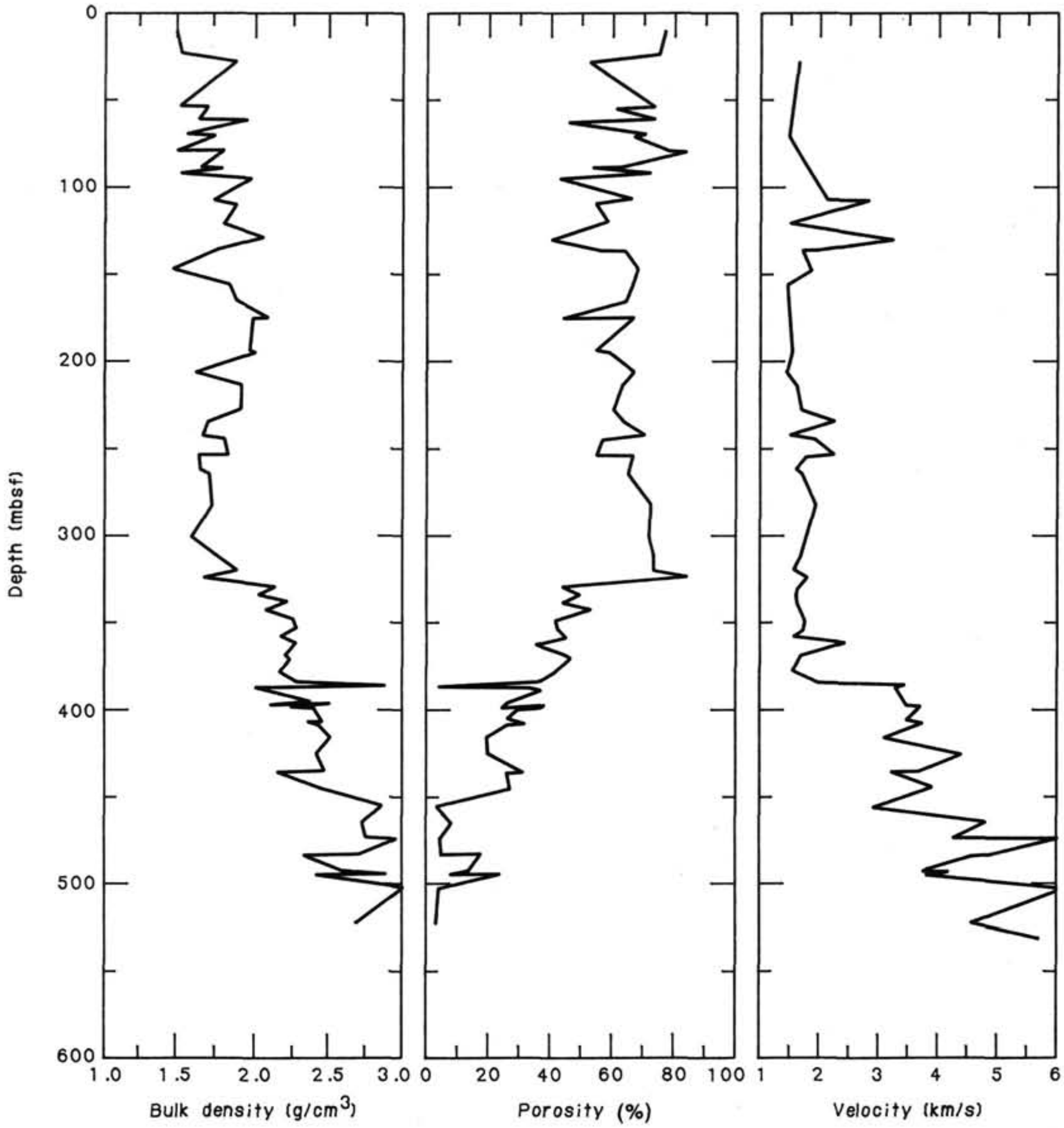

Figure 24. Bulk density, porosity, and velocity vs. depth at Site 651.

Plotting of the compressional wave velocity shows the following main trends:

1. From the mud line to 386 mbsf the velocities measured on samples are constant at about 1.6–1.7 km/s. This homogeneity is interrupted only at 100 to 120 mbsf by high velocities around 2.6 km/s.

2. Between 386 and 465 mbsf: this interval is clearly separated from the previous one. The measured velocities range from 3.4 to 4.8 km/s.

3. The deepest interval, below 465 mbsf, shows values between 3.9 and 6.1 km/s which reflect the heterogeneity of the basement complex.

Velocity measurements were done on the orthogonal axis of three hard rock samples (Table 5) and show a notable anisotropy of velocity. In Table 5, Axis A is parallel to the core liner and Axis B and Axis C are orthogonal to the core liner but, because of the rotary drilling technique, cannot be oriented.

Correlation with Lithology and Petrology Results

The physical properties analysis at Site 651 underlines the main lithologic units and their boundaries as follows:

1. Lithostratigraphic Unit I (see "Lithostratigraphy" section, this chapter) is well underlined by a porosity trend. The base of this unit, where cemented breccia and tuff were recovered, presents high velocity values between 100 and 120 mbsf. The high velocity interval separates this unit from the next one.
2. Lithostratigraphic Unit IIa is characterized, between 309 and 347 mbsf, by a constant density and a constant velocity. Only an increasing porosity vs. depth allows us to distinguish this unit from the previous one.
3. The limit between lithostratigraphic Units IIa and IIb is marked by an important change of density and porosity at 347 mbsf which correlates well with the appearance of a front of dolomitization.
4. The grain density shows a well defined interval between 320 and 385 mbsf. This interval can be explained by increased carbonate in the lower part of Unit IIa and in Unit IIb.

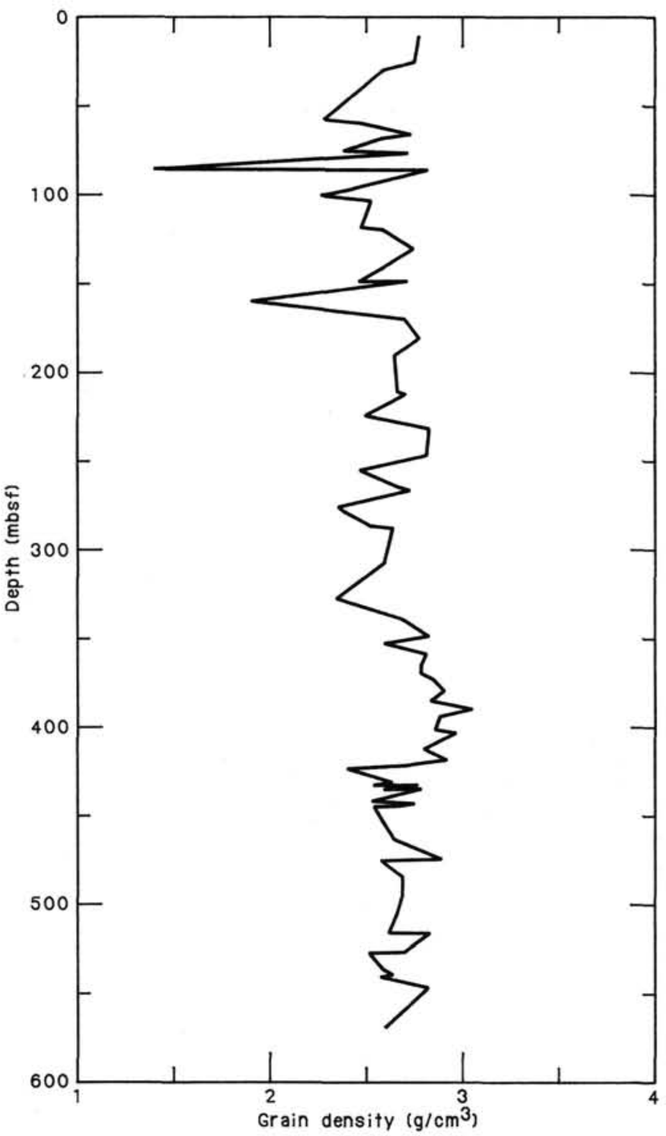

Figure 25. Grain density vs. depth at Site 651.

Table 3. Physical properties index for Site 651.

Core section	Interval or piece no. (cm)	Depth sub-bottom (m)	Bulk density (g/cm^3)	Porosity (%)	Grain density (g/cm^3)
3R-1	15–18	10.48	1.47	76.9	2.76
4R-3	19–22	23.02	1.51	74.5	2.73
4R-6	77–80	27.40	1.86	52.0	2.58
7R-3	10–15	52.52	1.50	73.7	2.27
7R-4	17–19	54.09	1.68	61.1	2.47
8R-1	83–85	60.05	1.62	73.6	2.72
8R-2	90–92	61.62	1.94	45.4	2.57
9R-1	10–11	68.91	1.55	70.5	2.37
9R-1	103–106	69.86	1.73	67.0	2.70
10R-1	47–48	78.78	1.77	83.8	2.81
11R-1	39–40	88.40	1.63	62.2	2.41
11R-1	55–57	88.57	1.77	53.3	2.43
11R-3	59–60	91.60	1.50	72.3	2.26
11R-5	59–60	94.60	1.96	42.2	2.52
13R-1	22–24	107.24	1.71	65.9	2.46
13R-2	104–106	109.56	1.87	54.3	2.57
14R-2	110–114	119.34	1.79	58.8	2.73
15R-C	8–12	129.43	2.05	39.6	2.58
16R-1	7–10	136.10	1.75	55.7	2.46
16R-1	17–19	136.19	1.74	64.2	2.71
18R-2	74–77	155.67	1.82	66.5	2.70
19R-1	50–51	165.11	1.87	64.3	2.77
20R-C	10–12	174.32	2.08	42.9	2.62
20R-C	15–17	174.37	1.97	67.4	2.65
22R-1	14–15	193.65	1.95	55.5	2.66
22R-1	26–27	193.77	1.99	59.2	2.69
23R-2	85–88	205.58	1.60	67.8	2.50
24R-1	16–18	213.08	1.91	63.4	2.82
25R-1	7–9	226.69	1.90	60.8	2.82
26R-2	54–57	234.24	1.68	65.1	2.47
27R-1	27–29	242.27	1.65	71.2	2.66
27R-2	8–10	244.30	1.79	57.3	2.73
28R-2	26–28	253.36	1.82	55.3	2.36
28R-2	82–85	253.92	1.62	67.2	2.39
29R-1	64–66	261.84	1.64	66.5	2.53
29R-2	8–10	263.50	1.69	66.2	2.64
31R-1	142–144	281.84	1.71	73.9	2.60
33R-C	10–11	300.11	1.58	73.1	2.35
34R-2	35–36	311.05	1.74	74.6	2.69
35R-1	97–99	319.89	1.88	74.2	2.83
35R-4	90–92	324.02	1.66	85.0	2.60
36R-1	100–102	329.62	2.13	44.8	2.82
36R-4	88–90	334.00	2.02	50.0	2.79
37R-1	3–6	338.26	2.20	44.4	2.79
37R-3	118–120	342.40	2.07	53.9	2.85
38R-1	48–50	348.30	2.24	41.9	2.91
38R-4	47–49	352.78	2.27	43.3	2.84
39R-1	43–45	357.94	2.17	45.6	3.05
39R-3	103–105	361.54	2.27	35.8	2.88
40R-1	126–128	368.46	2.20	45.0	2.86
40R-3	17–19	370.37	2.23	46.7	2.96
41R-1	8–10	377.60	2.16	41.8	2.81
41R-C	18–20	384.18	2.27	36.7	2.93
42R-1	8B	386.99	2.22	34.6	2.71
42R-1	21	387.80	2.00	37.6	2.41
43R-1	4	396.45	2.37	26.3	2.64
43R-1	10D	397.20	2.09	38.5	2.55
43R-1	13B	397.53	2.49	24.8	2.77
43R-2	7	398.30	2.23	37.5	2.72
43R-2	12D	398.72	2.38	30.1	2.60
43R-2	14	398.99	2.38	30.6	2.78
44R-1	3	406.17	2.42	26.4	2.54
44R-1	13	407.21	2.36	28.2	2.75
44R-2	5	407.78	2.40	32.0	2.68
44R-2	17	408.78	2.42	26.4	2.54
45R-1	6	416.06	2.49	19.5	2.59
46R-1	2	425.42	2.39	20.5	2.65
47R-1	6	435.37	2.46	31.9	2.90
47R-1	19	436.27	2.14	26.1	2.58
48R-1	10	445.21	2.42	27.7	2.70
52R-1	19	484.45	2.31	17.8	2.52
53R-1	13	494.10	2.57	14.1	2.61
53R-2	13	495.55	2.40	24.4	2.56

5. The limit between the sedimentary column and the basaltic breccia at 388 mbsf is poorly defined in the porosity and more evident in the density trend. However, the velocity data clearly indicate the contact between the sediments and Basement Unit 1.

6. The top of the Basement Unit 2 is underlined by a change of density, of porosity, and of velocity. The measurements obtained in Basement Units 2, 3, and 4 are highly variable and reflect the diversity of the basement petrology.

Correlation with the Seismic Data

It is interesting to compare the average velocity of each main interval with the velocity analysis of the site survey seismic line used for the choice of Site 651 (see "Seismic Stratigraphy" section, this chapter):

1. The average measured compressional velocity between the mud line and 386 mbsf is 1.88 km/s which is sensibly higher than the 1.64 km/s and 1.70 km/s velocities computed from the seismic line for Seismic Units 1 and 2. According to our data this change of velocity occurs at 386 mbsf and corresponds to the limit of seismic Subunits 3a and 3b which has to be located at the same depth.

2. The velocities measured between 386 and 465 mbsf have an average of 3.61 km/s which is very close to the seismic velocity attributed to the Seismic Unit 3b (3.70 km/s).

3. The deepest unit (465–551 mbsf) has a measured average velocity of 4.85 km/s which is sensibly higher than the com-

Table 4. Compressional velocity for Site 651.

Core section	Interval or piece no. (cm)	Depth sub-bottom (m)	Compressional velocity (km/s)
4R-6	77–80	27.40	1.738
9R-1	103–106	69.86	1.576
13R-1	22–24	107.24	2.240
13R-1	104–106	107.56	2.900
14R-3	72–76	120.16	1.595
15R-C	8–12	129.43	3.269
16R-1	7–10	136.10	2.063
16R-1	17–19	136.19	1.875
17R-1	66–68	146.38	1.967
18R-2	74–77	155.67	1.571
22R-1	26–27	193.77	1.700
23R-2	85–88	205.58	1.592
24R-1	16–18	213.08	1.764
25R-1	7–9	226.69	1.841
26R-2	54–57	234.24	2.360
27R-1	27–29	242.27	1.642
27R-2	8–10	244.30	2.048
28R-2	26–28	253.36	2.350
28R-2	82–85	253.92	1.892
29R-1	64–66	261.84	1.749
29R-2	8–10	263.50	1.837
31R-1	142–144	281.84	2.083
34R-2	35–36	311.05	1.845
35R-1	97–99	319.89	1.748
35R-4	90–92	324.02	1.927
36R-1	100–102	329.62	1.815
36R-4	88–90	334.00	1.770
37R-1	3–6	338.26	1.788
37R-3	118–120	342.40	1.823
38R-1	48–50	348.30	1.934
38R-4	47–49	352.78	1.890
39R-1	43–45	357.94	1.783
39R-3	103–105	361.54	2.560
40R-1	126–128	368.46	1.825
41R-1	8–10	377.60	1.756
41R-C	18–20	384.18	2.175
42R-1	4	386.70	3.499
42R-1	8B	387.00	3.325
42R-1	21	387.80	3.399
43R-1	10D	397.20	3.589
43R-1	4	397.53	3.752
43R-2	12D	399.00	3.710
44R-1	3	406.17	3.561
44R-1	13	407.21	3.794
44R-2	17	407.78	3.745
45R-1	6	416.06	3.204
46R-1	2	425.42	4.465
47R-1	6	435.35	3.760
47R-1	19	436.28	3.325
48R-1	10	445.20	3.994
49R-1	23	455.78	3.049
50R-1	13A	465.12	4.884
51R-1	3	473.75	4.372
51R-1	13	474.65	5.792
51R-1	15	475.05	5.969
52R-1	10	483.88	4.959
52R-1	19	484.50	4.641
53R-1	13	493.29	3.936
53R-1	15	493.47	4.258
53R-2	11	495.35	3.936
53R-2	13	495.55	3.865
54R-1	7	502.95	6.129
56R-1	24	523.14	4.626
57R-1	8	532.00	5.734

Table 5. Velocity anisotropy for Site 651.

Core section	Piece no.	Depth sub-bottom (m)	Compressional velocity (km/s)			Nature of sample
			Axis A	Axis B	Axis C	
51R-1	15	475.05	5.683	5.714	5.751	Albitite
56R-1	24	523.14	4.626	4.926	4.856	Serpentinized peridotite
58R-1	11	547.11	4.339	4.200	4.085	Serpentinized peridotite

puted velocities from the site survey seismic line (2.86 to 4.33 km/s) and the velocities calculated by Recq et al. (1984) with the refraction data (3.4 to 4.02 km/s) for a layer between 600 and 1300 mbsf. If the diverse computed data are correct this means that either our measurements are not good (which would be surprising according to the previous agreements between the different methods) or the basement sampled at Site 651 is not representative of the upper part of the regional acoustic basement. Possibly, only the harder levels have been recovered, with more altered or serpentinized intervals not sampled by the RCB drilling.

The anisotropy noted on hard rock samples is probably related to mineral orientations. Future studies should pinpoint the origin of this velocity anisotropy.

Conclusion

The physical properties measurements at Site 651 show clear trends and well-marked steps which are in good agreement with both the lithology and acoustic stratigraphy.

ORGANIC GEOCHEMISTRY

A total of 34 samples were analyzed for the abundance of organic carbon in sediments of Hole 651A following the procedures outlined in the "Explanatory Notes" chapter, this volume. Because of the questionable value of total nitrogen concentrations in organic-matter-lean sediments and because of very erratic C/N ratios resulting from low concentrations, these ratios are not given in Table 6. Figure 26 is a plot of inorganic carbon and organic carbon concentrations with depth.

Excursions of the plot from a background value of less than 0.3% C_{org} correlate with dark green, commonly laminated sa-

Table 6. Table of carbon and hydrogen concentrations in sediment at Site 651.

Core section interval (cm)	Depth (mbsf)	C_{org} (%)	C_{inorg} (%)	H (%)	Total C (%)
3-1, 35–36	10.65	0.00	3.08	0.67	3.08
4-2, 79–81	22.09	0.43	2.19	0.59	2.62
7-2, 140–150	52.40	0.00	0.73	0.31	0.31
9-1, 73–75	69.53	0.26	1.76	0.47	2.02
10-1, 76–78	79.06	0.00	1.80	0.49	1.36
12-1, 66–68	98.06	0.00	12.20	0.51	3.11
17-1, 66–68	146.36	0.15	0.81	1.32	0.96
18-5, 134–138	164.44	1.30	3.27	0.76	4.57
23-1, 28–30	203.48	0.27	2.40	0.63	2.67
25-2, 110–112	225.20	0.03	0.08	1.24	0.11
25-2, 115–119	225.25	0.04	0.05	1.51	0.09
26-1, 60–62	232.90	0.21	2.43	0.58	2.64
26-1, 145–146	233.75	0.11	0.55	0.68	0.60
27-2, 8–10	243.58	0.56	4.32	0.52	4.98
27-2, 68–70	244.18	1.97	4.29	0.71	6.26
27-2, 74–75	244.24	0.58	3.47	0.62	4.05
28-CC, 1–2	260.71	1.96	2.88	0.80	4.84
31-2, 16–19	282.06	0.04	0.12	1.17	0.16
33-CC, 10–11	308.90	0.14	2.20	0.81	2.34
34-1, 53–55	309.83	1.68	3.69	0.68	5.37
34-1, 140–150	310.70	0.22	4.12	0.58	4.34
35-1, 6–8	318.96	2.88	4.19	0.76	7.07
35-5, 88–90	325.78	0.12	1.06	0.73	1.18
36-1, 54–56	329.14	4.16	1.60	1.06	5.76
36-3, 7–10	331.67	1.35	3.28	0.70	4.63
36-5, 58–60	335.18	0.19	5.37	0.41	5.56
36-6, 82–85	336.92	1.78	3.33	0.68	5.11
37-2, 107–110	340.77	2.01	4.78	0.69	6.79
37-3, 36–38	341.56	1.74	2.82	0.70	4.56
37-4, 94–96	343.64	0.44	6.07	0.38	6.51
37-5, 140–142	345.60	2.94	3.57	0.70	6.51
39-3, 53–56	361.03	0.07	3.54	0.51	3.61
40-1, 64–65	367.84	0.00	3.58	0.61	3.31
41-2, 14–20	378.44	0.00	2.94	0.65	2.73

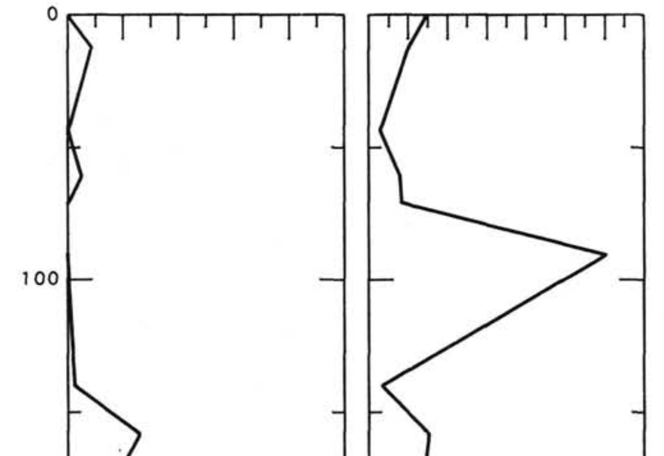

Figure 26. Concentrations of organic and inorganic carbon vs. depth at Site 651.

propel layers (C_{org} over 2%) and sapropelic muds, which were found scattered throughout Cores 107-651A-27R to 651A-38R (242–347 mbsf) of earliest Pleistocene age. Some of these centimeter-thin beds display burrowing features and traces of graded bedding. In smear slides, framboidal pyrite is a common constituent. Diatom frustules, opaline debris, and dinoflagellate debris are accessory components, as are calcareous microfossils. Dominated by light olive, amorphous organic material, detritus of higher plants is present only in minor amounts. Organic carbon values of sediments immediately bordering these sapropelic layers are invariably low to nil, while the maximum organic carbon value encountered in Sample 107-651A-36R-1, 54–56 cm (329.1 mbsf) was 4.19%. Within the Pleistocene succession of Hole 651A sedimentation of sapropels sensu strictu (C_{org} higher than 2% by weight) occurred in six samples (107-651A-27R-2, 68 cm, 651A-28R, CC, 1 cm, 651A-35R-1, 6 cm, 651A-36R-1, 10 cm, 651A-37R-2, 107 cm, and 651A-37R-5, 140 cm).

Cores were checked routinely for gas pockets and fluorescing hydrocarbon accumulations in the liner upon arrival on deck. No such accumulations were found, however, and analyses of gas pockets extracted from the liners of two cores yielded no evidence for the presence of volatile hydrocarbons in the range of C_1 to C_6.

INORGANIC GEOCHEMISTRY

Carbonate Analyses

A total of 88 sediment samples were analyzed for their carbonate content. In addition to samples taken exclusively for this purpose, subsamples of physical properties samples and samples taken adjacent to intervals investigated by smear slide analyses were used. Results are listed in Table 7, and Figure 27 is a plot of carbonate content versus depth for samples of Hole 651A.

As was the case in sediments from Site 650, the influx of turbidites into the sedimentary basin throughout the Pleistocene results in diverse lithologies and in a wide range of carbonate concentrations. Grain-size effects during turbidite emplacement generally lead to increasing fine-grained carbonate constituents in distal turbidites, while coarse-grained clastic and volcanogenic bases exhibit values generally less than 5%. This succession of facies is nicely documented by the proximity of extreme values: A minimum value of 0.2% $CaCO_3$ determined in a basal turbidite sample (Core 107-651A-25R, Section 2, 115–117 cm; 225.3 mbsf) is in close genetic and spatial relationship with the maximum value of 69.6% $CaCO_3$ encountered in a nannofossil chalk sample of the same turbidite sequence (Core 107-651A-25R, Section 1, 54–57 cm; 223.1 mbsf). Extremely high values above 40% $CaCO_3$ may delineate truly autochthonous hemipelagic nannofossil oozes representing background lithology, which is interrupted and diluted by siliciclastic and volcanogenic turbidite input.

Disregarding the possible introduction of artifacts by insufficient sampling density, the sedimentary column may coarsely be divided into two lithological units based on carbonate content. Each of these main units has two subunits. Unit 1 encompasses volcanogenic and siliciclastic sediments and turbidites of Cores 107-651A-1R to 651A-32R (0–290 mbsf). Carbonate content in this unit is characterized by extreme fluctuations characteristic of proximal turbidite sedimentation. Approximately with the onset of Core 107-651A-18R (150 mbsf), dolomite becomes an appreciable component in the carbonate fraction (as much as 50%). This occurrence of dolomite was not noticed in samples of Subunit 1a (Cores 107-651A-1R to about 651A-17R). From Table 7 and Figure 27 it appears that total carbonate values of sediments underlying Core 107-651A-33R (310 mbsf) are less widely scattered and generally reach higher values than those of younger sediments. Maxima in this Unit 2 cluster around 50%–60% carbonate and rarely drop below 10%, while calcite remains the dominant carbonate mineral.

The dominance of dolomite over calcite in samples underlying Core 107-651A-38R (348 mbsf) reaching to acoustic basement encountered in Core 107-651A-41R (386.5 mbsf) may be an appropriate characteristic to distinguish sediments of this Subunit 2b from overlying Subunit 2a. This massive occurrence of dolomite, associated with the basalt/sediment interface, is diagenetic in origin and results from the replacement of Ca^{2+} in calcium carbonate by Mg^{2+}. The magnesium was probably liberated during the alteration of the underlying basalt and peridotite units.

Interstitial Water Analyses

Subsamples of interstitial waters squeezed from 6 whole-round core segments of 10 cm length, 14 samples obtained from squeezing 50 cm^3 sections of the working half, and 1 reference sample of surface seawater were analyzed on board during drilling operations at Site 651. The results of these analyses are listed in Table 8 and depicted as depth plots in Figure 28.

Table 7. Calcium carbonate concentrations in Site 651 sediments.

Sample (interval in cm)	Depth (mbsf)	$CaCO_3$ (%)
651A-1R-3, 140–150	5.9	22.7
651A-3R-1, 35–36	10.7	23.5
651A-3R-1, 54–67	10.8	27.2
651A-4R-1, 97–98	20.9	17.9
651A-4R-2, 79–81	22.1	18.0
651A-4R-3, 53–67	23.3	18.5
651A-4R-6, 77–80	28.1	19.3
651A-7R-2, 140–150	52.4	1.9
651A-8R-1, 2–3	59.2	15.6
651A-8R-1, 87–88	60.1	25.2
651A-9R-1, 73–75	69.5	14.5
651A-10R-1, 70–71	79.0	15.0
651A-10R-1, 76–78	79.1	9.5
651A-11R-3, 37–40	91.4	2.8
651A-12R-1, 50–55	97.9	42.2
651A-12R-1, 66–68	98.1	18.7
651A-14R-1, 80–81	117.5	2.7
651A-14R-2, 59–60	118.8	18.2
651A-14R-2, 110–114	119.3	20.7
651A-14R-3, 72–76	120.4	13.0
651A-16R-1, 17–20	136.2	4.1
651A-17R-1, 66–68	146.4	6.7
651A-17R-3, 25–28	149.0	21.0
651A-18R-1, 74–77	155.6	34.9
651A-18R-5, 134–138	162.2	26.4
651A-18R-5, 140–150	162.3	34.1
651A-19R-1, 50–51	165.1	22.7
651A-20R-CC, 10–12	174.0	9.5
651A-20R-CC, 15–17	174.1	49.1
651A-22R-1, 14–15	193.6	6.8
651A-22R-1, 37–38	193.9	5.1
651A-22R-CC, 7–9	203.0	13.3
651A-23R-1, 28–30	203.5	20.6
651A-23R-1, 102–103	204.2	6.4
651A-23R-2, 85–88	205.6	6.5
651A-24R-1, 16–18	213.1	23.7
651A-24R-1, 68–70	213.5	35.4
651A-25R-1, 7–9	222.7	50.9
651A-25R-1, 54–57	223.1	69.6
651A-25R-2, 110–112	225.2	0.6
651A-25R-2, 115–117	225.3	0.2
651A-25R-3, 78–81	226.4	10.5
651A-26R-1, 60–62	232.9	20.0
651A-26R-1, 87–88	233.2	51.5
651A-26R-1, 145–146	233.7	4.4
651A-27R-1, 27–29	242.3	1.7
651A-27R-2, 8–10	243.6	35.8
651A-27R-2, 68–69	244.2	35.6
651A-27R-2, 74–75	244.2	28.5
651A-28R-1, 109–110	252.7	12.7
651A-28R-2, 82–85	253.9	9.4
651A-28R-3, 33–34	254.9	31.0
651A-29R-1, 64–66	261.8	7.3
651A-29R-1, 81–82	262.0	27.8
651A-29R-2, 8–10	262.8	8.3
651A-31R-1, 142–144	281.8	0.9
651A-31R-2, 16–18	282.1	0.7
651A-34R-1, 53–55	309.8	30.5
651A-35R-1, 6–8	319.0	34.9
651A-35R-1, 97–99	319.9	8.4
651A-35R-1, 116–117	320.1	10.5
651A-35R-3, 16–17	322.1	49.7
651A-35R-5, 88–90	325.8	9.0
651A-36R-1, 54–56	329.1	13.0
651A-36R-3, 7–10	331.7	27.1
651A-36R-3, 47–48	332.1	60.4
651A-36R-5, 58–60	335.2	44.3
651A-38R-2, 107–110	350.4	39.7
651A-38R-3, 36–38	351.2	23.1
651A-38R-3, 107–108	351.9	54.0
651A-38R-4, 67–68	352.9	37.1
651A-38R-4, 94–96	353.2	50.2
651A-38R-4, 140–142	353.7	29.8
651A-39R-1, 43–47	357.9	63.4
651A-39R-1, 100–102	358.5	44.7
651A-39R-1, 104–111	358.6	59.5
651A-39R-2, 68–74	359.7	45.1
651A-39R-3, 125–135	360.8	45.1
651A-39R-3, 140–150	361.0	44.0
651A-39R-4, 19–21	362.2	52.7
651A-39R-4, 68–75	362.6	49.9
651A-39R-4, 119–121	363.2	59.3
651A-40R-2, 55–60	369.3	49.3
651A-40R-4, 55–60	372.3	50.4
651A-41R-1, 48–49	377.3	55.0
651A-41R-4, 14–20	381.4	60.9
651A-41R-5, 104–106	383.8	12.4
651A-41R-CC, 2–3	386.2	64.9

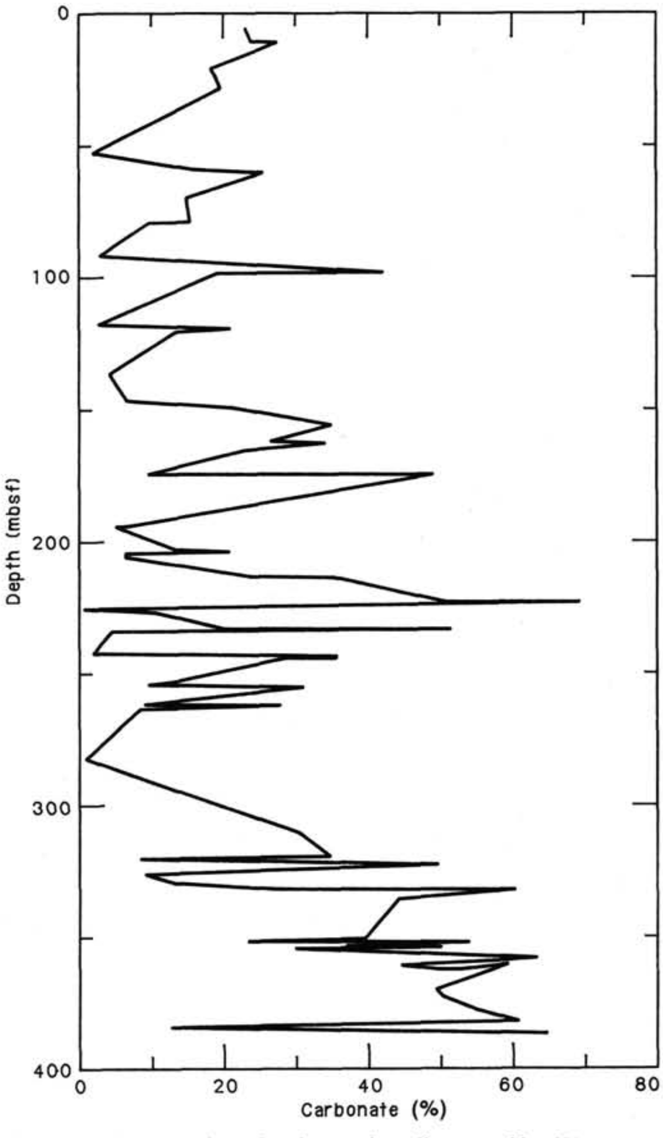

Figure 27. Concentration of carbonate in sediment at Site 651.

When comparing the results of Site 651 and those of Site 650 with previously published interstitial water results (e.g., Sayles and Manheim, 1975; Gieskes, 1975), several unusual features characterize downhole variations of interstitial water composition in Tyrrhenian sites: While magnesium concentrations in pe-

Table 8. Chemical analyses of interstitial water samples for Site 651.

Sample no. (interval in cm)	Depth	Sal.	Alk.	pH	Cl^-	SO_4^{2-}	Ca^{2+}	Mg^{2+}	Ca/Mg
Surface water		39.5	2.46	8.11	582	15.1	3.5	30.7	0.11
1R-3, 140-15	4.4	39.5	3.59	7.54	663	28.2	11.6	59.9	0.19
3R-1, 54-67	10.8	37.0	5.01	7.84	574	13.6	9.8	26.7	0.37
4R-3, 54-67	23.3	40.0	6.34	7.78	493	20.6	18.3	40.3	0.45
7R-2, 140-150	52.4	39.0	2.49	8.19	612	13.1	2.9	25.2	0.12
12R-1, 50-55	97.9	40.0	n.d.	n.d.	621	20.9	48.7	11.2	4.33
14R-3, 25-29	120.0	39.5	1.47	7.09	584	26.0	50.7	13.5	3.76
18R-5, 140-150	162.3	39.0	1.99	7.59	594	18.62	23.5	22.5	1.05
23R-1, 140-150	204.6	39.0	1.68	7.65	559	19.7	24.6	15.8	1.56
26R-1, 140-150	233.7	39.2	2.07	7.48	582	28.8	19.5	41.4	0.47
34R-1, 140-150	310.7	39.0	2.53	7.50	587	11.0	6.7	15.6	0.43
37R-2, 20-27	339.9	40.5	n.d.	n.d.	567	28.7	24.2	37.6	0.64
37R-4, 20-27	342.9	36.0	n.d.	n.d.	574	34.1	27.8	47.7	0.58
39R-1, 104-111	358.5	36.0	n.d.	n.d.	n.d.	31.6	25.8	48.0	0.54
39R-2, 68-74	359.7	34.0	n.d.	n.d.	545	27.3	21.6	43.9	0.49
39R-3, 127-135	361.8	39.0	2.05	7.5	576	31.8	30.7	50.6	0.61
39R-4, 69-75	362.7	36.0	n.d.	n.d.	564	24.9	19.4	40.8	0.48
40R-2, 55-60	369.3	36.0	n.d.	7.46	522	24.9	19.4	40.8	0.48
40R-3, 39-44	370.6	34.0	n.d.	n.d.	535	17.6	25.9	41.9	0.62
41R-2, 14-20	378.4	32.0	2.05	7.59	509	26.4	13.1	39.9	0.33
41R-4, 14-20	381.4	35.0	n.d.	n.d.	543	27.6	14.5	42.0	0.35

Hole 651A. Sample no.: Hole 651A, Core-Section, Interval. Depth is given in meters below seafloor. Sal.: Salinity in parts per thousand; Alk.: Alkalinity in mmol/L; Cl^-, SO_4^{2-}, Ca^{2+}, Mg^{2+} are given in mmol/L.

lagic and hemipelagic sediments usually decrease with depth—balanced by an equivalent increase in calcium—the palagonitization of abundant volcanic ash appears to counterbalance this diagenetic loss in Site 650 and 651 pore waters. It is assumed that magnesium is either taken up by carbonates (formation of dolomite, $CaMg(CO_3)_2$) or by neoformed silicate minerals, i.e., trioctahedral smectite ($(Na,1/2\ Ca)\ Mg_6Si_8O_{20})OH_4{\cdot}nH_2O$ and chlorite $(Mg,Al,Fe)_{12}(Si,Al)_8O_{20}(OH)_{16}$.

According to Fischer and Schmincke (1984), chemical changes during weathering of volcanic glass of basaltic composition release predominantly sodium, calcium, and magnesium. Calcium may immediately precipitate as calcite at elevated alkalinity values. The massive release of magnesium from the basement (Core 107-651-42R) is presumably responsible for the conspicuous alteration of primary nannofossil chalk to reddish brown dolostone in immediately overlying sediments, presumably at low temperatures: at temperatures encountered in young oceanic crust formed at mid-ocean ridges, magnesium usually is quantitatively removed from the pore waters (Mottl and Holland, 1978; Rona and Lowell, 1980). At Site 651, no convincing evidence for both extensive hydrolysis of silicate minerals and high-temperature hydrothermal alteration of fresh basalt can be detected: pH values do not increase significantly above 7.5, alkalinity values remain close to the baseline value of 2 mmol/L encountered throughout the sedimentary section (except for the slightly elevated values in the not too prominent zone of sulfate reduction at about 20-50 mbsf), and sulfate concentrations do not decrease. Sedimentological observations and smear slides give no indication of pyrite and sulfide formation in general. The depletion of chloride in the lowermost samples of Cores 107-651A-40R and 651A-41R is quite puzzling. Under these low-temperature conditions, the formation of ferro-apatites or mica containing chloride seems unlikely.

SEISMIC STRATIGRAPHY

Seismic Units

Site 651 is located on the eastern flank of a broad basement swell bisecting the Vavilov Basin at shot point 168 on MCS line ST12 (Fig. 29). Inspection of this seismic line as well as line ST03 and other single-channel seismic lines (Moussat, 1983) shows two main seismic characteristics: (1) strongly diffractive and irregular surface relief on the acoustic basement, and (2) a well-layered series of alternatively low- and high-amplitude reflectors filling basement depressions. Three main seismic units can be distinguished by both differentiated seismic characteristics and slight unconformities.

Seismic Unit One

This unit extends from the seafloor to the top of a high-amplitude reflector detected throughout the entire basin. Unit One shows a rather constant thickness (except near the top of the basement swell) of about 0.13 s. Interval velocity as given by MCS line processing is 1.64 km/s; the base of the unit should thus be at about 100-110 m sub-bottom. A few internal reflectors are seen within Unit One, particularly at the site location and in the vicinity of the top of the basement high (Fig. 29).

Seismic Unit Two

This unit, made of alternating high- and low-amplitude reflectors, is slightly unconformable with Unit One. This is particularly seen along the basement slope (Fig. 29) where Unit Two seems to have been eroded. The base of Unit Two is marked by a series of closely-spaced reflectors also slightly unconformable with Unit Three. At Site 651 the interval velocities vary from 1.64 to 1.70 km/s. These values indicate that the base of the unit lies at about 290 m sub-bottom (190 m thick). However, Unit Two thickens considerably toward the eastern and western Vavilov sub-basins. There the thickness may locally be as much as 0.6 s (about 500 m).

Seismic Unit Three

At Site 651 (Fig. 29) Unit Two rests unconformably on Unit Three, which can be divided into two subunits, Subunits 3A and 3B. Subunit 3A is made of slightly undulating reflectors. Subunit 3B comprises discontinuous high-amplitude reflectors progressively pinching out against the acoustic basement slope. At the site location Subunit 3A is rather thin (about 0.03 s) while Subunit 3B is about 0.05 s thick. Evaluation of sub-bottom depths of both subunits is difficult due to a sharp jump of interval velocities occurring between Subunits 3A and 3B (from 1.70 to 3.70 km/s). The base of Unit Three may be at about 450 to

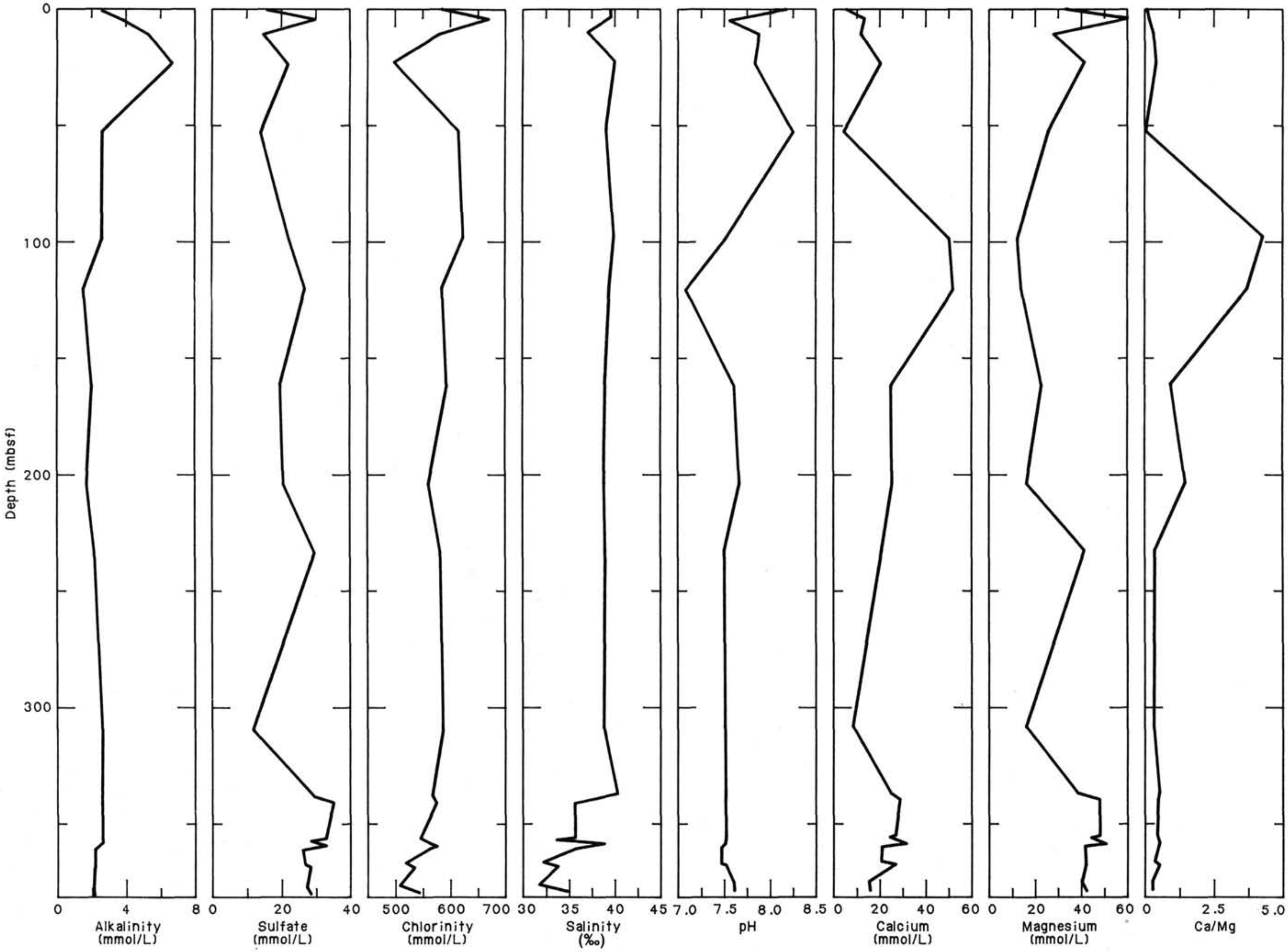

Figure 28. Summary of pore water chemistry at Site 651.

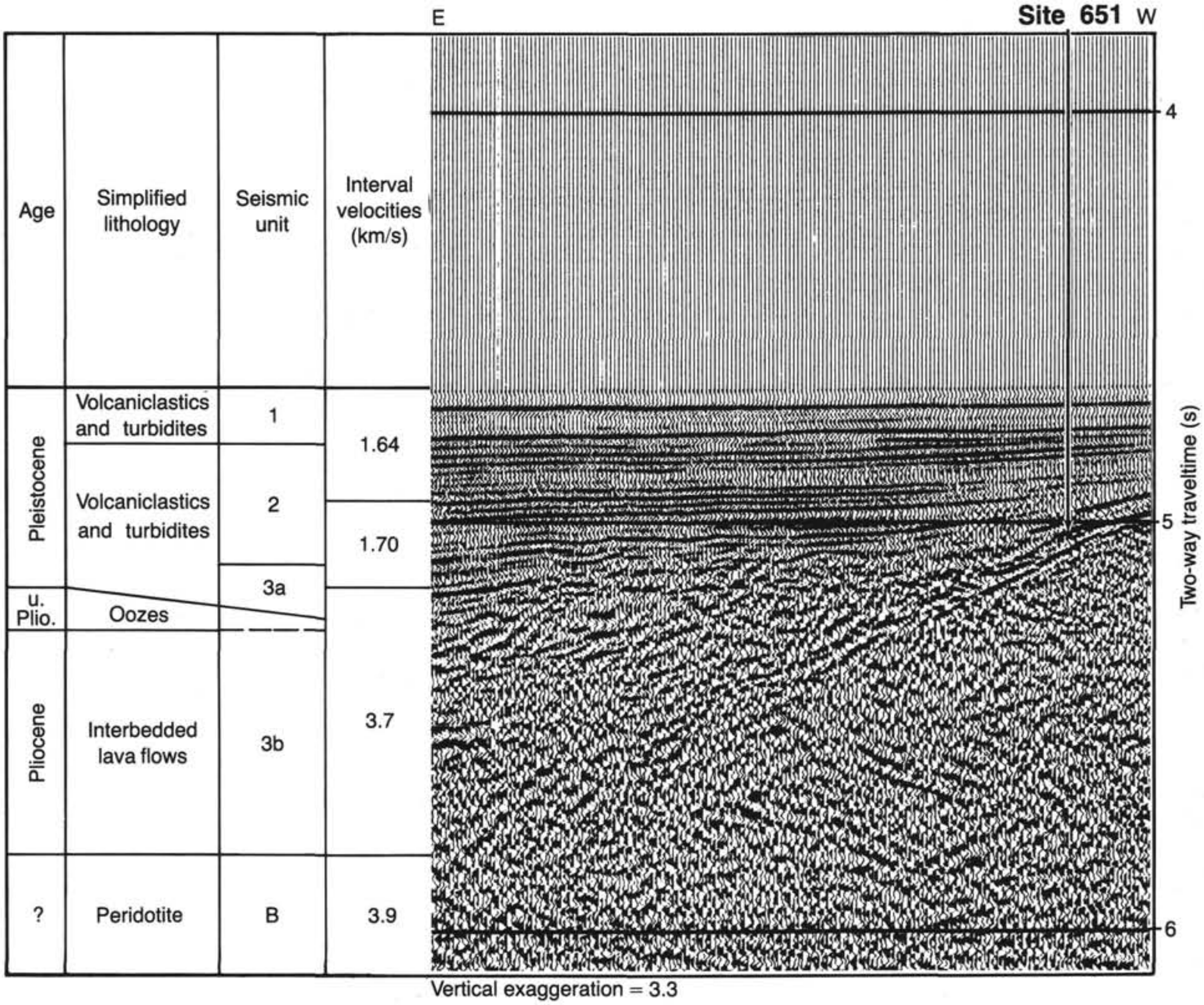

Figure 29. Summary of seismic stratigraphy from MCS Line ST12.

480 m below sub-bottom (thickness on the order of 160–190 m) or it may be shallower (about 350–380 m).

Acoustic Basement

The lowermost unit, referred to as acoustic basement, is bounded at its top by a very strong reflector gently dipping eastward beneath the preceding units. Toward the west the reflector rises progressively toward the top of the basement high. Interval velocities from multichannel processing range from 3.9 to 4.33 km/s, depending on the area. A few refraction data reported from the Vavilov Basin (Recq et al., 1984) indicate values between 3.4 and 4.02 km/s at a depth of 600 m to 1.3 km below seafloor.

Previous Lithologic and Stratigraphic Interpretations

As for the Marsili Basin (Site 650), correlation between seismic reflection lines and lithostratigraphy is not easy for the Vavilov Basin. Fabbri and Curzi (1979) believe that the entire Vavilov Basin contains mostly Pleistocene to Pliocene sedimentary sequences referred to as "A" and "B." Possibly the basin fill includes marginal-type Messinian evaporites, but there is no direct seismic evidence of their occurrence. Malinverno et al. (1981) also believe that the well-layered seismic reflectors represent Pliocene to Pleistocene deposits, possibly overlying Messinian clastic and thin lacustrine deposits. Moussat (1983) proposes that the basin is floored by an oceanic-type crust, but only of very small extent. Moussat (1983) indicates also the possible occurrences of Messinian volcaniclastics, particularly in the vicinity of large volcanoes such as Vavilov Seamount.

Synthetic *P*-Wave Seismogram

A synthetic *P*-wave seismogram was calculated based on physical-properties measurements of velocity and bulk density. The laboratory results used are shown graphically in Figure 24. The data were linearly interpolated onto an evenly spaced 1-m grid and then input to a simple 1-D convolutional synthetic seismic program. The wavelet used was 25-Hz Ricker type. Attenuation and spreading effects are unaccounted for in the synthetic seismogram. Internal multiples are included but seabed multiples are not.

The seismogram calculated here, shown in Figure 30, should be compared with the site survey reflection line ST12 (Fig. 29). The quality of correlation indicates that synthetic seismograms based on physical properties data are an effective tool for monitoring progress while drilling.

A brief comparison between seismic line ST12 at Site 651 and the synthetic seismogram points out the following features:

1. The base of Seismic Unit One (4.790 sbsl) appears as a prominent reflector on the synthetic seismogram at about 120 mbsf. Polarity is probably the same as that for the reflection line.

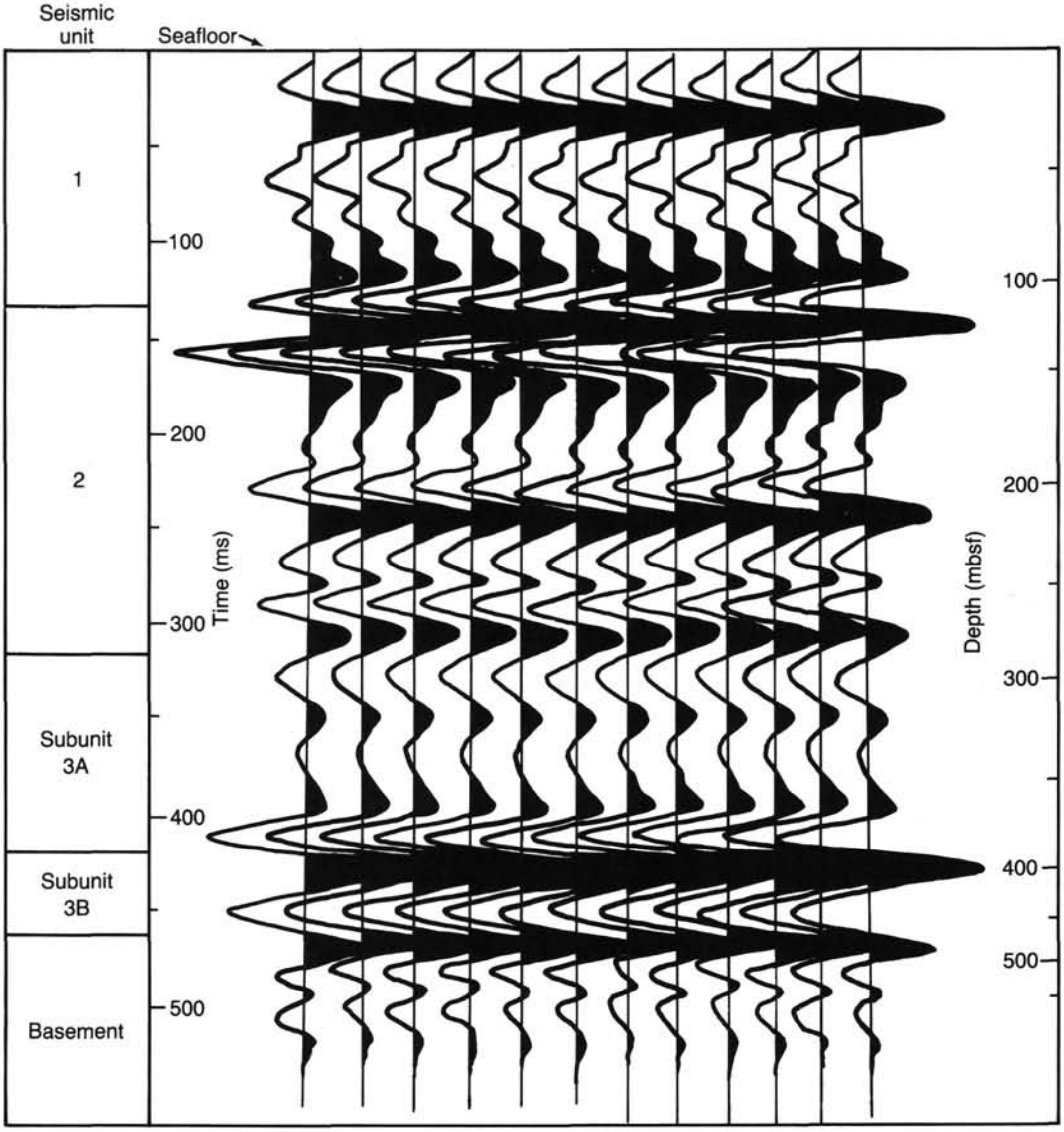

Figure 30. Synthetic seismogram constructed from physical-properties data (see "Physical Properties" section, this chapter). Scale in milliseconds (twtt) from the sea bottom on the left. Scale in meters on the right (note that the scale is not linear).

2. Seismic Unit Two is a complex series of interfering low-amplitude reflectors. The base of the unit at 5.02 sbsl on the reflection line is poorly resolved on a synthetic seismogram calculated from physical-properties measurements. The most likely depth for the base of this unit is 300 mbsf.

3. The base of Seismic Subunit 3A is seen as a major basal reflector on the synthetic seismogram at 5.08 sbsl. This corresponds to the sediment/basalt contact, occurring at a depth of about 390 mbsf.

4. The last high-amplitude reflector seen on the synthetic seismogram corresponds to an increased velocity and density which occurs near the top of the basement. Laboratory compressional wave velocities indicate that less important changes in physical properties occur below this level.

Comparison with Drilling Results

Drilling at Site 651 established the following points:

1. Seismic Unit One clearly corresponds to dominantly volcanogenic sediments interbedded with marly mud. The few discontinuous, high-amplitude reflectors seen on profile ST12 probably correlate with distinct pumiceous sand and gravel cemented breccia. There is a slight discrepancy (about 20 m) between Seismic Unit One and sedimentary Unit I. This may be an effect of interval velocities. According to shipboard velocity measurements, compressional wave velocity reaches values around 2.5 km/s in samples between 100 and 120 mbsf. This depth is consistent with a bottom of Unit One at about 100–110 mbsf.

2. Seismic Unit Two correlates with the upper levels of sedimentary Subunit IIa, consisting of nannofossil chalk with subordinate volcanogenic turbiditic claystone and siltstone.

3. Seismic Unit Three (Subunit 3A) correlates with the remaining levels of sedimentary Unit II, consisting of nannofossil chalk to colored dolomite with sediment lying just above the basalt contact. Subunit 3B is correlative with the lava flows and basaltic breccias drilled from 388 to 464 mbsf.

4. Site 651 bottomed in a serpentinized peridotite complex. This basement unit correlates with the seismic basement reflector. One observes a difference between interval velocities as derived from seismic (3.9–4.33 km/s, depending on the area) and

shipboard compressional wave velocities (5-6 km/s). One may suspect that the basement is strongly altered (serpentinized peridotites) and that shipboard measurements have been performed on better-preserved pieces.

DOWNHOLE MEASUREMENTS

Summary of Logging Operations

Logging operations at Site 651 began at 0030 hr 17 January 1986. Drill pipe was positioned downhole at 119 mbsf to avoid possible disturbances above. Four logging runs were planned: (1) gamma ray-caliper-velocity-resistivity (GR-CALI-LSS-DIL) and (2) density-porosity-spectral gamma ray (LDT-CNT-NGT), over the entire length of the drill hole; (3) borehole televiewer (BHTV); and (4) induced spectral gamma ray (GST) in the crystalline basement.

The velocity-resistivity combination tool would not pass below 339 mbsf because of a hole obstruction. It was decided to log the first two runs from this depth before attempting to ream deeper with the drill string. The density-porosity string would not pass below 273 mbsf and was logged up from that depth. As seen on the caliper log, this is the top of a severe hole constriction. Attempts to clear the hole failed when the drill string became stuck at the same depth. In light of the apparent danger to the drill string all further logging runs were abandoned.

Discussion of Results

A summary of the logged intervals and measurements obtained at Site 651 is given in Table 9. The original logging data are displayed in this chapter, before the barrel sheets.

Log-stratigraphic Interpretation

Logs permitted an accurate determination of stratigraphic boundaries as well as inferences about unrecovered intervals. Log data indicate that four log-stratigraphic units are present within the logged section at Site 651; the division into log-stratigraphic units is shown in Figure 31, along with the core recovery, the computed relative percentages of volcaniclastic and pelagic sediments, and the results of carbonate analysis obtained on board.

Unit 1: 119–155 mbsf

This unit is marked by high levels of uranium and thorium, and velocity > 1.75 km/s. The high-velocity–high-radioactivity intervals are interpreted as coarse-grained volcaniclastic rocks and sediments in a siliceous cement. The increase in velocity (as much as 2.3 km/s) and density (as much as 1.9 g/cm^3) and the lower porosity values (about 50%) in the interval from 120 to 131.5 mbsf indicate an even higher degree of cementation, but may also be due to variations in water content. Intercalations of carbonate oozes are rare; the low radioactivity, velocity, and resistivity indicate these intervals are thin interbeds in a predominantly volcanic section extending roughly to the base of Core 107-651A-17R (155 mbsf).

Unit 2: 155–267 mbsf

Log interpretation indicates Unit 2 to be primarily composed of volcaniclastic sediments, with a somewhat lower pelagic input. This unit is divided into four subunits based on calculated relative percentages of volcanic and pelagic sediments.

Unit 2a: 155–180 mbsf
Unit 2b: 180–208 mbsf
Unit 2c: 208–237 mbsf
Unit 2d: 237–267 mbsf

The uppermost interval, Unit 2a (155–165 mbsf), is characterized by generally lower radioactivity, and velocity less than 1.75 km/s. Beginning at the top of Core 107-651A-18R (155 mbsf) the unit is dominantly composed of homogeneous pelagic carbonates, the volcanic material gradually increasing downward. The sequence from 160 to 180 mbsf, with steadily increasing velocity, density, and resistivity, is interpreted as a coarsening downward, possibly turbiditic, deposit. The high density and velocity and low radioactivity readings at the base of the unit suggest this is a well-cemented low porosity carbonate.

In Unit 2b, both radioactivity and velocity logs appear to be good indicators of high volcanic input. Unit 2b is predominantly composed of volcanic sands and gravels as in Unit 1. Smaller layers of pelagic oozes are also evident but contribute only a small fraction (<20%) to the total sediment thickness.

Unit 2c is dominantly chalk. At least two distinct volcanic deposits are recognized as high radioactivity intervals at 222 and 227 mbsf.

Unit 2d is interpreted as consisting of mainly volcaniclastic sediments interbedded with chalks.

Unit 3: 267–315 mbsf

The top of Unit 3 is marked by a sharp reduction in hole diameter on the caliper log, to below 6 in. (15 cm). Log analysis becomes more difficult in this unit because density, porosity, and spectral gamma ray tools were unable to pass below the constriction at the top of the unit. Velocity, resistivity, and natural gamma ray logs reveal the section to be quite homogeneous. Recovery in this unit, Cores 107-651A-30R to 651A-34R, averaged only 10% of dominantly pelagic sediments. Nonetheless, high natural radioactivity and increased velocity indicate a significant thickness of volcaniclastic sediments similar to Unit 2d. The tendency of the hole toward ledging and bridging off is unique to this unit. Pelagic sediments recovered in Cores 107-

Table 9. Summary of log measurements at Hole 651A.

Mnemonic	Tool	Measurement	Unit	Depth (mbsf)
CALI	Caliper	Hole size	in.	119.0–328.0
GR	Natural Gamma Ray	Natural radioactivity	GAPI	119.0–329.0
DIL	Dual Induction	Deep, medium, and focused resistivity	$\Omega \cdot m$	119.0–338.0
LSS	Long Spacing Sonic	Sonic transit time (short and long spacing)	μs/ft	119.0–324.0
LDT	Lithodensity	Bulk density photoelectric effect	g/cm^3 b/elec	119.0–269.0
CNT	Compensated Neutron	Porosity	%	119.0–262.0
NGT	Natural Gamma Spectrometry	Total (Th + U + K) and computed (Th + K) natural radioactivity uranium, thorium, potassium	GAPI ppm wt%	119.0–258.0

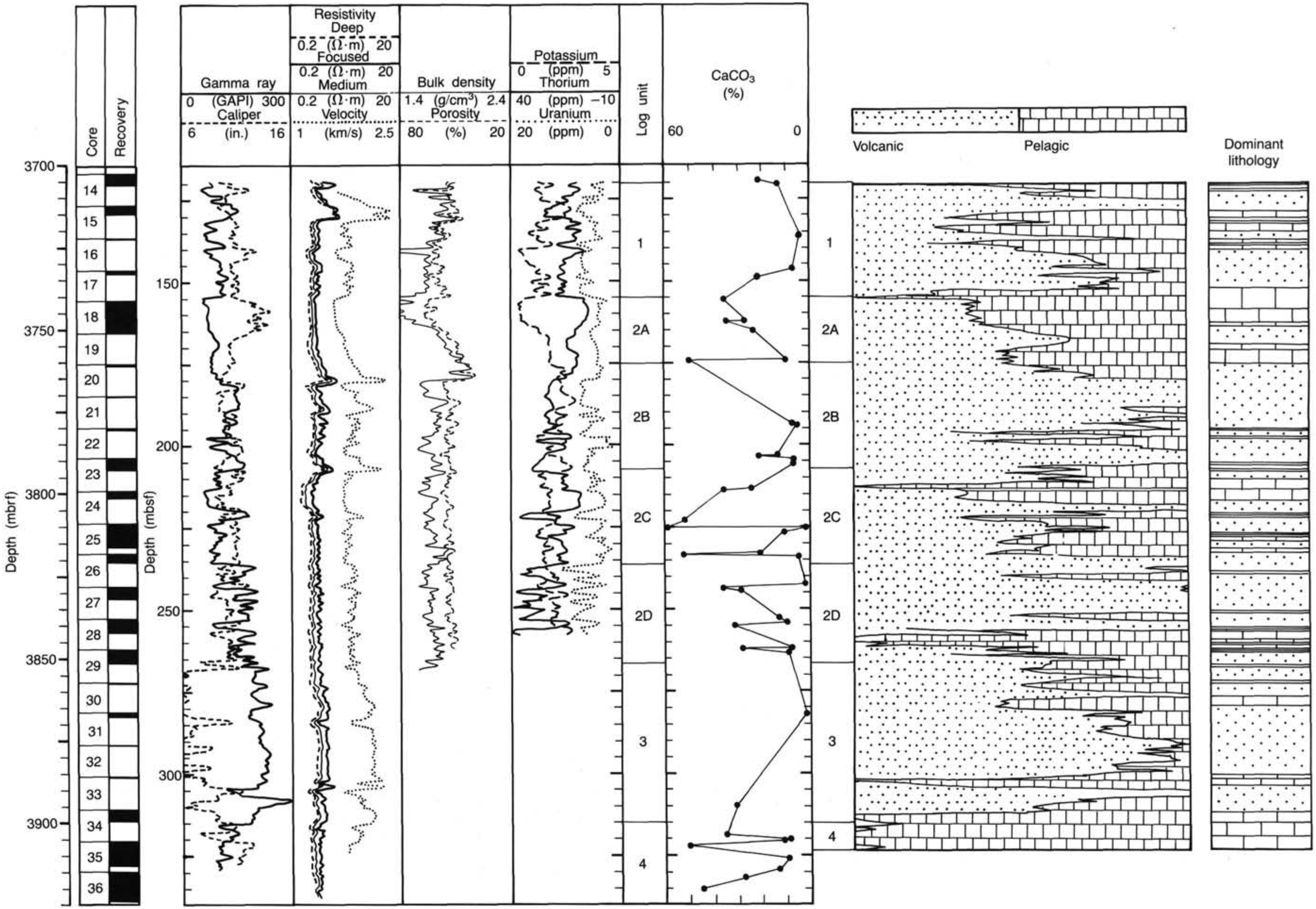

Figure 31. Logging data and log stratigraphic interpretation as a function of depth at Site 651. Relative percentages of volcanogenic and pelagic sediments are least-square estimates computed from gamma ray and velocity data. Volcanic sediments account for roughly 55% of the total sedimentary thickness of the logged interval. Results of carbonate analysis obtained on board are shown as well. Logging data are smoothed using a 5-point running average filter. Data are acquired every 0.15 m.

651A-30R to 651A-33R are seen on the logs as distinct intervals at 283 and 305 mbsf.

Unit 4: 315–338 mbsf, Bottom of the Logged Interval

Unit 4, on the basis of low radioactivity, low velocity, and low resistivity, is interpreted as indicating a predominantly pelagic sediment. Excellent core recovery confirms this result. Low radioactivity indicates an absence of volcaniclastic sediments in this interval.

Volcaniclastics

The rough percentages of volcanogenic and pelagic sedimentation in each of the log-stratigraphic units are shown in Figure 31. Relative percentages are least-square estimates calculated from gamma ray and velocity log data. Volcanic sediments account for roughly 55% of the total sediment thickness in the logged interval, 119–335 mbsf. This implies core recovery is sharply biased in favor of pelagic sediments at the expense of coarser volcanogenic sediments. Thus the importance of volcanic sedimentation would be seriously underestimated from examination of the recovered rocks alone.

Table 10 shows the average values of Th, U, and K in the first two log-stratigraphic units. The distinctively high concentrations of U and Th (Adams and Weaver, 1958) and the proximity of Site 651 to land would suggest either the Roman or Campanian volcanic province as origin of the volcaniclastic material. The Quaternary alkaline volcanites of the northern Roman province exhibit unusually high contents of thorium and uranium, at least five times larger than those typically observed in rocks of similar chemical composition (Locardi, 1967). The average values for products erupted since the beginning of the volcanic activity in this area (0.5–0.06 m.y.b.p.) range from 40 to 222 ppm and from 3 to 50 ppm for thorium and uranium respectively, with a Th/U ratio ranging from 4.3 to 5.5 (Civetta and Gasparini, 1973). These concentrations are much lower in the volcanics from the southern Roman province (Civetta et al., 1981) and from the Campanian province. In the latter, U and Th values range from 4 to 15 and from 15 to 50 respectively, the Th/U ratio ranging from 2.8 to 4 (Civetta and Gasparini, 1973). The average values of Th/U ratio computed at Site 651 from the spectral gamma ray log in the high radioactivity intervals fall in the 4.4–4.8 range, comparable to data from northern Roman province, but the absolute Th and U concentrations are markedly lower. Indeed, concentrations are closer to those of samples from the Campanian province, which show, however, lower ratios. Alternatively, one can imagine a dilution effect taking place as volcanogenic sediments are mixed with pelagic or terrigenous fragments during sedimentation. This would account for lower absolute uranium and thorium concentrations while maintaining a high Th/U ratio. The origin of the abundant volcanic material recovered at this site is therefore debatable: knowledge of the chemical composition and of the degree of alteration of these sediments is required to determine their provenance.

Logs indicate that the contribution of abundant clastic volcanic material to the sediment starts at 315 mbsf (Core 107-651A-34R, bottom of log-stratigraphic Unit 3). According to paleomagnetic and biostratigraphic data (see those sections, this chapter) this depth coincides with a break in the sedimentation rate, which changes from 2 cm/1000 yr (below 310 mbsf) to 27 cm/1000 yr. This break has been approximately dated to 0.73 m.y.b.p. and roughly corresponds to the onset of volcanic activity in the southern Roman province (Locardi et al., 1976).

Table 10. Average U, Th, and K concentrations at Site 651.

Log-stratigraphic unit	U	Th	K	Th/U
1 (119–155 mbsf)	5.8 ± 1.5	14.4 ± 4.8	1.5 ± 0.6	2.5 ± 0.6
2 (155–257 mbsf)	5.0 ± 1.9	18.6 ± 8.8	1.8 ± 0.6	4.0 ± 2.1
2A (155–180 mbsf)	4.1 ± 0.6	9.4 ± 3.5	1.4 ± 0.7	2.3 ± 0.8
2B (180–208 mbsf)	5.5 ± 1.8	22.2 ± 4.4	2.3 ± 0.4	4.8 ± 2.8
2C (208–237 mbsf)	4.2 ± 1.7	16.5 ± 6.7	1.6 ± 2.3	4.2 ± 1.6
2D (237–257 mbsf)	6.6 ± 2.1	28.1 ± 8.5	1.9 ± 0.4	4.4 ± 1.3

Note: No data below 257 mbsf.

Comparison of Logs and Physical-Property Measurements

Average core recovery in the logged interval was only about 28%. In zones of low recovery, depth matching between core and logs is difficult, but poor or biased recovery makes the definition of the physical properties by logs even more important.

Procedures and data from laboratory measurements are reported in the "Explanatory Notes" chapter, this volume, and in the "Physical Properties" section, this chapter. Data include bulk density, porosity, and compressional wave velocity. All physical property measurements were made at atmospheric conditions. Figure 32 displays the log curves superimposed on the core data. Log quality is quite good throughout the entire section; only in the 155–168 mbsf interval are the tool readings affected by severe hole enlargement.

In the uppermost interval, from 119 to 180 mbsf (log-stratigraphic Units 1 and 2a), log and core data display the same trends, even though core data must be depth-shifted 5–7 m (core recovery here was 31.7%). Log density ranges from 1.6 to 2.1 g/cm^3 opposite a well-cemented carbonate layer at 180 mbsf; porosity ranges from 40% to 65%; velocity from 1.65 to 2.3 km/s.

A fair agreement between log and sample velocity can be observed throughout the hole. The velocity below 180 mbsf is quite uniform down to 267 mbsf (bottom of Unit 2) with an average value of 1.83 ± 0.1 km/s, but tends to increase to 2.1 km/s in Unit 3. Scatter between log and sample velocities is largely attributed to small-scale heterogeneity, differences in confining pressure, elastic rebound, and depth-matching errors.

Throughout the entire hole, bulk density and porosity logs indicate values systematically lower than the laboratory measurements. Low neutron porosities (relative to benchtop samples) are probably more realistic estimates of *in-situ* porosities, primarily because of the elastic rebound experienced by the samples as they come to the surface. On the other hand, pressure rebound should decrease the measured sample densities with respect to the logs, the opposite of what is seen at Site 651. We believe an underestimate of bulk densities by logs is caused by infiltration of the drilling fluid between the formation and the detector skid. This condition is commonly accentuated by rugosity of the borehole wall (evidenced by Site 651 caliper measurements). As with velocity measurement, some scatter is also due to small-scale heterogeneity and depth mismatch.

Heat Flow

One downhole temperature measurement was made at a sub-bottom depth of 29.4 m by the Uyeda thermal probe. The temperature vs. time record shown in Figure 33. The bottom water temperature is 13.4°C as estimated from the 10-min station at about 20 m above the mud line on the way down and up. The temperature in the bottom sediment was found to fluctuate between 17.4°C and 18.0°C in this experiment. Although the fluctuations are probably caused by instability of the probe at the bottom, alternative causes are difficult to evaluate. At least two possible reasons for the fluctuations may be considered: (1) peaks represent frictional heating; (2) lows represent partial pullout or interference of bottom water. In any case, these fluctuations are relatively minor along the 20-min station so we take 17.7°C ± 0.3°C as the mean value for the sediment temperature. The temperature increase in the 29.4-m interval is thus 4.3°C, giving a geothermal gradient (Fig. 34) of 14.6°C ± 1.0°C/100 m considering the margin of error.

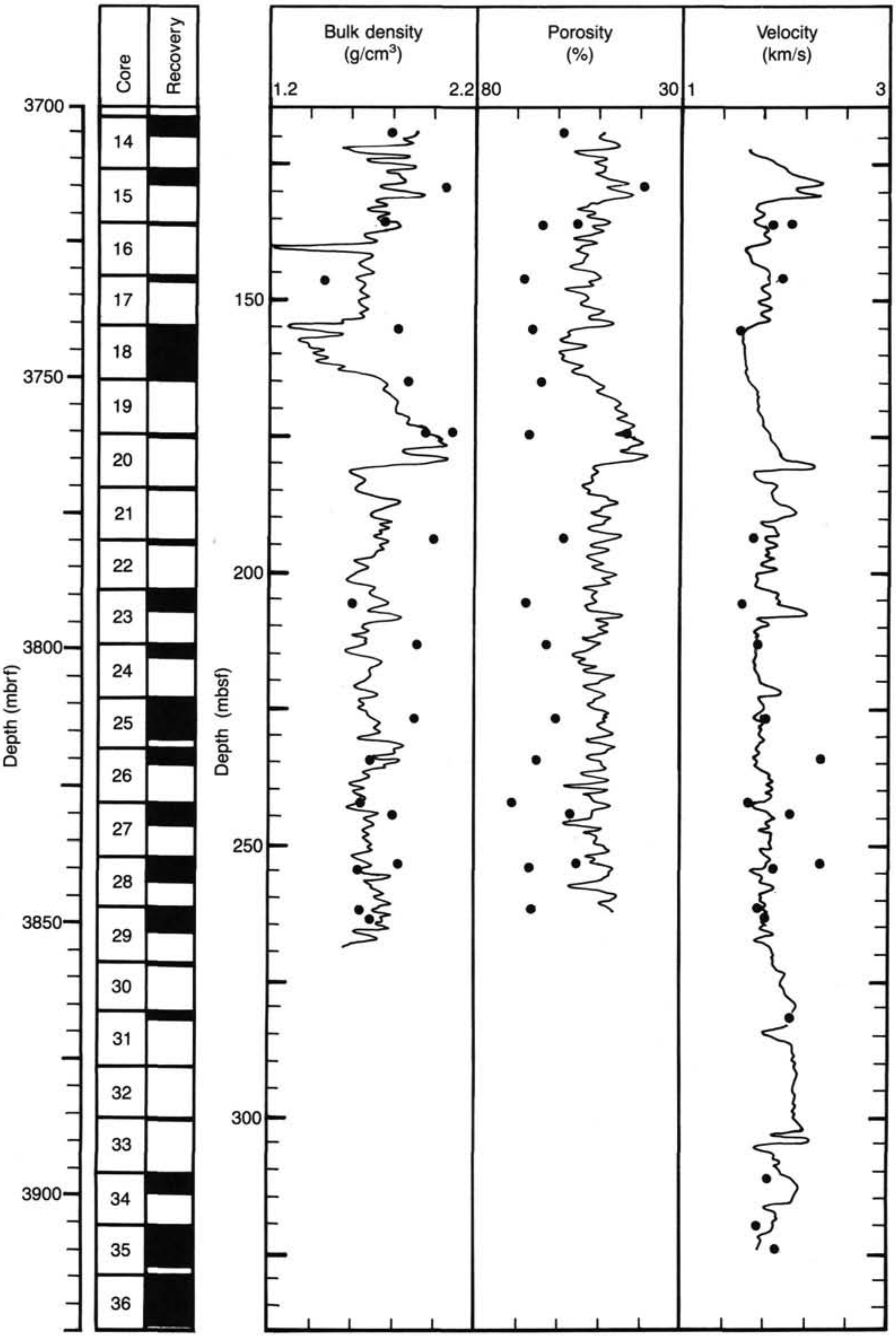

Figure 32. Logging and physical property data vs. depth at Site 651. Logs are smoothed using a 5-point running average filter. Data are acquired every 0.15 m. Dots indicate laboratory measurements on cored samples.

Only three thermal conductivity values are available for the interval considered (due to malfunction of the resistance-temperature conversion program on board). After reading other values measured on board, some improvement may be made to this estimate. The measurements at 9.2 m, 10.64 m, and 23.54 m are 0.980, 1.021, and 0.959 W/m/°C = 2.36 mCal/cm/s, respectively. The heat flow value at Site 651 is thus estimated to be 3.45 HFU = 144 mW/m^2.

Comments

It is difficult to make definitive conclusions on a determination based on one value. One can notice that it is within the

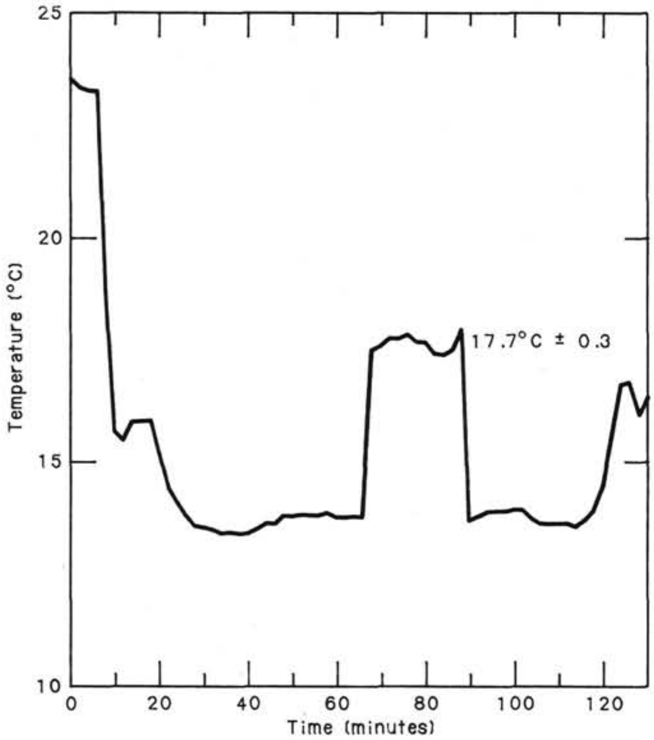

Figure 33. Downhole temperature measurement in Hole 651A at sub-bottom depth 29.4 m.

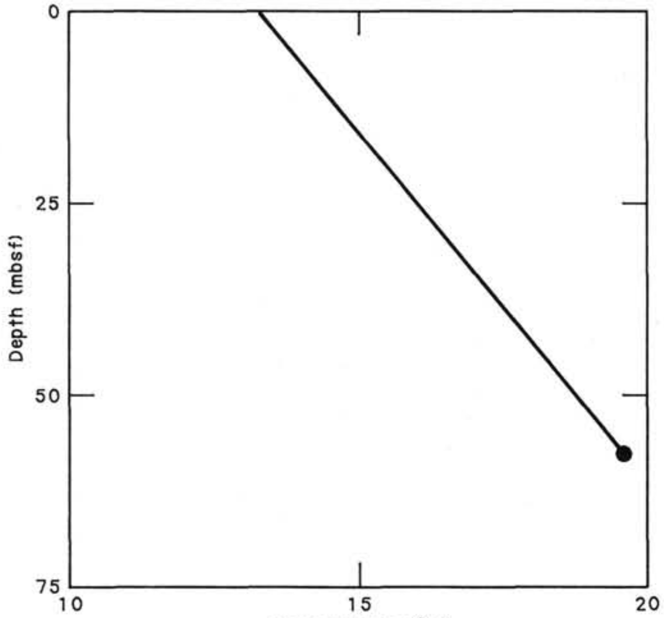

Figure 34. Downhole temperature vs. sub-bottom depth at Site 651.

range of the shallow probe measurements in nearby areas. This value fits especially closely with measurements made by Foucher and Rehault on a transect of the Vavilov Basin (Della Vedova et al., 1984; Rehault et al., 1984). A nearly symmetric heat flow anomaly overlies the axis of the northern Vavilov Basin with values ranging from around 90 mW/m^2 above both sides of the basement swell and 220 mW/m^2 above the top of the structure (Fig. 35). Our position on the flank of the basement for Site 651 indicates flow values similar to shallow probe measurements. The sediment blanketing effect here minimizes hydrothermal circulation within the structure (Sclater et al., 1980).

The scheduled heat flow program was canceled after this measurement because of poor hole conditions. The hole was unstable due to abundant coarse detrital and volcaniclastic formations; by the time drilling had penetrated deep enough for the hole to be sufficiently stable, the sediments were too firm to penetrate with the Uyeda probe.

DISCUSSION AND CONCLUSIONS

Site 651 achieved its primary objectives of identifying the nature of basement in the Vavilov Basin, and dating the overlying sediments. The basement turned out to be more complex, and the sediment younger, than had been anticipated.

Basement

Nature of the Basement

Drilling at Site 651 has established that, at least locally, basement consists of serpentinized peridotite, overlain by basalts and basaltic breccia, overlain in turn by an assemblage of dolerite, metasediments, and metadolerite, and then by a second unit of basalt. The horizontal extent of this basement complex is unknown, but it seems likely that the presence of peridotite near the sediment contact is not typical of the whole of the Vavilov Basin basement. We think it more likely that the recovered section is representative of Vavilov Basin's axial swell only. Our reasoning is as follows: The compressional wave velocities measured on samples from the upper basalt vary from 3.4 to 4.8 km/s with an average of 3.6 km/s. These laboratory measurements are compatible with an interval velocity of 3.7 km/s obtained for the seismic subunit 3A by processing of multichannel seismic data across the site. The 3.7 km/s layer extends across the basement swell and several kilometers eastward from the site; however, it does not appear to be present on the western side of the basement swell, suggesting that the basement there is significantly different in composition. The dolerite, lower basalt, and peridotites have an average velocity of 4.85 km/s on the samples measured on board. This average velocity is sensibly higher than the computed velocities from the site survey seismic line in the area (2.86–4.33 km/s) and the velocities calculated by Recq et al. (1984) with the refraction data (3.4–4.02 km/s) for a layer between 600 and 1300 mbsf. Once again, the basement complex recovered at Site 651 is not typical of the whole of the Vavilov Basin basement.

The observation of chilled margins in the basalts of both the first and third basement units suggests that both basalt units were emplaced as flows. The origin of the peridotite is more problematic; at least three different hypotheses can be considered. First, the peridotite could belong to an ophiolite complex which predates the opening of the Tyrrhenian. Within the circum-Tyrrhenian, ophiolite complexes of Mesozoic age are found in the Apennines, mostly in the Ligurian oceanic domain (Elter, 1975), in the Alpine Piemontese oceanic Tethyan realm (Dal Piaz, 1974; Lemoine, 1980), and in Alpine Corsica (Ohnenstetter, 1979). It seems plausible that the preexisting crust that was stretched and thinned during the rifting phase of Tyrrhenian extension might have included ophiolite slivers as well. As rifting and subsidence proceeded, fragments of preexisting crust, potentially including such Mesozoic ophiolites, might be left as islands amid basaltic oceanic crust. Secondly, the Site 651 peridotites could represent a sliver or protrusion of mantle material emplaced during the final phase of continental rifting, analogous to the case of other rifted passive margins such as the Red Sea or the Atlantic Iberian margin (Bonatti et al., 1981; Boillot

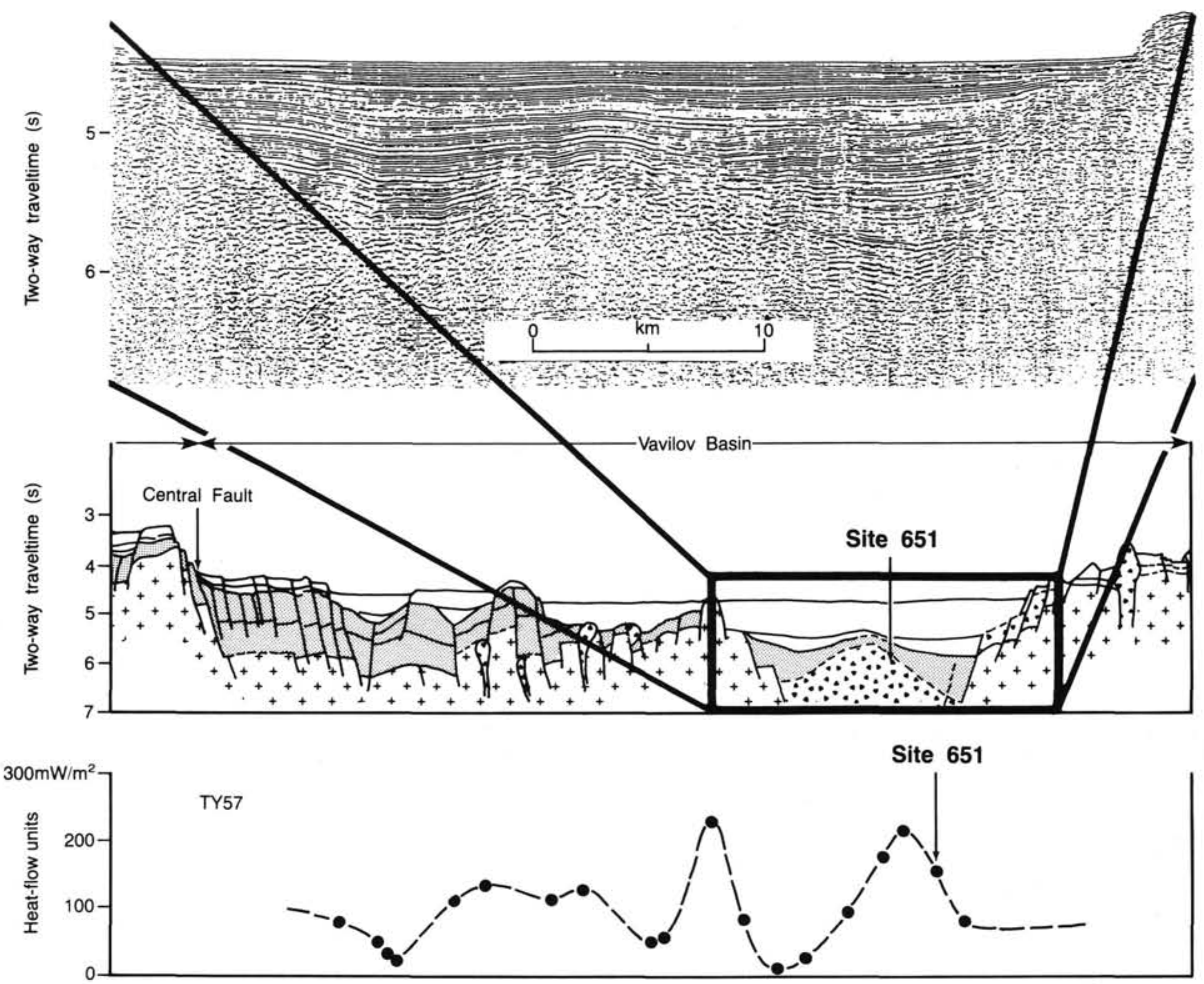

Figure 35. Reflection seismic profile, geological sketch, and surficial heat flow measurements across the Vavilov Basin in the vicinity of Site 651 (after Della Vedova et al., 1984; Rehault et al., 1984).

et al., 1980). Finally, the peridotite could be associated with faulting within oceanic crust, along either a transform fault or a normal fault oriented perpendicular to the direction of regional extension, as in the case of the Mid-Atlantic Ridge (Bonatti, 1976).

A hypothetical sequence of events which could account for the varied basement lithologies at Site 651 is as follows: (1) an upper mantle body protruded through thinned continental crust, (2) basaltic flows covered the peridotite body, (3) a thin layer of sediment was deposited on top of the basalt, (4) additional basalt flows were emplaced on top of the sediment, and (5) a new basaltic injection formed a dolerite sill at the level of the thin sedimentary layer, altering the sediment by contact metamorphism.

Age of Basement at Site 651 and Age of the Vavilov Basin Basement

Site 651 was located on the slope of a basement swell; consequently, an estimate of regional basement age requires first an estimate of the local basement age at Site 651, and then an extrapolation to the apparently older parts of the basin away from the basement swell.

The dolomite-rich, red-brown sediments immediately above the sediment/basalt boundary has not been directly dated: alteration has apparently destroyed the fossils and overprinted the magnetic signature. The oldest biostratigraphic age from Site 651 was derived from planktonic foraminifers (Zone MPl6) and nannoplankton (Zone NN18) found in chalk about 40 m above the upper basalt flows (348 mbsf). This age (about 2 m.y.) is consistent with the occurrence of the base of the Olduvai magnetic event (1.87 m.y.) at 345 mbsf and with the tentatively identified top of the Reunion magnetic event (2.01 m.y.) at 347 mbsf. The sedimentation rate for the deepest datable interval (from 310 mbsf to 345 mbsf, Brunhes/Matuyama magnetic epoch boundary to base of Olduvai) was approximately 3 cm/1000 yr. Extrapolation of this rate down to the sediment/basalt contact gives an age of 3.6 m.y. for the base of the sedimentary section; however this extrapolation is based on the unsupported assumption that sedimentation rate in the red-brown basal sediments is the same as in the overlying sediments.

Globoratalia crassaformis has been tentatively identified in thin section within the carbonate cement of a basalt breccia at 465 mbsf. The possible presence of this species would suggest an age of approximately 3.1 m.y. for the breccias just overlying the peridotite basement complex.

The seismic signature of the sedimentary section at the depth of Site 651's deepest reliable biostratigraphic date (about 2 m.y.; 348 mbsf) is numerous subparallel, slightly undulating, subhorizontal reflectors. Individual lithologic units cannot be assigned to these reflectors on a one-to-one basis; instead the reflectors presumably represent interference patterns between the seismic wavelet and the sediment structure. Nonetheless the subparallel reflectors are assumed to approximate time horizons. On this basis, it is possible to extrapolate along the seismic profiles, from the position of Zone MPl6/NN18 at Site 651, to that part of eastern half of Vavilov Basin where the sediment column is thickest. The lateral equivalent of MPl6/NN18 then falls at 420 ms below seafloor, within a total sediment column 850 ms thick. Thus, if the sedimentation rate in the lower half of the sedimentary column had been comparable to that in the upper half, the age of sediment just above basement would be early Pliocene.

Although an absolute age cannot be assigned to the oldest sediments overlying the basement of Vavilov Basin, we can state with confidence that the oldest sediments in Vavilov Basin predate the oldest sediments of the Marsili Basin, possibly by several million years. The oldest biostratigraphic unit identified at both Sites 650 (Marsili Basin) and 651 was MPl6/NN18, with an age of slightly less than 2 m.y. However, in the Marsili Basin MPl6/NN18 coincided with the deepest sedimentary seismic unit in the basin, whereas in the Vavilov Basin MPl6/NN18 coincided with an acoustic reflector which is only halfway down through the sediment column.

Sediments

The sediments overlying the upper basalt unit comprise two lithologic units. Unit I, between 0 and 136 mbsf, consists of volcanogenic sediments interbedded with volumetrically subordinate (<15%) marly, nannofossil-rich mud. Unit II (136–388 mbsf) consists mostly of nannofossil chalk with subordinate volcanogenic claystone and siltstone.

Clastic Sediments

Sedimentary Unit I (0–136 mbsf) is dominated by pumiceous sand, gravel, and cemented breccia; pelagic sediment is clearly subordinate. Siliciclastic as well as volcaniclastic sediments are present. The provenance of the siliciclastic sediments is mainly igneous source areas, but occurrences of sedimentary and metamorphic rocks indicate continental source areas as well. Sedimentary structures in the clastic sediments indicate reworking and redeposition by mass flows and turbidity currents. Occurrences of shelf-derived microfauna as well as metamorphic lithic fragments suggest that these gravitationally-driven flows have originated on the Italian mainland to the east and northeast of the site. From 107 to 126 mbsf, a thick layer of cemented breccias results from lithification of breccia clasts by both carbonate and opaline silica. The siliceous cement probably formed by dissolution of volcanic glass during early diagenesis.

Subunit IIa (136–309 mbsf) is lithologically heterogeneous and comprises volcaniclastic siltstones and sandstones interbedded within fine-grained carbonates. The abundance of clastic sediment decreases downsection within the subunit. The natural gamma ray log through this interval suggests that the volcaniclastic sediments have a relatively high content of U and Th, which may indicate a provenance in the Roman (or Tuscanian) volcanic province.

Changes in Sedimentation Regime Through Time

The curve of sediment depth vs. age (Fig. 15) shows two breaks in slope, both indicating an increase in sedimentation rate through time. The lower break in slope, from 3 to 27 cm/1000 yr, occurs approximately at the Brunhes/Matuyama boundary (0.73 m.y.b.p.), in the lower part of sedimentary Unit IIa (310 mbsf). Below this depth, the sediments are dominated by planktonic foraminiferal chalks with only thin interbedded calcareous siltstones and mudstones. The sediments immediately above this break in slope (upper part of sedimentary Subunit IIa; 136–309 mbsf) still contain abundant planktonic chalk, but graded siltstones and graded sandstones become more abundant upsection. Reference to the seismic reflection profile suggests that sediments below this depth were deposited on a bathymetric high isolated from all but the thickest turbidity currents.

The second break in slope of the sediment age vs. depth curve, from 27 to >70 cm/1000 yr, occurs within the *E. huxleyi* Zone (<250,000 yr ago; <180 mbsf). This change may coincide with the transition from sedimentary Unit I to II, marked by an upsection increase in the abundance of volcaniclastics, volcanic ashes, and lapilli tuffs. We also noted an upsection marked increase in slope of the age vs. depth curve within the Pleistocene of Site 650, also accompanied by an upsection increase in abundance of clastic sediments. At Site 650, the break in slope occurred within, or at the base of, nannofossil Zone NN20 (450,000–250,000 yr ago), whereas at Site 651 the break in slope occurs within the *E. huxleyi* Zone (<250,000 yr). Various hypotheses for the cause of this intra-Pleistocene change in sedimentation regime were presented in the "Discussion and Conclusions" section, Site 650 chapter. Had the change in sedimentation regime been simultaneous at Sites 650 and 651, this could have supported the hypothesis that changes in glacial/interglacial climate or glacial-eustatic sea level were the driving force behind the sedimentation trend. However the diachroneity of the change in sedimentation rate in Marsili and Vavilov Basins argues instead for a tectonic or volcanic control.

Basal Sediments

The lowermost 40 m (Subunit IIb; 348–388 mbsf) of the sedimentary column consists of dolostone, probably enriched in iron and manganese, characterized by bright red and brown coloration. A similar basal unit of reddish-brown, dolomite-rich nannofossil chalk was encountered at Site 650 in the Marsili Basin. However, the basal sediments at 651 are four times as thick as at Site 650. Metal-enriched sediments typically occur at the contact between oceanic crust and normal deep sea sediments, both in the oceans and in ophiolite complexes. Several hypotheses may explain why the basal sediments at Site 651 are thicker than at Site 650: First, the sediment overlying basement at Site 651 may be as much as twice as old as at Site 650, allowing more time for post-depositional alteration. Second, the presence of basaltic breccias at Site 651 suggests that the basement was more fractured than the basement at Site 650, which would allow more pathways for water to circulate through the basalt. (On the other hand, within the thin unit of basement recovered at Site 650, the basalts appeared to be more heavily altered than at Site 651, which is incompatible with this hypothesis.) Third, the peridotite of basement Unit 4 provides an extra source of magnesium for dolomitization. Fourth, the inferred injection of a dolerite sill could have occurred after some thickness of sediment had accumulated above the upper basalt flows; if so, the elevated temperature associated with the sill injection could have accelerated alteration processes. Finally, precipitation from hydrothermal fluids (as opposed to post-depositional alteration) may have played a larger role in forming the basal sediments at Site 651 than at Site 650.

REFERENCES

Adams, J.A.S., and Weaver, C. E., 1958. Thorium to uranium ratios as indicative of sedimentary processes: Example of concept of geochemical facies. *AAPG Bull.*, 42:387–430.

Barberi, F., Bizouard, H., Capaldi, G., Ferrara, G., Gasparini, P., Innocenti, F., Joron, J. L., Lambret, B., Treuil, M., and Allegre, C., 1978. Age and nature of basalts from the Tyrrhenian abyssal plain. *In*, Hsü, K. J., Montadert, L., et al., *Init. Repts. DSDP*, 42, Pt. 1: Washington (U.S. Govt. Printing Office), 509–516.

Boillot, G., Grimaud, S., Mauffret, A., Mougenot, D., Mergoil-Daniel, J., Kornprobst, J., and Torrent, G., 1980. Ocean-continent boundary off the Iberian margin: a serpentinite diapir west of the Galicia Bank. *Earth Planet. Sci. Lett.*, 48:23–34.

Bolis, G., Capelli, V., and Marinelli, M., 1981. Aeromagnetic data of the Italian area: instrumental to a better comprehension of the basement main characteristic in Italy, Carta Magnetica d'Italia. AGIP–43rd E.A.E.G. meeting in Venezia (Italy).

Bonatti, E., 1975. Metallogenesis at oceanic spreading centers. *Ann. Rev. Earth Planet. Sci.*, 3:401–431.

________, 1976. Serpentinite protrusions in the oceanic crust. *Earth Planet. Sci. Lett.*, 32:107–132.

Bonatti, E., Hamlyn, P. R., and Ottonello, G., 1981. The upper mantle beneath a young oceanic rift: peridotite from the island of Zabargad, Red Sea. *Geology*, 9:474–479.

Bonatti, E., Kolla, V., Moore, W. S., et al., 1979. Metallogenesis in marginal basins: Fe-rich basal deposits from the Philippine Sea. *Mar. Geol.*, 32:21–37.

Broecker, W. S., and Van Donk, J., 1970. Insolation changes, ice volume, and the ^{18}O record in deep-sea cores. *Rev. Geophys. Space Phys.*, 8:169–198.

Cita, M. B., 1975. Studi sul Pliocene e gli strati di passaggio del Miocene e Pliocene, VIII. Planktonic foraminiferal biozonation of the Mediterranean deep sea record: a revision. *Rev. Ital. Paleontol. Stratigr.*, 81: 527–544.

Civetta, L., and Gasparini, P., 1973. A review of U and Th distribution in recent volcanics from southern Italy: magmatological and geophysical implications. *In* Adams, Gesell, and Lowder (Eds.), *Symposium on Natural Radiation*, 483–515.

Civetta, L., Innocenti, F., Manetti, P., Peccerillo, A., and Poli, G., 1981. Geochemical characteristics of potassic volcanics from Mts. Ernici (southern Latium, Italy). *Contrib. Mineral. Petrol.*, 78:37–47.

Colalongo, M. L., Pasini, G., Pelosio, G., Raffi, S., Rio, D., Ruggieri, G., Sartoni, S., Selli, R., and Sprovieri, R., 1982. The Neogene/Quaternary boundary definition: a review and a proposal. *Geogr. Fis. Din. Quat.*, 5:59–68.

Dal Piaz, G. V., 1974. Le métamorphisme de haute préssion et basse température dans l'évolution structurale du bassin ophiolitique alpino-appénninique. Pt. 1: considerations paleogéographiques. *Boll. Soc. Geol. Ital.*, 93:437–468.

Della Vedova, B., Pellis, G., Foucher, J. P., and Rehault, J. P., 1984. Geothermal structure of the Tyrrhenian Sea. *Mar. Geol.*, 55:271–289.

Dietrich, V., Emmerman, R., Puchett, H., and Keller, J., 1978. Oceanic basalt from the Tyrrhenian basin, DSDP Leg 42A, Hole 373A. *In* Hsü, K. J., Montadert, L., et al., *Init. Repts. DSDP*, 42, Pt. 1: Washington (U.S. Govt Printing Office), 515-530.

D'Onofrio, S., 1981. I foraminferi bentonici della sezione Vrica (Calabria, Italia). *G. Geol.*, 32:327-364.

Elter, P., 1975. Introduction à la géologie de l'Apennin septentrional. *Bull. Soc. Geol. Fr.*, (7) XVII, 6:956–962.

Emiliani, C., 1978. The cause of the ice ages. *Earth Planet. Sci. Lett.*, 37:349–352.

Erickson, A. J., Simmons, G., and Ryan, W.B.F., 1977. Review of heat flow data from the Mediterranean and Aegean Seas. *In* Biju-Duval, B., and Montadert, L. (Eds.), *International Symposium on the Structural History of the Mediterranean Basins*. Paris (Technip) 263–279.

Fabbri, A., and Curzi, P., 1979. The Messinian of the Tyrrhenian Sea: seismic evidences and dynamic implications. *G. Geol.*, 43, 2:215–248.

Ferruci, F., Makris, J., Nicolich, R., Snoeck, M., Steinmetz, L., and Weige, W., 1982. Deep seismic sounding by OBS in Tyrrhenian Sea. CIESM (28th meeting), Cannes, 2-6 Dec. 1982.

Finetti, I., and Morelli, C., 1973. Geophysical exploration of the Mediterranean Sea. *Boll. Geofis. Teor. Appl.*, 15:263–340.

Fischer, R. V., and Schmincke, H.-U., 1984. *Pyroclastic Rocks*: Heidelberg (Springer).

Gennesseaux, M., Rehault, J.-P., Thomas, B., Colantini, P., Fabbri, A., Lepvrier, C., Mascle, G., Mauffret, A., Polino, R., Robin, C., and Vanney, J.-R., 1986. Les bloc basculés de la mer Tyrrhénienne centrale et le volcan sous-marin Vavilov: résultats des plongées en submersible Cyana. *C.R. Acad. Sci. Paris, Ser. AII*, 302:785–792.

Gieskes, J. M., Kastner, M., Einsele, G., Kelts, K., and Niemitz, J., 1982. Hydrothermal activity in the Guaymas Basin, Gulf of California: A synthesis. *In* Curray, J. R., Moore, D. G., et al., *Init. Repts. DSDP*, 64, Pt. 2: Washington (U.S. Govt. Printing Office), 1159-1167.

Gieskes, J. M., 1975. Chemistry of interstitial waters of marine sediments. *Ann. Rev. Earth Planet. Sci.*, 3:433–453.

Hsü , K. J., Montadert, L., et al., 1978. *Init. Repts. DSDP*, 42, Pt. 1: Washington (U.S. Govt Printing Office).

Hutchison, I., Von Herzen, R., Louden, K., Sclater, J., and Jemsek, J., 1985. Heat flow in the Balearic and Tyrrhenian basins, Western Mediterranean. *J. Geophys. Res.*, 90(B1):685–701.

Lemoine, M., 1980. Serpentinites, gabbros, and ophicalcites in the Piemont-Ligurian domain of the Western Alps: Possible indicators of oceanic fracture zones and of associated serpentinite protusions in the Jurassic-Cretaceous Tethys. *Arch. Sci. Geneve*, 33:103–115.

Locardi, E., 1967. Uranium and thorium in the volcanic processes. *Bull. Volcanol.*, 31:235–260.

Locardi, E., Lombardi, G., Funiciello, R., and Parotto, M., 1976. The main volcanic groups of Latium (Italy): relations between structural evolution and petrogenesis. *Geol. Rom.*, 15:279-300.

Malinverno, A., Cafiero, M., Ryan, W.B.F., and Cita, M. B., 1981. Distribution of Messinian sediments and erosional surfaces beneath the Tyrrhenian Sea: geodynamic implications. *Oceanol. Acta*, 4: 489–496.

Mottl, M. J., and Holland, H. D., 1978. Chemical exchange during hydrothermal alteration of basalt by seawater—I. Experimental results for major and minor components of seawater. *Geochim. Cosmochim. Acta*, 42:1103–1115.

Moussat, E., 1983. Evolution de la Mer Tyrrhénienne centrale et orientale et de ses marges septentrionales en relation avec la néotectonoque dans l'Arc Calabrais [Thesis]. Univ. P. et M. Curie, Paris.

Ohnenstetter, M., 1979. Contribution à l'étude des ophiolites du domaine méditerranéen [Thesis]. Univ. Nancy.

Panza, G. F., Calcannile, G., Scandone, P., and Mueller, S., 1980. La struttura profonda dell area Mediterranea. *Le Scienze*, 141:60–69.

Raffi, I., and Sprovieri, R., 1984. Calcareous plankton in DSDP Hole 125–Leg 13 (Ionian Sea–Eastern Mediterranean): a review. *Boll. Soc. Paleontol. Ital.*, 23:53–73.

Recq, M., Rehault, J.-P., Steinmetz, L., and Fabbri, A., 1984. Amincissement de la croute et accrétion au centre du bassin Tyrrhénien d'aprés la sismique réfraction. *Mar. Geol.*, 55:411–428.

Rio, D., Sprovieri, R., Di Stefano, I., and Raffi, I., 1984a. *Globorotalia truncatulinoides* (d'Orbigny) in the Mediterranean upper Pliocene geologic record. *Micropaleontology*, 30:121–137.

Rio, D., Sprovieri, R., and Raffi, I., 1984b. Calcareous plankton biostratigraphy and biochronology of the Pliocene–lower Pleistocene succession of the Capo Rossello area, Sicily. *Mar. Micropaleontol.*, 9:135–180.

Robertson, A.H.F., and Boyle, J. F., 1983. The origin and tectonic setting of metalliferous sediments in the Tethys Ocean. *In* Rona, P. A., Bostrom, D., Laubier, L., and Smith, K. L. (Eds.), *Hydrothermal Processes at Seafloor Spreading Centers*: New York (Plenum Press).

Rona, P. A., and Lowell, R. P. (Eds.), 1980. *Seafloor Spreading Centers/Hydrothermal Systems*. Benchmark Papers in Geology 56. Dowden, Hutchinson and Ross (Stroudsburg, PA).

Ruggieri, G., Rio, D., and Sprovieri, R., 1984. Remarks on the chronostratigraphic classification of Lower Pleistocene. *Boll. Soc. Geol. Ital.*, 103:251–259.

Ruggieri, G., and Sprovieri, R., 1983. Recenti progressi nella stratigraffia del Pleistocene inferiore. *Boll. Soc. Paleontol. Ital.*, 22.3:315–321.

Sayles, F. L., and Manheim, F. T., 1975. Interstitial solutions and diagenesis in deeply buried marine sediments: results from the Deep Sea Drilling Project. *Geochim. Cosmochim. Acta*, 39:103–127.

Selli, R., and Fabbri, A., 1971. Tyrrhenian: a Pliocene deep sea. *Rend. Cl. Fis. Mat. Acc. Nat. Lincei*, 50:104–116.

Selli, R., Lucchini, F., Savelli, C., and Del Monte, M., 1977. Dati geologici, petro-chimici e radiometrici sui vulcani centrotirrenici. *G. Geol.*, 42, 1:221–246.

Steinmetz, L., Ferrucci, F., Hirn, A., Morelli, C., and Nicolich, R., 1983. A 550 km long Moho traverse in the Tyrrhenian Sea from O.B.S. recorded Pn waves. *Geophys. Res. Lett.*, 10(6):428–431.

Tauxe, L., Opdyke, N., Pasini, G., and Elmi, C., 1983. Age of the Plio-Pleistocene boundary in the Vrica section, southern Italy. *Nature.*, 304:125–129.

Summary Log for Hole 651A

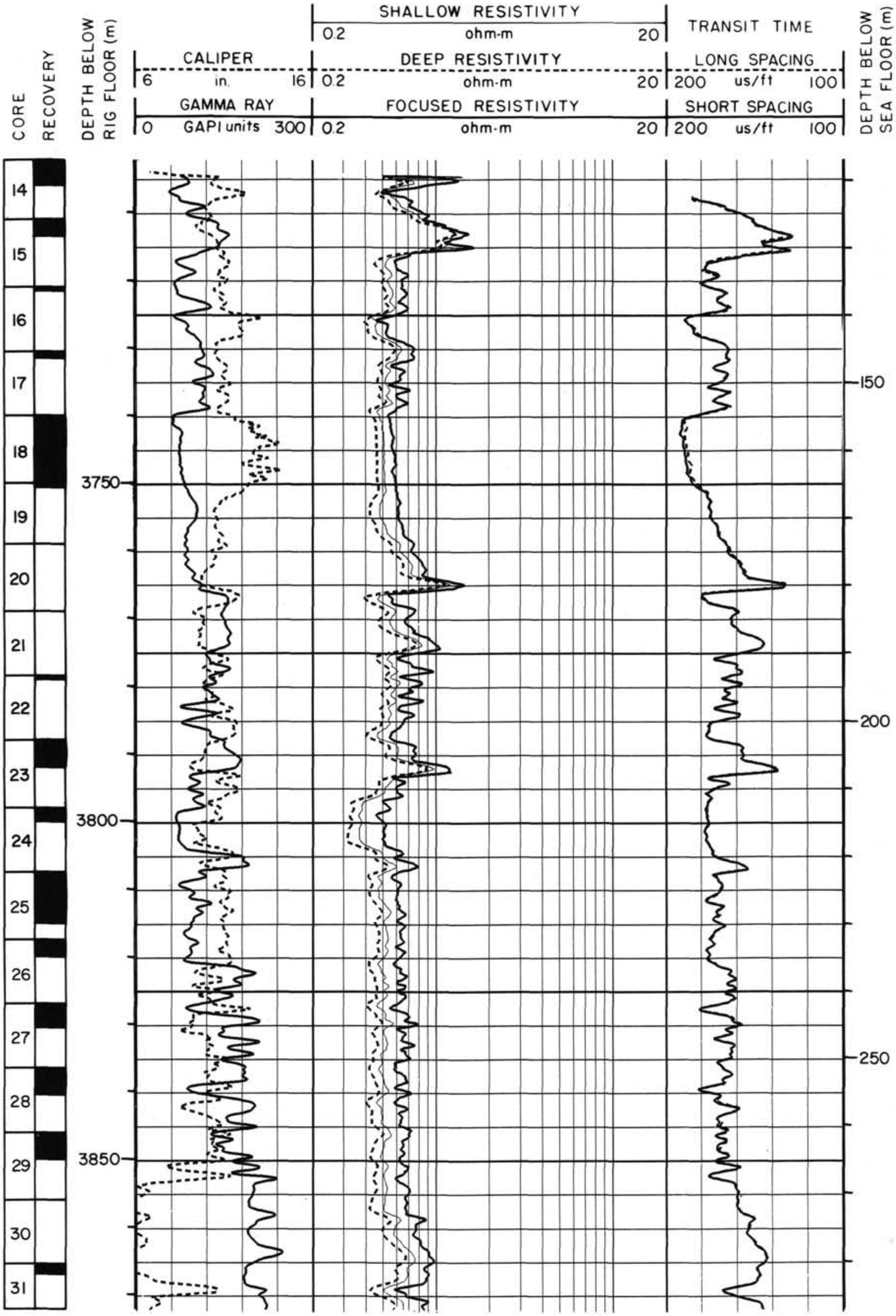

Summary Log for Hole 651A (continued)

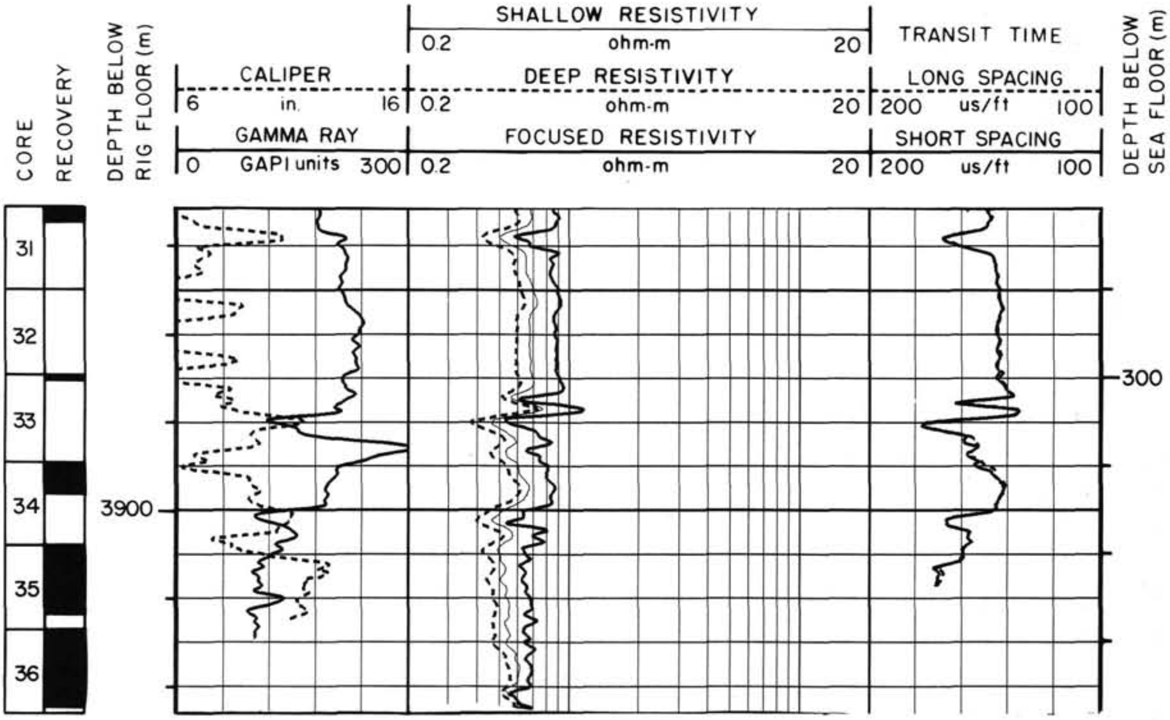

Summary Log for Hole 651A (continued)

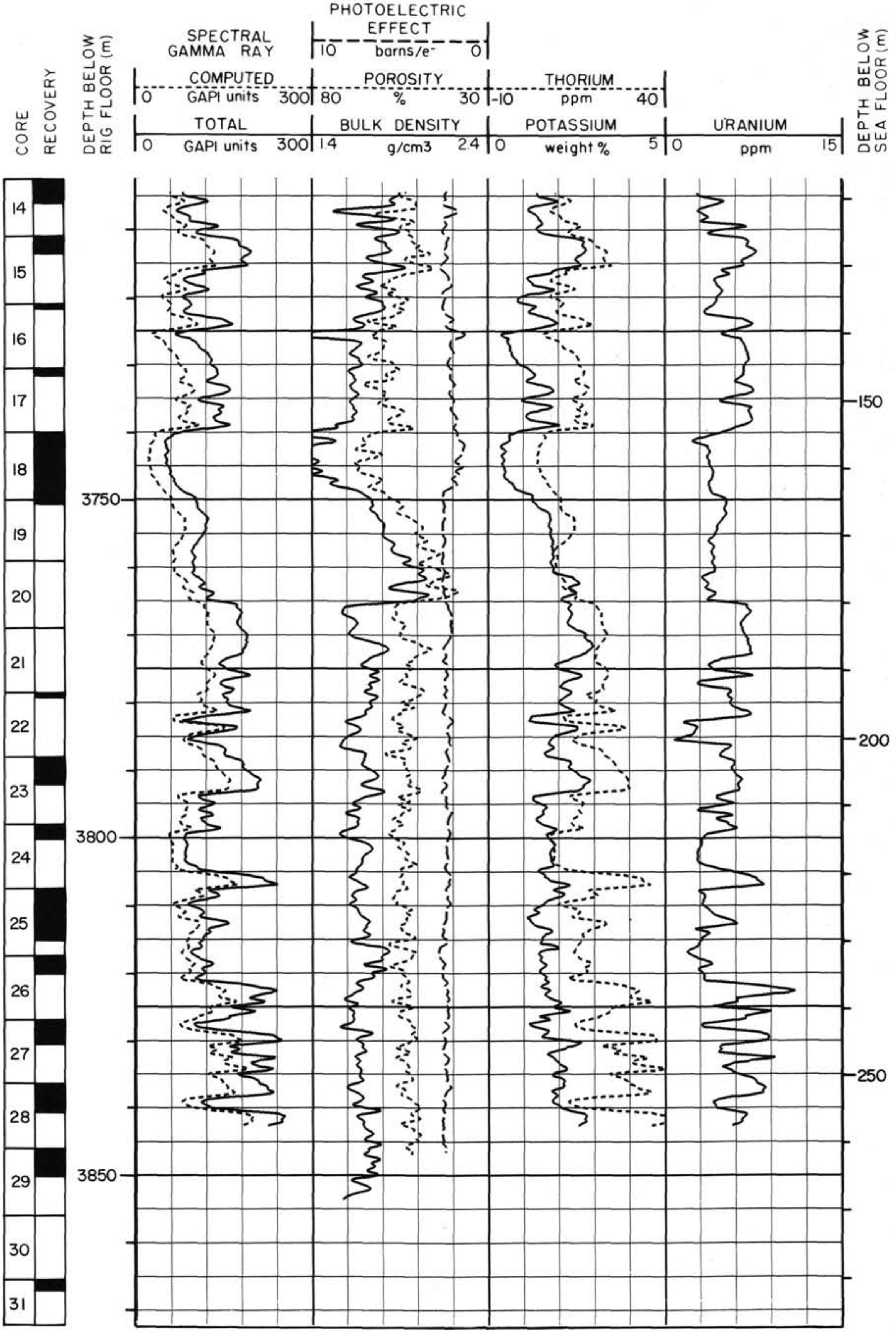

SITE 651 HOLE A CORE 1 R CORED INTERVAL 3578.0-3581.7 mbsl; 0.0-3.7 mbsf

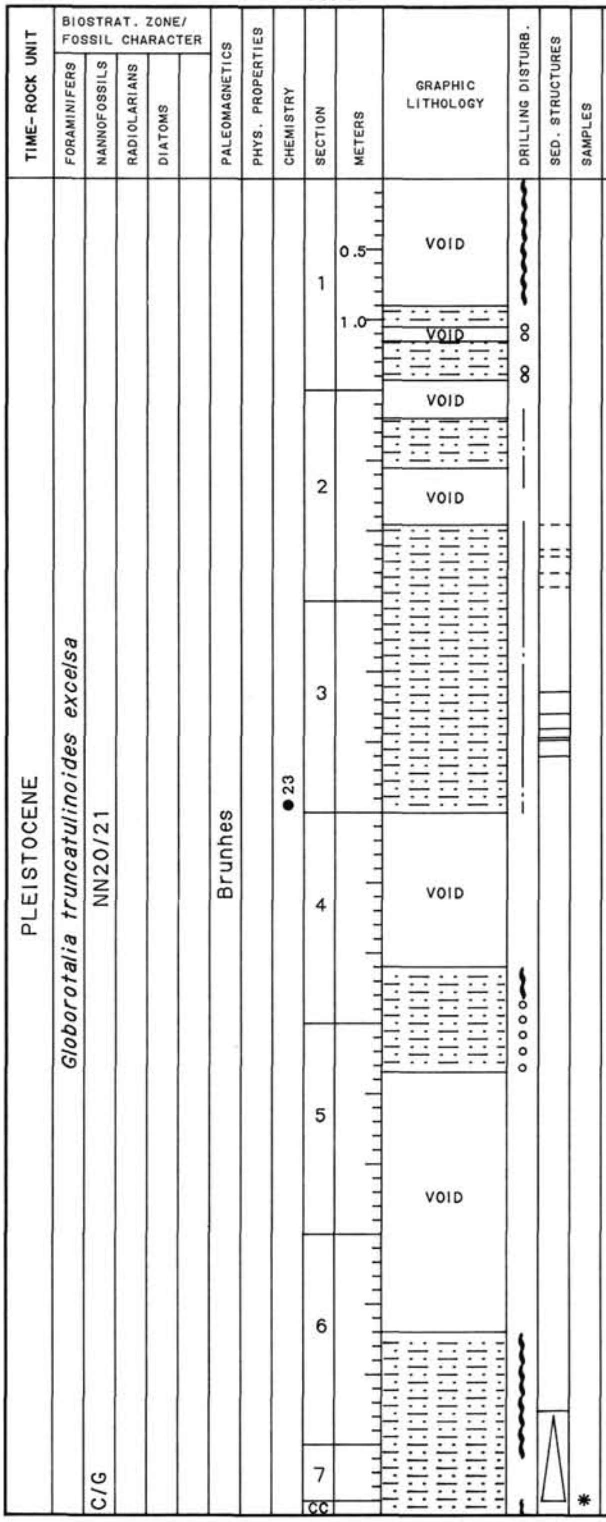

LITHOLOGIC DESCRIPTION

MUD

Homogeneous mud, slightly oxidized, pale olive (2.5Y 6/4), soupy and elongated through the core liner, becomes light gray (5Y 7/1); slightly laminated with brown and clear gray mud in Section 2, where the first silty layer occurs at 118 cm; downcore mud is clear yellowish gray to yellowish gray (2.5Y 8/0); Section 7 is a dark olive-gray (5Y 3/2), graded, volcaniclastic sand.

SMEAR SLIDE SUMMARY (%):

	7, 36 D
TEXTURE:	
Sand	60
Silt	40
Clay	—
COMPOSITION:	
Quartz	20
Feldspar	5
Volcanic glass	45
Calcite/dolomite	1
Accessory minerals	8
Foraminifers	20

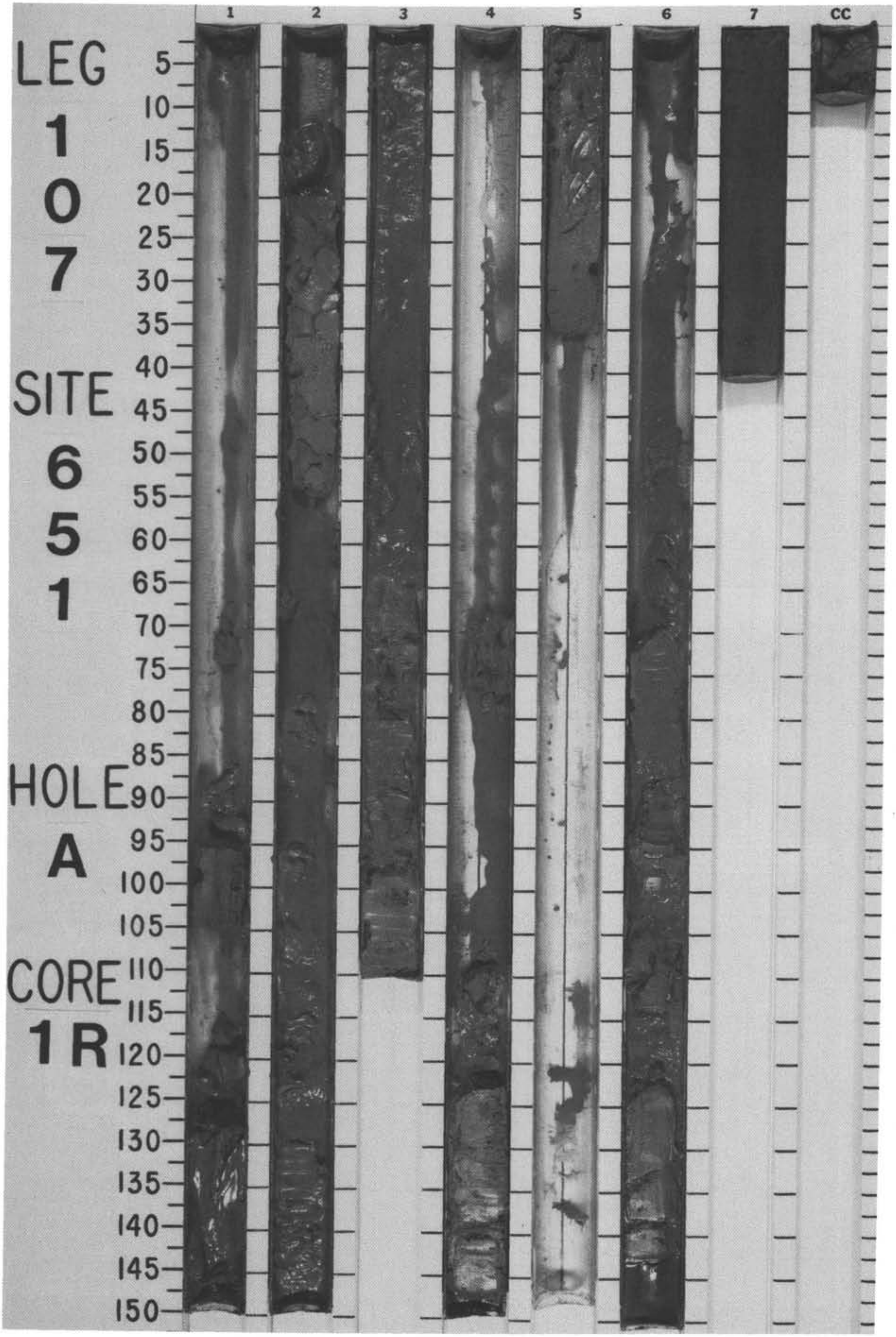
LEG
1
0
7
SITE
6
5
1
HOLE
A
CORE
1R
1
2
3
4
5
6
7
CC
5
10
15
20
25
30
35
40
45
50
55
60
65
70
75
80
85
90
95
100
105
110
115
120
125
130
135
140
145
150

SITE 651 HOLE A CORE 2 R CORED INTERVAL 3581.7-3588.3 mbsl; 3.7-10.3 mbsf

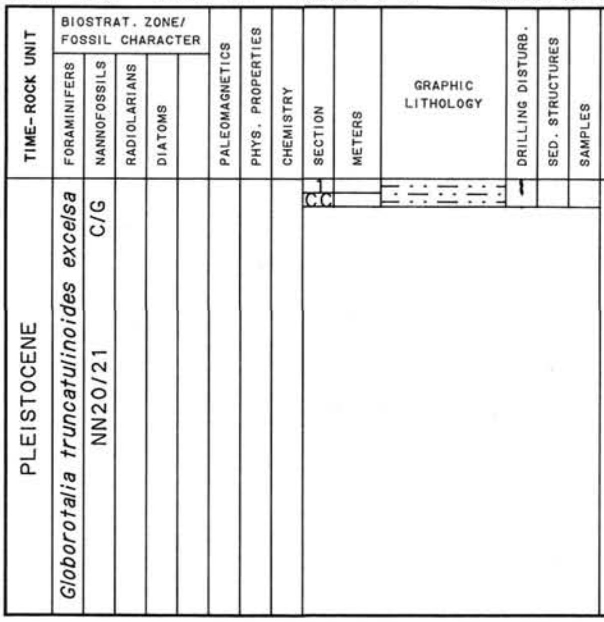

LITHOLOGIC DESCRIPTION

MUD

Soupy mud.

SITE 651 HOLE A CORE 3 R CORED INTERVAL 3588.3-3597.8 mbsl; 10.3-19.8 mbsf

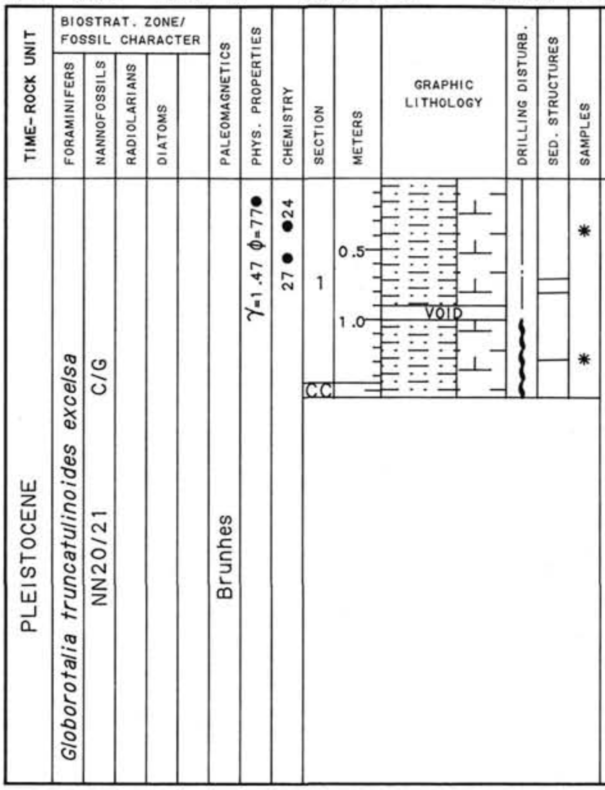

LITHOLOGIC DESCRIPTION

NANNOFOSSIL-RICH CALCAREOUS MUD

Homogeneous, nannofossil-ooze mud, olive-gray (5Y 5/2), with thin intercalations of soupy silt and volcaniclastic nannofossil ooze.

SMEAR SLIDE SUMMARY (%):

	1, 39 D	1, 132 D
TEXTURE:		
Sand	—	40
Silt	5	20
Clay	95	40
COMPOSITION:		
Quartz	—	10
Feldspar	2	10
Clay	7	15
Volcanic glass	5	15
Calcite/dolomite	2	15
Micrite	7	10
Accessory minerals	1	—
Foraminifers	1	10
Nannofossils	75	25

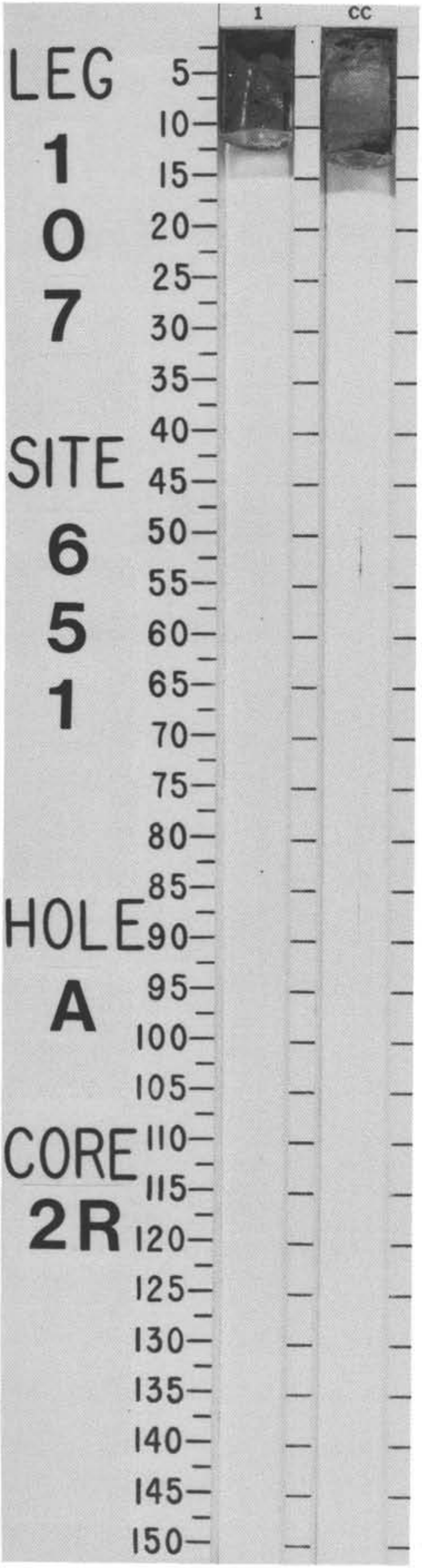
1
CC
LEG
107
SITE
651
HOLE
A
CORE
2R
5
10
15
20
25
30
35
40
45
50
55
60
65
70
75
80
85
90
95
100
105
110
115
120
125
130
135
140
145
150

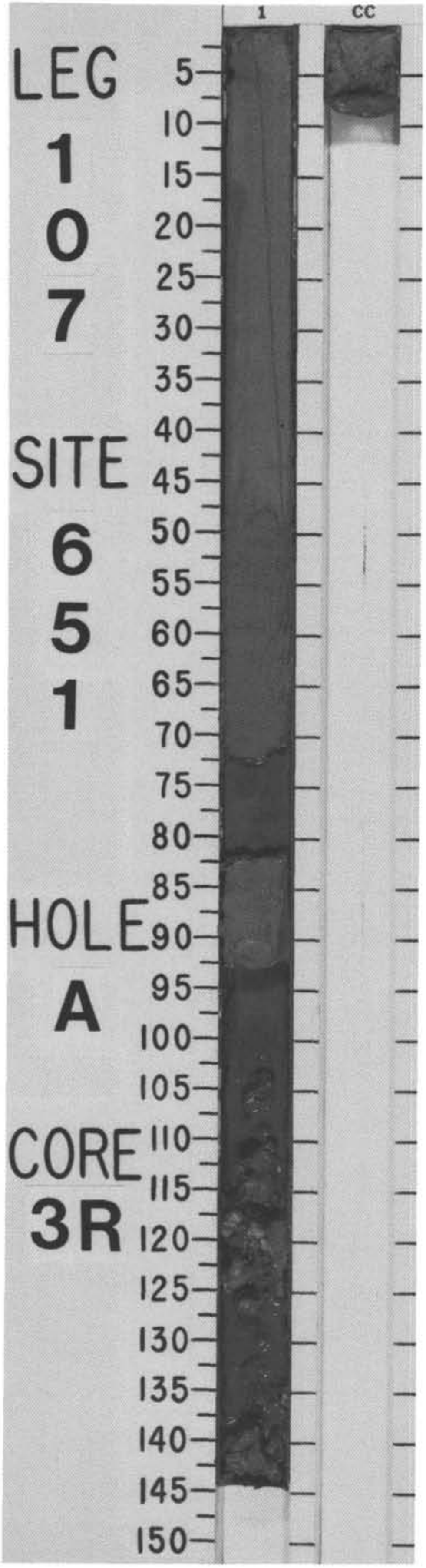
1
CC
LEG
107
SITE
651
HOLE
A
CORE
3R
5
10
15
20
25
30
35
40
45
50
55
60
65
70
75
80
85
90
95
100
105
110
115
120
125
130
135
140
145
150

SITE 651 HOLE A CORE 4 R CORED INTERVAL 3597.8-3607.4 mbsl; 19.8-29.4 mbsf

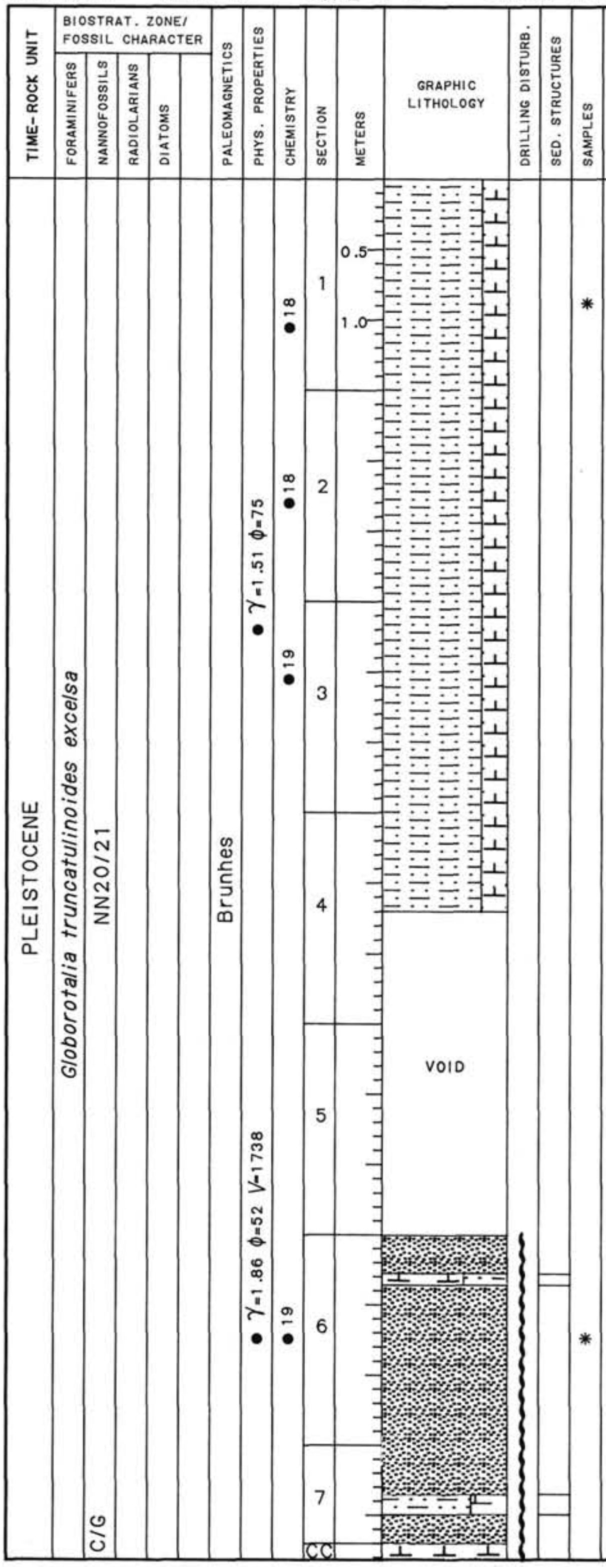

LITHOLOGIC DESCRIPTION

NANNOFOSSIL-RICH CALCAREOUS MUD

Homogeneous, nannofossil-ooze mud, gray (5Y 5/1), with gray sand (5Y 5/1) in Section 6.

SMEAR SLIDE SUMMARY (%):

	1, 97 D	6, 73 D
TEXTURE:		
Sand	—	60
Silt	—	20
Clay	100	20
COMPOSITION:		
Quartz	2	20
Feldspar	1	5
Rock fragments	—	10
Clay	19	10
Volcanic glass	5	1
Calcite/dolomite	2/1	5/1
Micrite	20	10
Accessory minerals	—	1
Foraminifers	—	10
Nannofossils	60	20
Sponge spicules	—	1
Fish remains	—	5

5R-NO RECOVERY

6R-NO RECOVERY

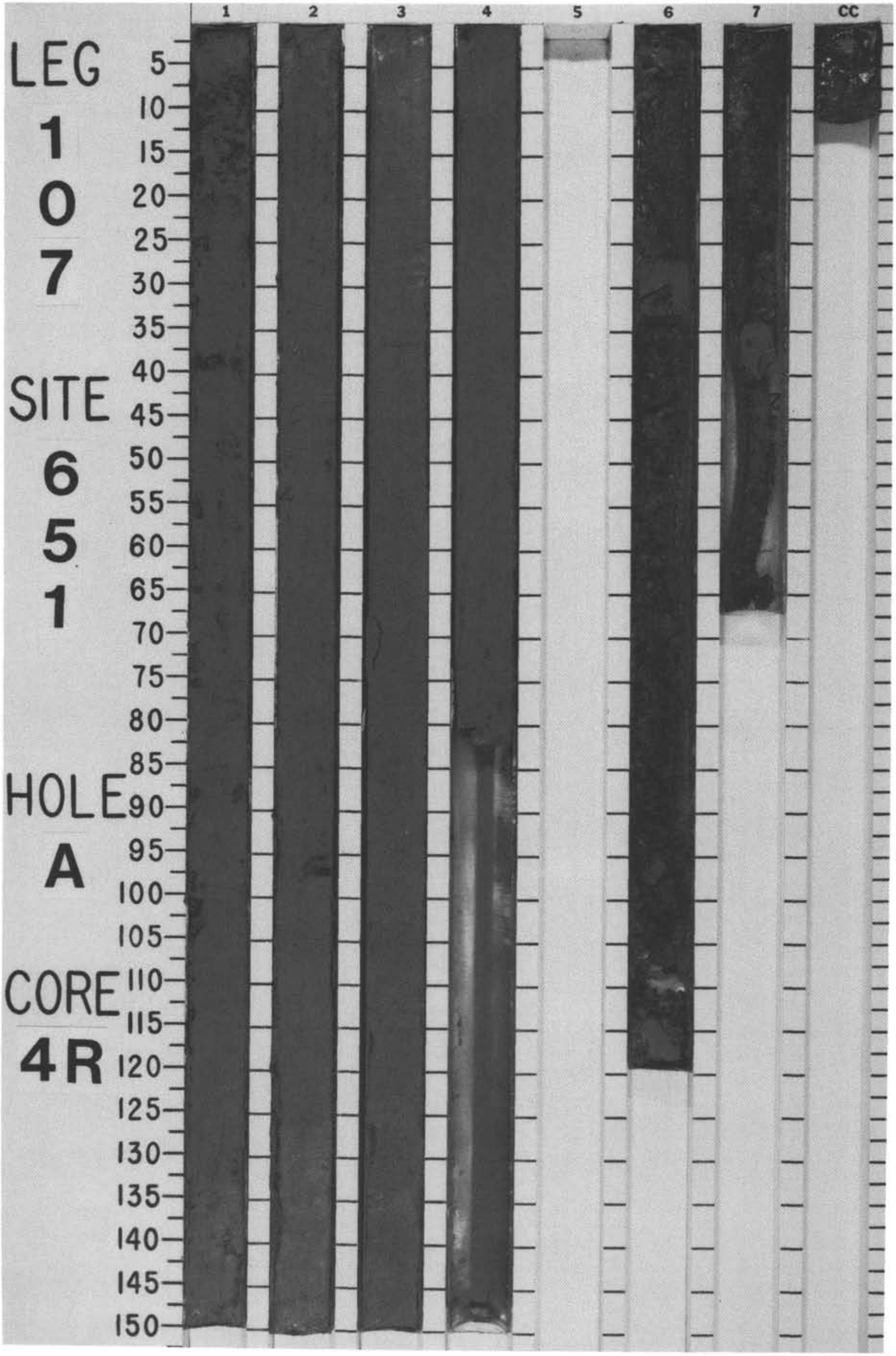
LEG
107
SITE
651
HOLE
A
CORE
4R
1
2
3
4
5
6
7
CC
5
10
15
20
25
30
35
40
45
50
55
60
65
70
75
80
85
90
95
100
105
110
115
120
125
130
135
140
145
150

SITE 651 HOLE A CORE 7 R CORED INTERVAL 3627.5-3637.2 mbsl; 49.5-59.2 mbsf

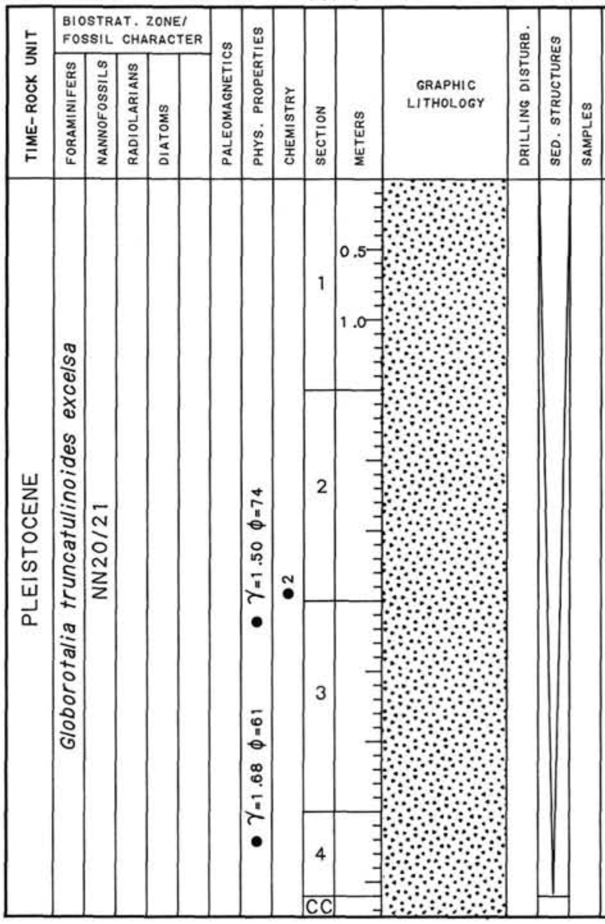

LITHOLOGIC DESCRIPTION

PUMICE

Pumice, gray (10YR 5/1), with inverse-graded bedding suggested by gravity flow.

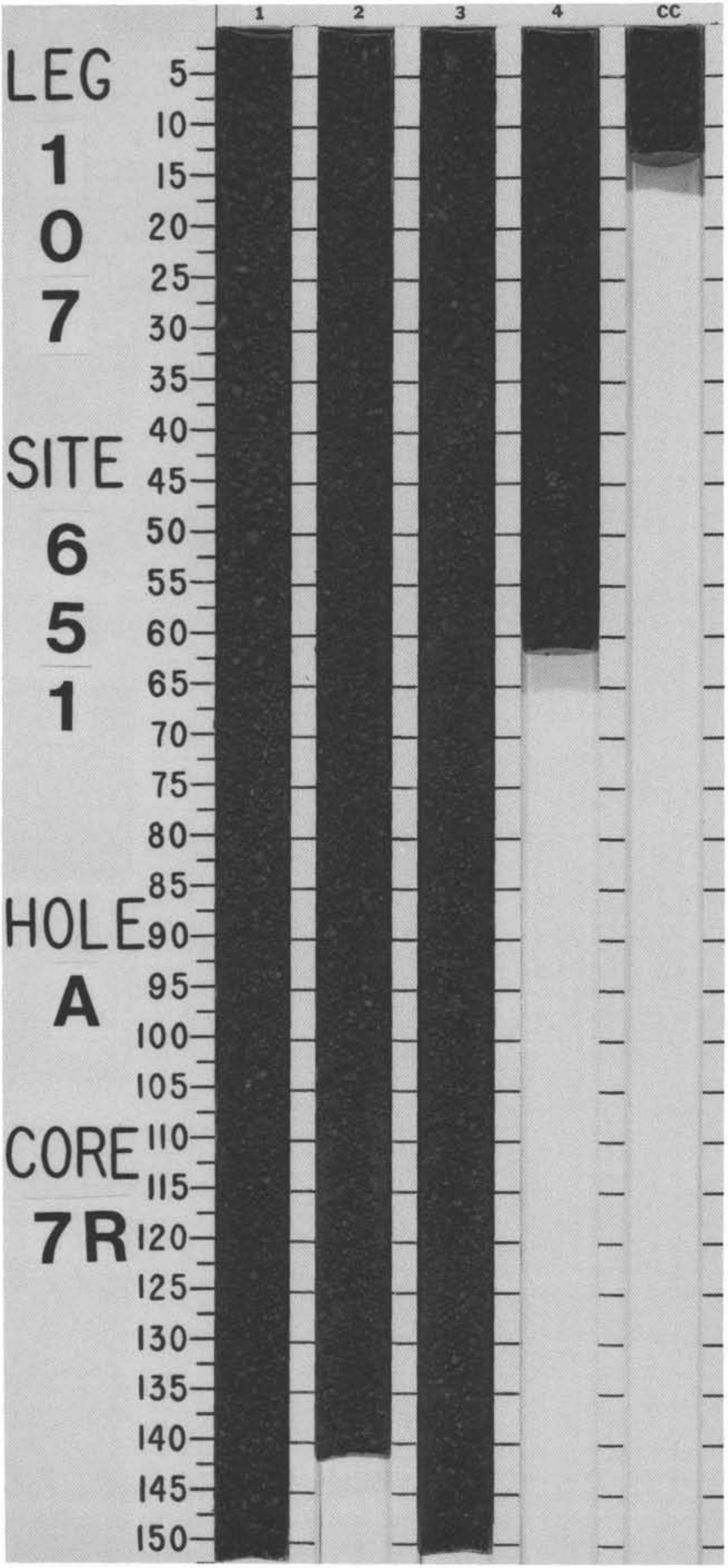
LEG
1
0
7
SITE
6
5
1
HOLE
A
CORE
7R
1
2
3
4
CC
5
10
15
20
25
30
35
40
45
50
55
60
65
70
75
80
85
90
95
100
105
110
115
120
125
130
135
140
145
150

SITE 651 HOLE A CORE 8 R CORED INTERVAL 3637.2-3646.8 mbsl; 59.2-68.8 mbsf

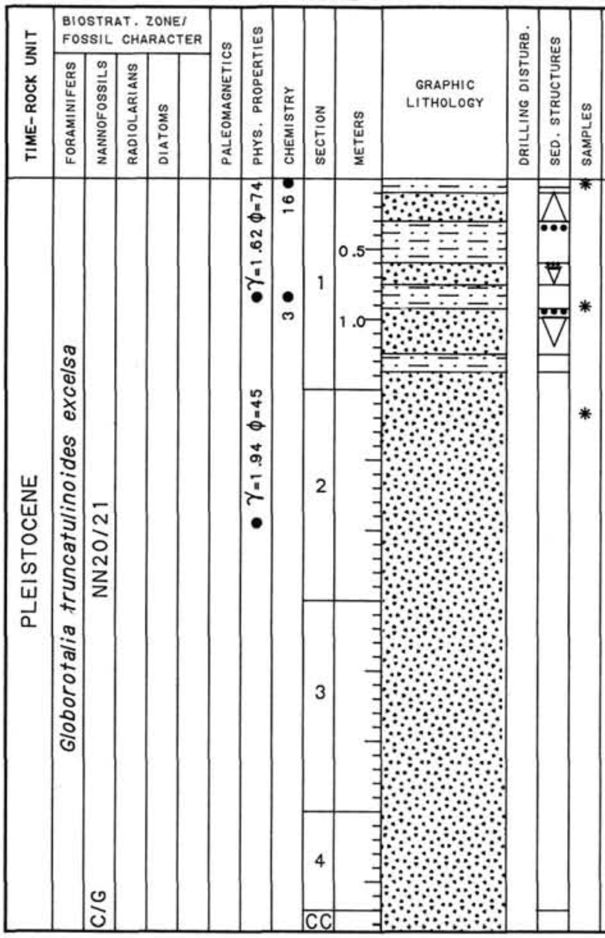

LITHOLOGIC DESCRIPTION

VOLCANIC LAPILLI and NANNOFOSSIL MUD

Dark gray (5Y 4/1) to light gray (5Y 7/2), nannofossil mud interbedded with volcanic ash in Section 1, 15–30 cm; lapilli are dark olive-gray (5Y 3/1), but also include white (5Y 8/1), black (5Y 2.5/1), and yellowish green (1.6Y 4/4) material. Distribution of lapilli indicates that reverse grading may be present.

SMEAR SLIDE SUMMARY (%):

	1, 3 M	1, 88 D	2, 21 D
TEXTURE:			
Sand	30	—	—
Silt	10	10	10
Clay	60	90	90
COMPOSITION:			
Quartz	6	1	—
Feldspar	8	—	3
Rock fragments	4	—	—
Mica	Tr	—	—
Clay	6	15	5
Volcanic glass	23	5	83
Calcite/dolomite	—	3/2	2
Accessory minerals	4	Tr	—
Foraminifers	6	3	—
Nannofossils	35	68	Tr
Radiolarians	—	2	—
Micrite	—	2	—
Inorganic calcite	—	—	2
Zoolites	—	—	5

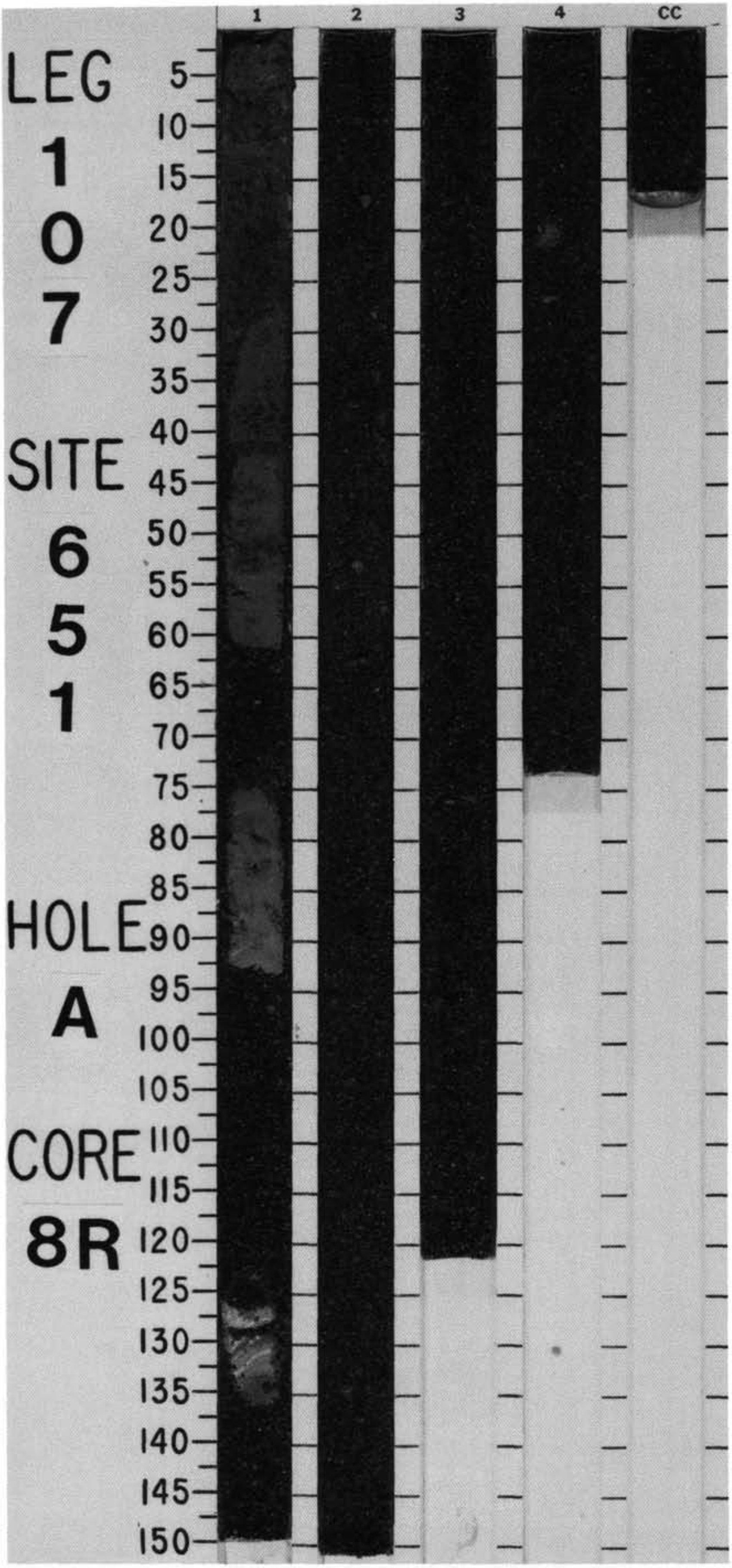
LEG
107
SITE
651
HOLE
A
CORE
8R
1
2
3
4
CC
5
10
15
20
25
30
35
40
45
50
55
60
65
70
75
80
85
90
95
100
105
110
115
120
125
130
135
140
145
150

SITE 651 HOLE A CORE 9 R CORED INTERVAL 3646.8-3656.3 mbsl; 68.8-78.3 mbsf

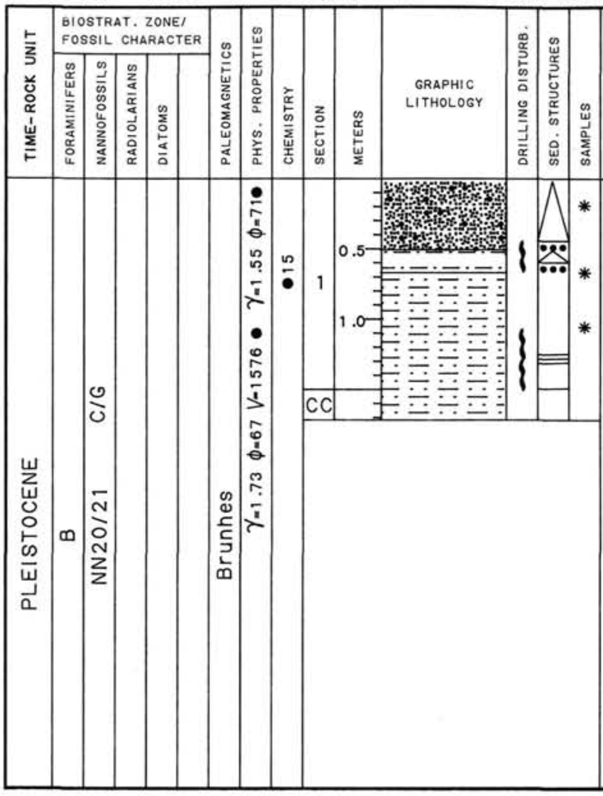

LITHOLOGIC DESCRIPTION

MUDSTONE and SANDY PUMICE MUDSTONE

Poorly laminated to homogeneous mudstone alternating with sandy mudstone, dark gray (5Y 4/1) with "salt and pepper" texture and pumice pebbles; extensive drilling disturbance. The two graded units suggest a gravity flow depositional mechanism.

SMEAR SLIDE SUMMARY (%):

	1, 22 D	1, 73 M	1, 105 M
TEXTURE:			
Sand	90	—	5
Silt	5	5	15
Clay	5	95	80
COMPOSITION:			
Quartz	15	5	5
Feldspar	5	2	2
Mica	—	—	1
Clay	10	15	35
Volcanic glass	40	5	—
Calcite/dolomite	—	5	—
Accessory minerals	5	1	—
Foraminifers	10	2	10
Nannofossils	10	50	40
Bioclasts	5	—	—
Micrite	—	15	7

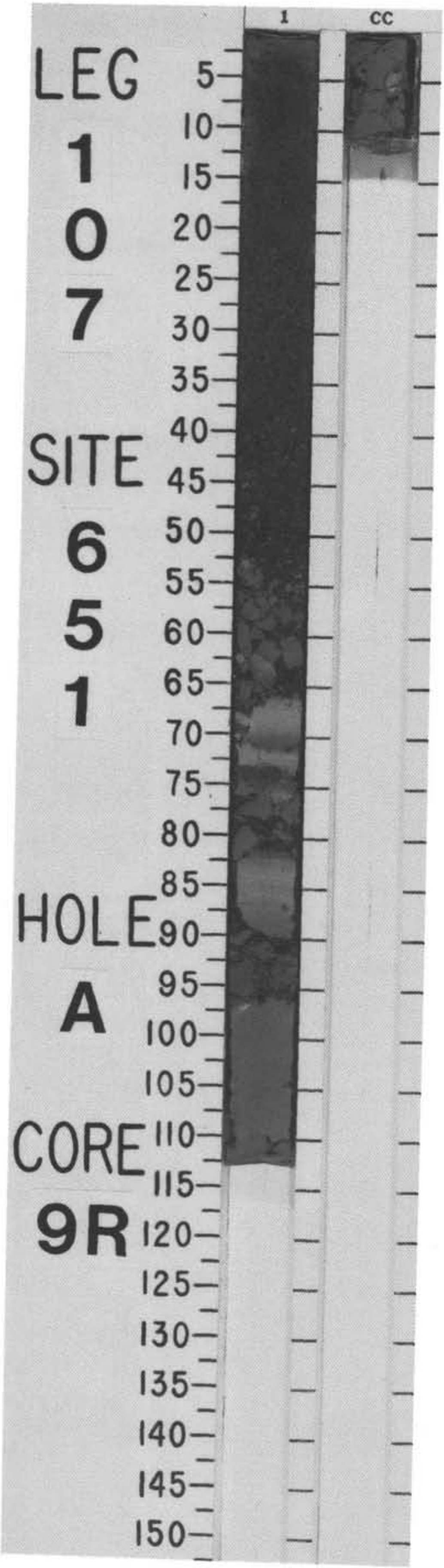
LEG
1
0
7
SITE
6
5
1
HOLE
A
CORE
9R
1
CC
5
10
15
20
25
30
35
40
45
50
55
60
65
70
75
80
85
90
95
100
105
110
115
120
125
130
135
140
145
150

SITE 651 HOLE A CORE 10 R CORED INTERVAL 3656.3-3666.0 mbsl; 78.3-88.0 mbsf

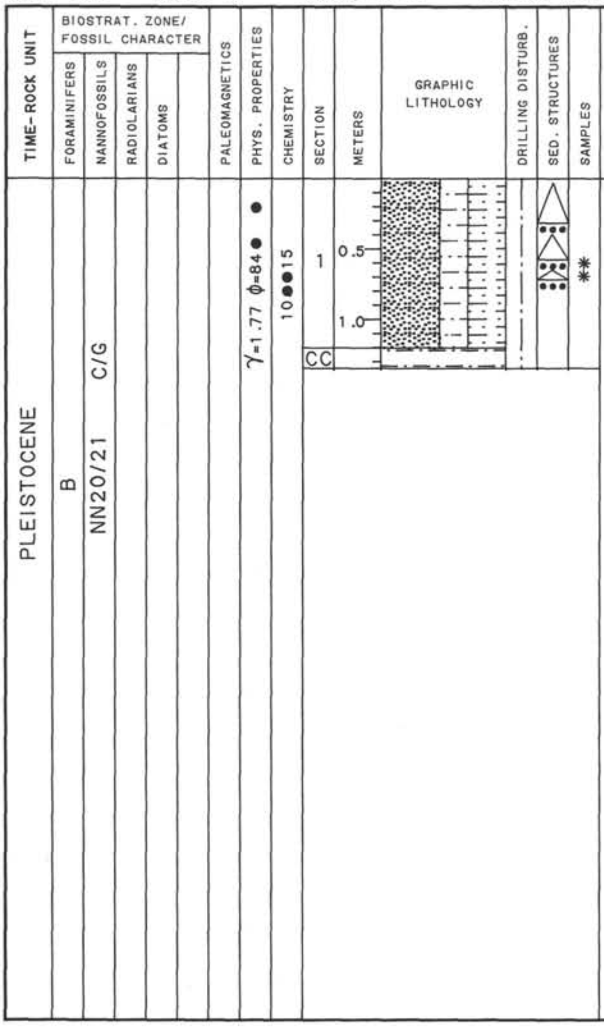

LITHOLOGIC DESCRIPTION

MUDSTONE and SANDSTONE

Recovered intervals dominated by three graded turbidites composed of sand grading into sandy mudstone and mudstone ranging from light olive-gray (5Y 6/2) to pale olive (5Y 6/3); pebble horizon rich in quartz and metamorphic rock pebbles in Section 1, 60–65 cm; sediment is slightly darker from Section 1, 69–70 cm.

Interpretation: mixed detrital and volcanogenic turbidites.

SMEAR SLIDE SUMMARY (%):

	1, 60 D	1, 70 M
TEXTURE:		
Sand	20	5
Silt	15	15
Clay	65	80
COMPOSITION:		
Quartz	10	15
Feldspar	Tr	5
Mica	5	3
Clay	54	47
Volcanic glass	1	5
Accessory minerals	—	5
Nannofossils	25	15
Bioclasts	—	5
Micrite	5	—

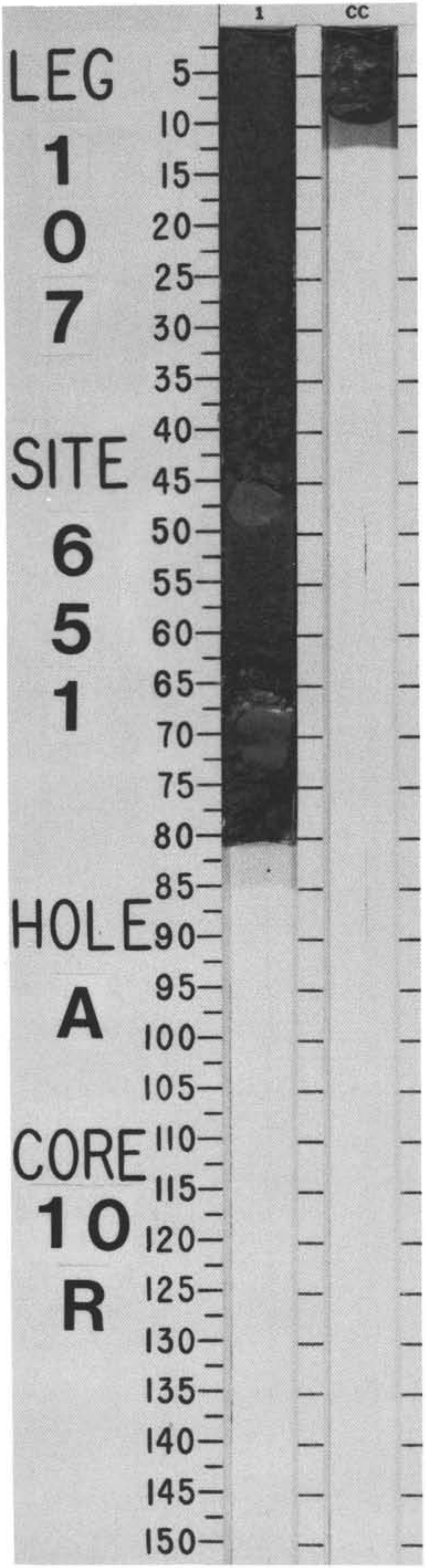
LEG
1
0
7
SITE
6
5
1
HOLE
A
CORE
1 0
R
1
CC
5
10
15
20
25
30
35
40
45
50
55
60
65
70
75
80
85
90
95
100
105
110
115
120
125
130
135
140
145
150

SITE 651 HOLE A CORE 11 R CORED INTERVAL 3666.0-3675.4 mbsl; 88.0-97.4 mbsl

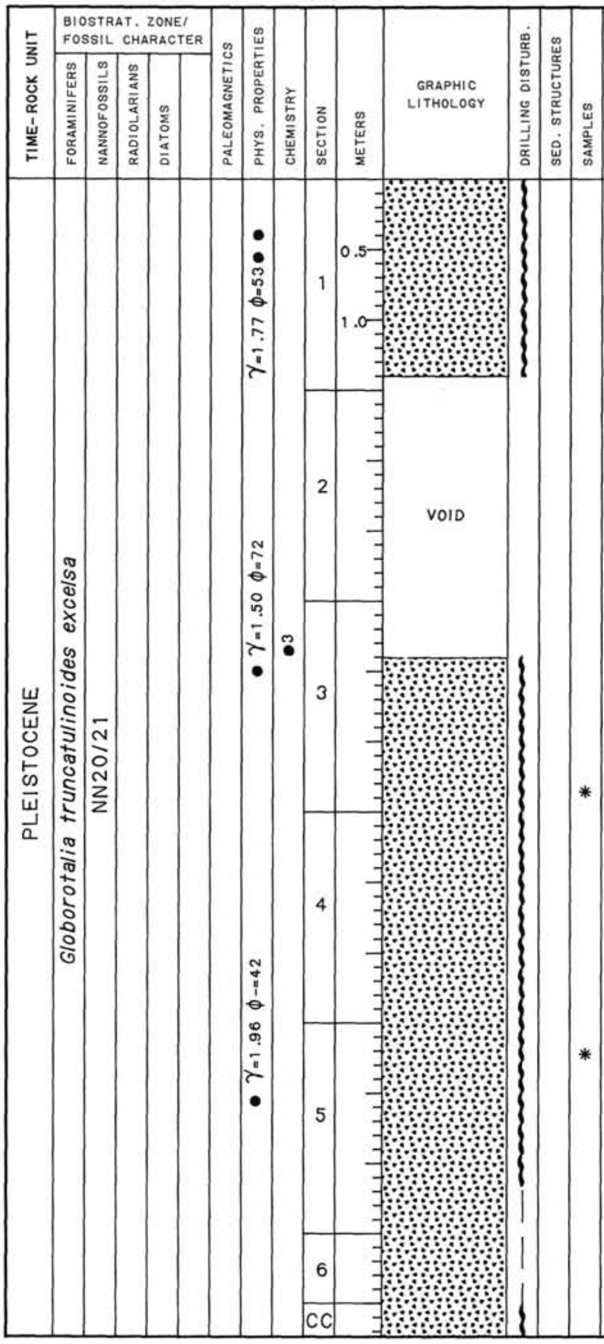

LITHOLOGIC DESCRIPTION

SAND and GRAVEL

Unconsolidated sand and gravel, dark olive-gray (5Y 3/2); in Section 1, 80 cm, a small piece of mud, and at 135 cm, a small piece of more indurated material; in Section 3, 115–135 cm, an indurated interval, and at 129–134 cm, 3-cm-thick micritic mudstone bed; in Section 5, 77 cm, a small piece of crustacean shell.

Interpretation: coarse clastic facies mainly of volcanogenic origin. The apparent homogeneity of this volcaniclastic sand may be an artifact of drilling.

SMEAR SLIDE SUMMARY (%):

	3, 135 M	5, 21 M
TEXTURE:		
Sand	5	—
Silt	10	10
Clay	85	10
COMPOSITION:		
Quartz	5	5
Feldspar	1	—
Clay	36	23
Volcanic glass	Tr	2
Dolomite	1	—
Micrite	—	5
Accessory minerals	2	—
Foraminifers	Tr	Tr
Nannofossils	45	60
Diatoms	5	5

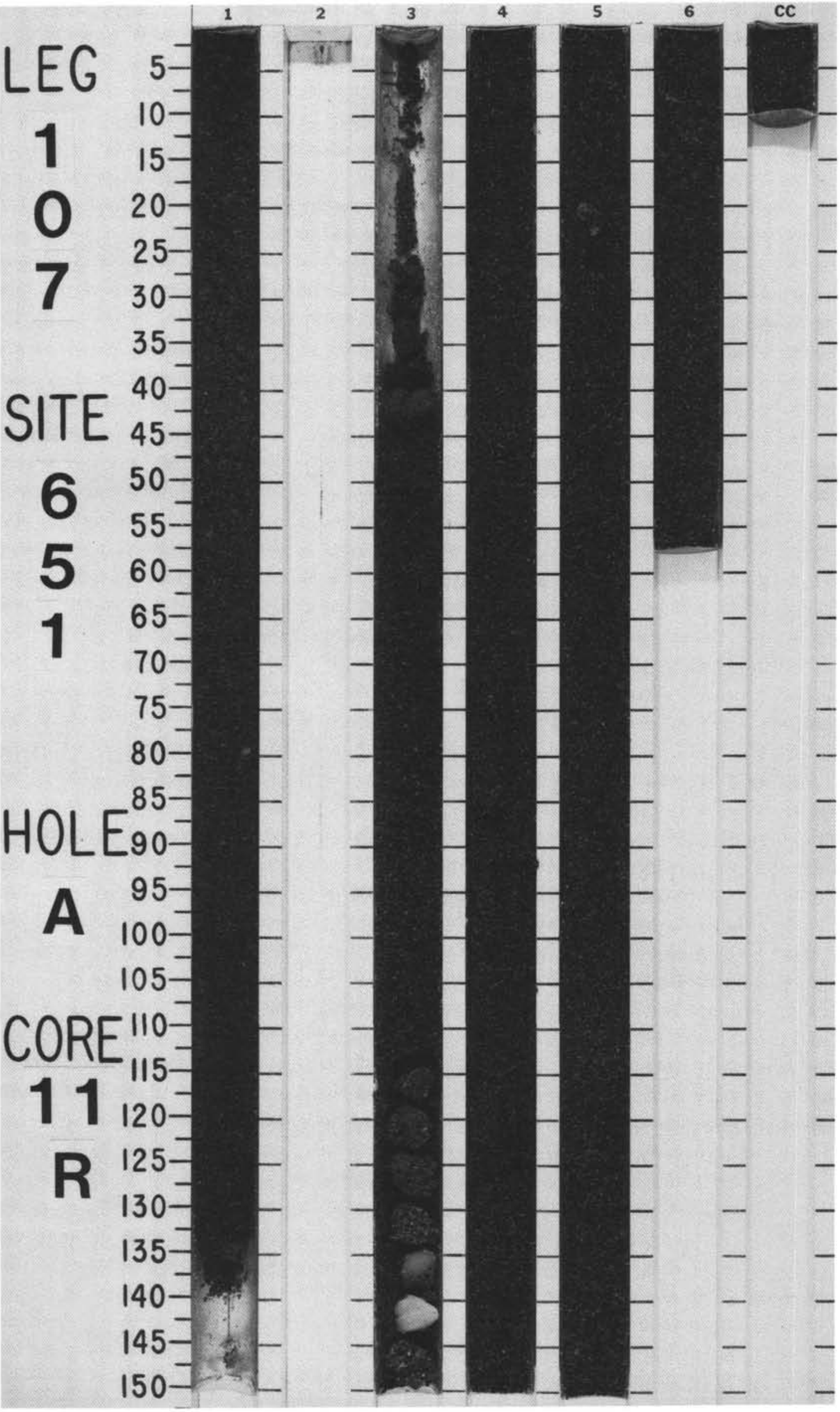
LEG
107
SITE
651
HOLE
A
CORE
11
R
1
2
3
4
5
6
CC
5
10
15
20
25
30
35
40
45
50
55
60
65
70
75
80
85
90
95
100
105
110
115
120
125
130
135
140
145
150

SITE 651 HOLE A CORE 12 R CORED INTERVAL 3675.4-3685.0 mbsl; 97.4-107.0 mbsf

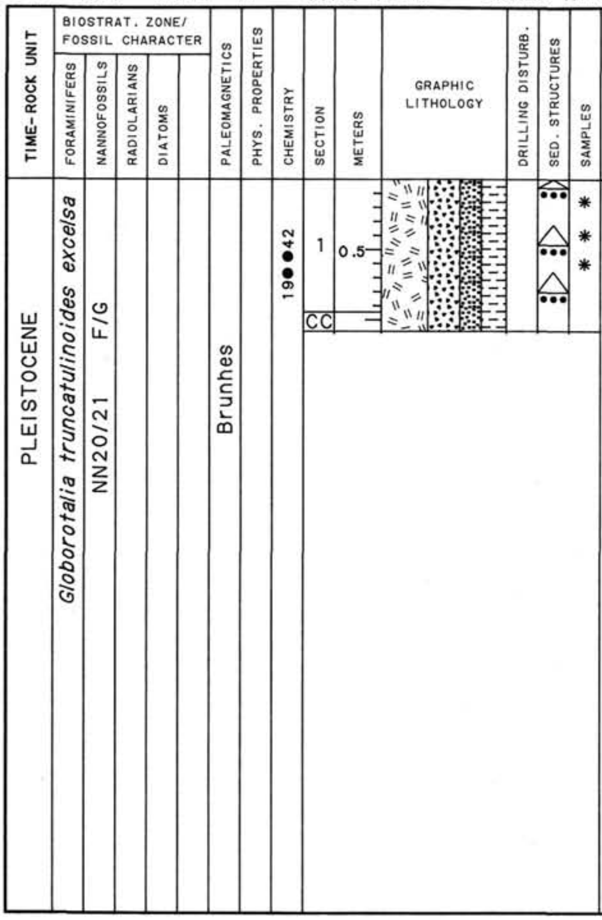

LITHOLOGIC DESCRIPTION

BRECCIA, SAND, GRAVEL, CLAY, MUDSTONE, and NANNOFOSSIL OOZE

Color ranges from dark gray (5Y 4/1) and gray (5Y 5/1) to olive-gray (5Y 4/2) and very dark gray (5Y 3/1); in Section 1, three graded units composed of indurated breccia and sand with gravel passing into clay and mudstone; clast size reaches 5 mm; clasts are heterogeneous and appear to include material of extrusive, sedimentary, and possibly metamorphic origin; at 19 cm, piece of indurated clay dated as late Pliocene on the basis of nannofossil content.

Interpretation: coarse clastic facies showing the beginning of increased cementation downward.

SMEAR SLIDE SUMMARY (%):

	1, 19 D	1, 45 D	1, 67 M
TEXTURE:			
Sand	—	40	—
Silt	1	30	5
Clay	99	30	95
COMPOSITION:			
Quartz	—	10	—
Feldspar	1	10	1
Rock fragments	—	—	1
Clay	38	21	1
Volcanic glass	5	2	20
Calcite/dolomite	5	15/2	5/0
Cement	—	—	2
Accessory minerals	—	10	5
Micrite	40	—	30
Amphibole	—	—	Tr
Opal cement	—	—	5
Foraminifers	1	10	Tr
Nannofossils	20	—	30

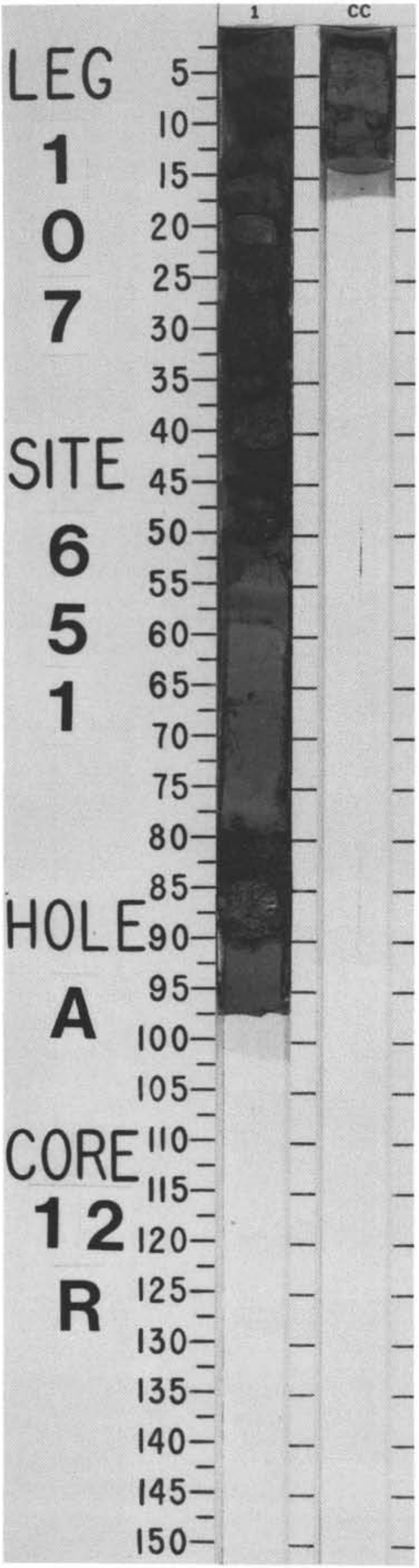
LEG
107
SITE
651
HOLE
A
CORE
12R
1
CC
5
10
15
20
25
30
35
40
45
50
55
60
65
70
75
80
85
90
95
100
105
110
115
120
125
130
135
140
145
150

SITE 651 HOLE A CORE 13 R CORED INTERVAL 3685.0-3694.7 mbsl; 107.0-116.7 mbsf

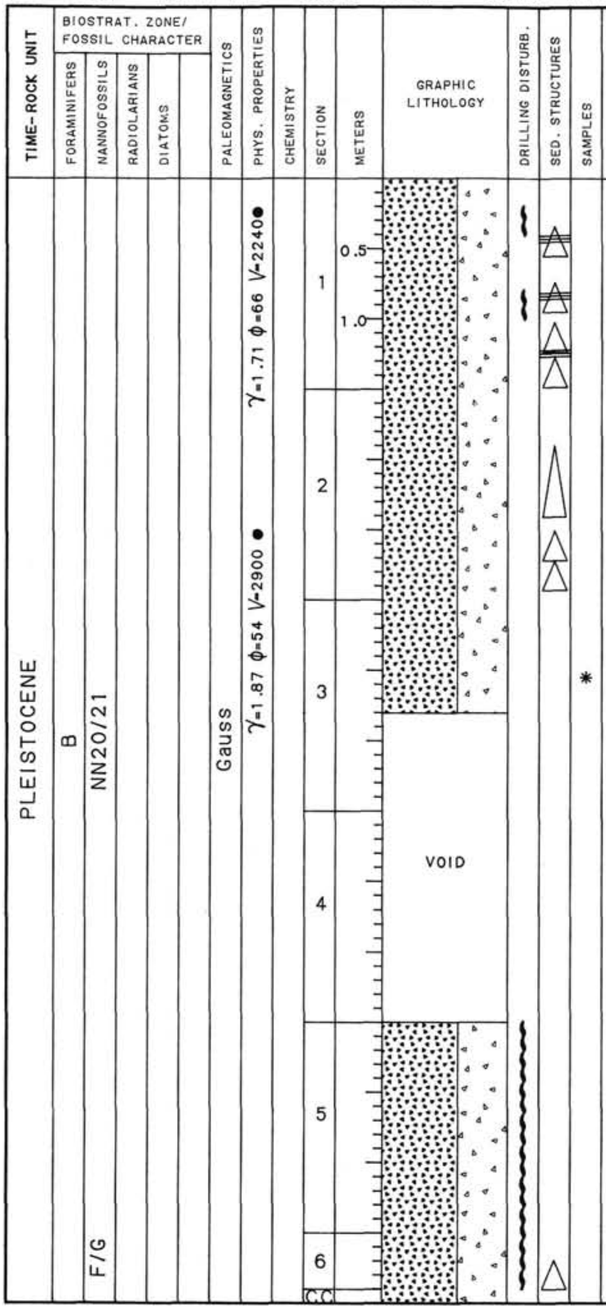

LITHOLOGIC DESCRIPTION

BRECCIA, SAND, and SANDSTONE

Sand and sandstone with breccia ranging gradually from well-indurated with silica (opal?) cement to totally unconsolidated; some of the unconsolidated sediment may be washdown material and not *in situ*; very dark gray (5Y 3/1) to dark gray (5Y 4/1); a number of graded units are interpreted as discrete depositional pulses.

Clastic grains are as large as 1 cm in diameter; under the binocular microscope grains of angular quartz and green translucent glass are seen with pyroxene, amphibole, olivine, basalt, obsidian, and fine-grained limestone, which fizzes in HCl.

Interpretation: a largely turbidite, volcaniclastic facies.

SMEAR SLIDE SUMMARY (%):

	3, 52 D
TEXTURE:	
Sand	90
Silt	10
Clay	—
COMPOSITION:	
Quartz	5
Feldspar	5
Rock fragments	40
Volcanic glass	50

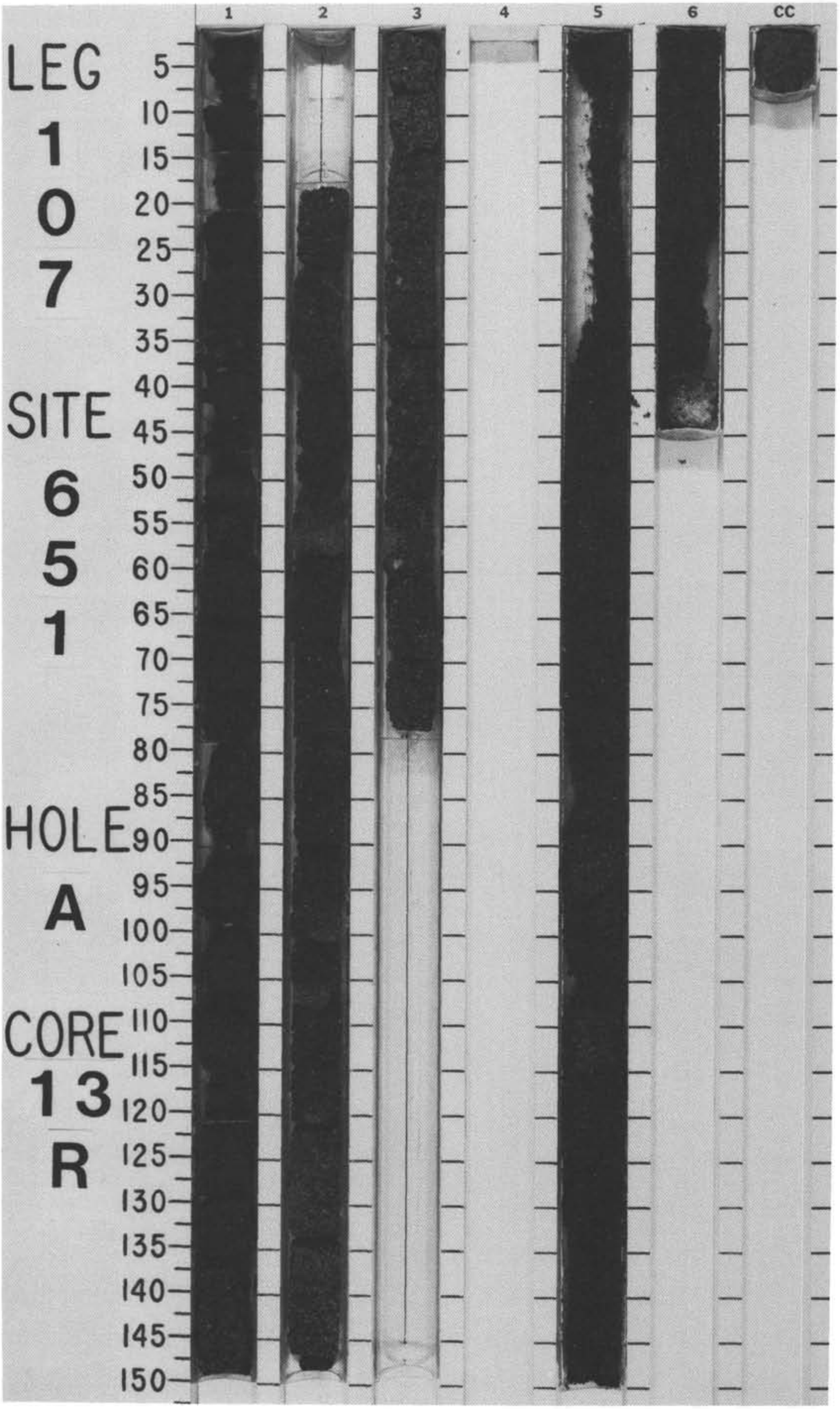
LEG
107
SITE
651
HOLE
A
CORE
13
R
1
2
3
4
5
6
CC
5
10
15
20
25
30
35
40
45
50
55
60
65
70
75
80
85
90
95
100
105
110
115
120
125
130
135
140
145
150

SITE 651 HOLE A CORE 14 R CORED INTERVAL 3694.7-3704.3 mbsl; 116.7-126.3 mbsf

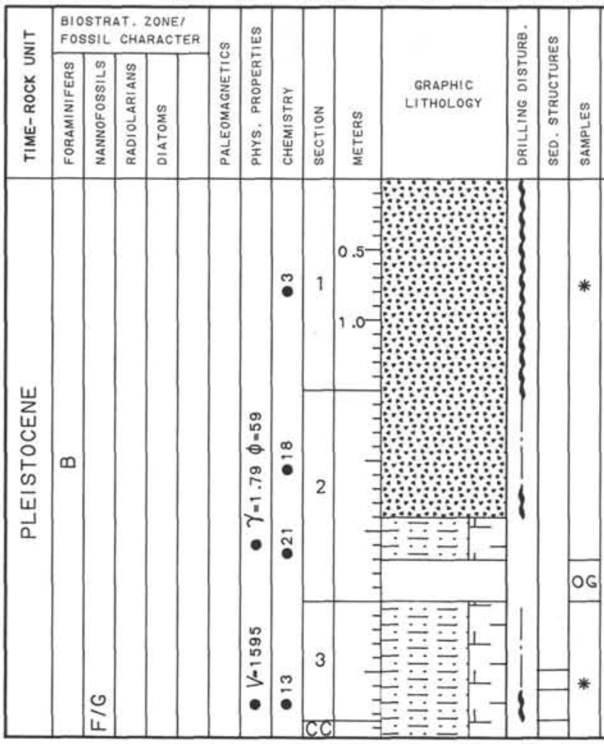

LITHOLOGIC DESCRIPTION

SAND and CALCAREOUS MUD

Volcaniclastic sand (lapilli), well-sorted, very dark gray (5Y 3/1), with possible drilling disturbance; from Section 2, 95 cm, homogeneous calcareous mud.

SMEAR SLIDE SUMMARY (%):

	1, 80 D	3, 59 D
TEXTURE:		
Sand	80	—
Silt	10	20
Clay	10	80
COMPOSITION:		
Quartz	15	5
Feldspar	10	5
Rock fragments	5	—
Clay	Tr	32
Volcanic glass	50	10
Calcite/dolomite	10	10/2
Accessory minerals	10	3
Micrite	Tr	20
Foraminifers	Tr	2
Nannofossils	Tr	10
Sponge spicules	—	1

SITE 651 HOLE A CORE 15 R CORED INTERVAL 3704.3-3714.0 mbsl; 126.3-136.0 mbsf

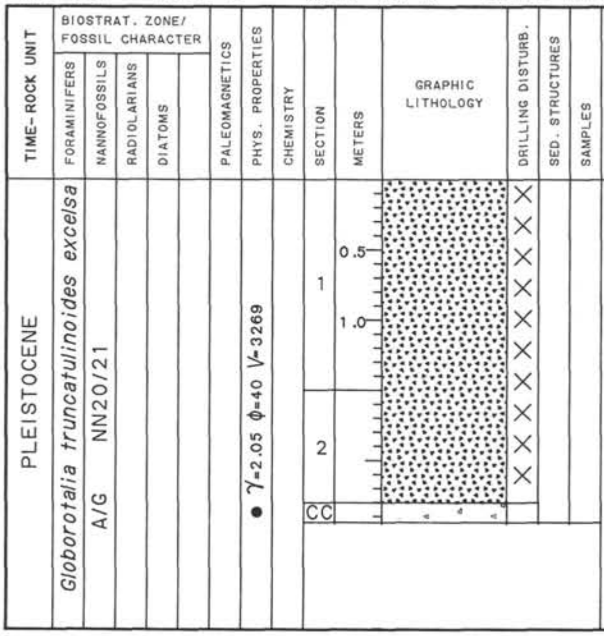

LITHOLOGIC DESCRIPTION

VOLCANIC LAPILLI

Lapilli tuff and volcanic breccia, very dark gray (5Y 3/1), mostly composed of vitric fragments in various stages of alteration in Section 2; light olive-gray (5Y 6/2), calcareous clay with plastic consistency at 17 cm (± 2 cm).

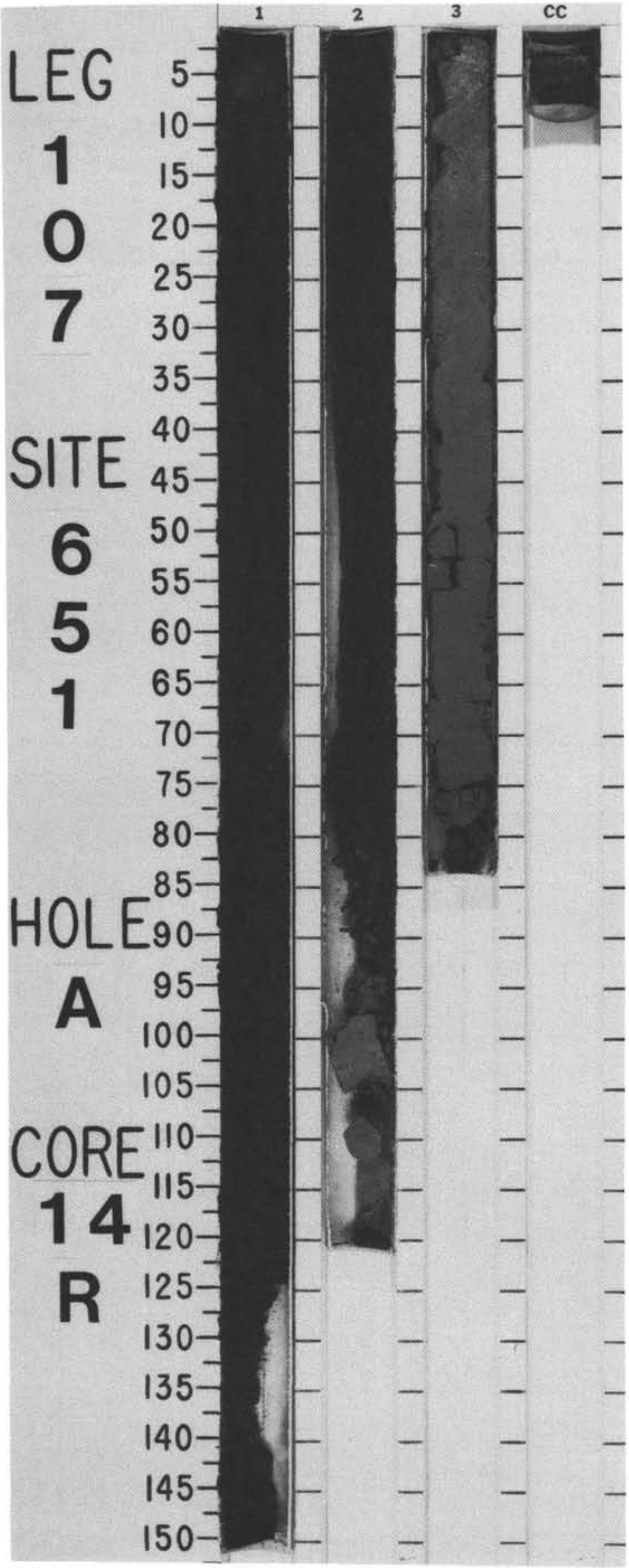
LEG
107
SITE
651
HOLE
A
CORE
14
R
1
2
3
CC
5
10
15
20
25
30
35
40
45
50
55
60
65
70
75
80
85
90
95
100
105
110
115
120
125
130
135
140
145
150

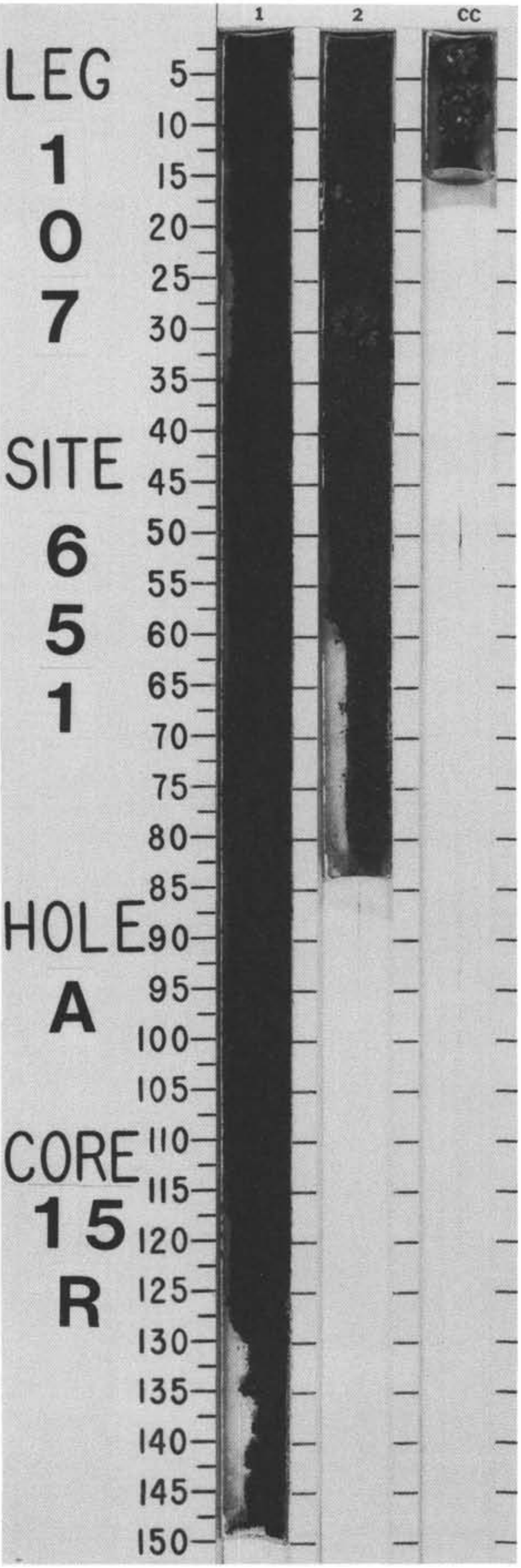
LEG
107
SITE
651
HOLE
A
CORE
15
R
1
2
CC
5
10
15
20
25
30
35
40
45
50
55
60
65
70
75
80
85
90
95
100
105
110
115
120
125
130
135
140
145
150

SITE 651 HOLE A CORE 16 R CORED INTERVAL 3714.0-3723.7 mbsl; 136.0-145.7 mbsf

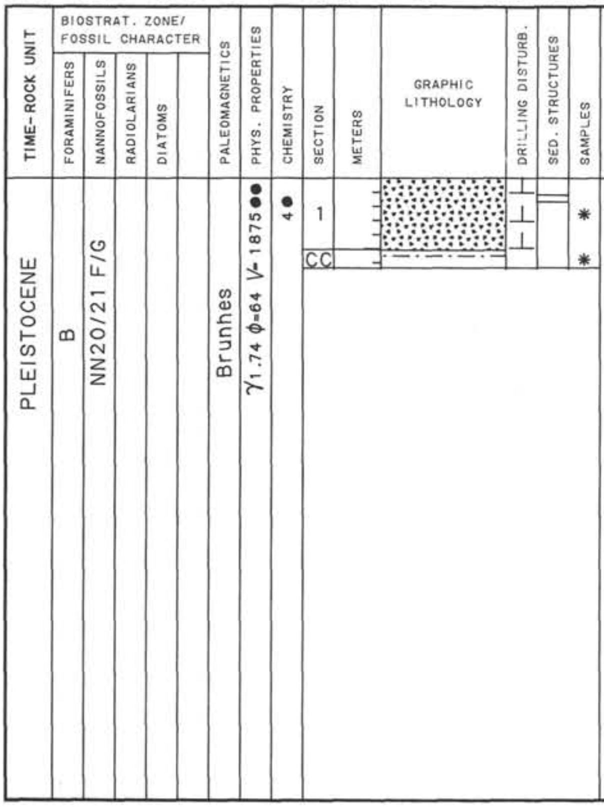

LITHOLOGIC DESCRIPTION

VOLCANIC ASH and SAND

Interbedded ash and layers of finely laminated, moderately bioturbated ash containing marly chalk, gray (10Y 5/1); CC composed of fine-grained, light gray (10Y 6/2), millimeter-thick laminations of sand mudstone.

SMEAR SLIDE SUMMARY (%):

	1, 25 D	CC, 11 M
TEXTURE:		
Sand	5	15
Silt	30	35
Clay	65	50
COMPOSITION:		
Quartz	7	15
Feldspar	10	10
Rock fragments	—	1
Mica	Tr	—
Clay	29	14
Volcanic glass	15	10
Calcite/dolomite	5	10
Micrite	20	20
Accessory minerals	2	5
Foraminifers	2	5
Nannofossils	10	10
Sponge spicules	Tr	—

SITE 651 HOLE A CORE 17 R CORED INTERVAL 3723.7-3732.9 mbsl; 145.7-154.9 mbsf

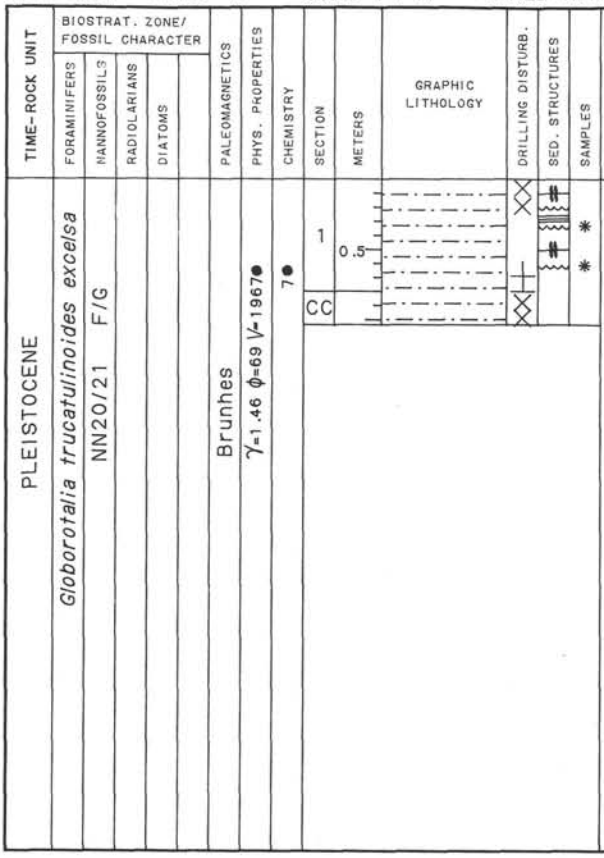

LITHOLOGIC DESCRIPTION

SILTY MUD

Silty mud, olive-gray (5Y 5/2) to dark gray (5Y 4/1), with thin (<0.5-mm) layers of detrital foraminifer sandy mud; possible fine-grained turbidites.

SMEAR SLIDE SUMMARY (%):

	1, 37 M	1, 65 D
TEXTURE:		
Sand	20	5
Silt	35	15
Clay	45	80
COMPOSITION:		
Quartz	10	4
Feldspar	6	7
Clay	37	33
Volcanic glass	5	5
Calcite/dolomite	5/Tr	5/2
Micrite	5	10
Accessory minerals	2	—
Foraminifers	15	Tr
Nannofossils	6	34
Diatoms	6	—
Radiolarians	3	—
Sponge spicules	Tr	—
Fish remains	—	Tr

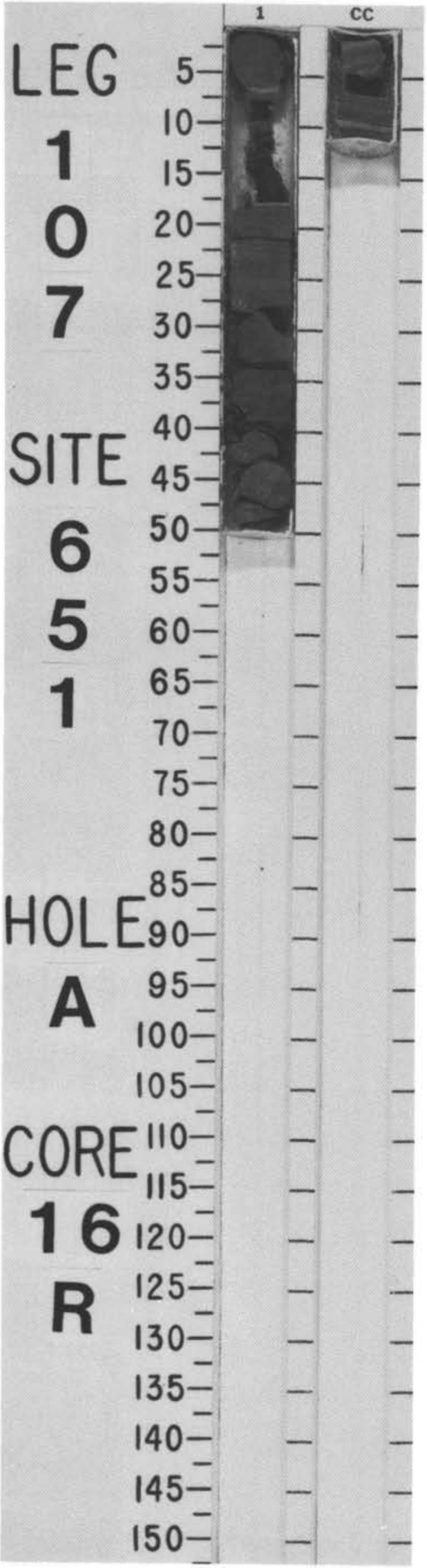
1
CC
LEG
107
SITE
651
HOLE
A
CORE
16
R
5
10
15
20
25
30
35
40
45
50
55
60
65
70
75
80
85
90
95
100
105
110
115
120
125
130
135
140
145
150

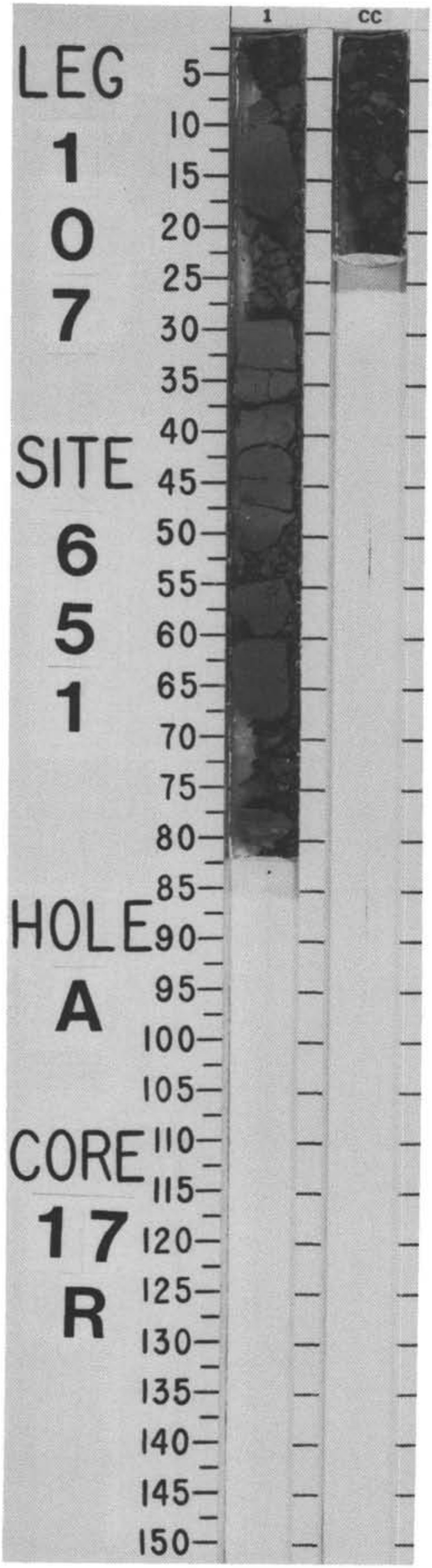
1
CC
LEG
107
SITE
651
HOLE
A
CORE
17
R
5
10
15
20
25
30
35
40
45
50
55
60
65
70
75
80
85
90
95
100
105
110
115
120
125
130
135
140
145
150

SITE 651 HOLE A CORE 18 R CORED INTERVAL 3732.9-3742.6 mbsl; 154.9-164.6 mbsf

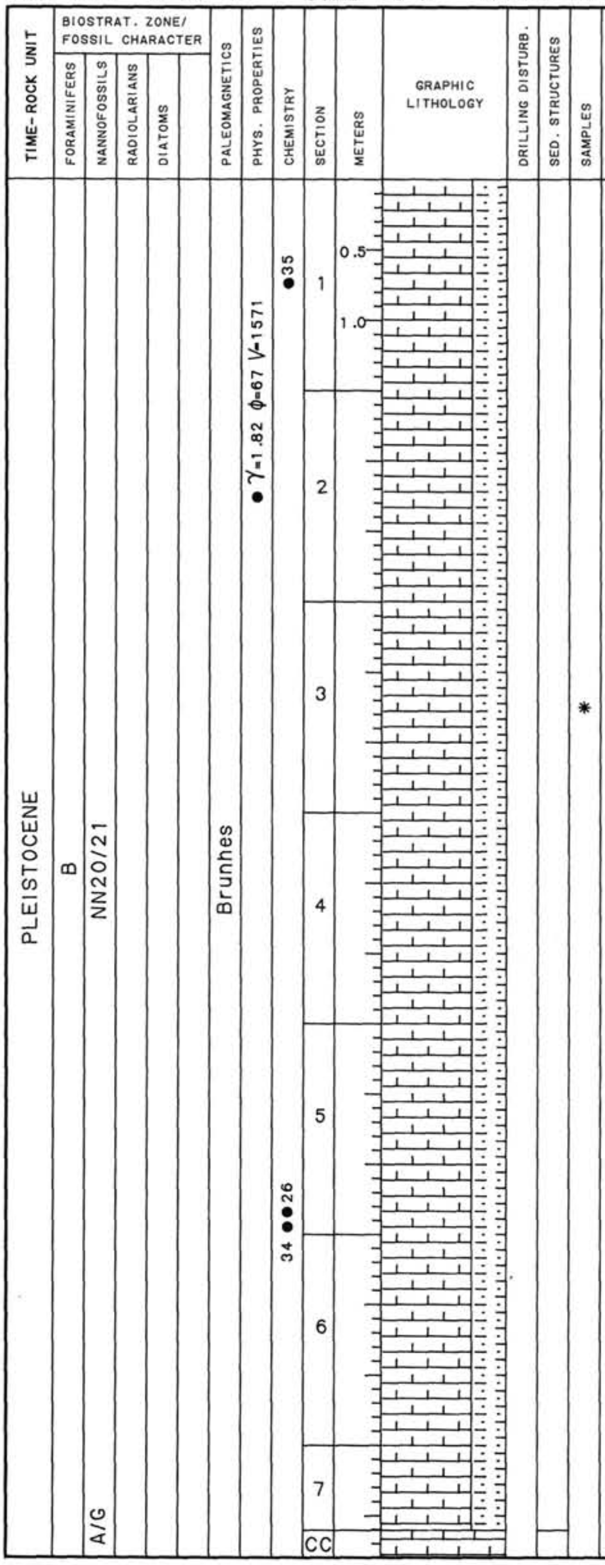

LITHOLOGIC DESCRIPTION

MARLY CHALK

Light gray (5Y 5/1), homogeneous, marly chalk.

SMEAR SLIDE SUMMARY (%):

	3, 75 D
TEXTURE:	
Sand	5
Silt	15
Clay	80
COMPOSITION:	
Quartz	1
Mica	1
Clay	10
Volcanic glass	15
Micronodules	5
Micrite	10
Accessory minerals	2
Foraminifers	3
Nannofossils	53
Sponge spicules	Tr

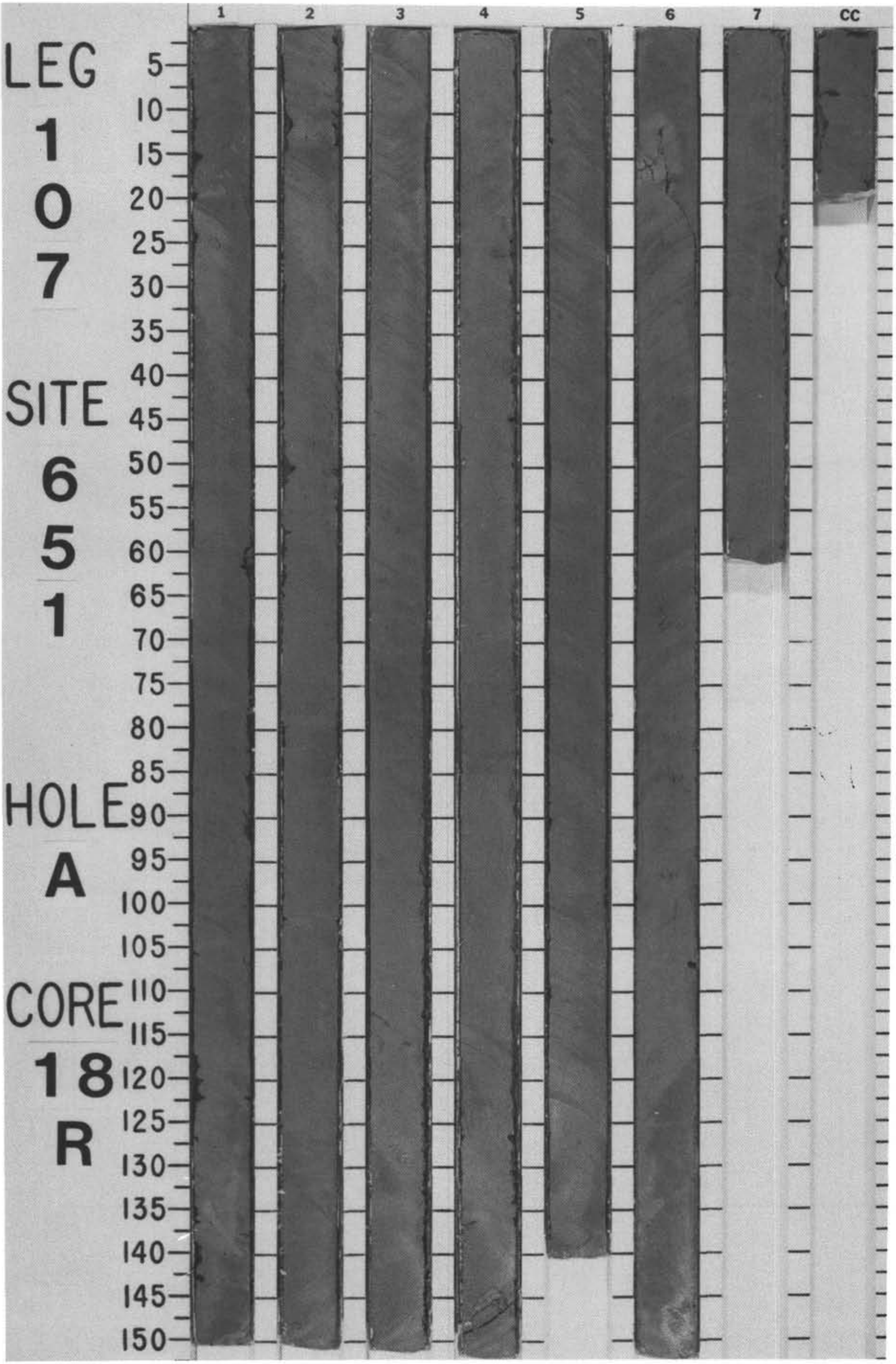
LEG
107
SITE
651
HOLE
A
CORE
18R
1
2
3
4
5
6
7
CC
5
10
15
20
25
30
35
40
45
50
55
60
65
70
75
80
85
90
95
100
105
110
115
120
125
130
135
140
145
150

SITE 651 HOLE A CORE 19 R CORED INTERVAL 3742.6-3752.2 mbsl; 164.6-174.2 mbsf

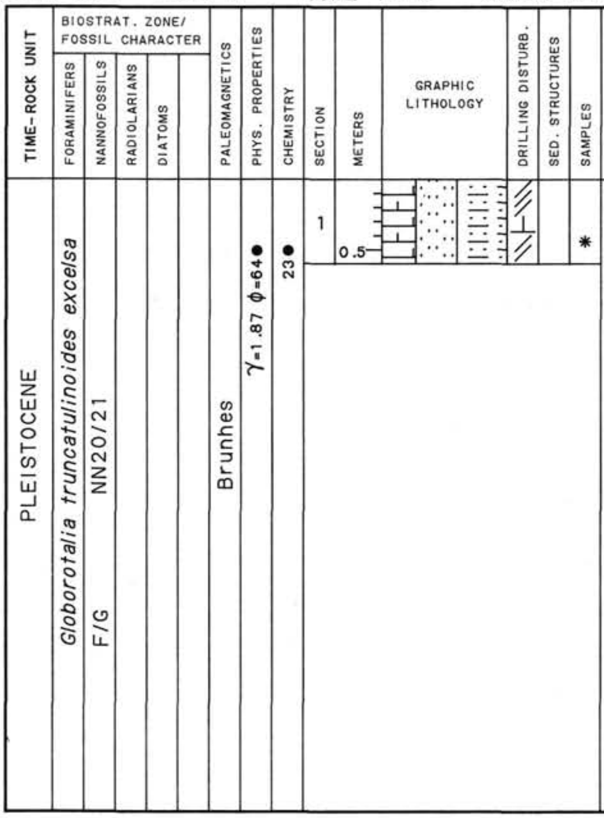

LITHOLOGIC DESCRIPTION

SILTY MUD

Highly laminated, silty nannofossil mud, light gray (5Y 5/1).

SMEAR SLIDE SUMMARY (%):

	1, 49 D
TEXTURE:	
Sand	20
Silt	35
Clay	45
COMPOSITION:	
Quartz	15
Feldspar	10
Rock fragments	6
Clay	9
Volcanic glass	6
Calcite/dolomite	8/2
Accessory minerals	2
Foraminifers	15
Nannofossils	20
Diatoms	4
Radiolarians	3
Fish remains	Tr

SITE 651 HOLE A CORE 20 R CORED INTERVAL 3752.2-3761.9 mbsl; 174.2-183.9 mbsf

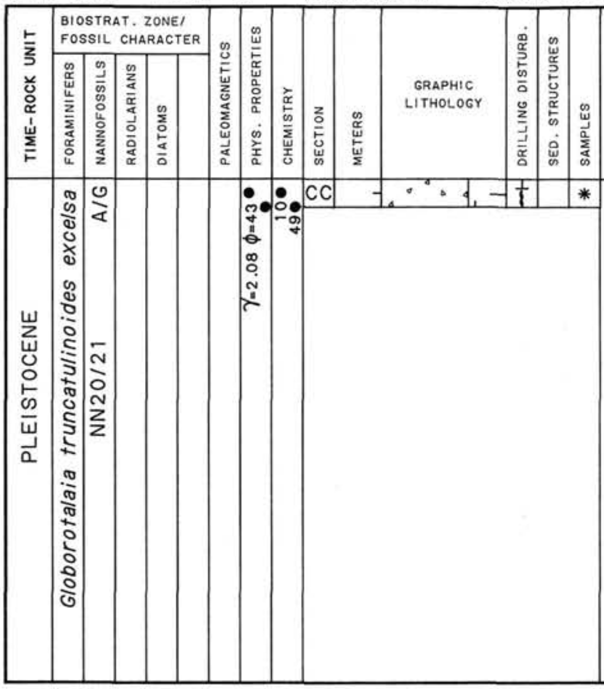

LITHOLOGIC DESCRIPTION

VOLCANIC BRECCIA and NANNOFOSSIL OOZE

Coarse to granular, cemented, volcanic breccia, gray (5Y 5/1); nannofossil ooze, light gray (5Y 6/1).

SMEAR SLIDE SUMMARY (%):

	CC, 14 D
TEXTURE:	
Sand	—
Silt	5
Clay	95
COMPOSITION:	
Quartz	3
Clay	10
Micrite	7
Foraminifers	6
Nannofossils	73
Fish remains	1

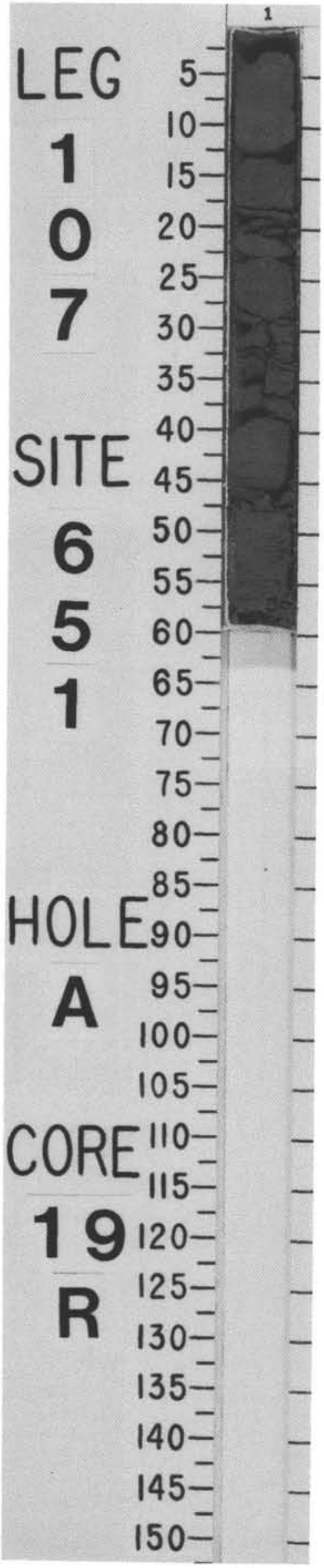
1
LEG
1
0
7
SITE
6
5
1
HOLE
A
CORE
19
R
5
10
15
20
25
30
35
40
45
50
55
60
65
70
75
80
85
90
95
100
105
110
115
120
125
130
135
140
145
150

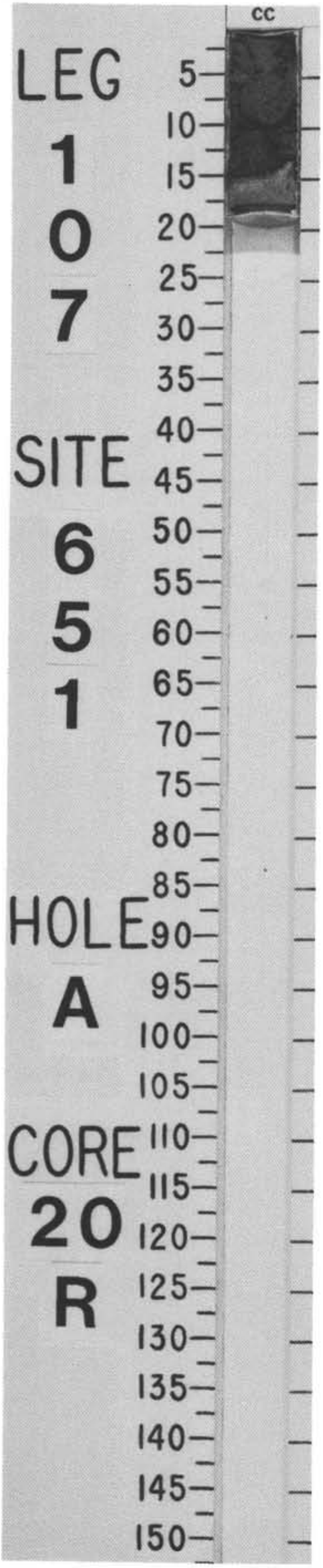
CC
LEG
1
0
7
SITE
6
5
1
HOLE
A
CORE
20
R
5
10
15
20
25
30
35
40
45
50
55
60
65
70
75
80
85
90
95
100
105
110
115
120
125
130
135
140
145
150

SITE 651 HOLE A CORE 21 R CORED INTERVAL 3761.9-3771.5 mbsl; 183.9-193.5 mbsf

TIME-ROCK UNIT	BIOSTRAT. ZONE/ FOSSIL CHARACTER					PALEOMAGNETICS	PHYS. PROPERTIES	CHEMISTRY	SECTION	METERS	GRAPHIC LITHOLOGY	DRILLING DISTURB.	SED. STRUCTURES	SAMPLES
	FORAMINIFERS	NANNOFOSSILS	RADIOLARIANS	DIATOMS										
PLEISTOCENE	B	NN20/21 R/G							CC		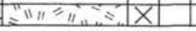			

LITHOLOGIC DESCRIPTION

VOLCANIC ASH

Fine-grained vitric tuff, very dark gray (5Y 3/1), laminated.

SITE 651 HOLE A CORE 22 R CORED INTERVAL 3771.5-3781.2 mbsl; 193.5-203.2 mbsf

TIME-ROCK UNIT	BIOSTRAT. ZONE/ FOSSIL CHARACTER					PALEOMAGNETICS	PHYS. PROPERTIES	CHEMISTRY	SECTION	METERS	GRAPHIC LITHOLOGY	DRILLING DISTURB.	SED. STRUCTURES	SAMPLES
	FORAMINIFERS	NANNOFOSSILS	RADIOLARIANS	DIATOMS										
PLEISTOCENE	*Globorotalia truncatulinoides excelsa*	NN20/21 A/G				Brunhes	γ=1.99 ϕ=59 V=1700 ● ● ● ●	● 7 ● 5 ● 13	1 CC	0.5	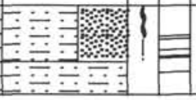			

LITHOLOGIC DESCRIPTION

GRAVEL, SAND, and CALCAREOUS MUDSTONE

Limited recovery of poorly laminated gravel and sand with some interbedded, weakly indurated clayey mudstone, dark olive-gray (5Y 5/2) to light olive-gray (5Y 4/2); CC recovery was disturbed, but a single lamination was observed at 5 cm.

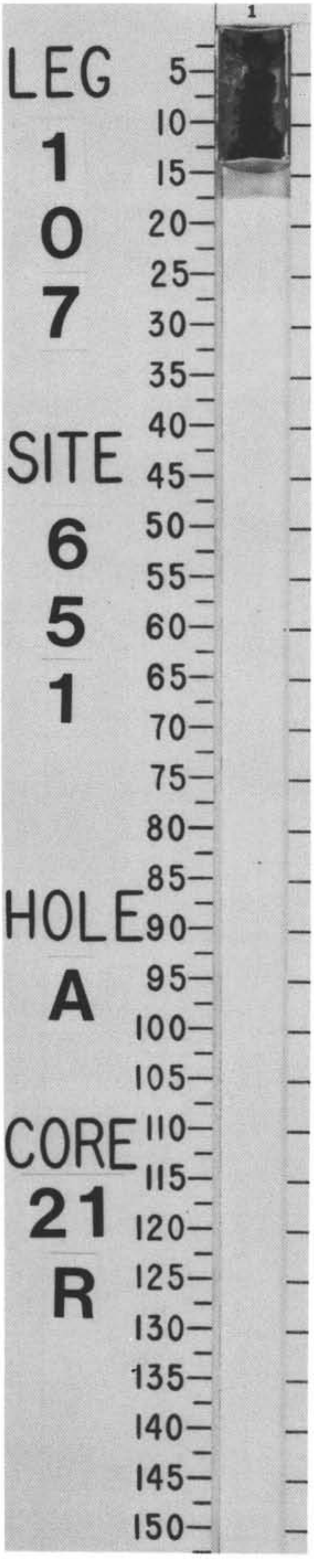
1
LEG
1
0
7
SITE
6
5
1
HOLE
A
CORE
21
R
5
10
15
20
25
30
35
40
45
50
55
60
65
70
75
80
85
90
95
100
105
110
115
120
125
130
135
140
145
150

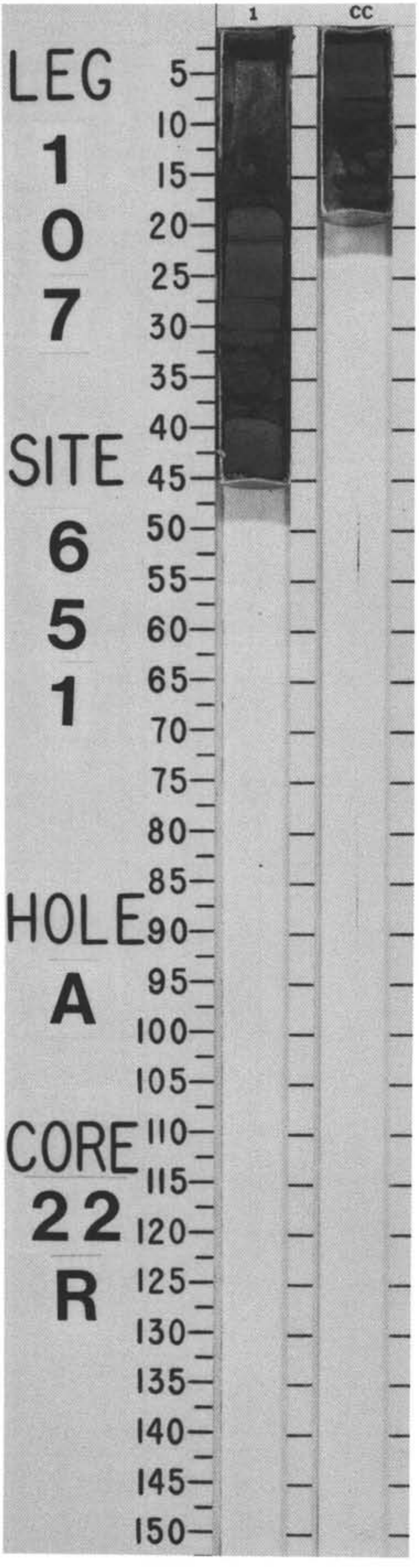
1
CC
LEG
1
0
7
SITE
6
5
1
HOLE
A
CORE
22
R
5
10
15
20
25
30
35
40
45
50
55
60
65
70
75
80
85
90
95
100
105
110
115
120
125
130
135
140
145
150

SITE 651 HOLE A CORE 23 R CORED INTERVAL 3781.2-3790.9 mbsl; 203.2-212.9 mbsf

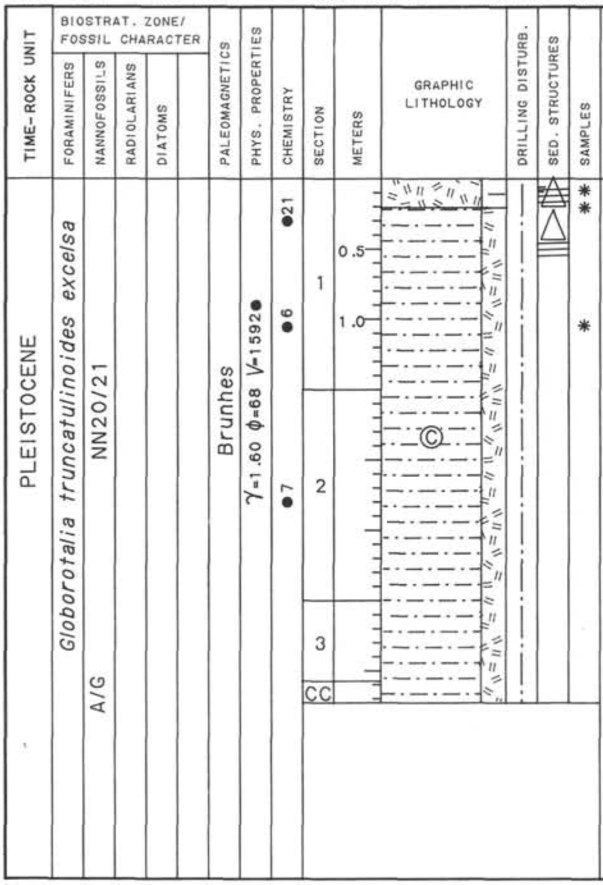

LITHOLOGIC DESCRIPTION

SILTY MUD, SILTY SAND, SAND, and SANDSTONE, partly VOLCANOGENIC

Homogeneous, silty mud, with a major volcanic input as seen in the smear slides; in Section 1, 0–20 cm, well-cemented, coarse sandstone containing moderately well rounded grains as large as 5 mm in diameter, two graded units; below, a thin layer of convoluted, laminated, sandy silt with graded bedding.

Interpretation: minor turbidite and gravity-enhanced grain flow input into "background" hemipelagic silty mud with marked volcanic provenance.

SMEAR SLIDE SUMMARY (%):

	1, 4	1, 23	1, 102
	D	M	D
TEXTURE:			
Sand	30	45	—
Silt	30	35	15
Clay	40	20	85
COMPOSITION:			
Quartz	5	5	Tr
Feldspar (sanidine?)	5	2	—
Rock fragments	Tr	—	—
Mica	Tr	2	—
Clay	30	25	20
Volcanic glass	30	10	35
Calcite/dolomite	—	—	Tr
Cement	5	—	—
Opaques	—	—	5
Pyroxene	3	10	Tr
Foraminifers	5	5	5
Nannofossils	15	25	25
Olivine?	2	3	—
Zeolite	Tr	5	Tr
Bioclasts	Tr	5	5

SITE 651 HOLE A CORE 24 R CORED INTERVAL 3790.9-3800.6 mbsl; 212.9-222.6 mbsf

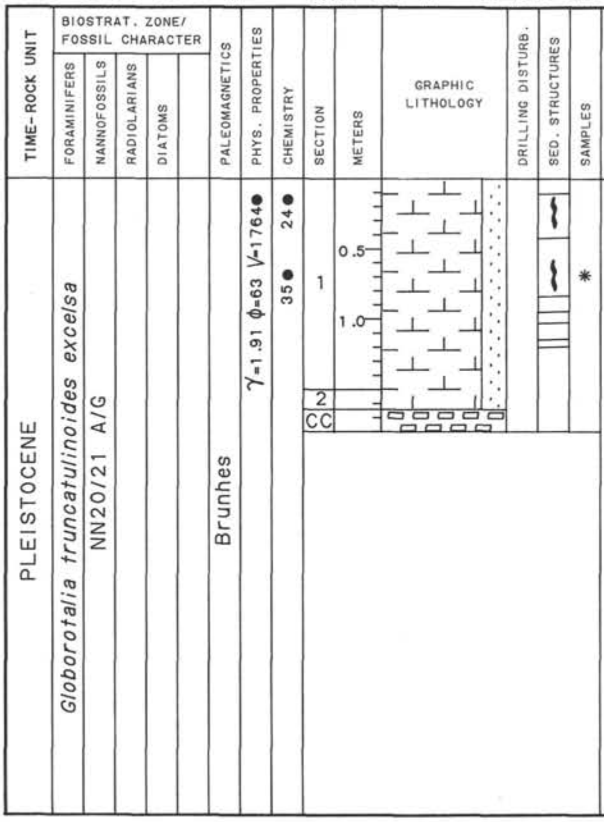

LITHOLOGIC DESCRIPTION

NANNOFOSSIL MUD with minor SILTSTONE

Repeated, thin (2–5-cm), nannofossil mud beds, plastic, often with massive or laminated basal portions and paler, burrowed upper portions; several discrete parallel-laminated siltstones with sharp bases and weak normal grading (e.g., Section 1, 103 cm); nannofossil mud is light olive-gray (5Y 5/2) and siltstone is dark olive-gray (5Y 3/2).

Interpretation: dominated by the nannofossil turbidites with rare, coarser (silt) turbidites of possibly different provenance. Mineralogy of the siltstone awaits shore-based determination.

SMEAR SLIDE SUMMARY (%):

	1, 70
	D
TEXTURE:	
Sand	5
Silt	10
Clay	85
COMPOSITION:	
Quartz	5
Mica	5
Clay	15
Calcite/dolomite	3
Opaques	2
Zircon	2
Foraminifers	17
Nannofossils	51
Bioclasts	5
Aragonite needles	Tr

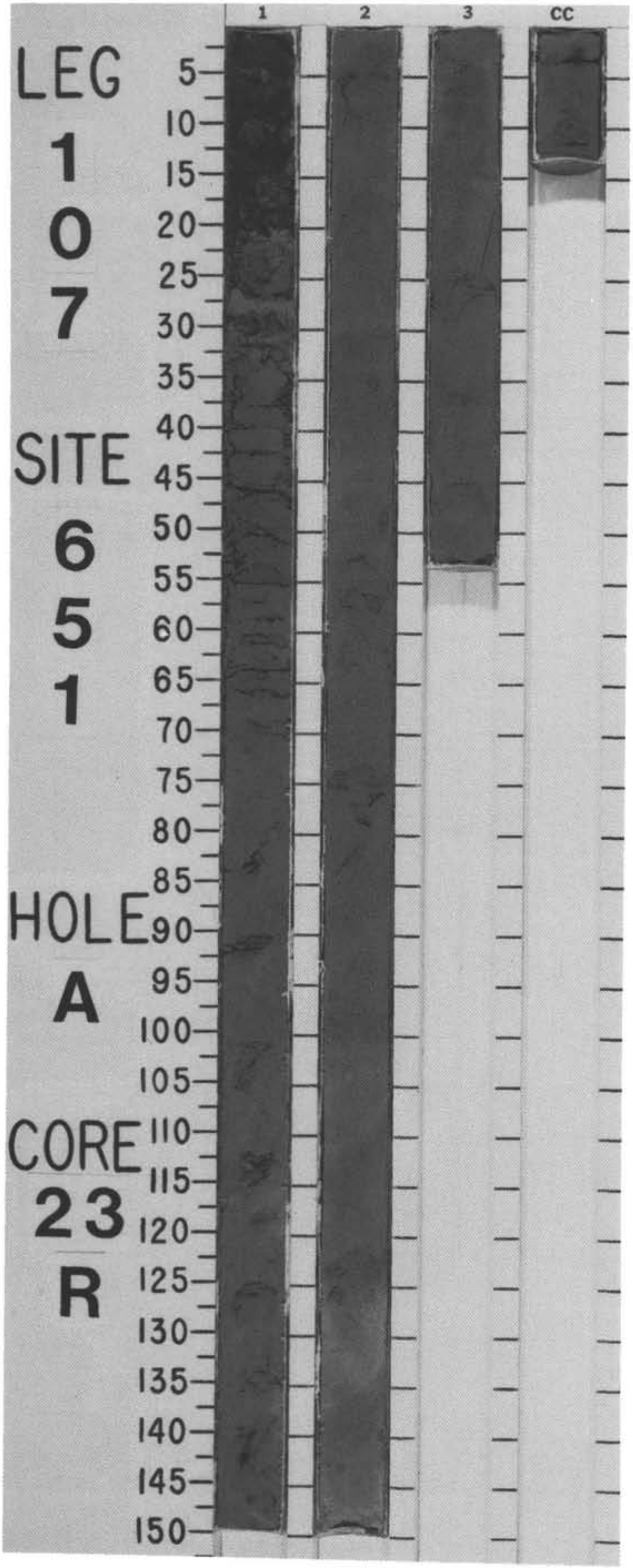
1
2
3
CC
LEG
107
SITE
651
HOLE
A
CORE
23
R
5
10
15
20
25
30
35
40
45
50
55
60
65
70
75
80
85
90
95
100
105
110
115
120
125
130
135
140
145
150

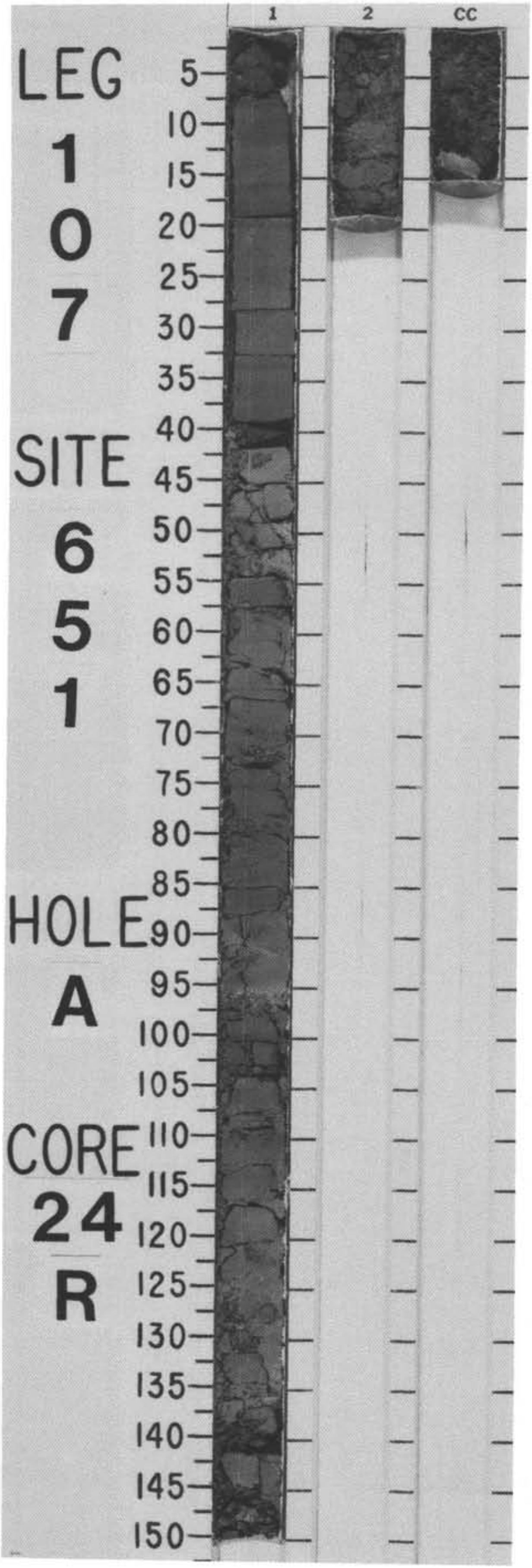
1
2
CC
LEG
107
SITE
651
HOLE
A
CORE
24
R
5
10
15
20
25
30
35
40
45
50
55
60
65
70
75
80
85
90
95
100
105
110
115
120
125
130
135
140
145
150

SITE 651 HOLE A CORE 25 R CORED INTERVAL 3800.6-3810.3 mbsl; 222.6-232.3 mbsf

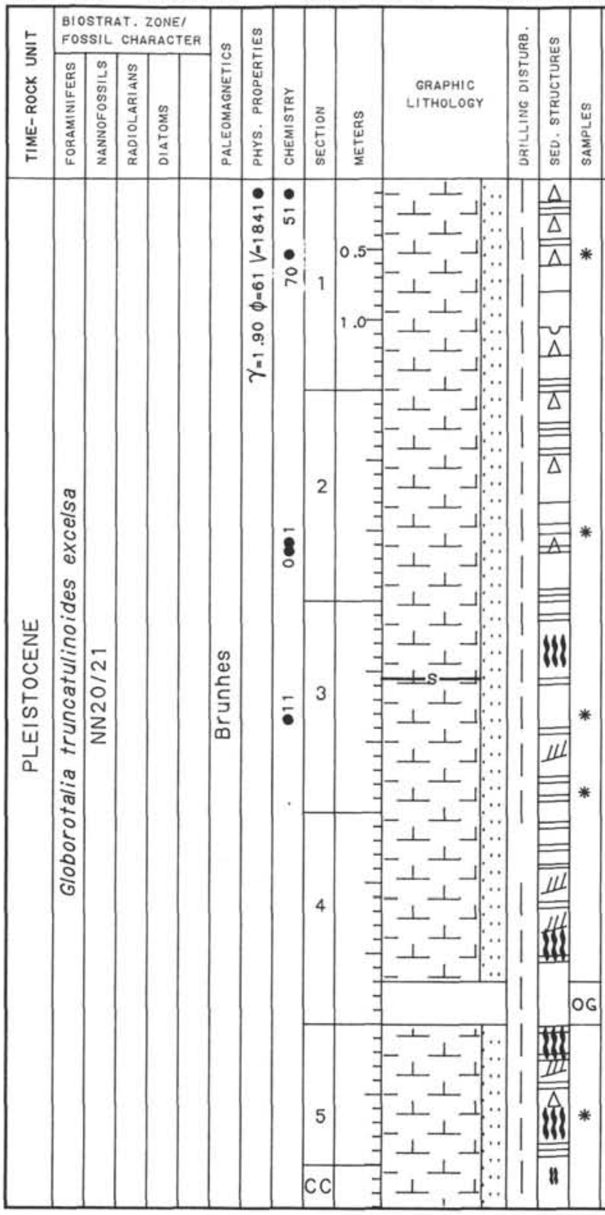

LITHOLOGIC DESCRIPTION

NANNOFOSSIL CHALK with subordinate CLAY and minor SILTSTONE

Thin (<12 cm) alternations of nannofossil ooze ranging from gray (5Y 5/1) to olive-gray (5Y 5/2) and light gray (5Y 6/1); in Section 4 and below, mud becomes more dominant; in Section 3, 144 cm, very dark gray (5Y 3/1) thin-bedded (2 cm) siltstone may contain garnet, and at 55 cm, a black, sapropelic horizon. Well-preserved, small-scale structures include grading, parallel lamination, low-angle micro-cross-lamination, and convolute lamination.

Interpretation: nannofossil ooze and mud turbidites, including both volcanic and siliciclastic provenance.

SMEAR SLIDE SUMMARY (%):

	1, 55 D	2, 114 D	3, 80 D	3, 145 M	5, 71 M
TEXTURE:					
Sand	5	5	—	10	—
Silt	10	15	9	70	2
Clay	85	85	91	20	98
COMPOSITION:					
Quartz	5	5	Tr	—	—
Feldspar	—	—	Tr	—	—
Mica	3	2	—	—	—
Clay	17	30	45	10	—
Volcanic glass	2	4	25	45	90
Calcite/dolomite	—	1	—	—	—
Opaques	2	3	—	—	5
Zircon	1	—	—	—	—
Accessory minerals	2	—	—	—	5
Foraminifers	10	5	—	—	—
Nannofossils	35	45	25	—	—
Zeolites	—	—	Tr	45	—
Bioclasts	5	5	5	—	—
Organics	—	—	—	Tr	—

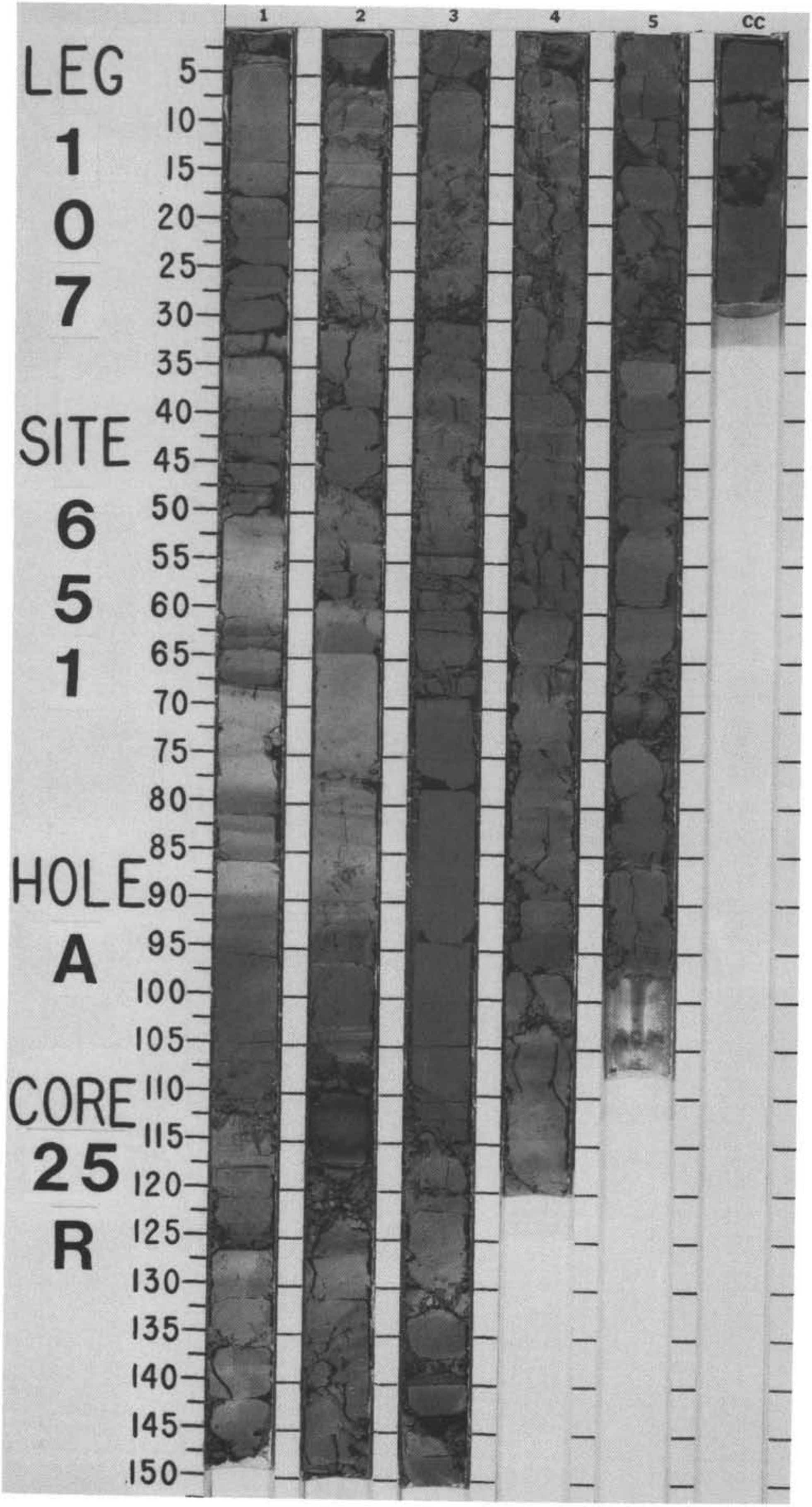
LEG
107
SITE
651
HOLE
A
CORE
25
R
1
2
3
4
5
CC
5
10
15
20
25
30
35
40
45
50
55
60
65
70
75
80
85
90
95
100
105
110
115
120
125
130
135
140
145
150

SITE 651 HOLE A CORE 26 R CORED INTERVAL 3810.3-3820.0 mbsl; 232.3-242.0 mbsf

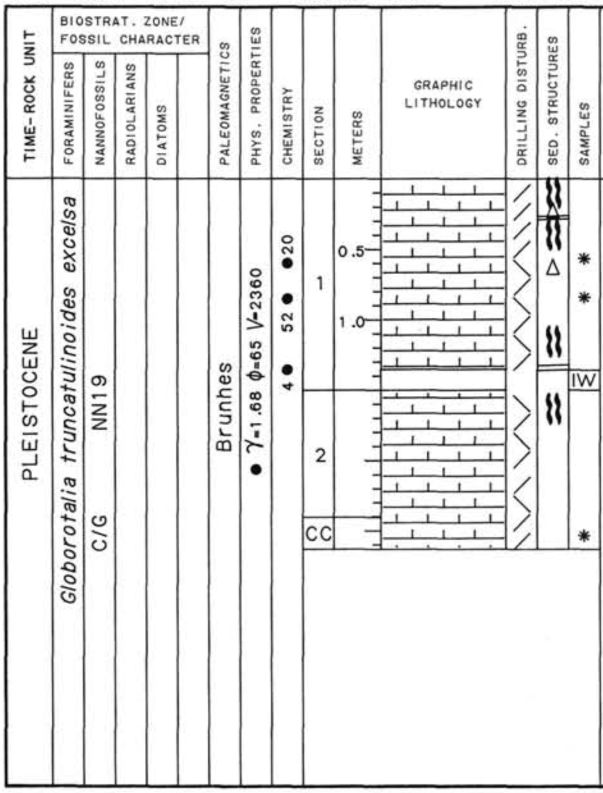

LITHOLOGIC DESCRIPTION

NANNOFOSSIL CHALK with rare SILTY PARTINGS

Olive-gray (5Y 5/2) to light olive-gray (5Y 5/1), nannofossil ooze, plastic but nonlithified, homogeneous except for rare burrowing and parallel laminations; in Section 2, 45–60 cm, well-lithified, nannofossil limestone.

SMEAR SLIDE SUMMARY (%):

	1, 63 M	1, 87 D	CC, 12 M
TEXTURE:			
Sand	—	—	—
Silt	20	5	25
Clay	80	95	75
COMPOSITION:			
Feldspar	5	—	—
Mica	—	—	Tr
Clay	15	—	25
Volcanic glass	—	1	40
Dolomite	1	1	Tr
Opaques	5	—	15
Zeolites	10	—	10
Analcite	—	—	5
Foraminifers	—	2	5
Nannofossils	54	96	Tr
Micrite	10	—	—

SITE 651 HOLE A CORE 27 R CORED INTERVAL 3820.0-3829.6 mbsl; 242.0-251.6 mbsf

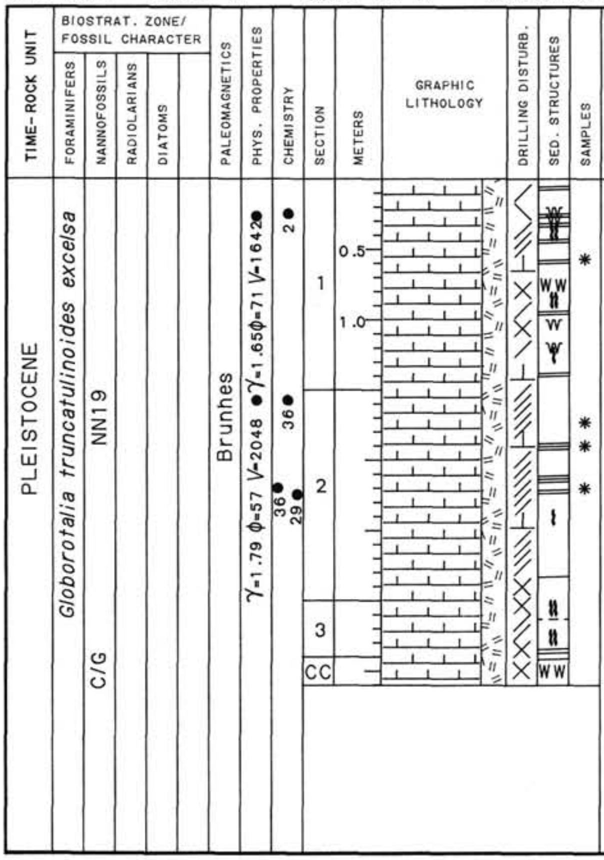

LITHOLOGIC DESCRIPTION

NANNOFOSSIL MUD and SANDY, SILTY, VOLCANIC ASH

Alternating nannofossil mud and sand, silt, and tuff; thin-bedded turbidite sequence with alternation of greenish gray (5GY 6/1), nannofossil chalk and dark gray (5Y 5/1), sandy, silty tuff.

SMEAR SLIDE SUMMARY (%):

	1, 65 M	2, 27 D	2, 41 M	2, 70 D
TEXTURE:				
Sand	20	—	15	5
Silt	30	10	30	15
Clay	50	90	55	80
COMPOSITION:				
Quartz	—	1	—	5
Feldspar	8	—	2	2
Mica	—	—	1	—
Clay	20	—	—	20
Volcanic glass	52	3	81	2
Calcite/dolomite	Tr	1	—	2/2
Accessory minerals	—	1	—	1
Analcime	1	—	6	—
Micrite	4	3	1	7
Other zeolites?	—	—	2	—
Foraminifers	2	2	2	4
Nannofossils	10	89	Tr	53
Diatoms	—	—	1	1
Radiolarians	2	—	4	1
Sponge spicules	1	—	—	—

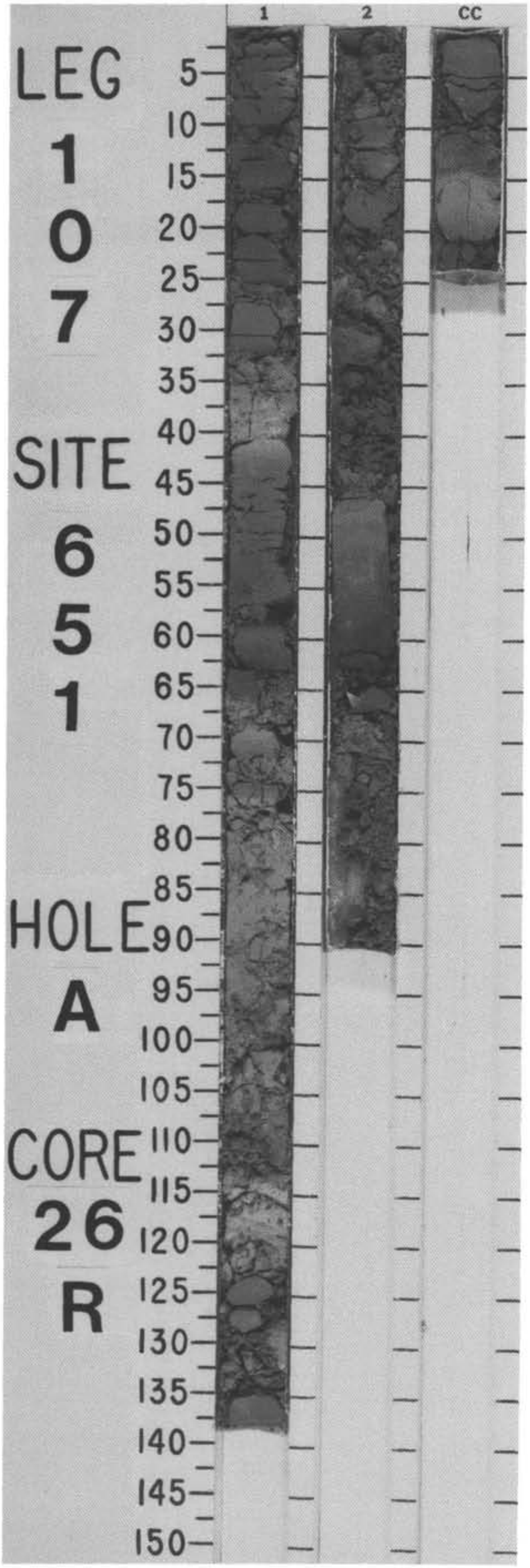
1
2
CC
LEG
107
SITE
651
HOLE
A
CORE
26
R
5
10
15
20
25
30
35
40
45
50
55
60
65
70
75
80
85
90
95
100
105
110
115
120
125
130
135
140
145
150

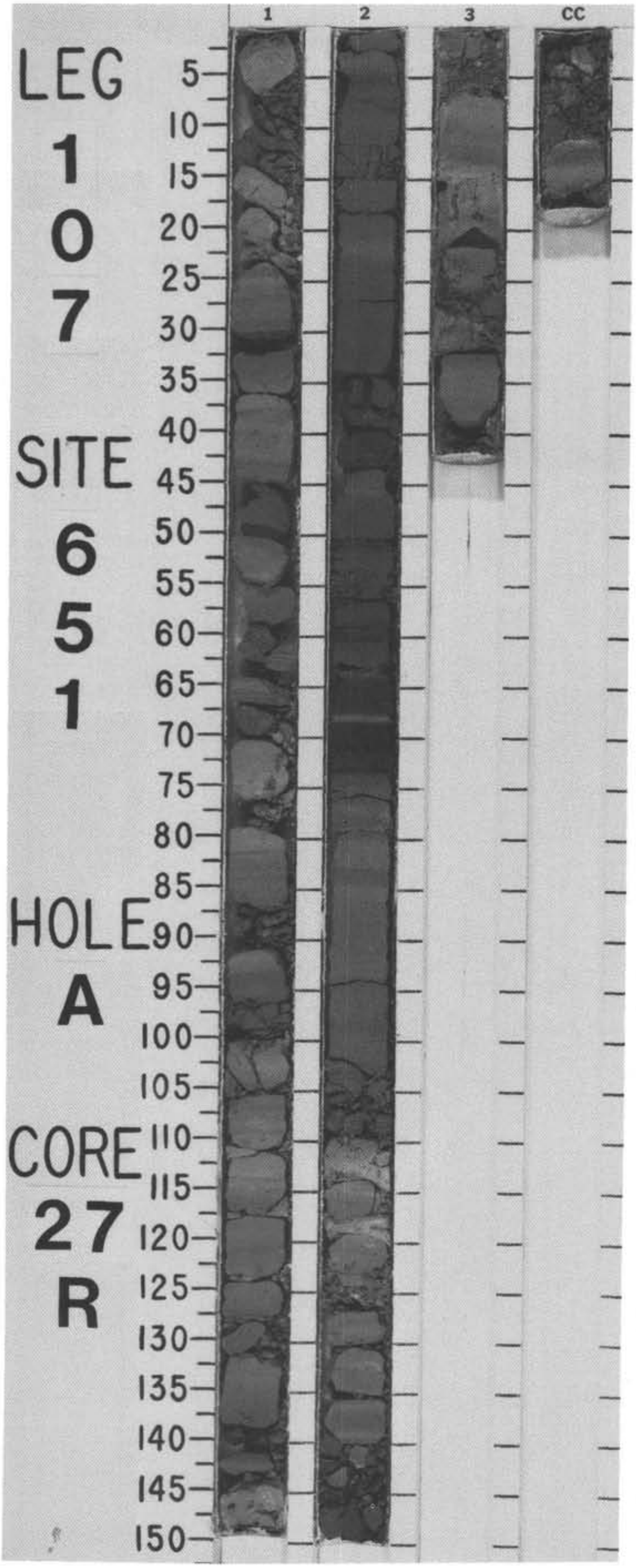
1
2
3
CC
LEG
107
SITE
651
HOLE
A
CORE
27
R
5
10
15
20
25
30
35
40
45
50
55
60
65
70
75
80
85
90
95
100
105
110
115
120
125
130
135
140
145
150

SITE 651 HOLE A CORE 28 R CORED INTERVAL 3829.6-3839.2 mbsl; 251.6-261.2 mbsf

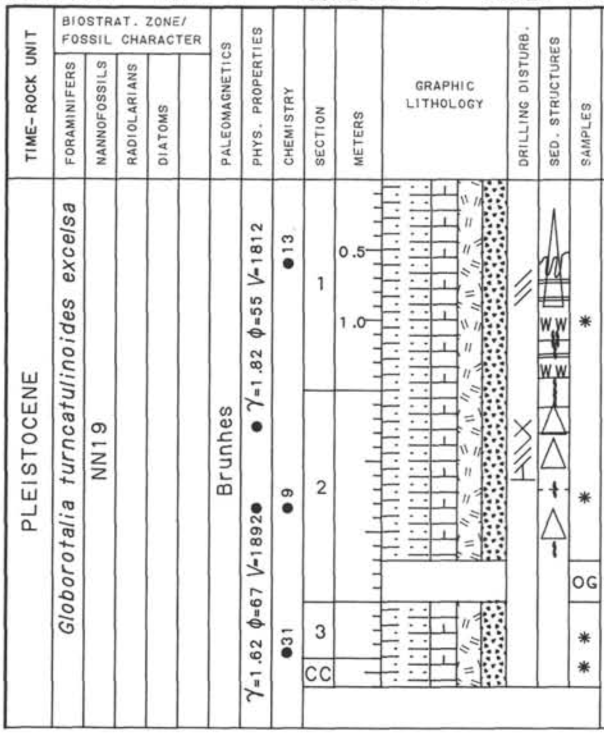

LITHOLOGIC DESCRIPTION

NANNOFOSSIL MUD, SILT, and SAND

Nannofossil mud with finely laminated, turbiditic layers of silty sand (tuff and volcanites).

SMEAR SLIDE SUMMARY (%):

	1, 107 M	2, 78 D	3, 34 D	CC, 1 M
TEXTURE:				
Sand	3	3	18	5
Silt	12	10	20	20
Clay	85	87	62	75
COMPOSITION:				
Quartz	5	Tr	1	2
Feldspar	3	Tr	1	2
Clay	35	20	15	40
Volcanic glass	4	Tr	4	6
Calcite/dolomite	1/Tr	2/Tr	—	—
Authigenic tiny needles	Tr	—	—	—
Micrite	3	6	5	—
Accessory minerals	2	—	—	—
Foraminifers	3	Tr	15	2
Nannofossils	40	70	55	40
Diatoms	3	1	1	6
Radiolarians	1	1	2	—
Sponge spicules	—	—	1	—
Analcine	—	Tr	—	—
Black spherules (pyrite?)	—	—	—	2

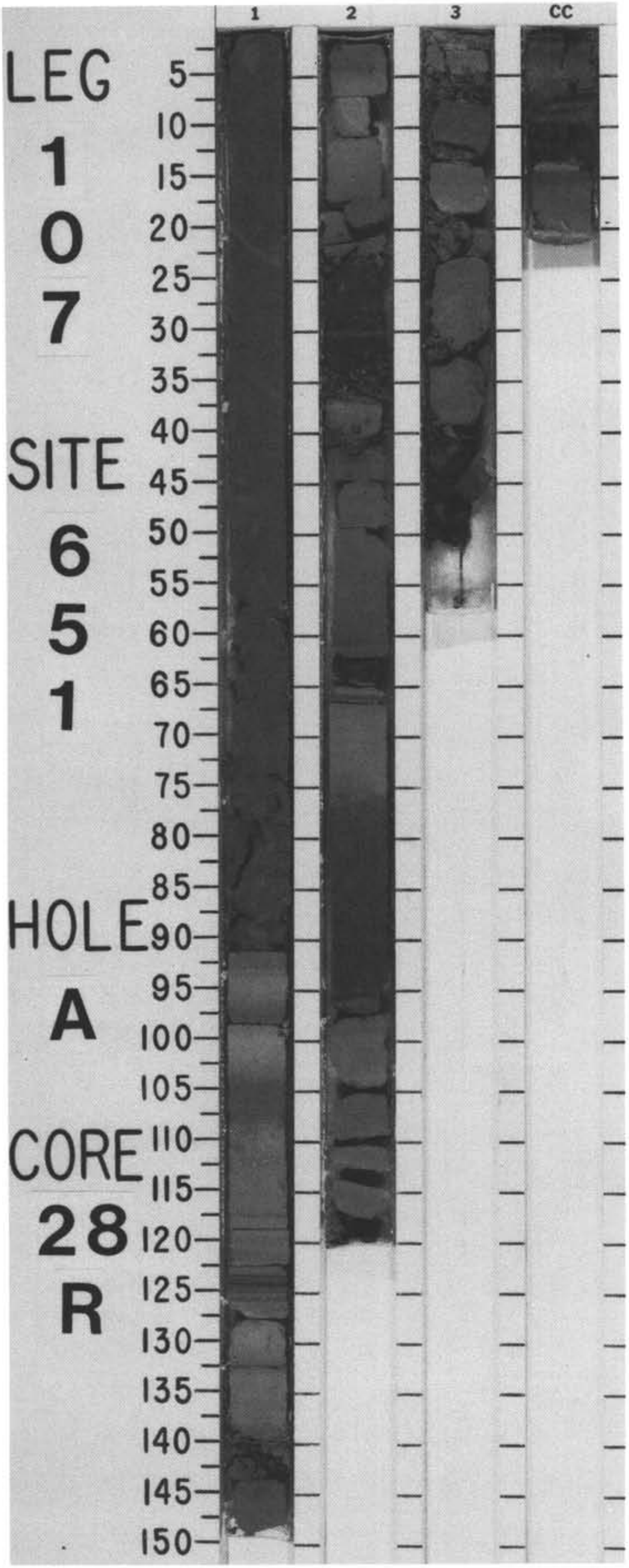
LEG
1
0
7
SITE
6
5
1
HOLE
A
CORE
28
R
1
2
3
CC
5
10
15
20
25
30
35
40
45
50
55
60
65
70
75
80
85
90
95
100
105
110
115
120
125
130
135
140
145
150

SITE 651 HOLE A CORE 29 R CORED INTERVAL 3839.2-3848.8 mbsl; 261.2-270.8 mbsf

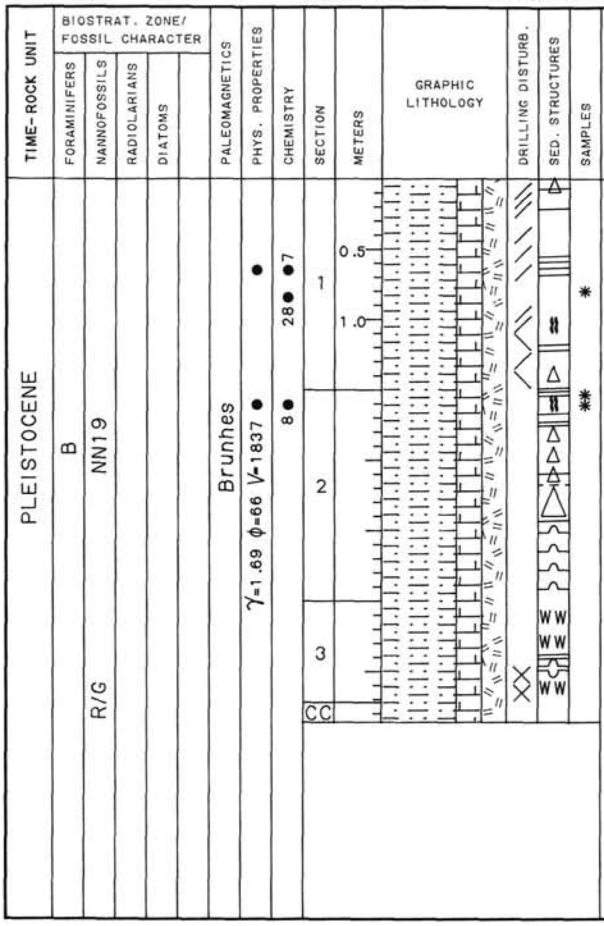

LITHOLOGIC DESCRIPTION

NANNOFOSSIL MUD and CALCAREOUS CLAY

Alternation of ash-bearing, nannofossil mudstone with diffuse laminations and clayey silty sand, foraminifers, and tuff; diffuse laminations in Section 1, with color alternations gray (5Y 5/1–6/1), dark gray (5Y 4/1), and light gray (5Y 7/1).

SMEAR SLIDE SUMMARY (%):

	1, 82 D	2, 4 M	2, 9 M
TEXTURE:			
Sand	5	—	2
Silt	15	15	15
Clay	80	85	83
COMPOSITION:			
Quartz	1	4	5
Feldspar	2	1	2
Clay	20	58	15
Volcanic glass	15	8	10
Calcite/dolomite	Tr	4	3/2
Micrite	4	9	5
Accessory minerals	—	1	2
Foraminifers	3	Tr	4
Nannofossils	51	15	52
Diatoms	1	—	Tr
Radiolarians	3	Tr	Tr
Fish remains	Tr	—	—

SITE 651 HOLE A CORE 30 R CORED INTERVAL 3848.8-3858.4 mbsl; 270.8-280.4 mbsf

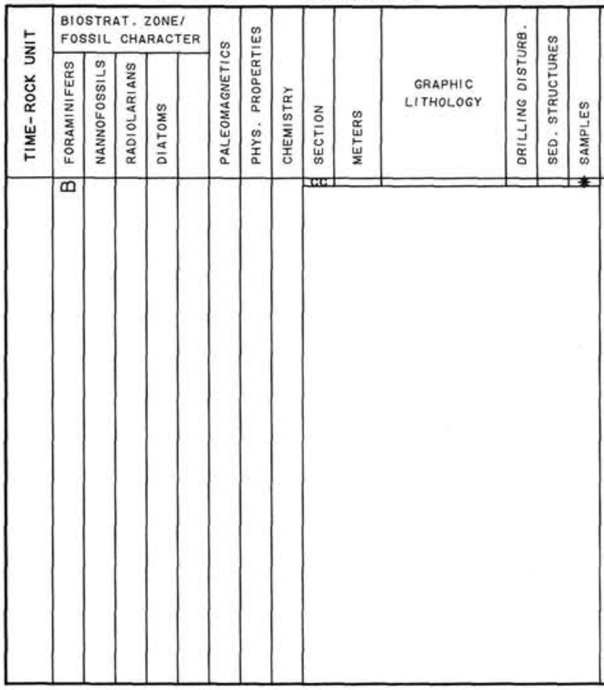

LITHOLOGIC DESCRIPTION

VOLCANIC ASH

Cemented tuff.

SMEAR SLIDE SUMMARY (%):

	CC, 0 D
TEXTURE:	
Sand	70
Silt	20
Clay	10
COMPOSITION:	
Quartz	2
Feldspar	1
Clay	10
Volcanic glass	85
Calcite/dolomite	Tr
Micrite	Tr
Accessory minerals	Tr
Nannofossils	2

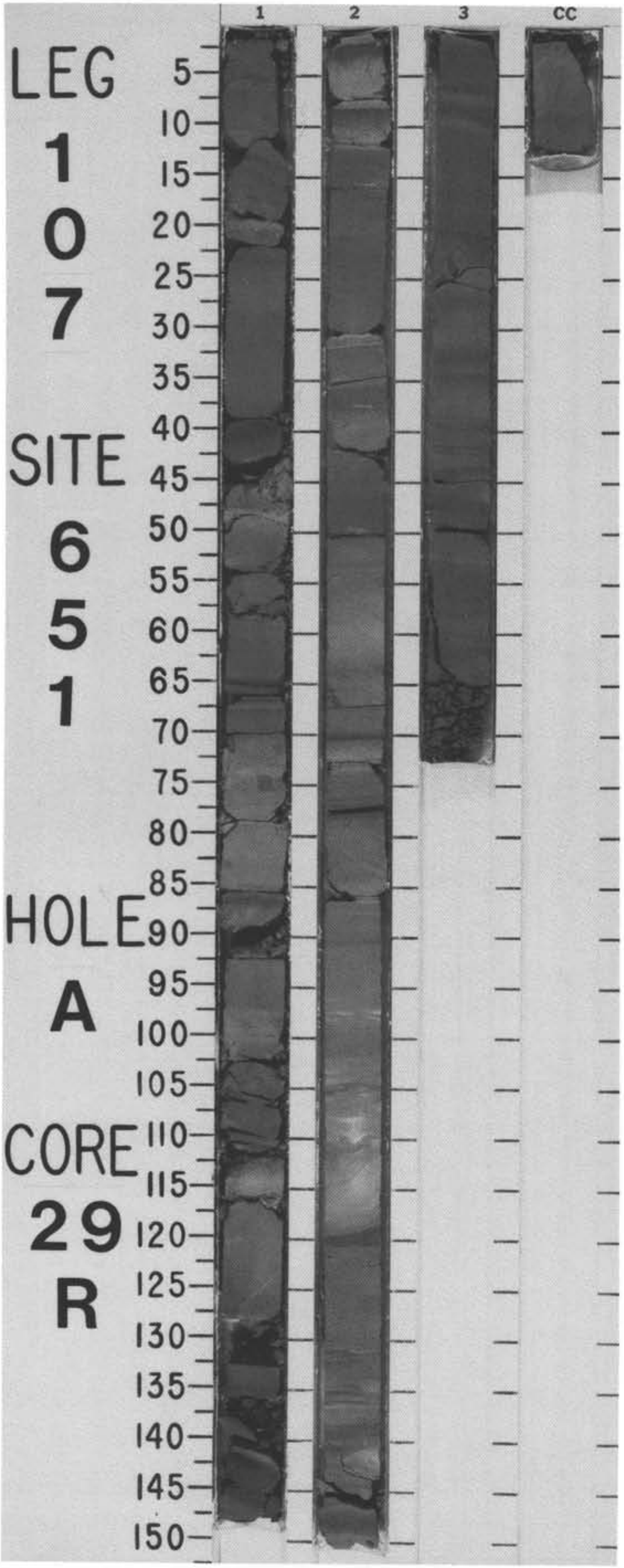
1
2
3
CC
LEG 107
SITE 651
HOLE A
CORE 29 R
5
10
15
20
25
30
35
40
45
50
55
60
65
70
75
80
85
90
95
100
105
110
115
120
125
130
135
140
145
150

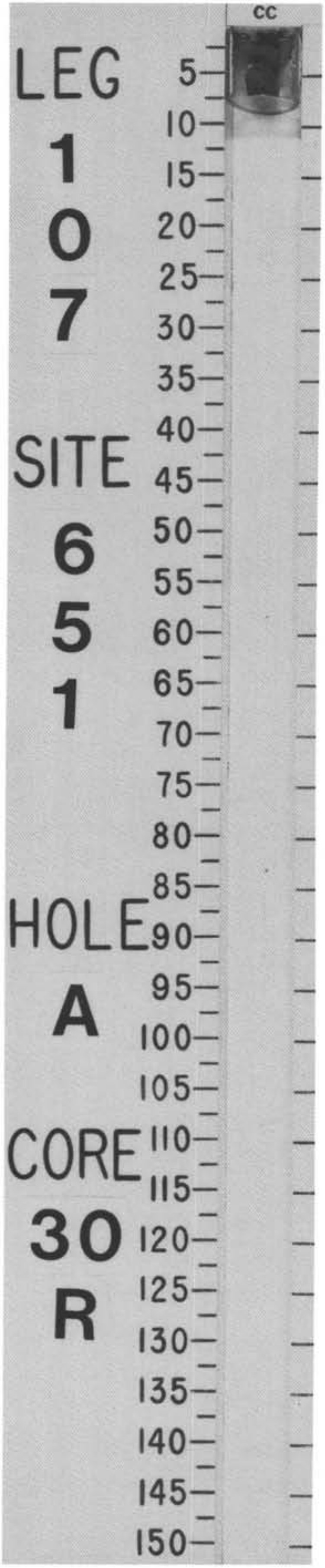
CC
LEG 107
SITE 651
HOLE A
CORE 30 R
5
10
15
20
25
30
35
40
45
50
55
60
65
70
75
80
85
90
95
100
105
110
115
120
125
130
135
140
145
150

SITE 651 HOLE A CORE 31 R CORED INTERVAL 3858.4-3868.0 mbsl; 280.4-290.0 mbsf

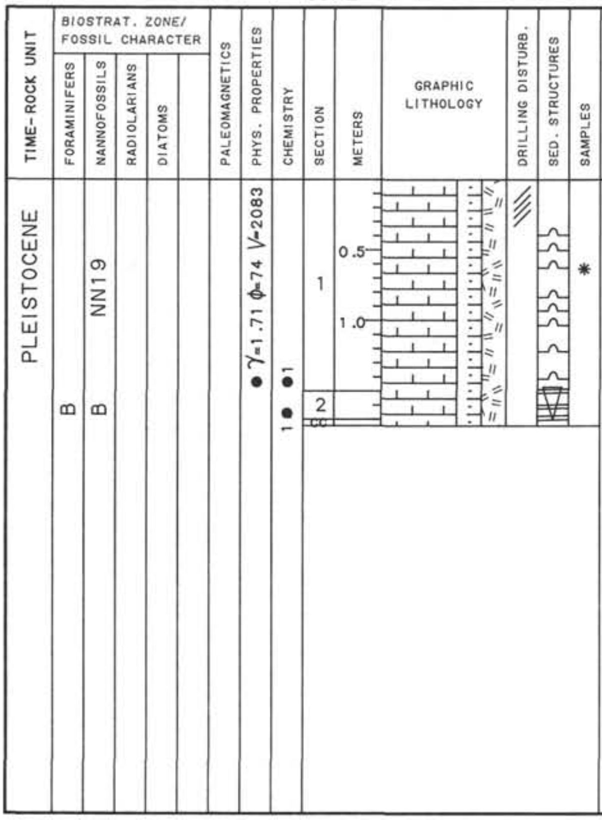

LITHOLOGIC DESCRIPTION

NANNOFOSSIL CHALK and CLAYSTONE

Homogeneous nannofossil chalk progressively more or less laminated toward top, mainly olive-gray (5Y 5/2); some slumplike structures and other disturbances at several horizons; nannofossil chalk, greenish gray (5Y 5/1), in CC.

SMEAR SLIDE SUMMARY (%):

	1, 64 D
TEXTURE:	
Sand	2
Silt	10
Clay	88
COMPOSITION:	
Quartz	1
Feldspar	3
Clay	30
Volcanic glass	Tr
Calcite/dolomite	2
Micrite	3
Foraminifers	1
Nannofossils	59
Radiolarians	Tr
Fish remains	1

SITE 651 HOLE A CORE 32 R CORED INTERVAL 3868.0-3877.6 mbsl; 290.0-299.6 mbsf

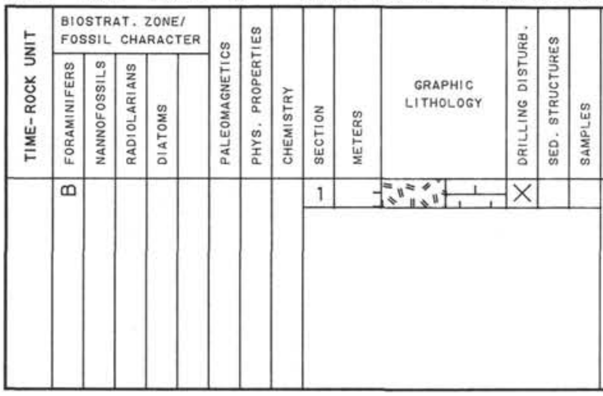

LITHOLOGIC DESCRIPTION

VOLCANIC ASH and CHALK

Dark greenish gray (5Y 4/1) nodules (drilling artifacts) of tuff and chalk.

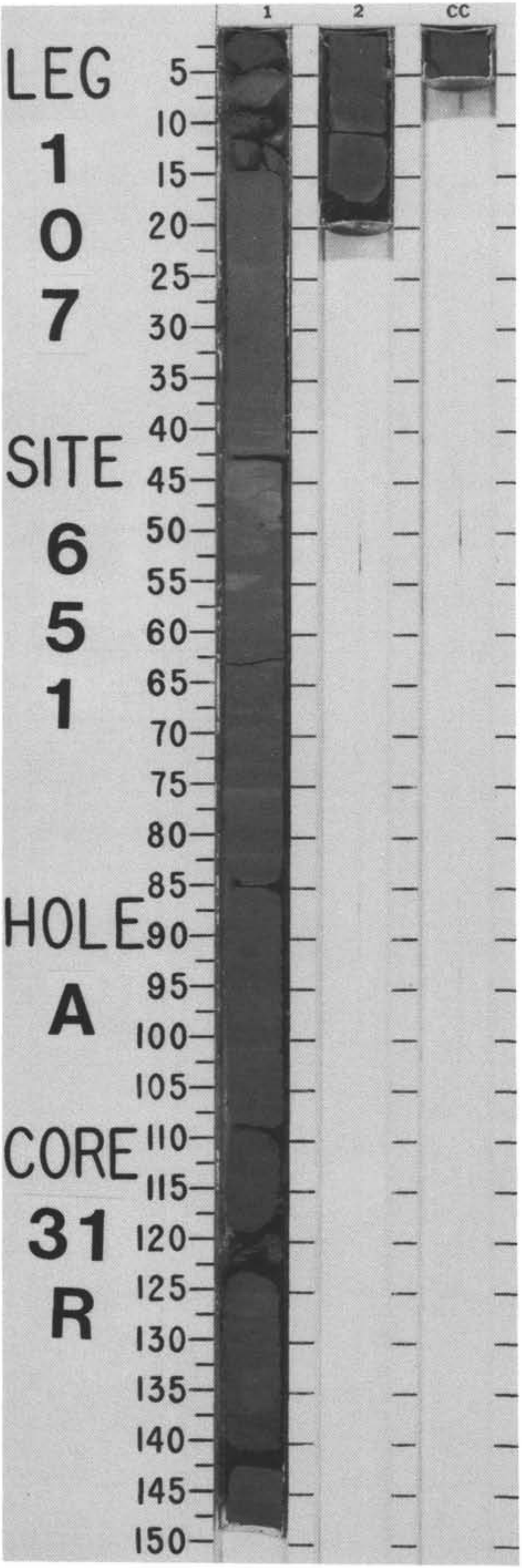
1
2
CC
LEG
1
0
7
SITE
6
5
1
HOLE
A
CORE
31
R
5
10
15
20
25
30
35
40
45
50
55
60
65
70
75
80
85
90
95
100
105
110
115
120
125
130
135
140
145
150

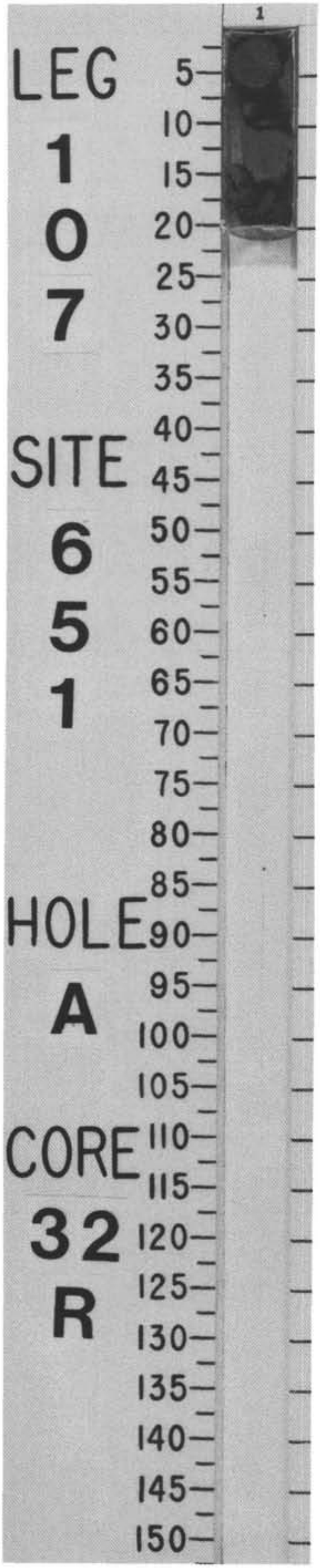
1
LEG
1
0
7
SITE
6
5
1
HOLE
A
CORE
32
R
5
10
15
20
25
30
35
40
45
50
55
60
65
70
75
80
85
90
95
100
105
110
115
120
125
130
135
140
145
150

SITE 651 HOLE A CORE 33 R CORED INTERVAL 3877.6-3887.3 mbsl; 299.6-309.3 mbsf

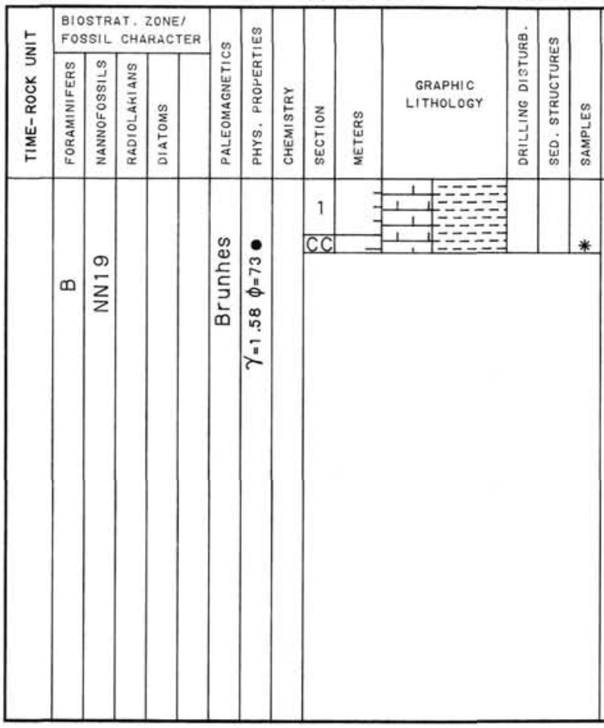

LITHOLOGIC DESCRIPTION

MARLY NANNOFOSSIL CHALK and CALCAREOUS CLAYSTONE

Greenish gray (5GY 5/1), homogeneous, marly nannofossil chalk.

SMEAR SLIDE SUMMARY (%):

	CC, 11 D
TEXTURE:	
Sand	2
Silt	17
Clay	81
COMPOSITION:	
Quartz	Tr
Clay	45
Volcanic glass	5
Calcite/dolomite	1
Micrite	12
Accessory minerals	Tr
Foraminifers	Tr
Nannofossils	35
Fish remains	2

SITE 651 HOLE A CORE 34 R CORED INTERVAL 3887.3-3896.9 mbsl; 309.3-318.9 mbsf

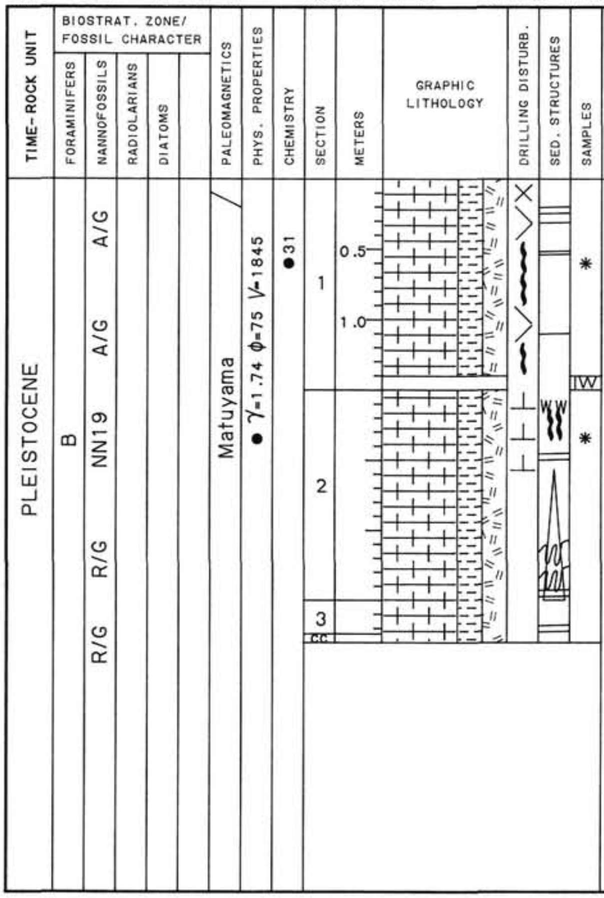

LITHOLOGIC DESCRIPTION

CALCAREOUS CLAYSTONE

A thin-bedded turbiditic sequence comprising alternations of gray (5Y 5/1) tuff and marly foraminifer chalk, passing into greenish gray (5GY 5/1) to marly nannofossil chalk (5GY 7/1); CC has gray tuff.

SMEAR SLIDE SUMMARY (%):

	1, 57 M	2, 36 D
TEXTURE:		
Sand	25	—
Silt	25	10
Clay	50	90
COMPOSITION:		
Quartz	—	1
Feldspar	2	—
Clay	45	61
Volcanic glass	5	Tr
Calcite/dolomite	Tr	—
Accessory minerals	—	Tr
Opaques	3	—
Micrite	12	15
Foraminifers	20	Tr
Nannofossils	10	20
Diatoms	Tr	Tr
Radiolarians	3	Tr
Fish remains	—	3

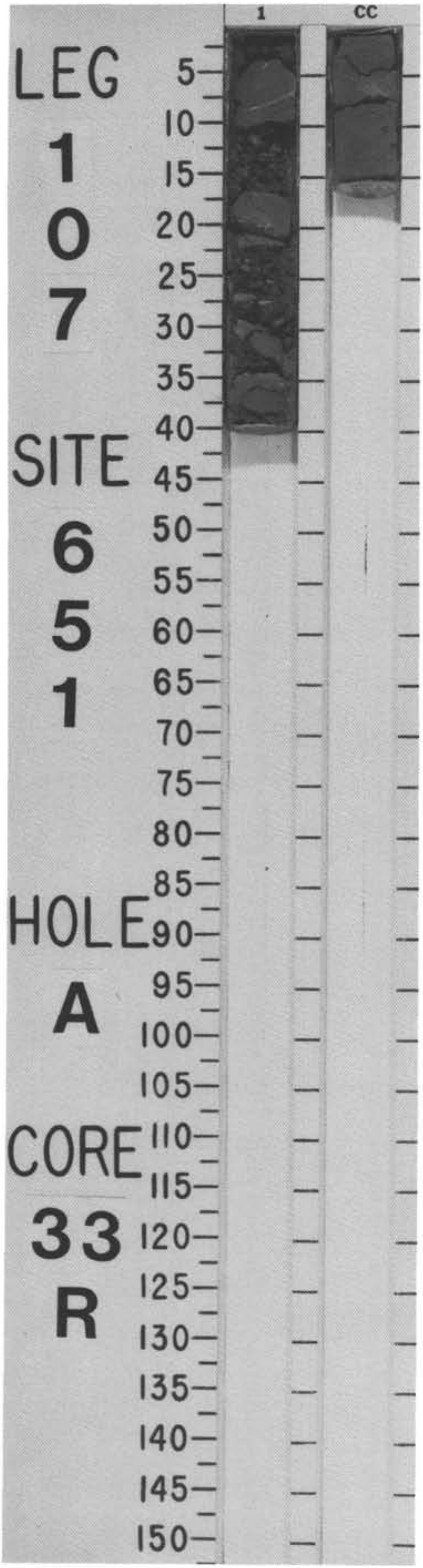
1
CC
LEG
107
SITE
651
HOLE
A
CORE
33
R
5
10
15
20
25
30
35
40
45
50
55
60
65
70
75
80
85
90
95
100
105
110
115
120
125
130
135
140
145
150

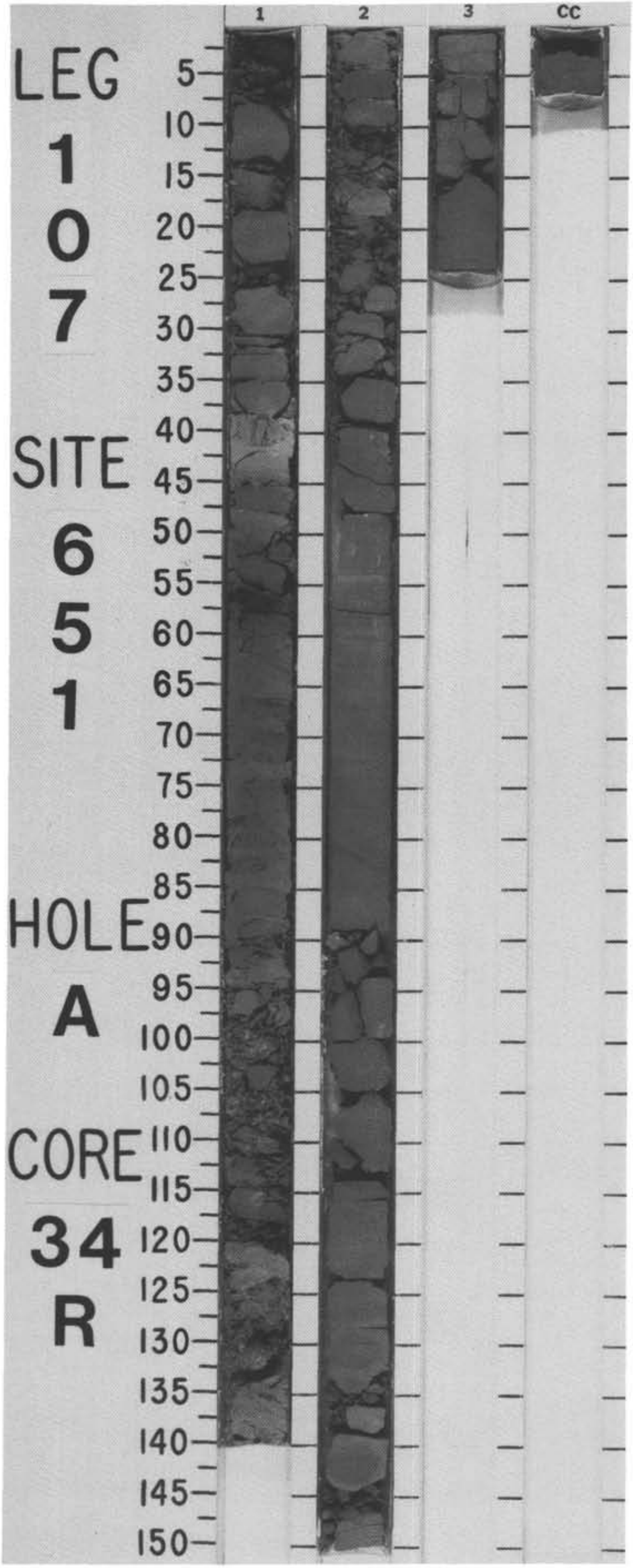
1
2
3
CC
LEG
107
SITE
651
HOLE
A
CORE
34
R
5
10
15
20
25
30
35
40
45
50
55
60
65
70
75
80
85
90
95
100
105
110
115
120
125
130
135
140
145
150

SITE 651 HOLE A CORE 35 R CORED INTERVAL 3896.9-3906.6 mbsl; 318.9-328.6 mbsf

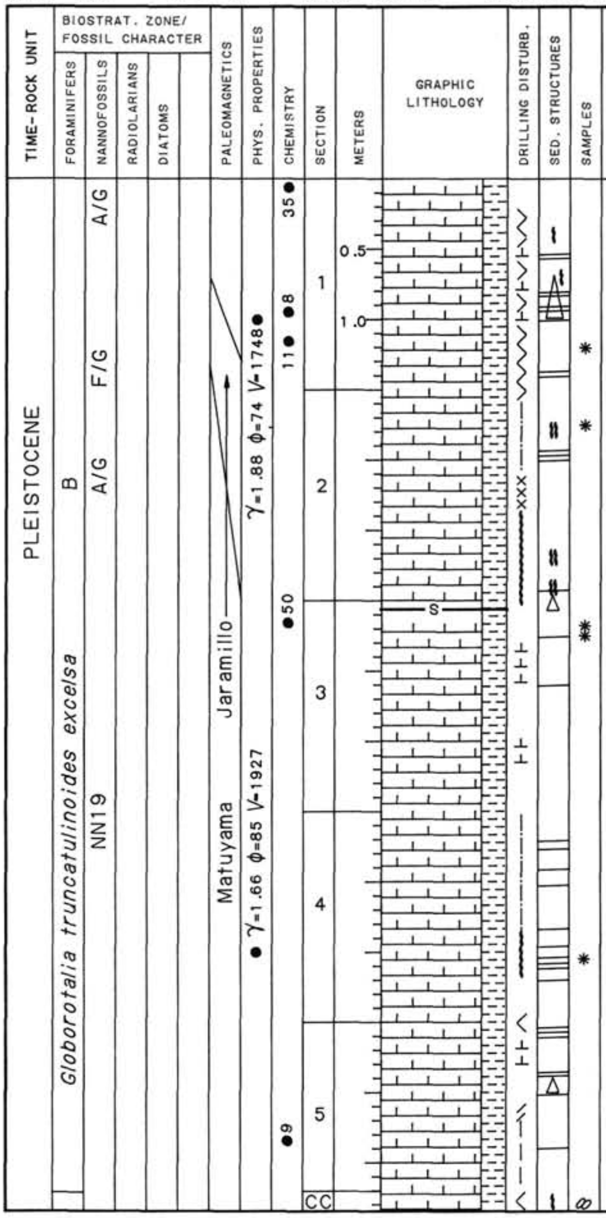

LITHOLOGIC DESCRIPTION

NANNOFOSSIL CHALK, CALCAREOUS CLAYSTONE, and minor VOLCANIC ASH

Greenish gray (5GY 6/1) nannofossil chalk and dark greenish gray (5GY 4/1) to greenish gray (5GY 6/1) calcareous claystone alternating with one another and with volcaniclastic horizons; some layers of finely laminated tuff (volcaniclastic ash layers); in Section 3, 5–9 cm, one finely laminated sapropel.

SMEAR SLIDE SUMMARY (%):

	1, 115 D	2, 30 D	3, 15 M	3, 28 M	4, 106 M
TEXTURE:					
Sand	1	1	—	—	—
Silt	10	10	5	10	10
Clay	89	89	95	90	90
COMPOSITION:					
Quartz	1	Tr	2	2	—
Feldspar	1	—	—	1	—
Clay	64	Tr	10	64	—
Volcanic glass	15	—	Tr	15	88
Calcite/dolomite	—	1	1	—	2
Micrite	10	6	5	5	—
Accessory minerals	Tr	—	2	Tr	—
Foraminifers	1	3	4	3	—
Nannofossils	5	90	76	10	—
Radiolarians	Tr	—	—	Tr	—
Fish remains	3	—	—	Tr	10

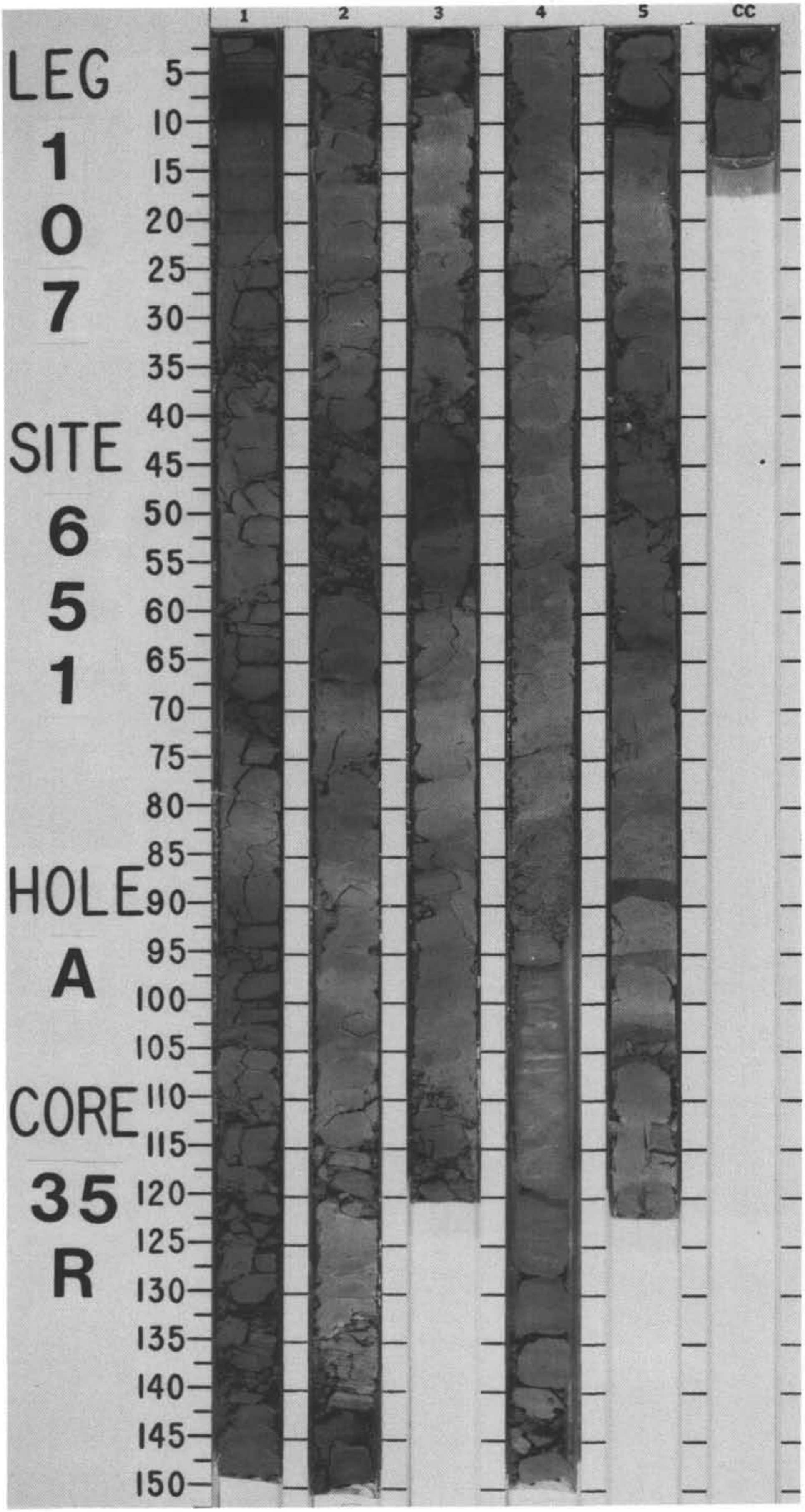
LEG
1
0
7
SITE
6
5
1
HOLE
A
CORE
35
R
1
2
3
4
5
CC
5
10
15
20
25
30
35
40
45
50
55
60
65
70
75
80
85
90
95
100
105
110
115
120
125
130
135
140
145
150

SITE 651 HOLE A CORE 36 R CORED INTERVAL 3906.6-3916.2 mbsl; 328.6-338.2 mbsf

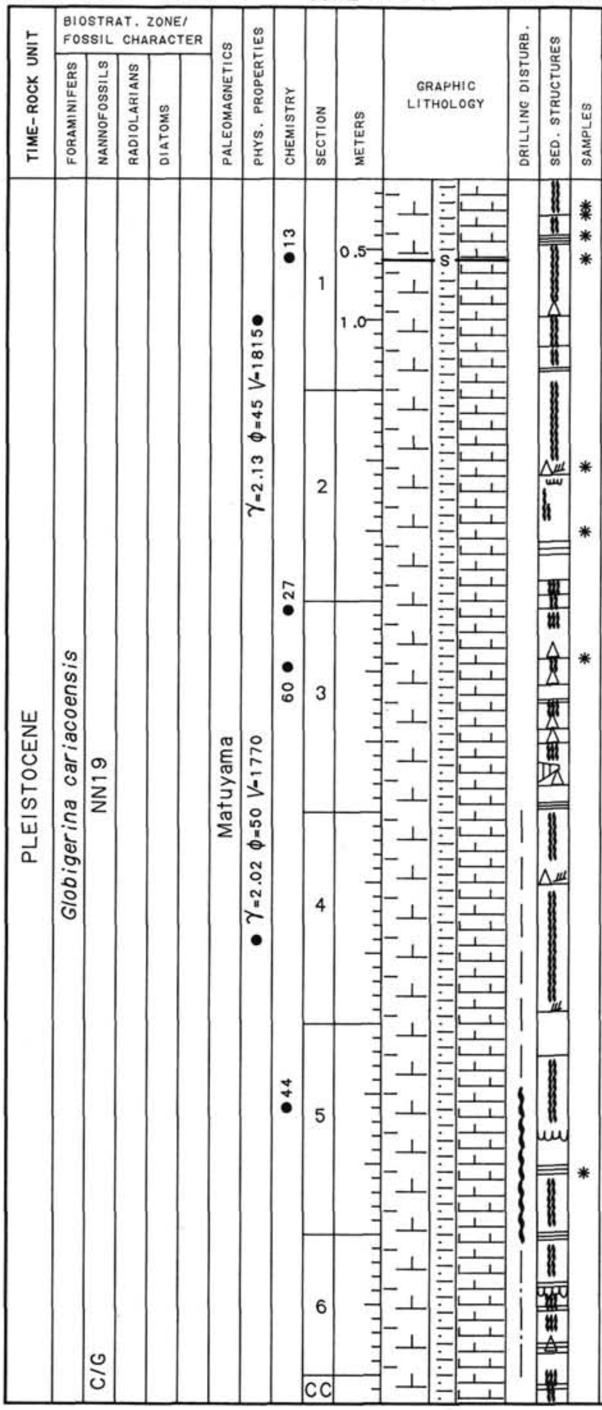

LITHOLOGIC DESCRIPTION

NANNOFOSSIL CHALK, NANNOFOSSIL OOZE, CALCAREOUS MUDSTONE, and CALCAREOUS CLAYSTONE

Heterogeneous assemblage of thin, interbedded, burrowed nannofossil claystone and nannofossil limestone, olive-gray (5Y 5/2) to dark greenish gray (5GY 5/1), with as much as 4 cm of thick, graded, locally micro-cross-laminated, calcareous claystones and mudstone, both dark greenish gray (5G 5/1); nannofossil chalk contains numerous disseminated planktonic foraminifers, which are absent from the laminated claystone and mudstone; in Section 1, 57–60 cm, a prominent sapropel; in Section 1, 132–134 cm, Section 3, 8–10 cm, Section 4, 0–6 cm, Section 5, 78–80 and 103–106 cm, and Section 6, 3–5 and 82–84 cm, grayish (5GY 5/1) horizons also occur.

Interpretation: background is nannofossil foraminifer ooze, into which fine-grained clay and mud turbidites have been introduced. The sapropels were possibly redeposited and contain nannofossil-rich limestone and partings (mass mortality?).

SMEAR SLIDE SUMMARY (%):

	1, 20 D	1, 28 M	1, 50 M	1, 58 M	2, 105 M	3, 45 D	5, 107 D
TEXTURE:							
Sand	—	—	—	—	—	—	—
Silt	5	10	35	10	5	5	5
Clay	95	90	65	90	95	95	95
COMPOSITION:							
Quartz	4	8	20	—	Tr	—	Tr
Feldspar	—	2	—	—	—	—	—
Mica	—	Tr	Tr	Tr	—	—	—
Clay	15	70	40	50	10	30	45
Volcanic glass	—	—	15	—	—	—	—
Calcite/dolomite	1	2	5	5	3	—	Tr
Accessory minerals	—	—	Tr	—	—	—	—
Orthopyroxene?	Tr	—	—	—	—	—	—
Clinoptilolite	—	Tr	Tr	Tr	—	Tr	—
Opaques	—	8	5	40	—	—	—
Foraminifers	10	Tr	5	—	7	15	5
Nannofossils	60	8	10	3	75	50	45
Sponge spicules	—	Tr	—	—	—	—	—
Bioclasts	5	2	5	2	5	5	5
Micrite	5	—	—	—	—	—	—
Aragonite needles	Tr	—	—	—	—	Tr	Tr
Analcite	—	—	Tr	—	—	—	—

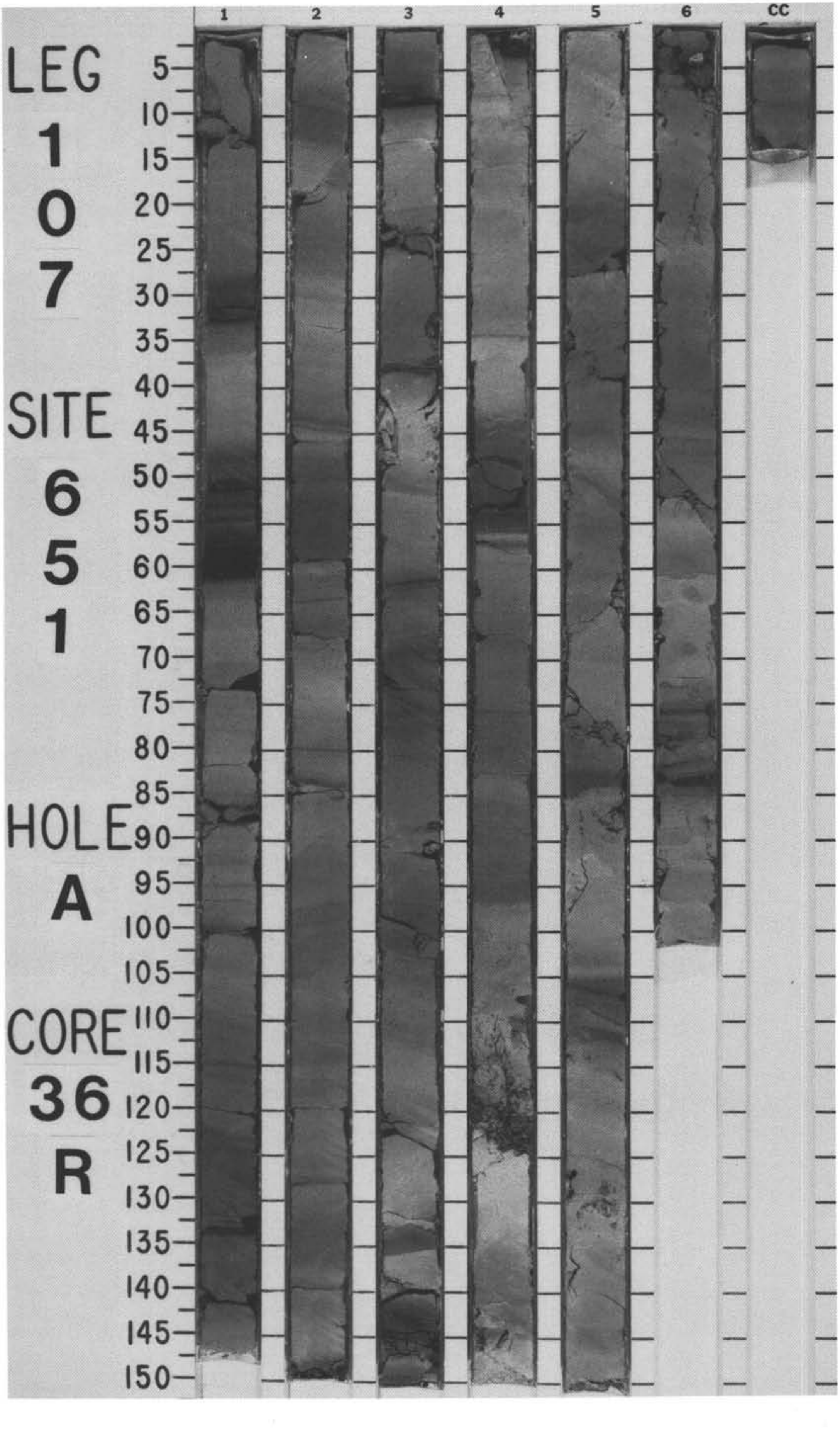
LEG
107
SITE
651
HOLE
A
CORE
36
R
1
2
3
4
5
6
CC
5
10
15
20
25
30
35
40
45
50
55
60
65
70
75
80
85
90
95
100
105
110
115
120
125
130
135
140
145
150

SITE 651 HOLE A CORE 37 R CORED INTERVAL 3916.2-3925.8 mbsl; 338.2-347.8 mbsf

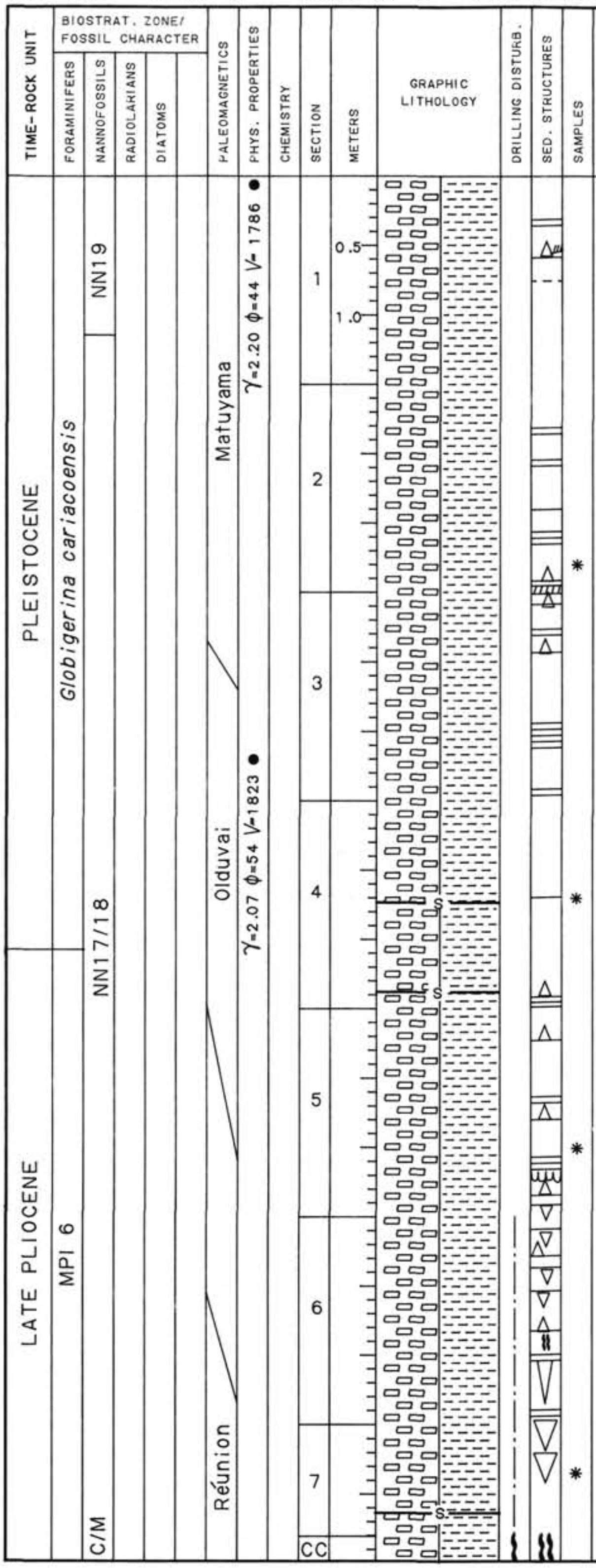

LITHOLOGIC DESCRIPTION

CALCAREOUS OOZE and CALCAREOUS CLAYSTONE

Burrowed, intergradational, stiff, calcareous ooze and weakly indurated, calcareous claystone, pale olive (5Y 6/4), olive-gray (5Y 5/2), and light gray (5Y 7/1) to greenish gray (5Y 6/1). Sediments are burrowed but traces of pre-existing, fine parallel lamination are locally preserved; some burrows exhibit black organic-rich fills, and many are rich in planktonic foraminifers, which commonly increase in number upward, imparting a general reverse grading. Interbedded, thin (<4 cm), parallel laminated, graded and locally micro-cross-laminated, olive-gray claystone (5Y 6/2) shows no burrowing except occasionally at the top.

In Section 1, 142–146 cm are Bouma C, B, and E divisions of a distal turbidite; in Section 4, 75–77 cm, is a dark gray (5Y 3/1) sapropelic layer, and at 137–140 cm, an olive-gray (5Y 4/2) sapropelic layer; in Section 7, 65–67 cm, is another sapropelic horizon with sharply defined, white laminations.

Interpretation: impure pelagic carbonate deposition with thin claystone turbidites.

SMEAR SLIDE SUMMARY (%):

	2, 103 M	4, 76 D	5, 100 D	7, 42 D
TEXTURE:				
Sand	—	—	—	—
Silt	5	—	9	10
Clay	95	100	91	90
COMPOSITION:				
Clay	55	—	45	60
Calcite/dolomite	—	100	—	5
Opaques	30	—	7	6
Zeolite	Tr	—	—	—
Foraminifers	—	—	20	10
Nannofossils	5	—	25	15
Bioclasts	10	—	3	4
Aragonite needles	—	—	Tr	Tr

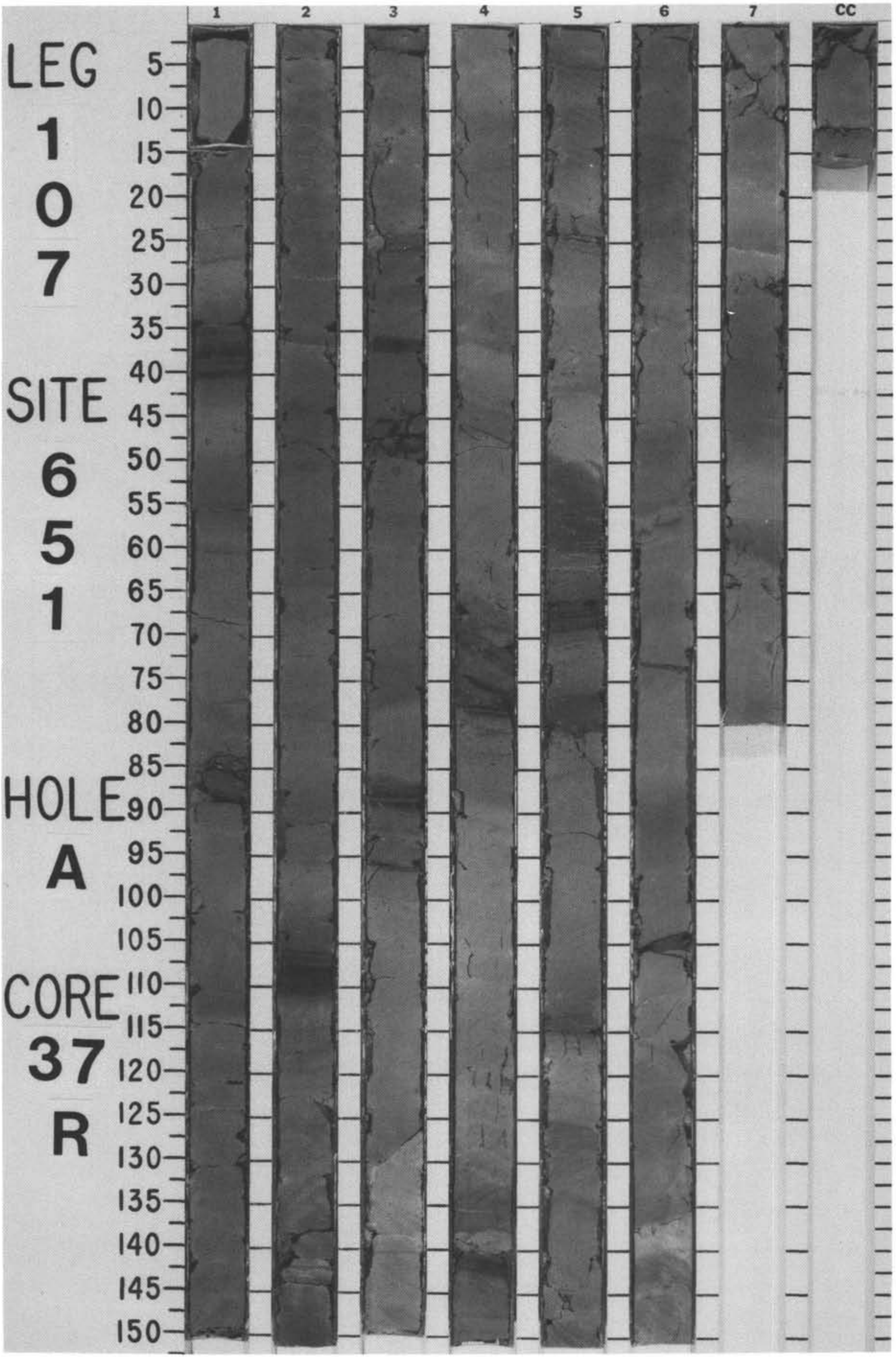
LEG
1
0
7
SITE
6
5
1
HOLE
A
CORE
37
R
1
2
3
4
5
6
7
CC
5
10
15
20
25
30
35
40
45
50
55
60
65
70
75
80
85
90
95
100
105
110
115
120
125
130
135
140
145
150

SITE 651 HOLE A CORE 38 R CORED INTERVAL 3925.8-3935.5 mbsl; 347.8-357.5 mbsf

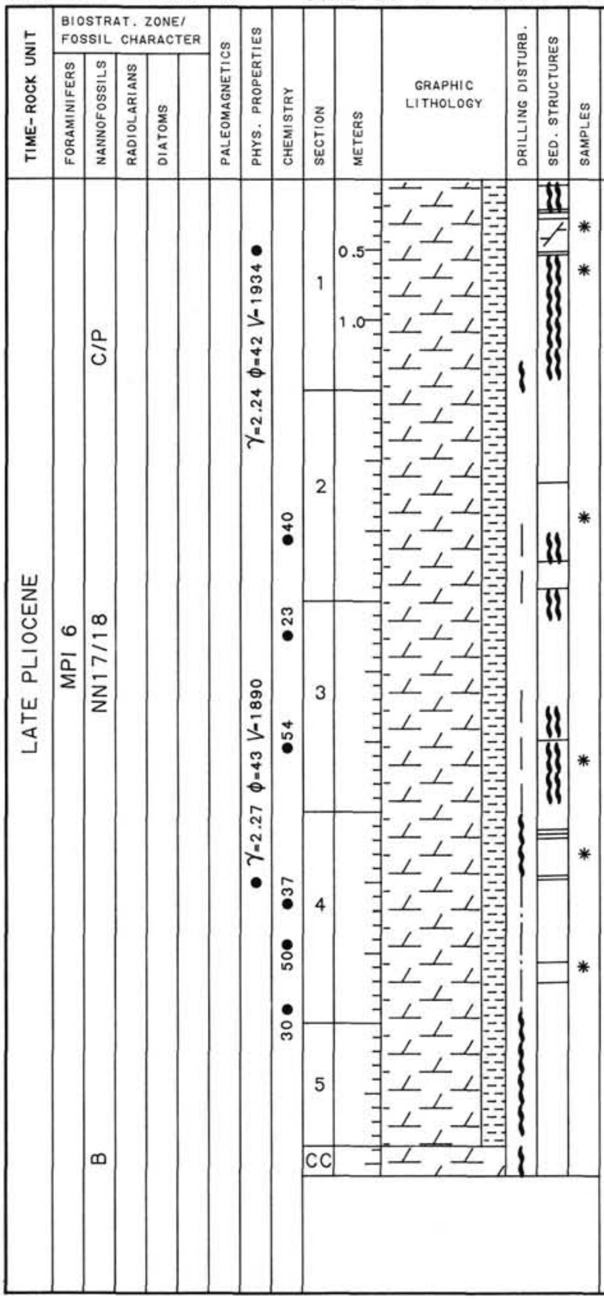

LITHOLOGIC DESCRIPTION

DOLOMITIC CLAYSTONE, DOLOSTONE, and METALLIFEROUS MUD with minor VOLCANIC ASH

Brightly colored, metal-rich (Fe, Mn?), dolomitic clay and dolostone that fizz only weakly or not at all with 5% HCl; ranging in color from light gray (5Y 7/1) to grayish green (5G 5/1), and gray (6GY 6/1) to pale olive (6Y 1/3) to light yellowish brown (2.5Y 6/4), olive-gray (5Y 5/3), greenish gray (5G 6/1, 5Y 2/2), light grayish brown (5YR 5/6), brownish red (5R 3/6), and black (10YR 5/4).

Recorded dips are as high as 45° but variable, a subhorizontal dip predominates; in Section 1, 30–42 cm, is a neptunian dike, roughly 1 cm wide x 10 cm long; in Section 1, 43–45 cm, rare parallel- and micro-cross-laminated volcanic ash, and at 110–130 cm, tiny (1–3-mm) reduced segregations; in Section 2, 12–130 cm, tiny manganese or sulfide segregations; in Section 3, a small (6 cm), elongate fracture with a green, 0.5-cm-wide reduced zone on either side; Section 4, 15–25 cm, is brightly colored, with small diagenetic metal oxide segregations; CC is crystalline dolomite.

SMEAR SLIDE SUMMARY (%):

	1, 43 M	1, 68 M	2, 90 D	3, 120 D	4, 36 M	4, 106 M
TEXTURE:						
Sand	5	—	—	—	—	—
Silt	85	80	50	25	20	20
Clay	10	20	50	75	80	80
COMPOSITION:						
Feldspar	Tr	—	—	—	5	5
Mica	3	—	—	—	—	—
Clay	15	10	15	30	10	5
Volcanic glass	80	—	—	Tr	—	—
Dolomite	—	70	75	65	65	70
Opaques	2	5	—	5	—	—
Orthopyroxene	Tr	—	—	—	—	—
Micrite	—	—	10	—	—	—
Foraminifers	—	Tr	—	—	—	—
Nannofossils	—	15		—	—	—
Geothite	—	—	—	—	15	10
Manganese oxide	—	—	—	—	5	10

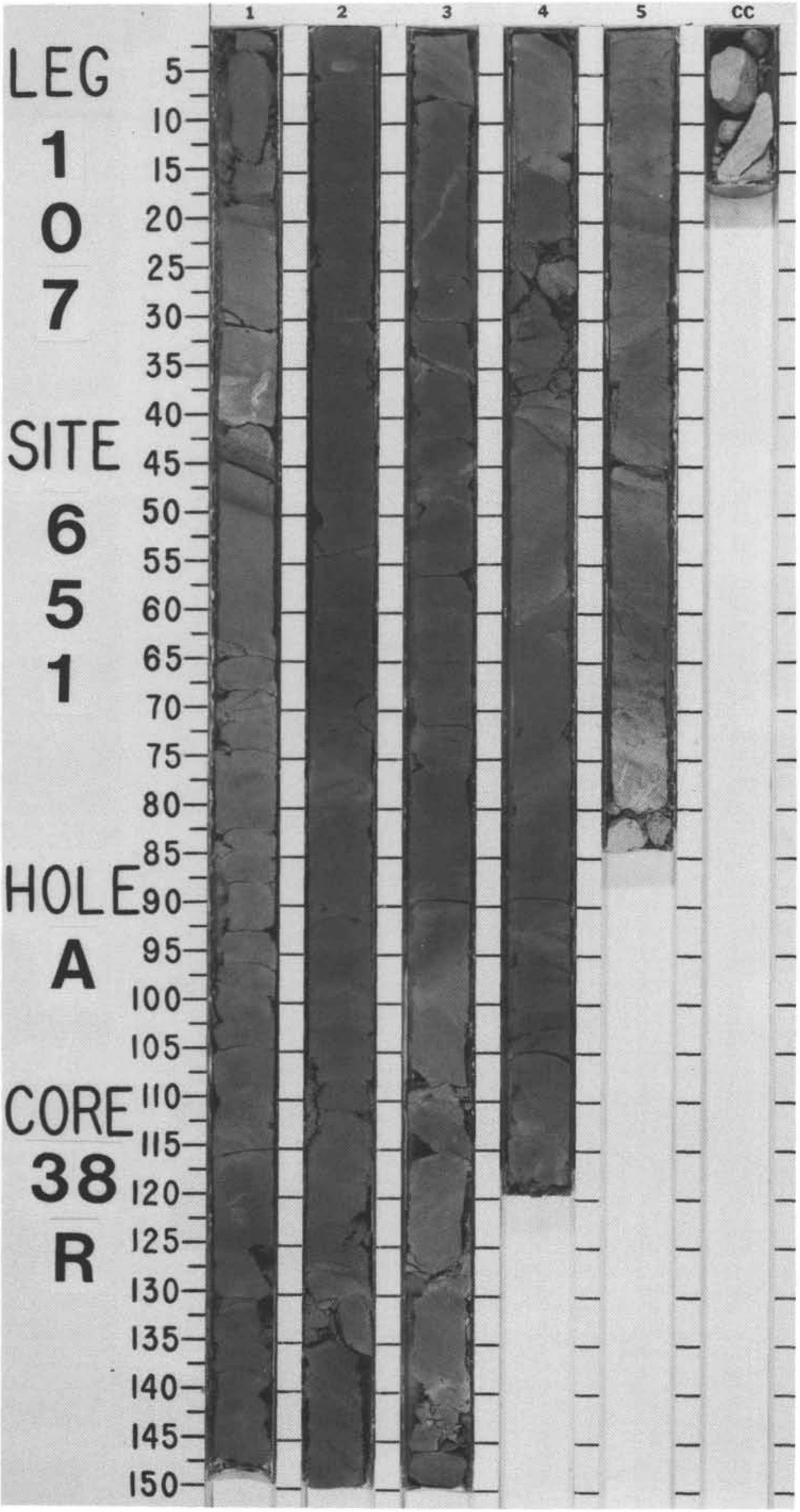
LEG
1
0
7
SITE
6
5
1
HOLE
A
CORE
38
R
1
2
3
4
5
CC
5
10
15
20
25
30
35
40
45
50
55
60
65
70
75
80
85
90
95
100
105
110
115
120
125
130
135
140
145
150

SITE 651 HOLE A CORE 39 R CORED INTERVAL 3935.5-3945.2 mbsl; 357.5-367.2 mbsf

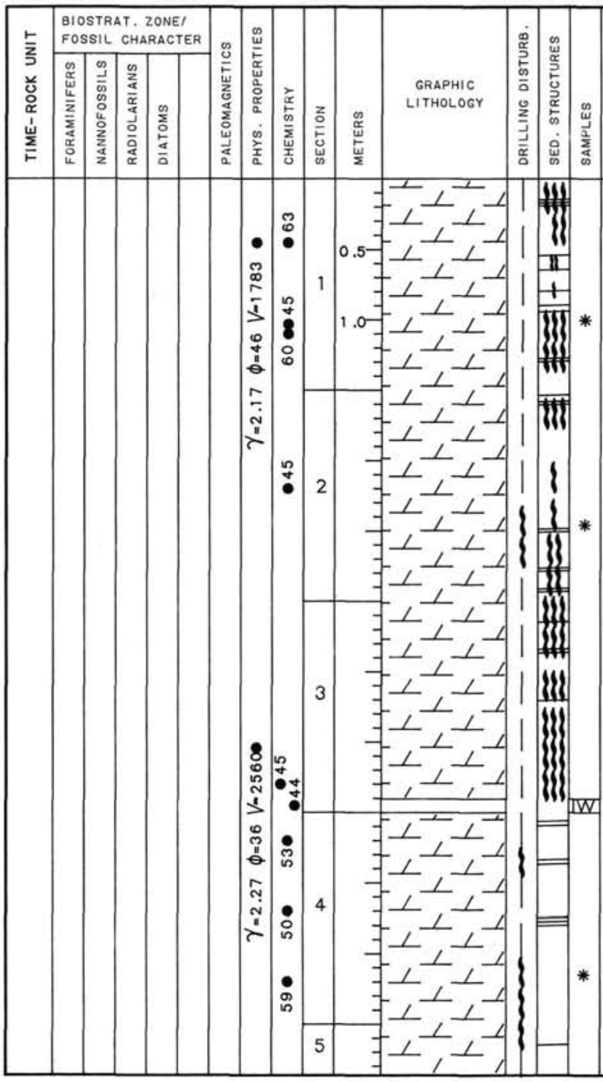

LITHOLOGIC DESCRIPTION

METALLIFEROUS DOLOSTONE

Brightly colored, variably burrowed, metal-rich dolostone, olive (5Y 5/3) and light olive-gray (5Y 6/2), to white (2.5Y 8/2), to olive-brown (2.5Y 4/3), light brownish gray (2.5Y 6/2), grayish brown (2.5Y 5/2), red (10R), light reddish brown (5YR 6/4), light yellowish brown (2.5Y 6/4), reddish yellow (7.5YR 6/6), and light gray (2.5Y 7/2); burrowing is ambiguous, but a parallel lamination is still preserved, indicating an apparent drop of dip to 35°; numerous, tiny (<3 mm), manganiferous, diagenetic segregations.

Interpretation: metalliferous oxide precipitated from volcanic centers and deposited above basaltic basement. Dolomite may be related to diagenetic alteration adjacent to the basalt.

SMEAR SLIDE SUMMARY (%):

	1, 100 D	2, 100 D	4, 120 D
TEXTURE:			
Sand	—	—	—
Silt	35	30	25
Clay	65	70	75
COMPOSITION:			
Clay	10	20	15
Volcanic glass	—	—	Tr
Dolomite	70	60	70
Zeolite	2	8	Tr
Opaques	3	2	Tr
Micrite	15	10	15

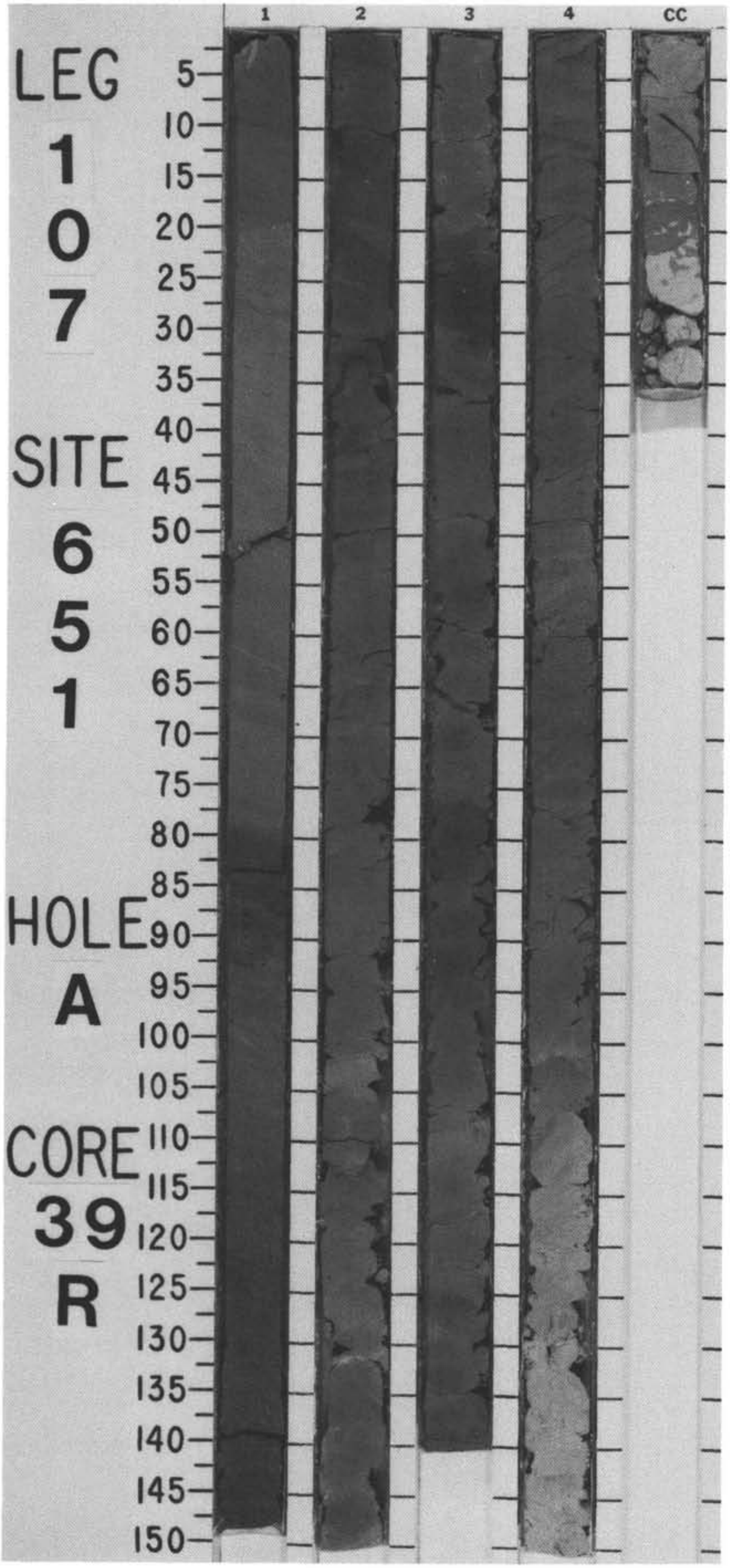
LEG
1
0
7
SITE
6
5
1
HOLE
A
CORE
39
R
1
2
3
4
CC
5
10
15
20
25
30
35
40
45
50
55
60
65
70
75
80
85
90
95
100
105
110
115
120
125
130
135
140
145
150

SITE 651 HOLE A CORE 40 R CORED INTERVAL 3945.2-3954.8 mbsl; 367.2-376.8 mbsf

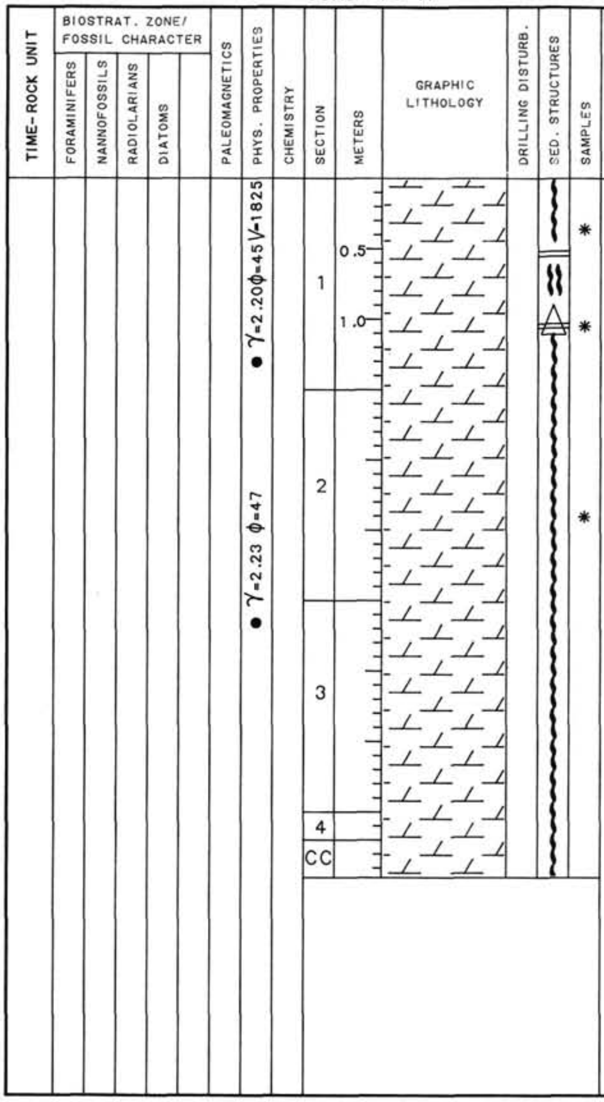

LITHOLOGIC DESCRIPTION

METALLIFEROUS DOLOSTONE

Brightly colored, metal-rich, burrowed dolostone; intergradational colors are black (3/1), dark gray (4/1), brown (10YR 5/3), light brownish gray (10YR 5/3), light reddish brown (5YR 6/3), dark grayish brown (2.5Y 3/2), light yellowish brown (2.5Y 6/6), reddish yellow (7.5YR 6/6), pinkish gray (7.5YR 7/2), light gray (10YR 7/2), pink (7.5YR), pale brown (10YR 6/3), very pale brown (10YR 7/3), and pale red (10R 6/4); in Section 1, 25–35 cm, are manganese dendrites(?), at 63–65 cm is a horizon of black crystalline material that may be manganese oxide (pyrolusite?), and at 103–105 cm is a parallel laminated horizon containing altered volcanic material.

Interpretation: sediments reflect probable precipitation of metalliferous oxides related to subseafloor hydrothermal activity. The dolomite genesis may reflect alteration within the sediment pile.

SMEAR SLIDE SUMMARY (%):

	1, 37 D	1, 111 M	2, 90 M	3, 38 D
TEXTURE:				
Sand	—	40	30	—
Silt	90	60	70	90
Clay	10	—	—	10
COMPOSITION:				
Feldspar/albite	Tr	2	1	Tr
Volcanic glass	—	1	—	Tr
Dolomite	100	84	80	100
Accessory minerals	—	3	19	Tr

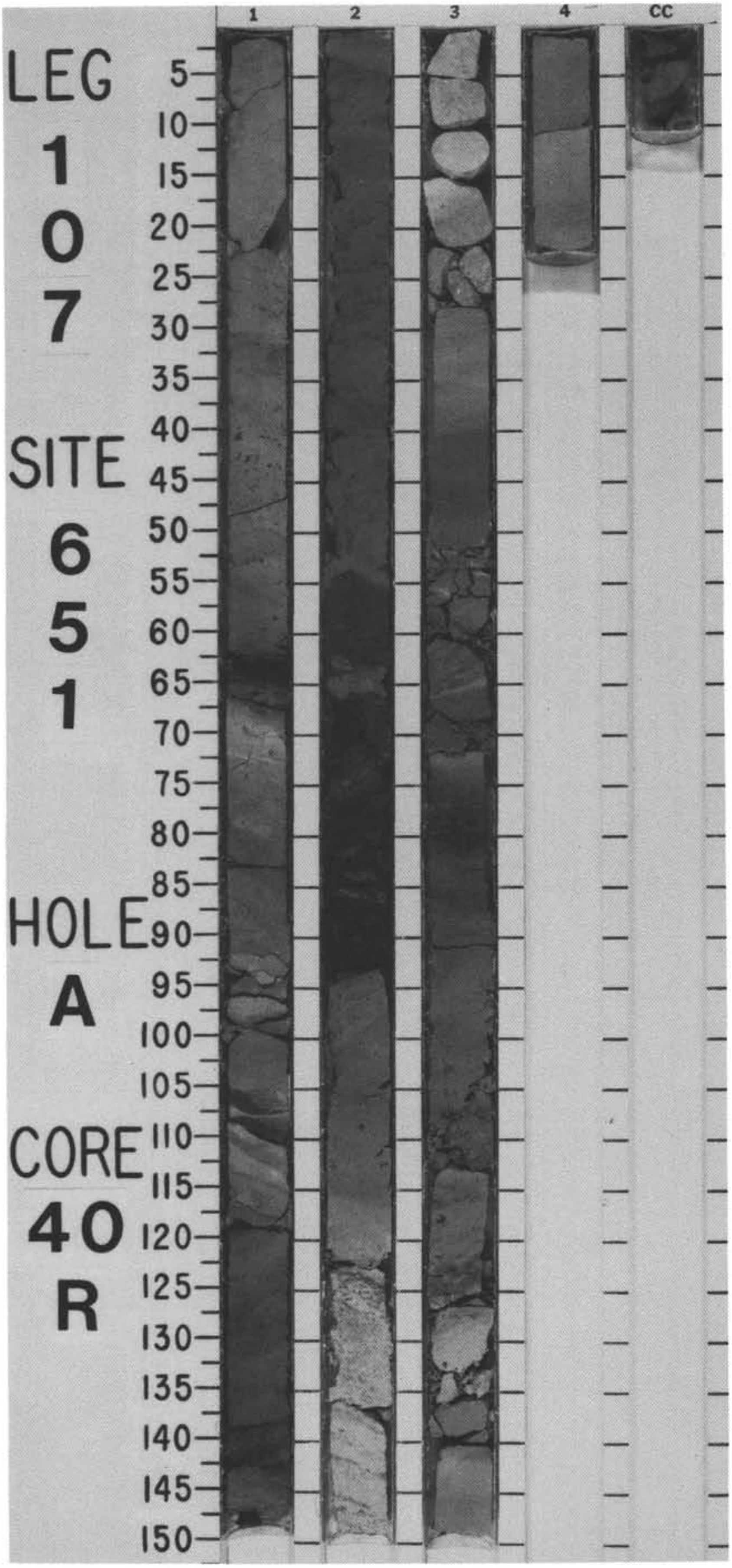
LEG
107
SITE
651
HOLE
A
CORE
40
R
1
2
3
4
CC
5
10
15
20
25
30
35
40
45
50
55
60
65
70
75
80
85
90
95
100
105
110
115
120
125
130
135
140
145
150

SITE 651 HOLE A CORE 41 R CORED INTERVAL 3954.8-3964.5 mbsl; 376.8-386.5 mbsf

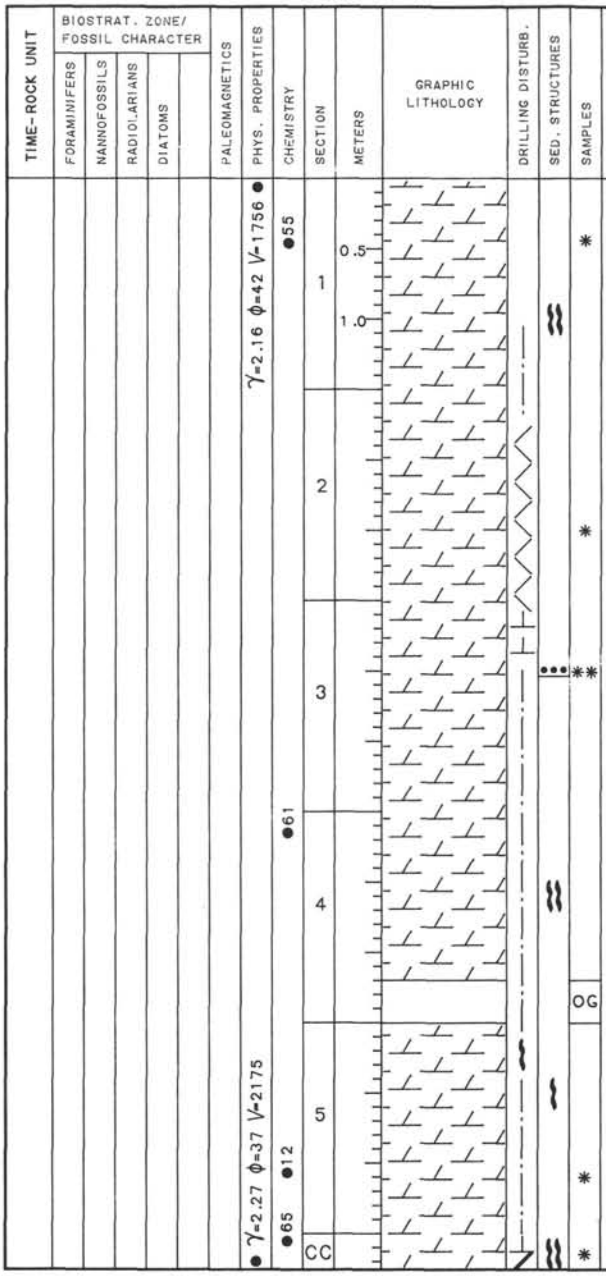

LITHOLOGIC DESCRIPTION

DOLOSTONE

Poorly lithified dolostone (dolomitic chalk) with many deformation-like structures, and many alternations in color from pale olive (5Y 6/3), pale brown (10YR 6/3), reddish yellow (7.5YR 6/6), to light yellowish brown (10YR 6/4); rare, fine-grained silt layers of feldspathized tuff, dusky yellow-green (5GY 5/2) and greenish gray (5G 6/1); marked diagenetic evolution of a probable nannofossil chalk; fine-grained turbiditic layers of silty volcanic glass; some dark gray (10YR 4/1) diffuse specks.

SMEAR SLIDE SUMMARY (%):

	1, 49 D	2, 97 D	3, 47 M	3, 48 M	5, 108 M	CC, 5 D
TEXTURE:						
Sand	—	—	5	—	—	—
Silt	5	5	30	15	20	10
Clay	95	95	65	85	80	90
COMPOSITION:						
Quartz	—	—	1	—	—	—
Feldspar	8	4	60	5	20	5
Clay	Tr	2	4	—	6	—
Volcanic glass	—	4	25	Tr	5	4
Dolomite*	92	90	3	92	54	88
Accessory minerals	—	—	2	—	—	1
*Dolomite auth. zeolite	Tr	Tr	—	3	Tr	—
Black grains	—	Tr	—	—	15	—
Foraminifers	—	—	—	Tr	—	—
Fish remains	Tr	Tr	—	—	—	—
Micrite	—	—	5	Tr	—	—
Red amorphous oxide	—	—	—	—	—	2

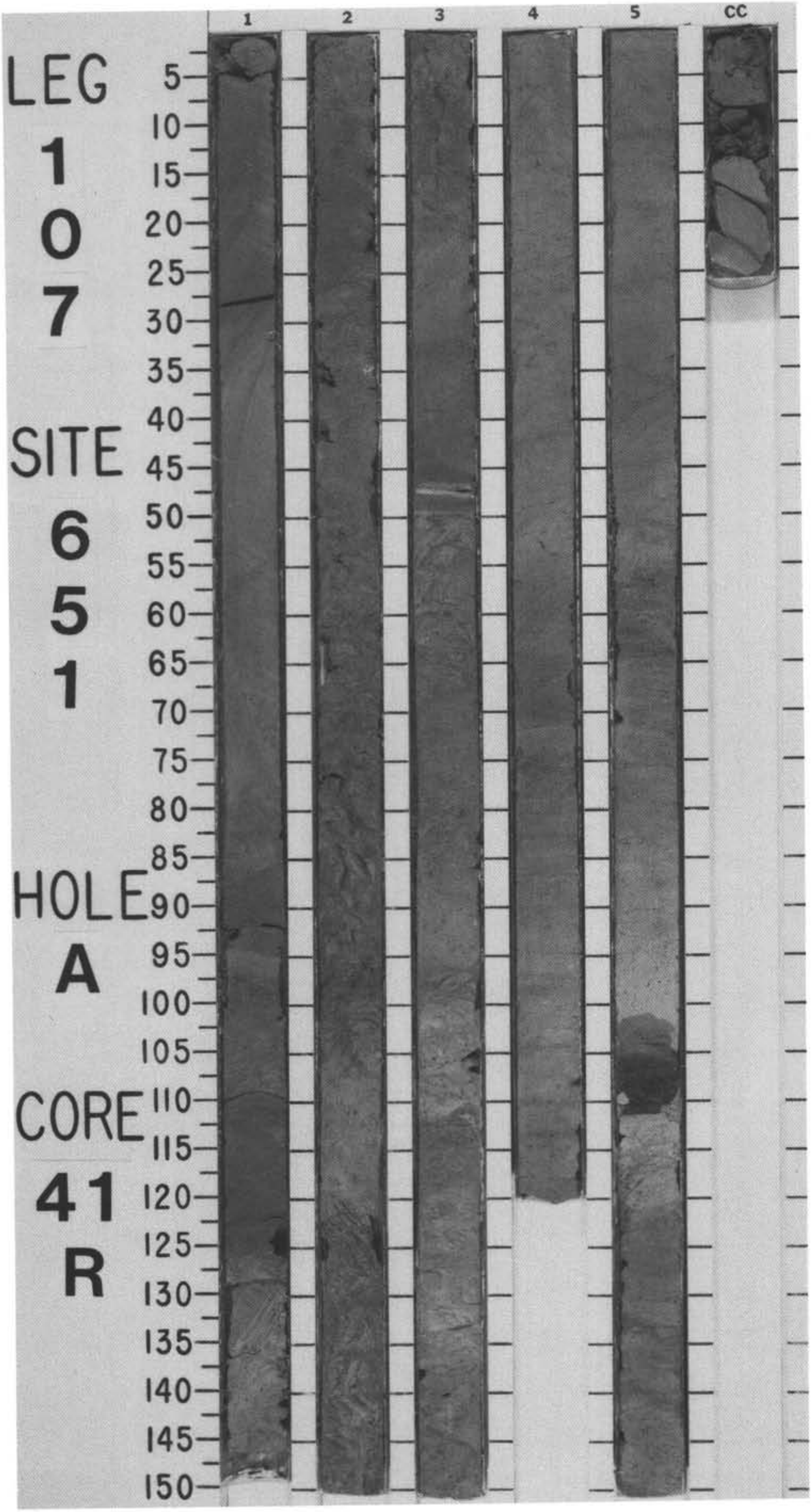
LEG
1
0
7
SITE
6
5
1
HOLE
A
CORE
41
R
1
2
3
4
5
CC
5
10
15
20
25
30
35
40
45
50
55
60
65
70
75
80
85
90
95
100
105
110
115
120
125
130
135
140
145
150

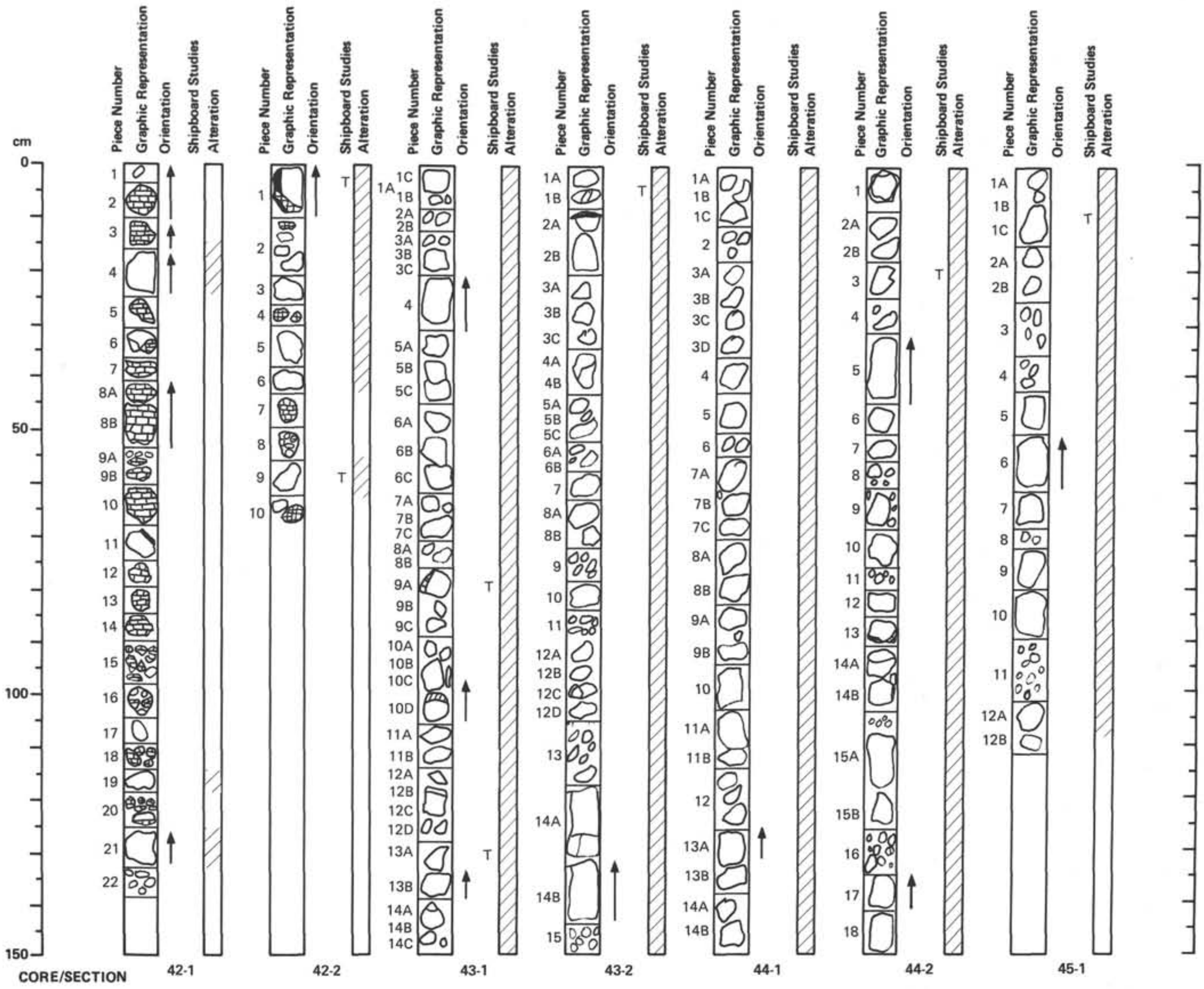

107-651A-42R-1

Alternations of gray to pink dolomite/limestones and basalt:

Piece 4	Altered basalt.
Piece 5-8	Dolomitic breccias with minor basaltic component.
Piece 9-10	Dolomitic breccias.
Piece 11	Basalt with glassy margin.
Piece 12-16	Dolomitic breccia with minor basaltic component.
Piece 17	Basalt.
Piece 18	Light, reddish-brown dolomite.
Piece 19	Highly altered basalt.
Piece 20	Light, reddish-brown dolomite.
Piece 21	Highly altered basalt.

107-651A-42R-2

Alternations of gray to pink, brecciated dolomite/limestone and basalt:

Piece 1	Basalt with relatively fresh glassy margin; crack in margin is filled by dolomitic breccia.
Pieces 4, 7, 8	Breccias of basalt and dolomite.
Piece 6	Highly altered basalt.
Piece 9	Basalt. Intergranular texture. Olivine and Ca-plagioclase microlites in altered groundmass.

107-651A-43R

Altered aphanitic basalt. Intergranular to intersertal texture. Pseudomorphs after olivine. Microlites of Ca-plagioclase and occasional olivine in an altered groundmass. Carbonate veins (become less abundant down section). Some chilled margins. Rare vesicles. 107-651A-43R-1, Pieces 9a and 10d are carbonate cemented basaltic breccias in contact with chilled glass margins.

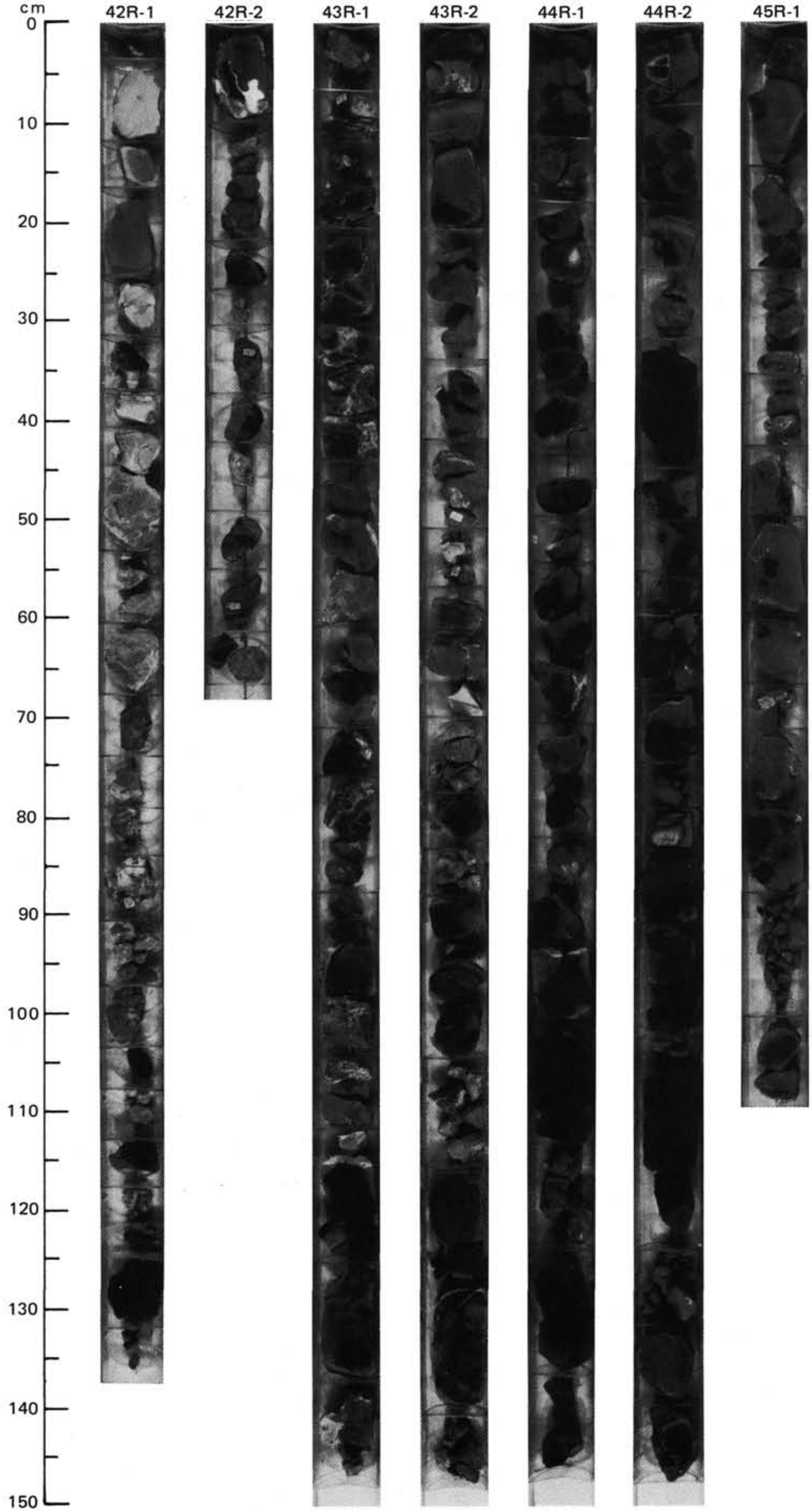
cm
0
10
20
30
40
50
60
70
80
90
100
110
120
130
140
150
42R-1
42R-2
43R-1
43R-2
44R-1
44R-2
45R-1

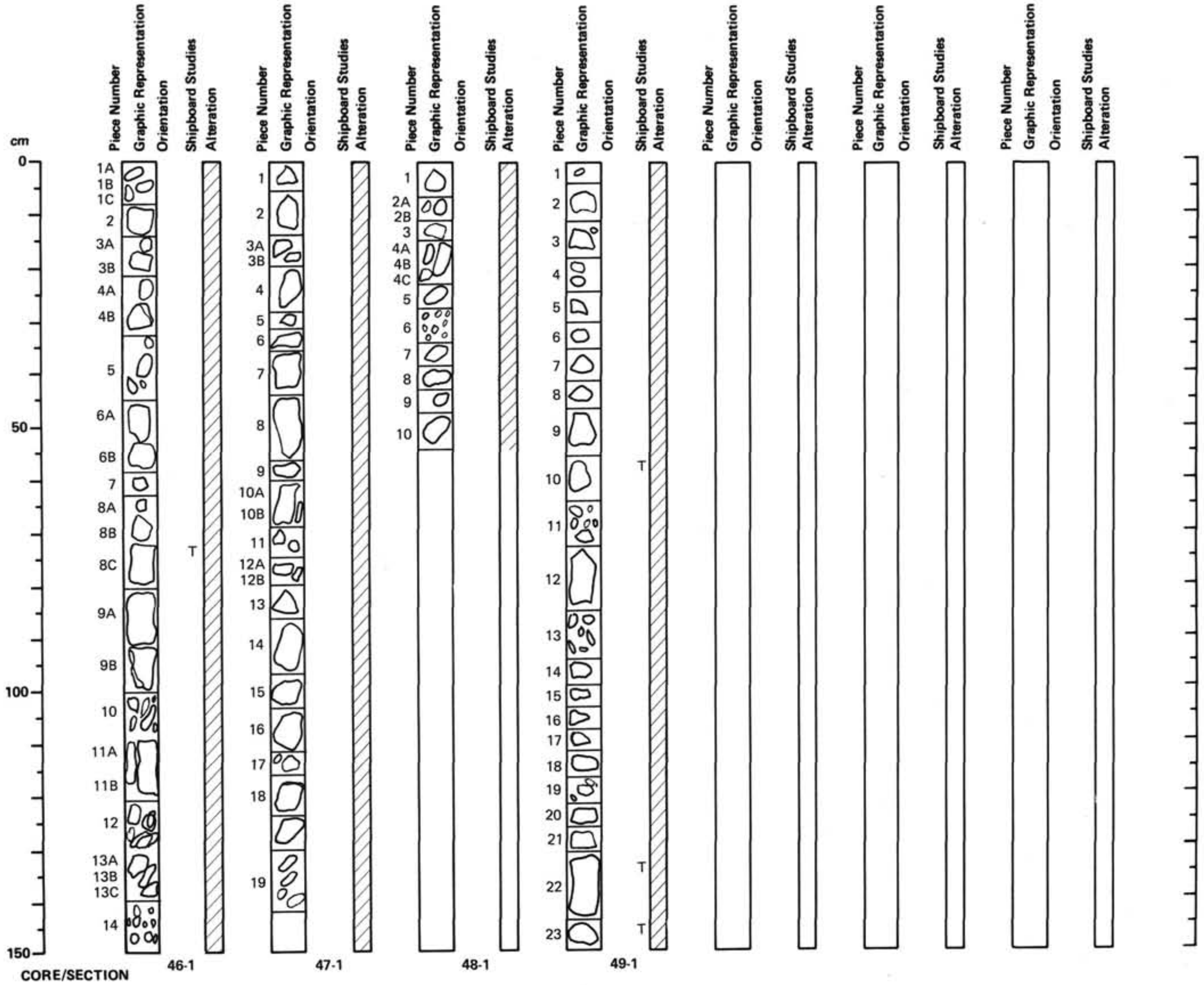

107-651A-46R×49R
Highly altered aphanitic basalt. Intergranular texture. Porphyroclasts of Ca-plagioclase and olivine in altered groundmass. Local vesicles. 107-651A-47R-1, Piece 9 is a basaltic breccia. Some chilled margins. Some carbonate crusts.

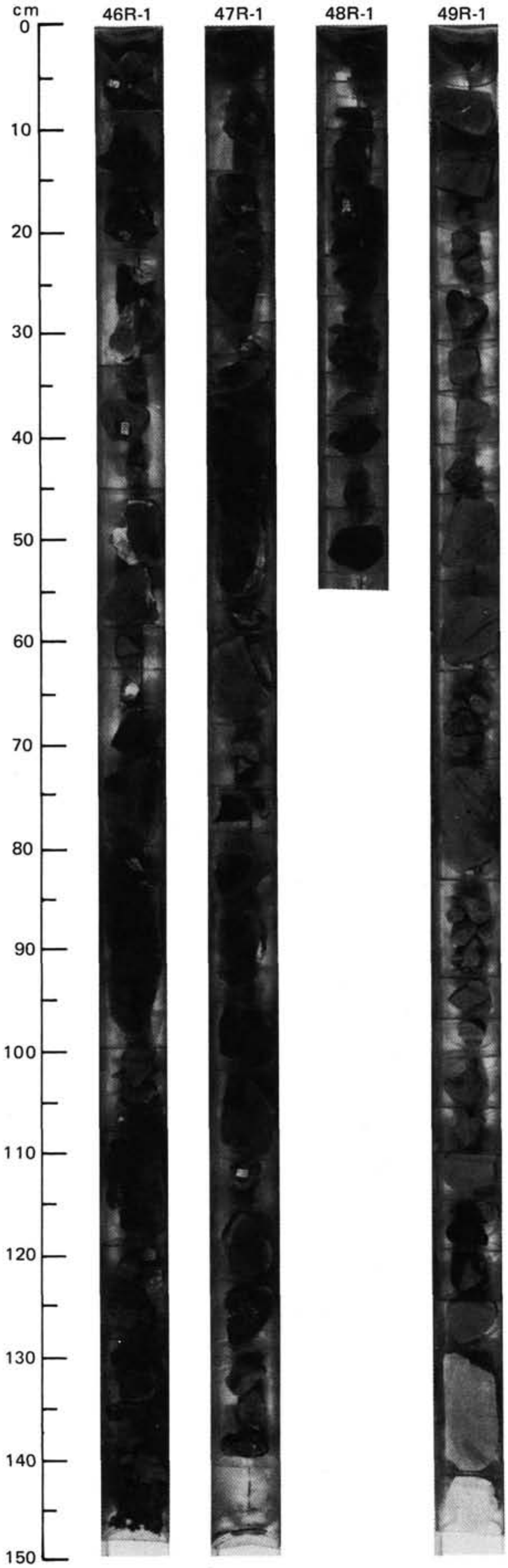
cm
0
10
20
30
40
50
60
70
80
90
100
110
120
130
140
150
46R-1
47R-1
48R-1
49R-1

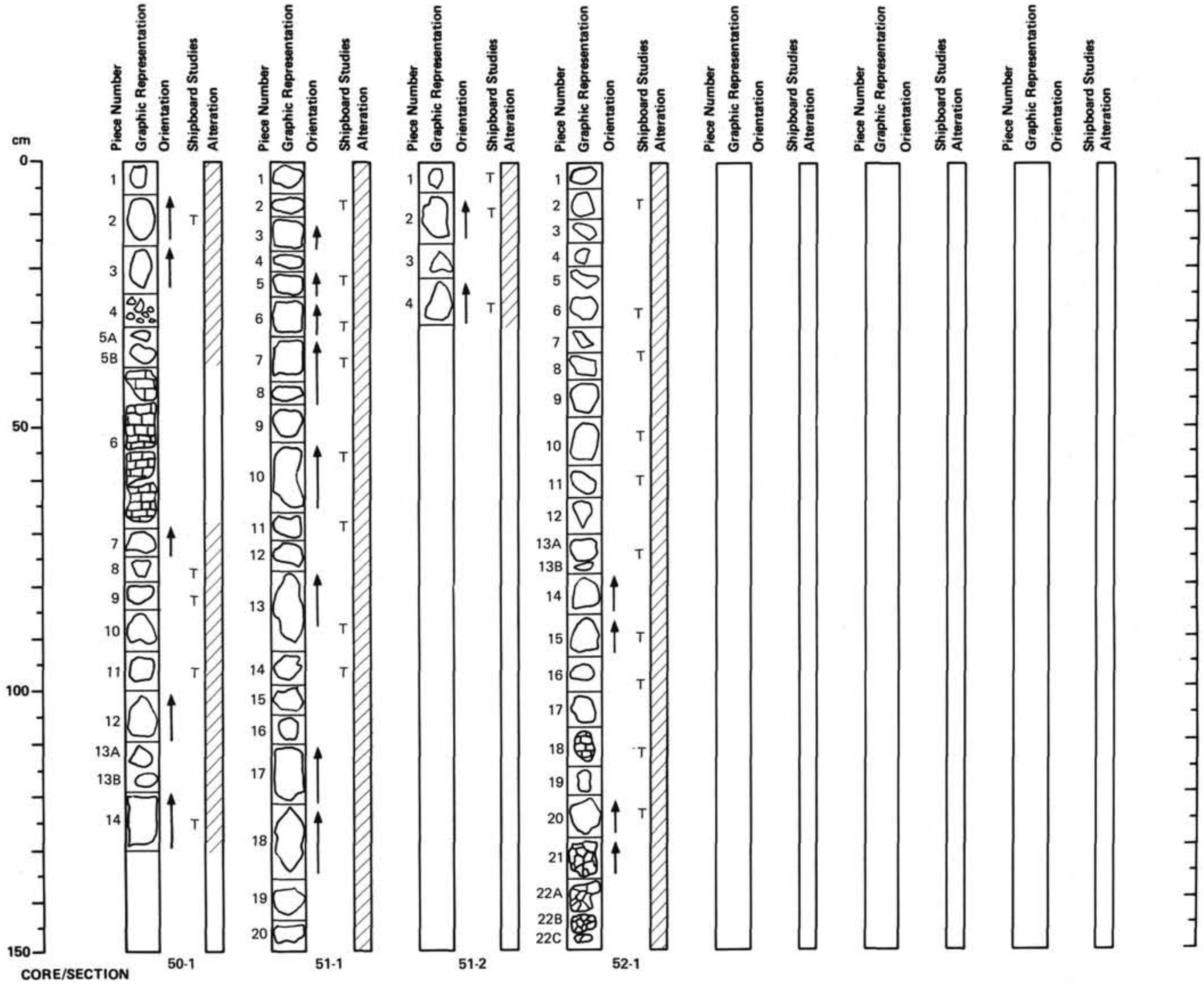

107-651A-50R×52R Intercalated layers of diabase and leucocratic feldspathic rocks, except as follows:

107-651A-50R-1, Pieces 1,2, and 3	Serpentinized peridotite.
107-651A-51R-1, Piece 17	Serpentinized peridotite.
107-651A-50R-1, Piece 6	Pale yellow to brown dolomite.
107-651A-52R-1, Pieces 19 and 20	Altered yellowish basalt.
107-651A-52R-1, Pieces 21 and 22	Carbonate cemented basaltic breccia.

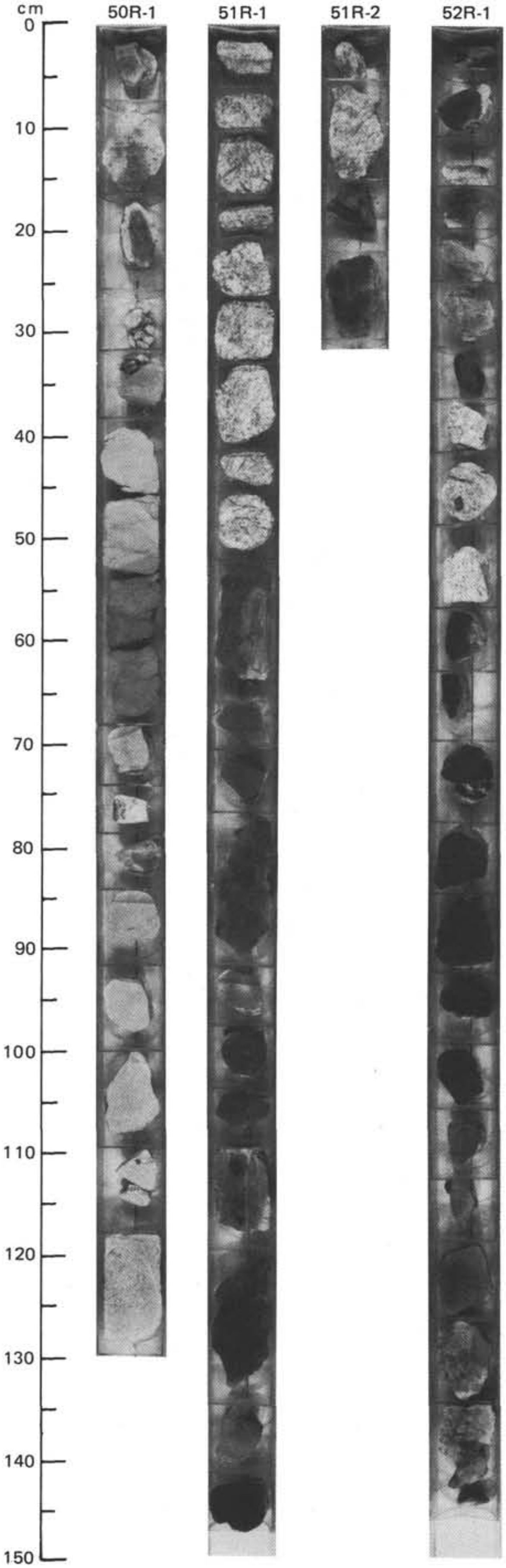
cm
0
10
20
30
40
50
60
70
80
90
100
110
120
130
140
150
50R-1
51R-1
51R-2
52R-1

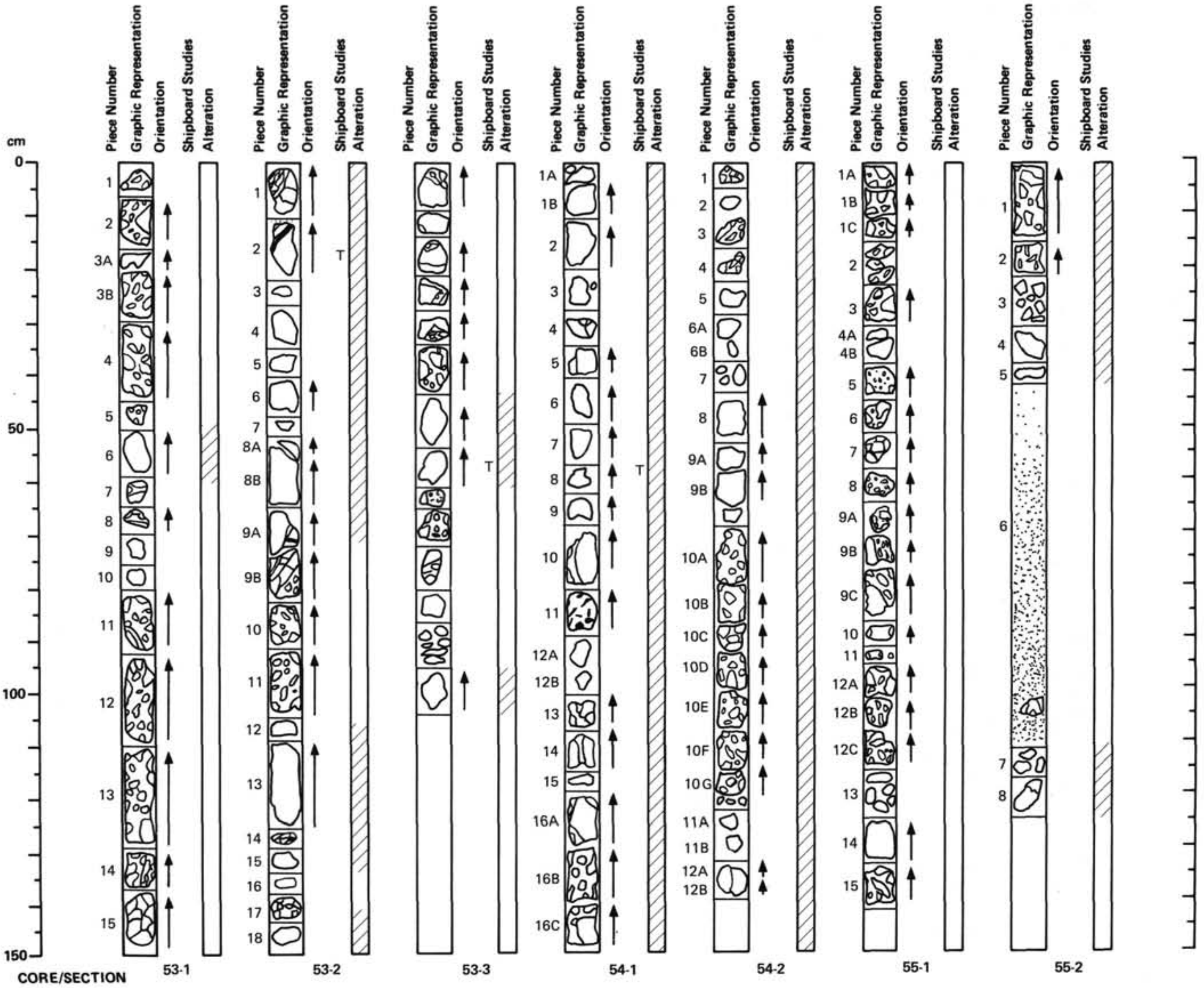

UNIT 3

Alternations of altered basalt and basaltic breccia cemented by carbonate. Basalt contains Ca-plagioclase and pseudomorphs after olivine in an altered groundmass. Former glass margins are observed occasionally.

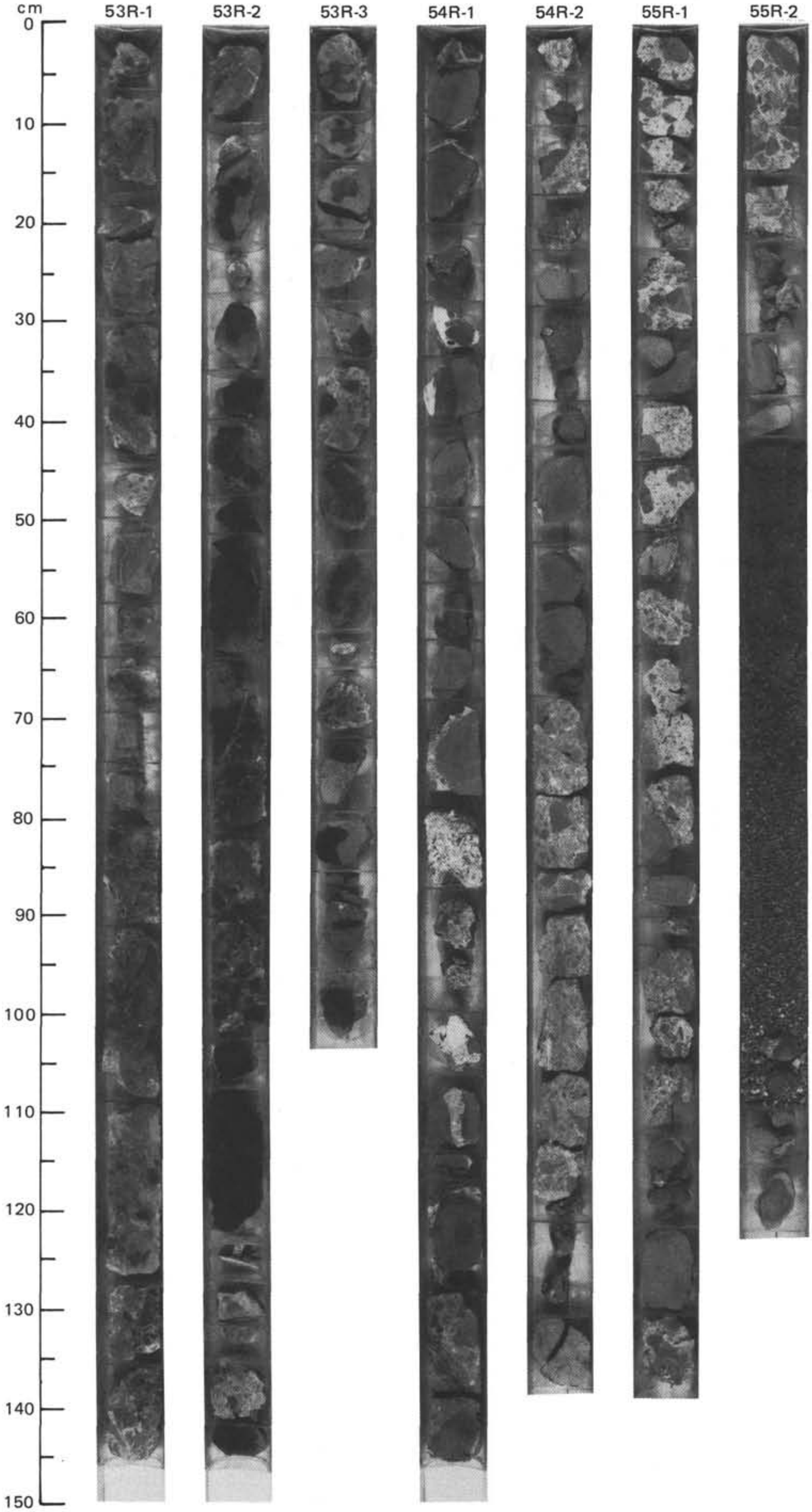
cm
0
10
20
30
40
50
60
70
80
90
100
110
120
130
140
150
53R-1
53R-2
53R-3
54R-1
54R-2
55R-1
55R-2

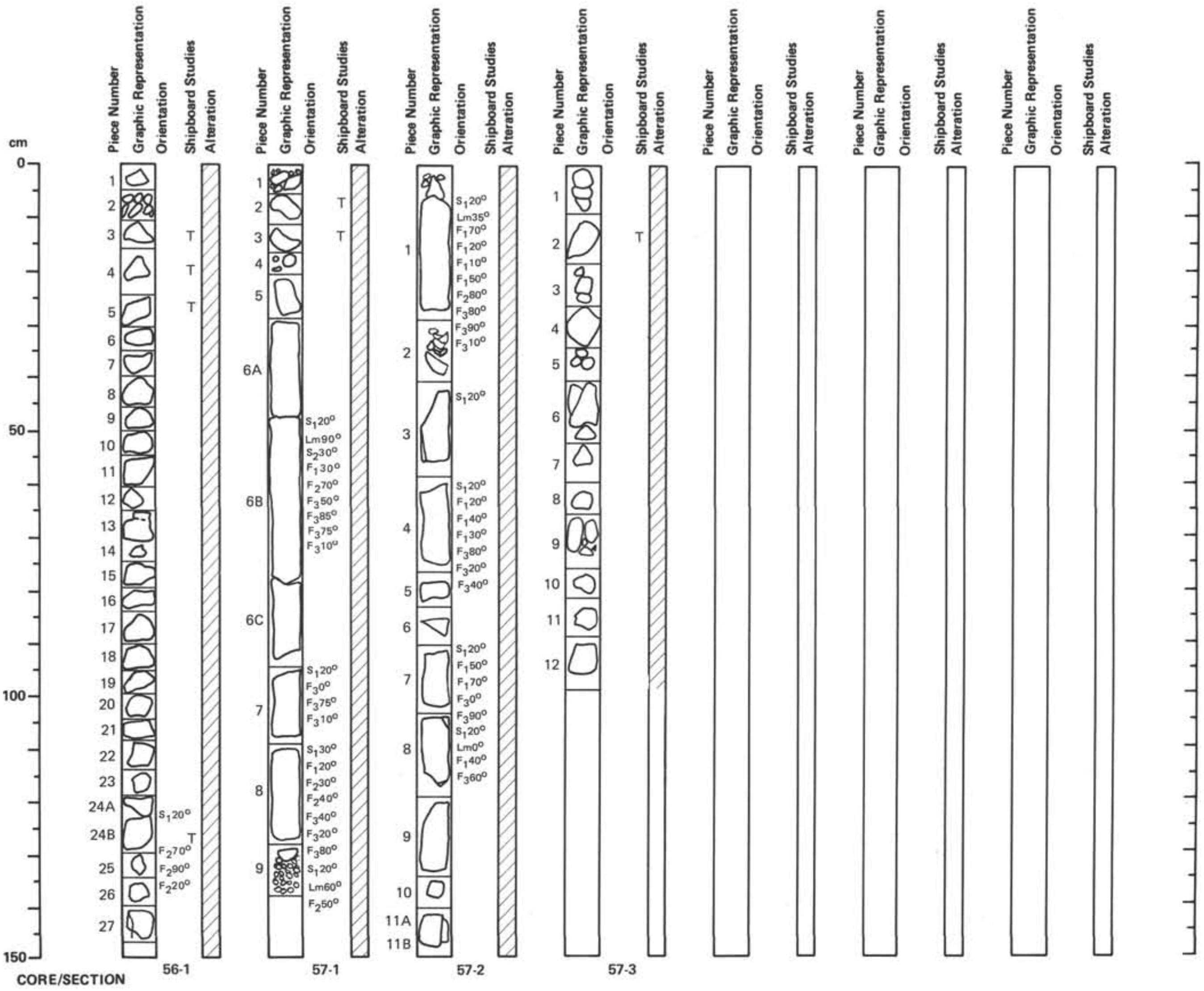

UNIT 4

Highly sheared and foliated serpentinized peridotite. Rock is criss-crossed by white veins of chrisotile. 107-651A-56R-1, Piece 2 contains small pebbles of garnet-bearing rock. All measured microstructures are related to the section plane which has been chosen perpendicular to the S_1 dip.

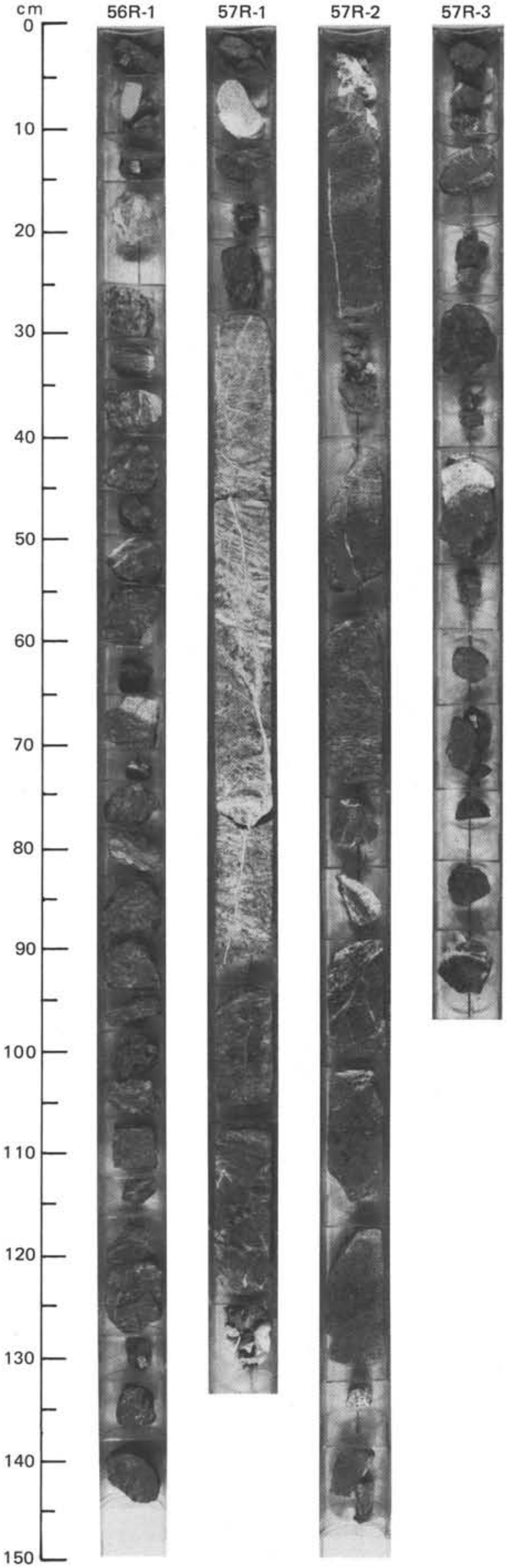
cm
0
10
20
30
40
50
60
70
80
90
100
110
120
130
140
150
56R-1
57R-1
57R-2
57R-3

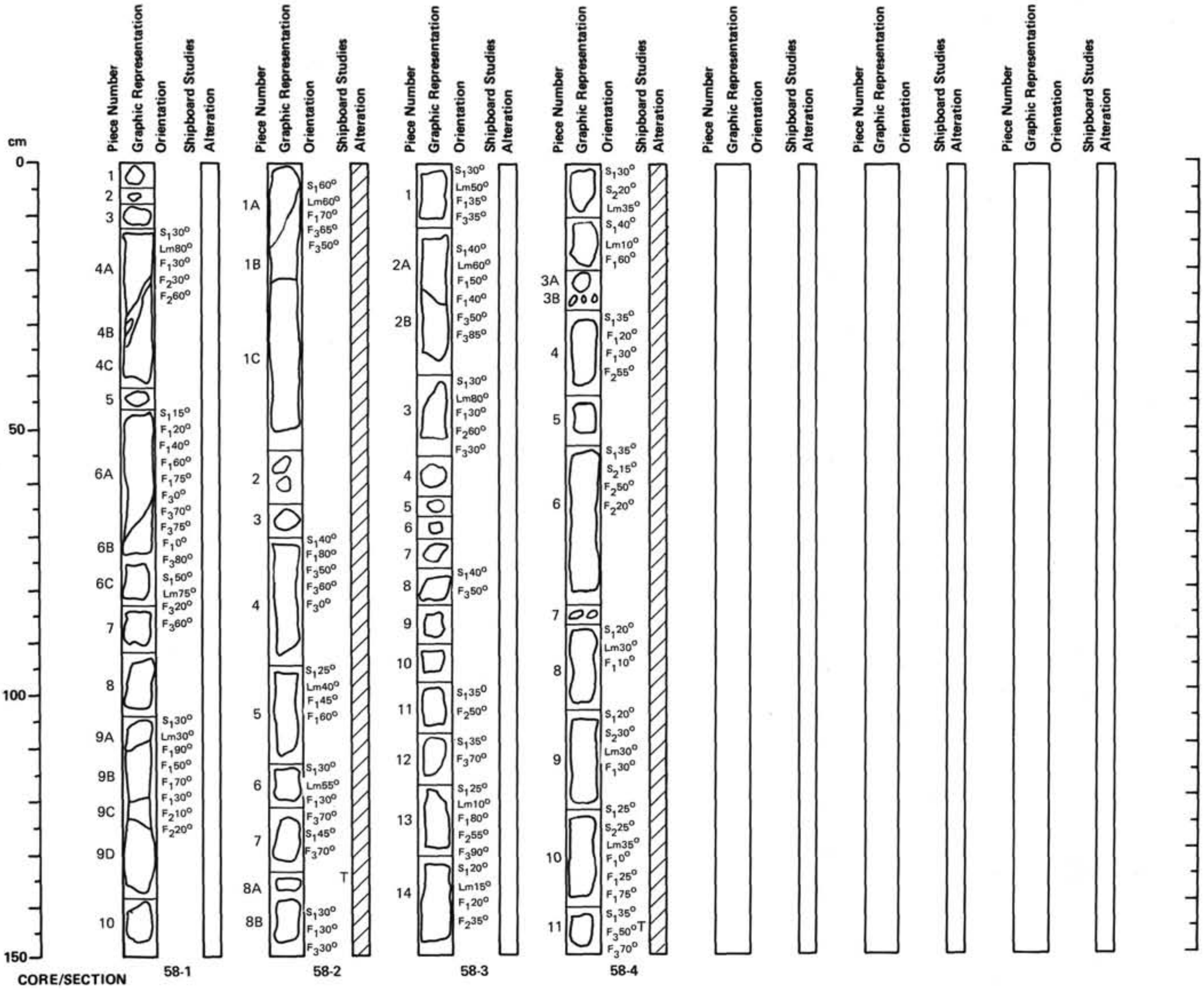

UNIT 4

107-651A-58R-1, Piece 1 is foliated granodiorite. The remainder of the core is criss-crossed by white veins of chrysolite. All measured microstructures are related to the section plane which has been chosen perpendicular to S_1 dip. Interval 107-651A-58R-4, 98 to 102 cm, brackets a fault plane parallel to the section plane. Dip is 50°; slickensides pitch is 60°. Interval 107-651A-58R-4, 0-15 cm brackets a fault plane dipping 65°; slickensides pitch is 70°.

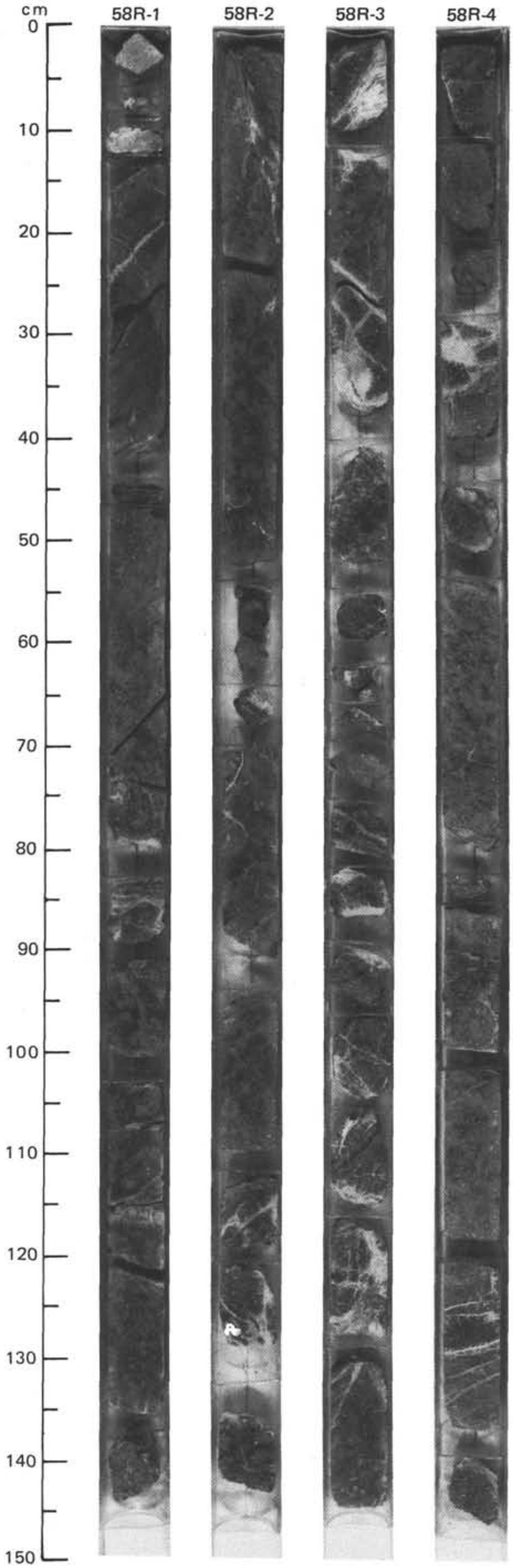
cm
0
10
20
30
40
50
60
70
80
90
100
110
120
130
140
150
58R-1
58R-2
58R-3
58R-4